CHARACTERIZING THE HYDROGEOLOGIC PROPERTIES OF THICK CLAYSTONE AQUITARDS IN THE WILLISTON BASIN USING GROUTED-IN PRESSURE TRANSDUCERS

A Thesis Submitted to the College of

Graduate Studies and Research

In Partial Fulfillment of the Requirements

For the Degree of Doctor of Philosophy

In the Department of Geological Sciences

University of Saskatchewan

Saskatoon

BY

LAURA A. SMITH

PERMISSION TO USE

In presenting this thesis in partial fulfilment of the requirements for a Postgraduate degree from the University of Saskatchewan, I agree that the Libraries of this University may make it freely available for inspection. I further agree that permission for copying of this thesis in any manner, in whole or in part, for scholarly purposes may be granted by the professor or professors who supervised my thesis work or, in their absence, by the Head of the Department or the Dean of the College in which my thesis work was done. It is understood that any copying or publication or use of this thesis or parts thereof for financial gain shall not be allowed without my written permission. It is also understood that due recognition shall be given to me and to the University of Saskatchewan in any scholarly use which may be made of any material in my thesis.

Requests for permission to copy or to make other use of material in this thesis in whole or part should be addressed to:

Head of the Department of Geological Sciences
University of Saskatchewan
114 Science Place
Saskatoon, Saskatchewan
S7N 5E2

ABSTRACT

Clay-rich (argillaceous) aquitards with low hydraulic conductivity ($K \leq 10^{-8}$ ms^{-1}) are widespread throughout the world. Managing and protecting groundwater resources is often dependent on accurate determinations of the hydrogeologic properties of a formation (bulk compressibility, α and K). However, characterizing such deposits has been difficult due to challenges associated with the slow response times of field-based methods, and the difficulty of collecting representative and competent core samples for laboratory analysis. Laboratory tests also tend to overestimate α and underestimate K. Due to these challenges, aquitards remain one of the least understood areas of hydrogeology. This work presents results of *in situ* measurements of α and K of Cretaceous-aged claystones obtained through the measurement and interpretation of pore pressure responses recorded by grouted-in vibrating wire pressure transducers (VWPs). Ten VWPs were installed in one borehole to a total depth of 325 m BG near the northeastern portion of the Williston Basin (Site 1). The loading efficiency (γ) was determined based on pore pressure responses to barometric pressure fluctuation and was found to decrease with increasing depth (0.93 to 0.6). The γ was then used to calculate the constrained one dimensional compressibility, m_v (2.5×10^{-7} to 2.2×10^{-6} kPa^{-1}), which also decreased with depth. Measurements of m_v from laboratory testing on core samples from the same borehole were as much as an order of magnitude greater than the *in situ* estimates. The vertical and horizontal hydraulic conductivity (K_v and K_h, respectively) of the claystone at Site 1 was evaluated at different spatial scales using numerical modeling and laboratory analysis. The results highlight the importance of accounting for scale (laboratory vs field) and consideration of the presence of possible secondary features (e.g. fractures) in the aquitard. The findings from Site 1 suggest that fully-grouted VWPs may provide an alternative method to determine the m_v and K of overconsolidated aquitards and become a useful tool to increase our understanding of the hydrogeology of aquitards. This conclusion was supported by the results obtained from an additional 27 VWPs installed in 5 boreholes at Site 2, also located in the Williston Basin.

ACKNOWLEDGMENTS

First and foremost, I extend my sincerest gratitude to my co-supervisors Dr. M. Jim Hendry and Dr. S. Lee Barbour for their constant encouragement, support, and guidance over the course of this research. I am deeply indebted to them for the many opportunities they have provided me, and consider myself incredibly lucky to have had the chance to be mentored by such inspiring, knowledgeable, and enthusiastic individuals.

I am grateful to Dr. Garth van der Kamp for countless thought-provoking discussions that in no small part, shaped this entire thesis. Your expertise, attention to detail, and thorough editing greatly improved these manuscripts.

I thank Dr. Jim Merriam and Dr. Grant Ferguson for their participation on my committee, and Dr. Matt Lindsay for serving as the chair of the advisory committee. I am also grateful for the contribution of my external examiner, Dr. David Rudolph, for thoroughly examining my thesis and asking both relevant and challenging questions during the defence. Your participation made the final hurdle of this degree both enjoyable and satisfying.

I acknowledge financial support provided to MJH by NSERC-IRC, and the contributions made by The Mosaic Company, Cenovus Energy, PotashCorp, and the Saskatchewan Potash Producers Association.

To my friends, both on campus and off, thank you for humoring me when all I could think about was the current problem I had to solve, and listening to me vent when nothing was going right. I am truly blessed to have such amazing people around me.

I must also thank my soon-to-be husband, Dylan Youngstrom. Your unwavering support and encouragement throughout this process instilled me with confidence every single day, and somehow you kept me laughing the whole way through.

Finally, I would like to thank my family. To my sisters, Rene and Christie, you are my biggest cheerleaders and my best friends. I am so thankful to have you in my life. To my parents, Mel and Carol Smith, you are the voices in my head encouraging me to keep going, and reminding me that if it was easy, everyone would do it. You inspire me to be my best self every single day.

TABLE OF CONTENTS

LIST OF FIGURES

LIST OF TABLES

LIST OF SYMBOLS AND ABBREVIATIONS

α	Bulk compressibility (MLT^{-2})
B	Bulk modulus (MLT^{-2})
B_{ave}	Average barometric pressure (MLT^{-2})
B_0	Barometric pressure at T=0 (MLT^{-2})
β	Bulk compressibility of water (MLT^{-2})
Cc	Compression index ( )
Cr	Recompression (or swell) index ( )
e	Void ratio ( )
e_o	Initial void ratio ( )
σ’	effective stress (MLT^{-2})
σ_t	Total stress (MLT^{-2})
F.S.	Full scale (%)
h	Hydraulic head (L)
h_f	Fresh water hydraulic head (L)
h_p	Point water pressure head (L)
m_v	1-D constrained compressibility ($M^{-1} L^{-1} T$)
m BG	meters below ground (L)
masl	meters above sea level (L)
M	Constrained modulus (MLT^{-2})
n	Total porosity ( )
OCR	Overconsolidation ratio ( )
ρ_f	Density of fresh water (ML^{-3})
ρ_p	Point water density (ML^{-3})
υ	Poisson’s ratio ( )
p*	Corrected porewater pressure (MLT^{-2})
p_t	Uncorrected absolute pore pressure (MLT^{-2})
P_C’	Preconsolidation pressure (MLT^{-2})

K	Hydraulic conductivity (LT^{-1})
K_h	Horizontal hydraulic conductivity (LT^{-1})
K_v	Vertical hydraulic conductivity (LT^{-1})
γ	Loading efficiency ( )
ρ_w	Density of water (ML^{-3})
ρg	Specific gravity of water ($ML^{-2}T^{-2}$)
q	specific discharge or Darcy flux (LT^{-1}),
RMSE	Root mean squared error (L)
S_S	Specific storage (L^{-1})
t	Time (T)
z	Depth (L)
BP	Before present
DST	Drill Stem Test
WB	Williston Basin
WCSB	Western Canada Sedimentary Basin
VWP	Vibrating wire piezometer

1.0 INTRODUCTION

1.1 Overview

Aquitards are geologic deposits with low hydraulic conductivity ($K \leq 10^{-8}$ m s^{-1}) and sufficient regional extent, thickness and competency to impede groundwater flow between or to aquifers (Cherry and Parker, 2004). In addition to the ability to control recharge and chemical transport to adjacent aquifers, aquitards can act as isolating units to protect shallow groundwater from contamination by fluids and gases injected into deeper formations. More recently, due to the low-K and high sorption capacity of thick basinal aquitards, many countries are investigating them as possible host formations for the sequestration of hazardous wastes (Hendry et al., 2015; Neuzil, et al. 2013; Mazurek et al., 2011). Managing and protecting groundwater resources is often dependent on accurate determinations of the hydrogeologic properties of a formation (1-D constrained compressibility, m_v; bulk compressibility, α; specific storage, S_S; and K). For these reasons, increased research on aquitards and their physical, chemical and hydrogeological properties has occurred over the last 20-30 years (c.f. Batlle-Aguilar et al., 2016). However, in spite of the additional focus on aquitards, they remain one of the least understood areas of hydrogeology. The lack of systematic studies of these systems arises primarily due to the logistical and technical difficulties associated with monitoring slow responses during conventional field tests, and the cost and challenge of collecting representative and competent core samples for laboratory analysis. Due to these challenges, research in this area is slow and often intermittent.

1.2 Research objectives

The goal of this thesis was to develop and apply alternative methods to characterize the hydrogeological properties of low-K formations and thus increase our understanding of deep (up to 400 m) aquitard systems in the Williston Basin (WB). The main research objectives were to: (1) determine the *in situ* compressibility through argillaceous aquitards in the WB by analyzing pore pressure responses from grouted-in vibrating wire pressure transducers (VWPs); (2) characterize the K of argillaceous aquitards using laboratory, *in situ*, and numerical modeling and compare the multi-scale results to each other and previous work; and (3) generate a detailed data set of hydrogeologic parameters for argillaceous aquitards in the WB using *in situ*, laboratory and numerical modeling methods to evaluate the potential of grouted-in VWPs for determining *in situ* parameters (α and K_h) of aquitards.

To achieve these objectives, the following actions were taken:

1) Six boreholes were drilled at two sites (Site 1, n=1; and Site 2, n=5) in the WB (100 to 325 m depth) from which cores were collected and multiple VWPs (3-10) were installed at varying depths;
2) Geotechnical and hydrogeological parameters were determined from core samples obtained from each site using conventional laboratory methods;
3) The short- and long-term pore pressure responses to barometric pressure fluctuations recorded by the VWPs were analyzed to determine *in situ* 1-D constrained compressibility (m_v) at Site 1;
4) The pore pressure recovery of each VWP following installation were numerically modeled to determine *in situ* K_h at Site 1;
5) A method was developed to numerically model the head profile at Site 1 to determine if the modeled *in situ* K_h was a reasonable estimate;
6) The *in situ* VWP methods were applied to VWPs installed at Site 2 in the WB to build the database and evaluate the reliability of the methods; and
7) A detailed suite of *in situ* and lab based data for overconsolidated shale aquitards was generated from the VWP and laboratory determined parameters for the WB.

This is a manuscript-style Ph.D. thesis in which three of the chapters (Chapters 3, 4 and 5) are written in journal manuscript format and have either been published, accepted, or in preparation for submission to a peer reviewed journal. Chapter 3 (Manuscript #1) presents a method developed to determine *in situ* compressibility of a thick claystone aquitard using high resolution pore pressure records from grouted- in vibrating wire pressure transducers. Chapter 4 (Manuscript #2) presents a multiscale approach to determine the hydraulic conductivity through the thick claystone aquitards using various field, laboratory and numerical modeling methods. Chapter 5 (Manuscript #3) presents a synthesis of the *in situ* hydrogeologic properties determined from pressure transducers and evaluates estimates provided in previous work on similar argillaceous materials.

In addition to the manuscript chapters, the thesis also contains the introduction (this chapter; Chapter 1) and a literature review (Chapter 2) undertaken from a broader perspective than that contained within each manuscript. The final chapter (Chapter 6) presents a summary of

conclusions and recommendations for the entire study. Because of the manuscript-based format of the thesis, there is some repetition between Chapters, particularly in the Introduction and Geologic Setting sections.

At the time of the defence of this thesis, the status of the manuscripts were:

- **Manuscript #1 (Chapter 3): A new technique for obtaining high-resolution pore pressure records in thick claystone aquitards and its use to determine *in situ* compressibility. Status:** Published by Water Resources Research, Vol., 49, 732-743, doi:10.1002/wrcr.20084, 2013.

- **Manuscript #2 (Chapter 4): A multiscale approach to determine hydraulic conductivity in thick claystone aquitards using field, laboratory and numerical modeling methods**. **Status:** Published by Water Resources Research doi: 10.1002/2015WR018448, 2016.

- **Manuscript #3 (Chapter 5): *In situ* hydrogeologic properties of argillaceous formations in the Williston Basin determined from grouted-in pressure transducers Status:** In preparation to be submitted to Hydrogeology Journal.

In addition to these manuscripts, the author has coauthored two additional manuscripts during the course of the graduate program that were published or submitted for publication in refereed journals. These manuscripts were based on the subject matter of this thesis. These were:

- Smerdon, B. D., L. A. Smith, G. A. Harrington, W. P. Gardner, C. Delle Piane, and J. Sarout (2014), Estimating the hydraulic properties of an aquitard from *in situ* pore pressure measurements, Hydrogeol. J., 22(8), 1875-1887, doi: 10.1007/s10040-014-1161-x.

- Hendry, M. T., M.J. Hendry, L.A. Smith, (in review), Analysis of the measured pore pressure response to atmospheric pressure changes to evaluate small strain moduli: Methodology and case studies. Submitted to Geotechnique.

1.3 Location

1.3.1 Geologic Setting

The WB is a sedimentary basin within the Western Canada Sedimentary Basin (WCSB). The WCSB is a wedge of sub-horizontal sedimentary rock that progressively thins from 5,500 m under the Rocky Mountains to 0 m near the eastern margins. The WB is a structural-sedimentary basin underlying approximately 250,000 km^2 in North Dakota, Manitoba, Saskatchewan, Montana and South Dakota (Vigrass, 2006). The basin is bordered by the exposed Canadian shield to the north and northeast, the Sioux uplift and Transcontinental arch to the east and southeast. A series of arches, domes and uplifts separate the WB from smaller basins in the southwest and the Alberta Basin in the northwest (Bachu and Hitchon, 1996). The WB contains a nearly complete record of Middle Cambrian to Tertiary aged sediments reaching up to 5,000 m in the center of the basin and thins outward to about 3,300 m near the basin boundary (Vigrass, 2006). The sedimentary rocks in the WB range from Cambrian to late Tertiary and can be divided into two main divisions: a lower succession of Cambrian to Jurassic age formations that are predominantly carbonate rocks and formed before the major uplift of the Canadian Cordillera; and an upper succession of mid-Jurassic to Tertiary aged rocks of predominantly shale and sandstone deposited following the uplift in the Cordillera. The upper succession is typically covered by glacial drift deposited during the Pleistocene Epoch (2 Ma- 11,000 years BP). The carbonate rocks in the lower succession make Canada the world's leading producer of evaporite minerals (anhydrite, halite and potash) (Jasinski, 2010), while the upper succession contains one of the world's richest reserves of petroleum and natural gas.

1.3.2 Hydrogeologic Setting

The current conceptual model of water flow in the WB assumes that the driving force behind basin scale flow is due to gravity gradients created by topography (Bachu and Hitchon, 1996; Bachu, 2002). Recharge areas at high elevations in the southwest of the basin in Montana and South Dakota (1100-1300 m range) discharge to low elevation areas in the northeast at Lake Winnipeg (200-300m range). In most areas of the basin, formation pressures are very close to hydrostatic, and formation flow is near steady state; however, smaller scale flow of formation waters in the basin are the result of local structure, stratigraphy and lithology (Bachu and Hitchon, 1996). For the purposes of this study, we are interested in the Cretaceous aquitard overlying the Mannville Group (aquifer). Drill stem tests (DSTs) conducted on the Mannville

Group indicate the same regional northeastward flow with hydraulic heads ranging from more than 1000 m in the south west to less than 400 m relative to sea level at the Manitoba escarpment in the northeast (Bachu and Hitchon, 1996). Previous work by Neuzil (1993) suggests that transient flow is occurring within these deposits as a result of unloading associated with erosional rebound in the Pierre Formation (youngest Cretaceous shale in the aquitard sequence) and that this mechanical rebound could account for the low pressures in the shale. This is consistent with Neuzil and Pollock's (1983) assertion that erosion will generate subhydrostatic conditions; however, they also indicate this may only apply to relatively deformable media. Due to these low pressures, it is suggested that groundwater will flow both downward and upward into the Cretaceous aquitard until equilibrium is attained (Figure 1.1) (Neuzil, 1993). The stratigraphic terminology for the Cretaceous deposits in the WCSB are not consistent across provinces; therefore, stratigraphic sections with local terminology are presented (Figure 1.2). For the purposes of this thesis, the terminology used is consistent with the locations of the sites in Southern Saskatchewan and Southern Manitoba (locations 8 and 9, respectively).

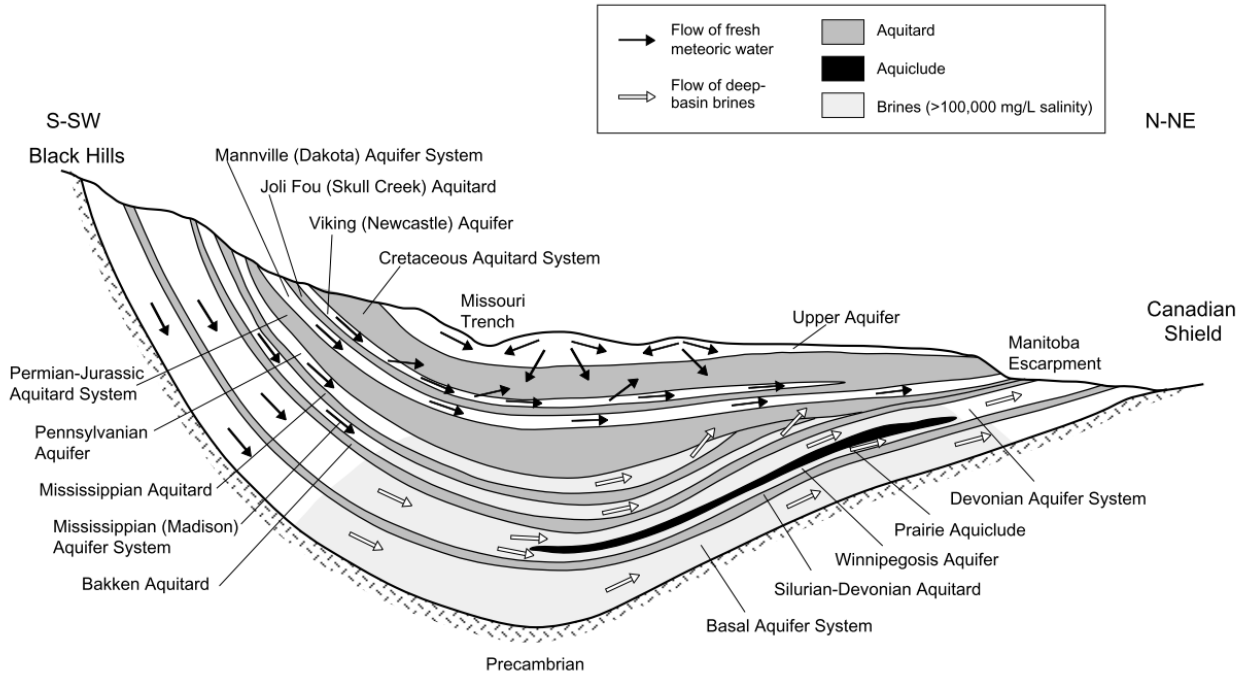

Figure 1.1: Cross section of the Williston Basin from the S-SW to N-NE of basin-scale flow of formation waters (Bachu and Hitchon, 1996. Reprinted by permission of the AAPG whose permission is required for further use).

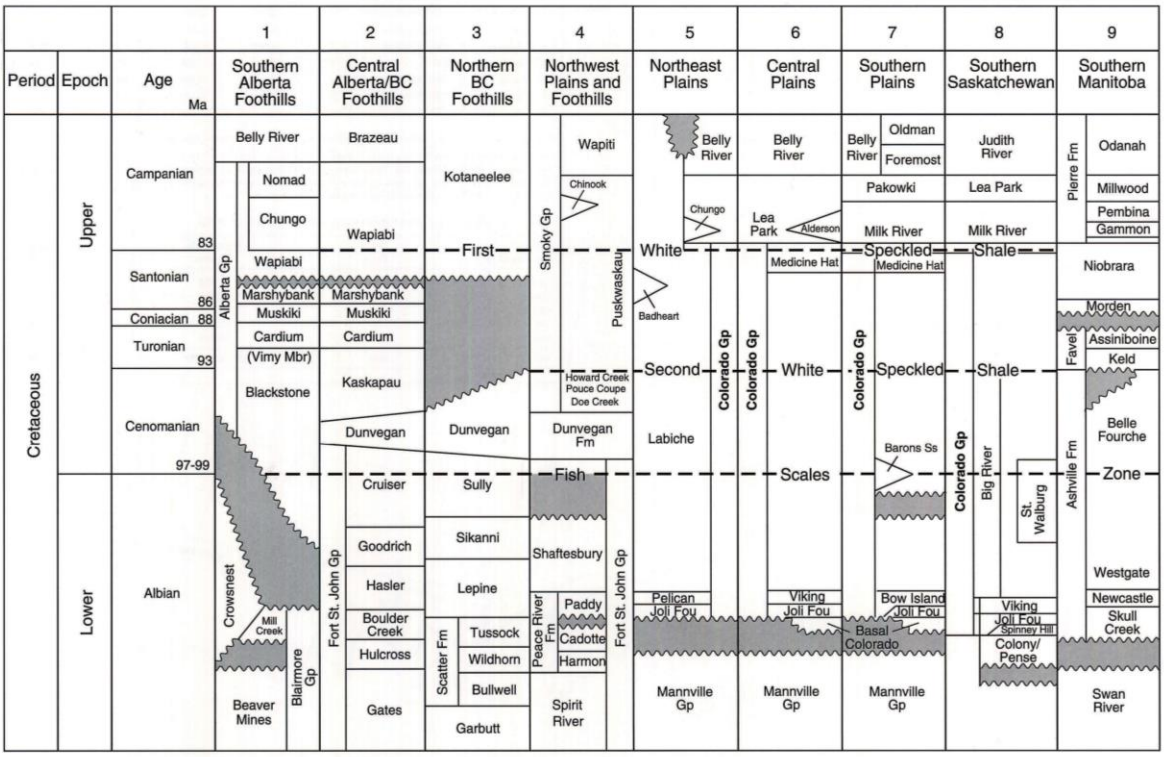

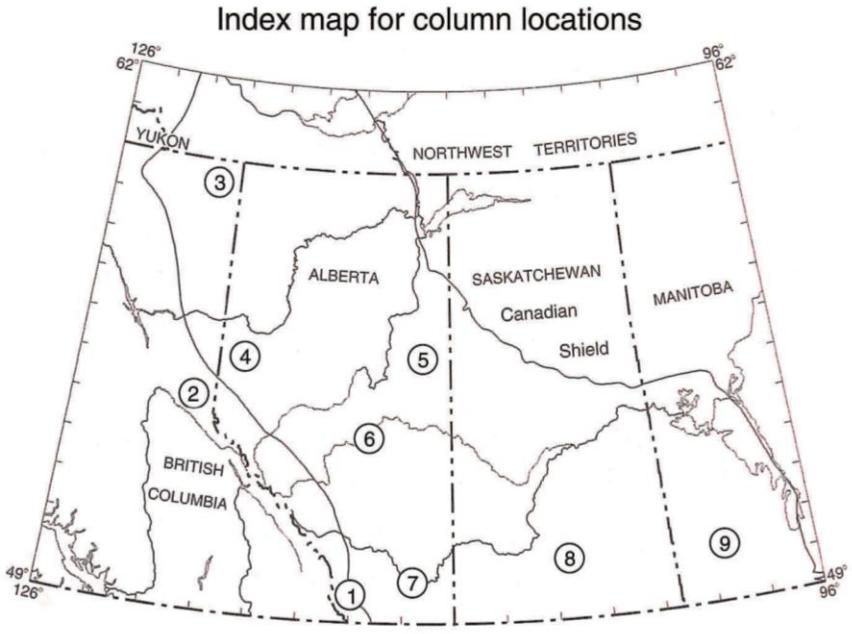

Figure 1.2: Stratigraphic terminology for the Cretaceous deposits in the Western Canada Sedimentary Basin (Alberta Geological Survey, 2016. Contains information licensed under the Open Government Licence – Alberta).

1.4 References

Alberta Geological Survey, (2016), Atlas of the Western Canada Sedimentary Basin, Chapter 20: Cretaceous Colorado/Alberta Group of the Western Canada Sedimentary Basin. [Available at: http://ags.aer.ca/publications/chapter-20-cretaceous-colorado-alberta-group.htm, accessed 29 Aug. 2016]

Bachu, S. and B. Hitchon (1996), Regional-scale flow in formation waters in the Williston Basin. *AAPG Bull.*, 80 (2), 248–264.

Bachu, S. (2002), Suitability of the subsurface in Saskatchewan and Manitoba for Geological Sequestration of Anthropogenic Carbon Dioxide. Alberta Geological Survey, Alberta Energy and Utilities Board.

Jasinski, S.M. (2010), Potash, *Mining Engineering*, 69-70.

Neuzil, C. E. (1993), Low fluid pressure within the Pierre Shale: A transient response to erosion. *Water Resour. Res., 29*, 2007–2020.

Neuzil, C. and Pollock, D. (1983), Erosional unloading and fluid pressures in hydraulically 'tight' rocks. *J. Geo*., 91, 179-193.

Vigrass, L. (2006), Williston Basin. Encyclopedia of Saskatchewan [Available at http://esask.uregina.ca/entry/williston_basin.html, accessed 23 Nov. 2015].

2.0 LITERATURE REVIEW

This chapter provides background information and theory related to the topic of this thesis, as well as a review of the relevant literature. Although Chapters 3-5 include a specific literature review for each manuscript, the same information presented here provides information and the literature context of the entire work.

2.1 Effective stress and pore pressure

Total vertical stresses (σ) (i.e. overburden stress) acting on a point below the ground can be calculated by the unit weight of the formation (soil and fluid) and the depth of the overburden. When stress is applied to a sediment (e.g. during burial or glaciation), the load is borne by both the pore fluid and the grain-grain soil matrix. The effective stress (σ') is the portion of the total stress that is borne by the soil or rock matrix, while the pore pressure (p) is the portion of the total stress taken up by the fluid (Terzaghi, 1936):

[2.1] $$\sigma' = \sigma - p$$

The pore water pressure also represents a component of the total mechanical energy causing ground water flow (the other being elevation or gravitational potential energy). The two main methods used to measure positive (gauge) pore pressures in soils and rock include the use of open wells or the use of sealed in pressure transducers.

2.1 Barometric and loading efficiency

It has long been established that the pore water pressure within a formation will respond to loading such as that created by surface barometric (or atmospheric) pressure. For a laterally homogenous formation, horizontal displacement due to atmospheric pressure change is negligible, and the stress change acting on the claystone aquitard will be essentially vertical and equal to the atmospheric pressure change at ground surface (van der Kamp and Gale, 1983). This applied load produces an instantaneous change in pore water pressure at depth (Jacob, 1940; Skempton, 1954); however, generally only a portion of the barometric pressure is borne by the porewater, with the remainder carried by the soil or rock matrix. The ratio of the observed pore pressure change to the applied surface load is referred to as the loading efficiency (γ). In open systems, (e.g. stand pipe piezometers) the full atmospheric pressure acts on the water within the well and in systems which the pore water can equilibrate quickly between the well and formation (e.g. confined aquifers) this results in a drop in the water level in the well if the formation pore

pressure has a γ which is less than unity. This change in water level is used in open wells to define the barometric efficiency (BE) of the aquifer as the change in water level caused by a change in barometric pressure divided by the barometric pressure change (Skempton, 1954; Clark, 1967; van der Kamp and Gale; 1983) such that:

[2.2] $$\gamma + BE = 1$$

In geotechnical engineering, the most commonly addressed problem associated with loading is the consolidation of soft clays, and in these conditions the loading efficiency is essentially equal to 1 (Terzaghi and Frohlich, 1936). However, in heavily overconsolidated soils where the compressibility approaches the compressibility of water, a portion of the applied load is shifted to the soil skeleton from the pore water, thereby decreasing the γ and increasing BE (Terzaghi, 1996). Assuming lateral strain is negligible, the γ of the formation can be determined, and the porosity is known, the m_v of the formation can be determined using the following relationship (van der Kamp and Gale, 1983):

[2.3] $$m_v = \frac{\gamma n \beta}{1-\gamma}$$

where m_v is the one dimensional (1-D) constrained compressibility of the formation, β is the compressibility of water at 20°C (4.6×10^{-7} kPa^{-1}), and *n* is the porosity of the formation. The value of m_v can be converted to a constrained modulus ($M=1/m_v$) and then to a bulk modulus (B) by assuming a Poisson's ratio and the following relationship (Duncan and Bursey, 2013):

[2.4] $$B = \frac{M}{3}\frac{(1+\nu)}{(1-\nu)}$$

where *ν* is Poisson's ratio. The inverse of B is bulk compressibility (α, kPa^{-1}). Again, assuming negligible lateral strain, specific storage (S_S) can be calculated using:

[2.5] $$S_S = \rho g(n\beta + \alpha)$$

where ρg is the unit weight of water (9.8 kN m^{-3}).

2.2 Hydrogeologic parameters of argillaceous aquitards

Hydrogeologic parameters (K and α) are historically difficult to determine in heavily overconsolidated, argillaceous aquitards. Conventional field testing (such as pump/slug tests), are often not suitable for determining *in situ* parameters of low-K deposits due both technical and logistical difficulties associated with slow response times. Further, collecting competent core

samples for laboratory analysis that are representative of *in situ* conditions is not only challenging, but costly as well. Regardless, the majority of K and α data for argillaceous formations are obtained from laboratory analysis. However, even in perfect conditions where the core sample is as competent and representative as it can be, the reliability of the method and the scale of application are both areas of concern. Sample deterioration such as desiccation or microfracturing (Neuzil, 1993; Neuzil and Provost, 2014), and equipment configuration or measurement uncertainties (Timms et al., 2014) can all introduce error and result in inaccurate estimates. These errors can only be quantified if other methods are applied to the same core at the same depth, otherwise, variances in the results can be attributed to spatial heterogeneity (Batlle-Aguilar et al., 2016). However, regardless of how carefully core samples are collected and preserved, laboratory values will always have some sort of error associated with them and should be treated as such.

2.2.1 Methods to determine hydraulic conductivity in aquitards

Various laboratory and field techniques exist to determine K in high-K formations (aquifers) but only a few are applicable to aquitards. For the purposes of this thesis, only those pertinent to aquitards are presented here. An open well installed in an aquitard can take years to recover to equilibrium, and once fully recovered, the magnitude and rate of water level changes in open wells can be affected by numerous factors, not related to barometric pressure fluctuations (e.g. precipitation, loading frequency, variable formation hydraulic properties, well storage capacity) (Rojstaczer, 1988). For these reasons, 'closed' system methods are favoured for monitoring instantaneous pore pressure responses due to loading (including barometric).

A traditional method to estimate the *in situ* bulk K of an aquitard involves installing a pumping well in an adjoining aquifer (preferably under the aquitard), and installing observation wells in both the aquifer and the overlying aquitard. Then, the drawdown is monitored with time in both the aquifer and the aquitard to estimate the bulk K. In aquitards where the K is $>10^{-8}$ ms^{-1}, this method may be suitable, but for aquitards with a very low-K, the response times are too slow for this method to be applicable. For this reason, a few *in situ* methods were developed to reduce wellbore storage, resulting in quicker response times. Neuzil (1993) installed multiple pressure transducers in an argillaceous aquitard and embedded them in 3 m sand packs at the bottom of a hole before being grouted in place to both reduce the volume of water (and time) required for the pore pressure to recover, and facilitate groundwater flow around the sand pack. Roberts et al.

(2011) and Beauheim et al. (2014) used a multi-port packer with two inflatable packers to isolate a specific interval in a borehole with a downhole shut in valve that either connects or isolates the test interval from the tubing on which the test tool is suspended in the hole. Pressure transducers measure pore pressure at the bottom of the hole below the packer, in the tubing string above the test tool, and in the annulus between the tubing and the borehole above the packer. These methods are similar in that they measure pore pressure changes in an isolated portion of the borehole without the long response times, but they can be a challenge to install successfully.

Additional methods include short-term packer tests and installation of multi-packer equipment (MP system) in deep boreholes specifically developed for hydrogeologic purposes by Westbay Ltd. The short-term packer tests can be reliable for K estimates, but are most successful when pressures are stable. Following drilling and installation, short-term packer tests are vulnerable to transient pressure responses, and these induced pressures can take years to dissipate in low-K formations. In addition, thermal, chemical, and physico-chemical effects due to fluid circulation can produce some uncertainty (Distinguin and Lavanchy, 2007). The MP systems can measure the pressure and temperature at several intervals in a borehole, while also allowing water sampling/pumping from each interval, giving this method a clear advantage over any other method. However, this equipment requires that the borehole be filled with freshwater for installation, which can result in considerable disturbances due to physico-chemical processes or technological effects. Additional issues can arise from the well bore storage (large volume of the chambers), the gradient between intervals or between the intervals and the lining causing short-circuiting, and the impact of surface effects (atmospheric pressure changes affecting the inner tubing before the interval) resulting in compressibility of the system (Distinguin and Lavanchy, 2007), all of which can influence the resulting determined K.

In the laboratory, both triaxial permeameter and 1-D consolidation tests are commonly used to determine K. These tests can help provide an measurement of the matrix K of the aquitard; however, the small size of the samples make it unlikely to be a representative value of K through the formation. This is further exemplified by a comparison between the larger scale *in situ* methods (above) and regional groundwater modeling. For example, Bredehoeft (1983) compared the results of a regional groundwater model of a Cretaceous Shale Fm (Pierre Shale, 1.8×10^{-9} ms^{-1}) with laboratory results obtained from consolidation and pulse tests (10^{-14}-10^{-12} ms^{-1}). The results indicated that the modeled K of the aquitard and the laboratory K were separated

by up to five orders of magnitude. This incidence was observed again by Hart et al. (2006) in the Maquoketa Fm in the Michigan Basin, USA. Using a regional groundwater flow model (1.8×10^{-11} ms^{-1}) and laboratory tests that were up to three orders of magnitude lower. It would appear that a comparison of groundwater modeling, field *in situ* methods, and laboratory tests can reveal large scale heterogeneities in the formation (e.g. fractures).

2.2.2 Laboratory compressibility of aquitard formations

The relationship between the deflection of a sample in response to applied load was first made by Terzaghi (1923) and lead to the definition of σ'. This fundamental relationship led to the development of the oedometer experimental apparatus where changes in void ratio could be measured in response to incremental increases (or decreases) in applied effective stress. The rate of deflection during each loading increment can be used to estimate the hydraulic diffusivity (D), or as described in geotechnical engineering, the coefficient of consolidation (C_v). The changes in void ratio (e, the ratio of the volume of voids to the total volume of the soil) between loading increments can be used to estimate the coefficient of compressibility of the soil (A_v) and the constrained 1-D compressibility of the soil (m_v) which are defined as follows:

[2.6] $$A_v = \frac{\Delta e}{\Delta \sigma}, \text{ and}$$

[2.7] $$m_v = \frac{A_v}{1+e_o}$$

where e_o is the initial void ratio.

The consolidation test can be used to apply a specified stress history to the sample that parallels the natural stress history of the sample in response to sedimentation, burial by additional sediments, glacial loading or unloading. This type of loading sequence helps to define how the compressibility of the soil varies with applied stress and the loading history (e.g. loading or unloading) (Freeze and Cherry, 1979).

Consolidation tests are the most commonly used method of obtaining estimates of m_v for soils – a typical range of values for various geologic media are summarized in Table 2.1. However, the errors associated with laboratory testing discussed earlier are also relevant here. Removing a core sample from the subsurface rapidly unloads the sample from confining pressure and forces the sample to adjust to the unloaded condition prior to reloading in the oedometer test. Expansion or swelling of the sample can lead to disturbance of the soil through the formation of

microfractures or the destruction of cementation or bonding between particles. Even when the sample is reloaded to *in situ* conditions, it may no longer be representative of the formation at depth and result in an overestimation of sample compressibility.

Table 2.1: Range of compressibility values (Freeze and Cherry, 1979)

Material	Compressibility (kPa^{-1})
Clay	10^{-3}-10^{-5}
Sand	10^{-4}-10^{-6}
Gravel	10^{-5}-10^{-7}
Jointed Rock	10^{-8}-10^{-7}
Sound Rock	10^{-6}-10^{-8}
Water (β)	4.4×10^{-7}

2.3 Fully-grouted VWPs

As discussed previously, pressure transducers are traditionally installed in a high-K material (e.g. sand) and sealed directly above and below with a bentonite grout or packers to measure K in aquitard formations. These installations are arduous and time consuming and can be so problematic that the installation is unsuccessful (Mikkelsen and Green, 2003). Approximately 40 years ago, Vaughan (1969) proposed a 'fully-grouted' method wherein the pressure transducers were lowered into the borehole and grouted-in place directly within the grout, eliminating the need for a high-K material (e.g. sand pack) around the piezometer. Due to the ease of installation, several VWPs can be installed in the same borehole, and the success rate of fully-grouted VWPs is high. Provided the grout is within three orders of magnitude greater than the permeability of the surrounding soil, the error is negligible (Contreras et al. 2008). While this method was largely overlooked for decades after it was proposed, it has started to gain traction over the past 20 years. McKenna (1995) published a review of the fully-grouted method and both laboratory and field analysis that supports the reliability of the method; although he notes that more field testing with other soils and over longer periods of time is warranted. Since then, the fully-grouted method has become a fairly common occurrence in both academia and industry practice. The success of the fully-grouted method lies with the development of sensitive vibrating wire pressure transducers (VWPs) that have the ability to measure very small fluid

volume changes over short distances. VWPs use a pressure sensitive diaphragm with an attached vibrating wire element. The diaphragm is protected by a porous filter stone that allows fluid to pass through but prevents soil particles from pressing directly on the diaphragm. Pore fluid acting on the diaphragm causes deflections of the diaphragm that change the tension and frequency of the vibrating wire. These changes are transmitted to a readout device and converted to pore pressure.

2.4 The evolution of using pore pressure to determine *in situ* parameters of aquitards

The first published observations of excess pore-pressure profiles generated due to both uniform surface loading and localized surface loads were by Terzaghi and Frohlich (1936). Building off this premise, Jacob (1940), van der Kamp and Gale (1983), Rojstaczer (1988) and Rojstaczer (1989) examined pore pressure responses to natural surface loading (such as barometric pressure fluctuations). Later work by van der Kamp and Maathuis (1991) and Bardsley and Campbell (1994) focused on measuring pore pressure changes due to moisture loading. This work enabled van der Kamp and Schmidt (1997) to develop a novel method to monitor moisture balance on a scale of hectares (the piezometric weighing lysimter method) where a single pressure transducer was installed in a shallow aquitard (<35 m BG) and connected to an electronic datalogger to monitor instantaneous pore pressure responses due to surface loading. Barr (2000) applied this method to a mature boreal aspen forest in central Saskatchewan, Canada, and demonstrated the use of the piezometric weighing lysimeter method. Both studies involved aquitards composed of clay-rich glacial till with low permeability and a high compressibility, leading to loading efficiencies only slightly less than 1.0. Anochickwa et al. (2012) then employed a coupled stress-strain and seepage finite element model to analyze pore pressure responses to moisture loading events to obtain *in situ* stress-strain and hydraulic properties (hydraulic diffusivity) in shallow aquitards using fully-grouted VWPs. Smerdon et al. (2014) used numerical modeling to simulate the transient pore pressure recovery from grouted-in pressure transducers to evaluate the hydraulic diffusivity of thick Cretaceous shale aquitards in the Great Artesian Basin, Australia, although no attempt was made to evaluate the reliability of these estimates using other methods. Marefat et al. (2015) applied multiple pore pressure response methods to determine elastic properties of soft marine clays in the lowlands of Quebec (Champlain Sea clays). Most recently, Hendry et al. (in review) developed a methodology to determine γ from pore pressure using filtering and numerical regression. The technique was

successfully applied to a 'simple' site, where groundwater conditions are relatively stable, as well as a dynamic site with changing groundwater conditions and complex stress changes due to landslides. The successful application to the latter site shows that robust analysis is possible, even for dynamic and complex environments, and that the method represents a viable alternative for estimating hydrogeologic parameters of formations that are historically difficult to characterize.

A timeline from the introduction to the fully-grouted method to using pore pressure analysis of grouted-in VWPs to determine the elastic and hydraulic properties of aquitards is presented (Figure 2.2). Although unconventional in a literature review, the work presented in this thesis was included to provide context of the contribution of this material.

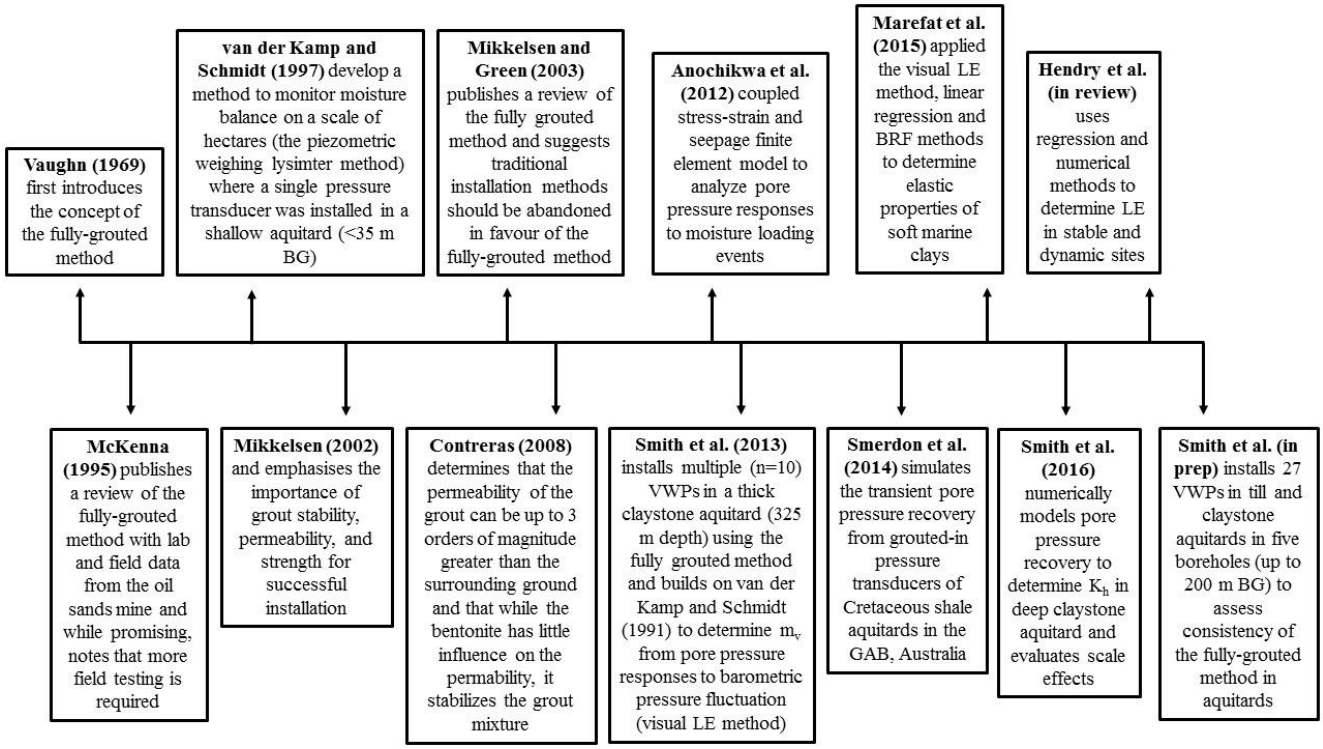

Figure 2.2: Timeline from the introduction to the fully-grouted method to using pore pressure analysis of grouted-in VWPs to determine the elastic and hydraulic properties of aquitards.

2.5 References

Anochickwa, C.I., G. van der Kamp, S. L. Barbour (2012), Interpreting pore-water pressure changes induced by water table fluctuations and mechanical loading due to soil moisture changes, Can. Geotech. J. (49) 357-366.

Bardsley, W. E. and D. I. Campbell (1994), A new method for measuring near-surface moisture budgets in hydrological systems. *J. Hydrol., 154*, 245–254.

Barr, A. G., G. van der Kamp, R. Schmidt, and A. Black (2000), Monitoring the moisture balance of a boreal aspen forest using a deep groundwater piezometer. *Agr. Forest Meteorol., 102*, 12–24.

Beauheim, R.L., R.M. Roberts, J.D. Avis (2014), Hydraulic testing of low-permeability Silurian and Ordovician strata, Michigan Basin, southwestern Ontario, *J. Hydrol*. 509, 163-178.

Bredehoeft, J. D., C. E. Neuzil, and P. D. Milly (1983), *Regional flow in the Dakota Aquifer: A study of the role of confining layers.* U.S. Geological Survey Water Supply Paper.

Bredehoeft, J.D., B.B. Hanshaw (1968), On the maintenance of anomalous fluid pressures: I, Thick sedimentary sequences, *Geol. Soc. Am. Bull*. 79(9), 1097-1106.

Clark, W.E. (1967), Computing the barometric efficiency of a well: Journal of the hydraulics division, *American Society of Civil Engineers*, 93, 93-98.

Contreras, I., A.T. Grosser, R.H. Ver Strate, 2008. The use of the fully- grouted method for piezometer installation, Part 1. *Geotech. News.* June, 2008.

Distinguin, M and J-M Lavanchy (2007), Determination of hydraulic properties of the Callovo-Oxfordian argillite at the bure site: Synthesis of the results obtained in deep boreholes using several in situ investigation techniques. *Physics and Chemistry of the Earth*, 32, 379-392.

Duncan, J. M., and A. Bursey (2013), Soil Modulus Correlations. Foundation Engineering in the Face of Uncertainty, in 2013 GeoCongress, San Diego, CA, March 3-7, 2013; pp. 321-336. doi: 10.1061/9780784412763.026

Freeze, R. A. and J. Cherry (1979), *Groundwater*, Prentice Hall, Englewood Cliffs, NJ, pp. 37, 158.

Hart, D.J., K.R. Bradbury, D.T. Feinstein (2006), The vertical hydraulic conductivity of an aquitard at two spatial scales, *Groundwater*, 44 (2), 201-211.

Hendry M.J, Kelln C.J, Wassenaar L.I (2004), Characterizing the hydrogeology of a complex clayrich aquitard system using detailed vertical profiles of the stable isotopes of water. *J. Hydrol* 293: 47-56.

Hendry, M., M.J. Hendry, L.A. Smith. Analysis of the measured pore pressure response to atmospheric pressure changes to evaluate small strain moduli: Methodology and case studies. Submitted to Geotechnique.

Jacob, C.E. (1940), On the flow of groundwater in an elastic artesian aquifer. *Trans. Am Geophys. Union*, 37, 574-586.

Marefat, V., F. Duhaime, R.P. Chapuis (2015), Pore pressure response to barometric pressure change in Champlain clay Prediction of the clay elastic properties, *Engineering Geology*, (198), 16-29.

McKenna, G. T. (1995), Grouted-in installation of peizometers in boreholes. *Can. Geotech. J.*, *32*, 355-363.

Mikkelsen, P. E. (2002), Cement-bentonite grout backfill for borehole instruments. *Geotech. News.* December 2002.

Mikkelsen, P.E., G.E. Green (2003), Piezometers in fully grouted boreholes. *Symposium on Field Measurements in Geomechanics, FMGM.* Oslo, Norway, September.

Mitchell, J. K. (2005), *Fundamentals of Soil Behavior*, 3rd edition, John Wiley & Sons, Hoboken, NJ.

Mitchell, J. K.., J.S. Younger (1967), Abnormalities in hydraulic flow through fine grained soils. Permeability and Capillary of soils, ASTM STP 417, *Am. Soc. Testing Mats.*, pp.106.

Neuzil, C. E. (1982), On conducting the modified 'slug' test in tight formations. *Water Resour. Res.*, *18* (2), 439–441.

Neuzil, C. E. (1986), Groundwater flow in low-permeability environments. *Water Resour. Res.*, *22* (8), 1163–1195.

Neuzil, C. E. (1993), Low fluid pressure within the Pierre Shale: A transient response to erosion. *Water Resour. Res., 29*, 2007–2020.

Neuzil, C. E. (1994), How permeable are clays and shales? *Water Resour. Res., 30*, 145–150.

Neuzil, C. and Pollock, D. (1983), Erosional unloading and fluid pressures in hydraulically 'tight' rocks. *J. Geo*., 91, 179-193.

Neuzil, C. E., C. Cooley, S. E. Silliman, J. D. Bredehoeft, and P. A. Hsieh (1981), A transient laboratory method for determining the hydraulic properties of "tight" rocks, 11, Application, *Int. J. Rock Mech. Min. Sci*., 18(3), 253-258.

Roberts, R., D. Chace, R. Beauheim, J. Avis (2011), Analysis of Straddle-Packer Tests in DGR boreholes. *Geofirma Engineering Ltd.* Berlin (890).

Rojstaczer, S. (1988), Determination of fluid flow properties from the response of water levels in wells to atmospheric loading. *Water Resour. Res., 24* (11), 1927–1938.

Rojstaczer, S., D. Carr Agnew (1989), The influence of formation material properties on the response of water levels in wells to Earth tides and atmospheric loading. *J. Geophys. Res., 94*, 12403-12411.

Skempton, A. W. (1954), The pore-pressure coefficients A and B. *Geotechnique, 4*, 146–147.

Smerdon, B. D., L. A. Smith, G. A. Harrington, W. P. Gardner, C. Delle Piane, and J. Sarout (2014), Estimating the hydraulic properties of an aquitard from *in situ* pore pressure measurements, Hydrogeol. J., 22(8), 1875-1887, DOI: 10.1007/s10040-014-1161-x.

Smith L. A., G. van der Kamp, and M. J. Hendry (2013), A new technique for obtaining high-resolution pore pressure records in thick claystone aquitards and its use to determine *in situ* compressibility, *Water Resour. Res*., 49, 732-743, DOI:10.1002/wcwr.20084.

Smith, L. A., S. L. Barbour, M. J. Hendry, K. Novakowski, G. van der Kamp (2016), A multiscale approach to determine hydraulic conductivity in thick claystone aquitards using field, laboratory and numerical modeling methods. *Water Resour. Res.* (DOI: 10.1002/2015WR018448).

Terzaghi, K. (1923), Die Berechnung der Durchlässigkeitsziffer des Tones aus dem Verlauf der hydrodynamischen Spannungserscheinungen. *Sitz. Akad. Wissen. Wien d. matem.-naturw.Kl., part IIa, 132*, pp. 125–138. [English translation by C. R. I. Clayton and H. Müller Seinhagen: A method of calculating the coefficient of permeability of clay from the variation of hydrodynamic stress with time. As cited in Clayton, C. R. I., H. M. Steinhagen, and W. Prowrie (1995), Terzaghi's theory of consolidation, and the discovery of effective stress. Proceedings of the Institution of Civil Engineers. *Geotech. Engin.* 113 (4), 191–205.]

Terzaghi, K. and K. O. Frohlich (1936), Theorie der Setzung von Tonshichten: eine einfuhrung in die analytische Tonmechanil, Leipzig, Franz Deuticke. [As cited in Terzaghi, K., R.B. Peck and G. Mesri (1996), Soil mechanics in egineering practice (third edition), John Wiley and Sons, New York. NY, USA.]

Terzaghi, K., R. B. Peck, and G. Mesri (1996), *Soil mechanics in engineering practice* (third ed.). New York, NY, USA: John Wiley and Sons

van der Kamp, G. and H. Maathuis (1991), Annual fluctuations of groundwater levels as a result of loading by surface moisture. *J. Hydrogeology* (127) 137-152.

van der Kamp, G. and J. E. Gale (1983), Theory of Earth tide and barometric effects in porous formations with compressible grains. *Water Resour. Res.*, *19* (2), 538–544.

van der Kamp, G. and R. Schmidt (1997), Monitoring of total soil moisture on a scale of hectares using groundwater piezometers. *Geophys. Res. Lett., 24* (6), 719–722.

van der Kamp, G. (2001), Methods for determining the in situ hydraulic conductivity of shallow aquitards - an overview. *Hydrogeol. J., 9*, 5–16.

Vaughan, P.R. (1969), A note on sealing piezometers in boreholes. *Geotechnique*, *19* (3), 405-413.

3.0 A NEW TECHNIQUE FOR OBTAINING HIGH-RESOLUTION PORE PRESSURE RECORDS IN THICK CLAYSTONE AQUITARDS AND ITS USE TO DETERMINE *IN SITU* COMPRESSIBITY

PREFACE

This chapter addresses Objective 1 of the thesis: to determine the *in situ* compressibility through argillaceous aquitards in the WB by analyzing pore pressure responses from grouted-in vibrating wire pressure transducers. The transducers at this site were the first to be installed at a depth exceeding 50 m to determine if surface loading was detectable at depth (up to 325 m BG). The pore pressure from these transducers were analyzed in conjunction with barometric pressure to determine high-resolution depth profiles of loading efficiency, compressibility, and specific storage through a thick (400 m) claystone aquitard, and provided the necessary parameters to progress to Objective 2.

The chapter is reproduced with permission from: Smith L. A., G. van der Kamp, and M. J. Hendry (2013), A new technique for obtaining high-resolution pore pressure records in thick claystone aquitards and its use to determine *in situ* compressibility, *Water Resourses Research*, 49, 732-743, DOI:10.1002/wcwr.20084. 0043-1397/13/10.1002/wrcr.20084. Minor editorial and formatting changes have been made to accommodate reproduction in this thesis.

In addition to the editorial and formatting changes, a few significant changes were made to this manuscript since publication, and are listed below:

1) The 1-D constrained compressibility was reported by the symbol α in the published manuscript. During the process of writing manuscript 2 (Chapter 4), this parameter was changed to the co-efficient of volume compressibility, m_v (equivalent to 1-D compressibility, α), while α was used to represent bulk compressibility. For consistency purposes throughout the thesis, all references to α in Chapter 3 were changed to m_v, and Equation 3.4 was added to this chapter to relate m_v to α.
2) Prior to publication of this chapter, there was some speculation that the deepest three transducers (A, B, and C) were mislabeled due to the resulting hydraulic head profiles, and a questionable labeling practice during installation. After publication, analysis of the transducer temperature profiles confirmed that these three transducers were mislabeled.

In this chapter, the transducers were re-labeled correctly (transducer A is now transducer C, transducer B is now transducer A, and transducer C is now transducer B). These changes have no significant impact on the interpretation discussed in the published manuscript, but Figures 3.5 and 3.7 and Table 3.1 were updated in this chapter to address transducer re-order.

3) Values of S_S in Table 3.1 and illustrated in Figure 3.5 were calculated from bulk compressibility (α) using an assumed Poisson's ratio of 0.33. In the published manuscript, S_S was calculated using m_v.
4) Uncertainty in the m_v value was estimated based on the relative uncertainty of γ and propagated to S_S. These uncertainties are illustrated by error bars in Figure 3.5. A detailed description of the method is presented in Appendix A.

3.1 SUMMARY

Laboratory tests are commonly used to determine properties (1-D constrained compressibility, m_v; bulk compressibility, α; specific storage, S_S; vertical hydraulic conductivity, K_v) of claystone aquitards; however, whether data representative of *in situ* conditions can be obtained from disturbed samples is questionable. Here, we present a method to determine the *in situ* m_v and S_S of a thick sequence of Cretaceous aged claystone by estimating the loading efficiency (γ) of a formation from pore pressure responses to barometric pressure fluctuations. We installed 10 vibrating wire pressure transducers at different depths (25 to 325 m below ground, BG) in a thick claystone aquitard by placing them directly within the cement-bentonite grout. Two years of continuous transducer records using this method appeared to provide pore pressure data with a resolution of better than one part in 10^5, equivalent to mm of hydraulic head change. Pore pressure responses to barometric pressure changes, earth tides and precipitation events can be clearly identified and the barometric responses can be easily analyzed. The resulting values of γ (0.6 to 0.93), m_v (2.5×10^{-7} to 2.2×10^{-6} kPa^{-1}), and S_S (2.6×10^{-5} to 4.5×10^{-6} m^{-1}) all decrease with depth. The results are comparable with the limited existing data for *in situ* estimates of S_S and are as much as an order of magnitude smaller than laboratory estimates of S_S for similar aquitard deposits. Our findings suggest that the fully-grouted transducer method can provide an accurate and reliable means to monitor pore pressure changes and to determine *in situ* parameters for bedrock aquitard systems.

3.2 INTRODUCTION

Clay-rich deposits (argillaceous aquitards) with low hydraulic conductivity ($K \leq 10^{-8}$ m s^{-1}) control recharge and contaminant transport to adjacent aquifers (Cherry and Parker, 2004), can serve as host formations for sequestration of hazardous wastes, and can act as isolating units to protect shallow groundwater from contamination by fluids and gases injected into deeper formations. Accurate determinations of hydrogeologic properties of aquitard formations are important to determine the hydraulic diffusivity and flow system response times through aquitards and their impact on adjoining aquifers. Furthermore, the compressibility and specific storage of aquitard formations can influence water yield to adjoining aquifers, subsidence resulting from fluid extraction, and propagation of stress changes.

Historically, researchers have generally relied on laboratory tests to determine elastic properties in low-K material (Neuman and Witherspoon, 1972; Keller et al., 1986, 1989; Shaver, 1997). However, whether data representative of *in* situ conditions can be obtained from disturbed samples is questionable due to unavoidable stress changes during sample collection (Clark, 1998) and resulting damage to the sample, and incomplete re-saturation or chemical effects from introduced water (Clayton, et al., 1982). The release of stress experienced by an overconsolidated sample as it is removed from the subsurface allows the material to re-equilibrate at surface pressure. If there is no damage to the sample, the effects of stress change can be reversed by re-loading the sample; however, stress changes combined with structural disturbances during sampling, can increase the compressibility of the material (Klohn, 1965; Radhakrishna and Klym, 1974). Subsequent analyses often underestimate the relative stiffness of the sample and lead to estimates of the values of vertical compressibility (m_v) and consequently of specific storage (S_S) greater than values that are representative of *in situ* conditions (Grisak and Cherry, 1975; van der Kamp and Schmidt, 1997; van der Kamp, 2001). Further, using laboratory determined parameters (m_v and S_S) to estimate vertical hydraulic conductivity (K_v) from field-determined hydraulic diffusivity K_v/S_S can yield over-estimates of K_v not representative of *in situ* conditions. Therefore, determining the hydrogeologic properties (m_v and S_S) of a claystone aquitard using *in situ* methods is preferable to estimates based on laboratory testing (van der Kamp, 2001).

A field method that can be used to determine the *in situ* elastic properties of a formation is monitoring the pore pressure response to surface loading (van der Kamp and Schmidt, 1997;

Barr et al., 2000). Atmospheric pressure changes are known to cause pore pressure fluctuations in aquifers (Rojstacer and Agnew, 1989; Bardsley and Campbell, 1994, 2007; Sophocleous et al., 2006) and aquitard formations (van der Kamp and Schmidt, 1997; Barr et al., 2000; Anochikwa et al., 2012). In both cases, sensitive pressure transducers coupled with electronic dataloggers are used to monitor instantaneous pore pressure responses to surface loading. Generally, aquitards are considered more suitable than aquifers for studying pore pressure responses because they are more hydraulically isolated from changing groundwater flow conditions (Rojstaczer, 1988; van der Kamp and Schmidt, 1997). However, the very low permeability of some aquitards presents a challenge with respect to installing instrumentation that is responsive with no significant time lag to pore pressure changes (Neuzil, 1993).

The objectives of our study were to determine if the *in situ* values of m_v and S_S through a thick claystone aquitard sequence could be determined by analyzing pore pressure responses to atmospheric pressure changes. We used several vibrating wire pressure transducers (VWPs) emplaced in a fully-grouted borehole without a permeable surround, such as a sandpack, around the transducers. While previous work focuses primarily on relatively shallow (<50 m BG) systems, to our knowledge, no other studies have used multiple pressure transducers through a deep (>75m BG) claystone aquitard of low-K to measure small natural variations of pore pressure, including responses to atmospheric pressure variations, and analyze these data to produce estimates of *in situ* m_v and S_S with increasing depth. The intrinsic difficulty in determining *in situ* parameters of low-K material makes this method particularly useful and potentially more reliable than current practices. The ability to determine accurate *in situ* S_S of such low-K formations at depth would provide a better understanding of transient leakage to aquifers (Konikow and Neuzil, 2007). High-resolution measurements of pore pressure changes within low-K formations can also contribute to characterizing and understanding the nature and origin of pressure anomalies.

3.3 THEORY

In a saturated profile, an applied surface load is shared by the porewater and the porous matrix of a formation. The applied load produces an instantaneous change in porewater pressure at depth (referred to as excess pore pressure) (Terzaghi and Frohlich, 1936; Jacob, 1940;

Skempton, 1954), and the difference between the total stress and the pore pressure is the effective stress, σ', assuming grains are incompressible (Terzaghi, 1923, van der Kamp and Gale, 1983):

[3.1] $$\sigma = \sigma' + p,$$

where σ is the total stress ($MT^{-2}L^{-1}$) and p is the pore pressure ($MT^{-2}L^{-1}$).

The same principle applies to atmospheric loading, wherein a portion of the barometric pressure transmitted through the underlying aquitard will be borne by the porewater and the remainder by the aquitard skeleton (Terzaghi, 1923; Anochikwa et al., 2012). The ratio of the pore pressure response to the applied load is known as loading efficiency (γ), (Skempton, 1954) and is related to soil and water compressibility by:

[3.2] $$\gamma = \frac{m_v}{n\beta + m_v}$$

where m_v is the 1-D constrained compressibility of the formation, β is the compressibility of water (4.6×10^{-7} kPa^{-1} at 20°C) and *n* is the porosity of the formation.

When the pore water is much less compressible than the formation structure, the pore water will essentially bear the full loading pressures, resulting in a value of γ only slightly less than 1. Typically, shallow clay-rich aquitards are much more compressible than water. However, for stiff, overconsolidated formations with m_v similar to water (β), the value of γ can be well below 1 and provide a means to estimate the m_v of the formation (Bishop, 1973; van der Kamp and Gale, 1983; Terzaghi et al., 1996; Anochikwa, 2012).

The magnitude of γ also depends on the degree of saturation, (Skempton, 1954; Bishop, 1973; Black and Lee, 1973; Terzaghi et al., 1996). Therefore, the magnitude of the pore pressure response depends only on the m_v and *n* of the aquitard under the assumption of full saturation. If γ can be determined from the measured response to barometric pressure changes, then m_v can be determined using:

[3.3] $$m_v = \frac{\gamma n\beta}{1-\gamma},$$

The value of m_v can be converted to a constrained modulus ($M=1/m_v$) and then to a bulk modulus (B) if a Poisson's Ratio is assumed, and using the following relationship (Duncan and Bursey, 2013):

[3.4] $$B = \frac{M}{3}\frac{(1+\nu)}{(1-\nu)}$$

where ν is Poisson's ratio. The inverse of B is bulk compressibility (α, kPa^{-1}). Specific storage (S_S) was then calculated using:

[3.5] $$S_S = \rho g(n\beta + \alpha)$$

where ρg is the unit weight of water (9.8 kN m^{-3}) and assuming a value for Poisson's ratio.

Earth tides can also cause pore pressure fluctuations by deforming the porous skeleton (Agnew, 2007, Toll and Rasmussen, 2007). The relationship between earth tide strain and water level responses to determine the hydrogeologic properties of an aquifer has been studied extensively (Bredehoeft, 1967; van der Kamp and Gale, 1983; Hsieh et al., 1987; Rojstaczer and Agnew, 1989; Toll and Rasmussen, 2007). S_S can in principle be determined from the earth tide response. However, the calculation requires an accurate value for the *in situ* Poisson's Ratio of the formation, which is generally not known, and the actual earth tide strain near the earth's surface may differ significantly in amplitude and phase from the theoretical strain (Cutillo and Bredehoeft, 2011). In consequence, values of S_S calculated from earth tide responses tend to be subject to large uncertainties.

3.4 HYDROGEOLOGIC SETTING

The Williston Basin underlies approximately 250,000 km^2 of North Dakota, South Dakota, and Montana, USA and Manitoba and Saskatchewan, Canada. Sedimentary thickness reaches approximately 5,000 m at the center of the basin (Vigrass, 2006); and repeated transgression and regression during the Upper Cretaceous resulted in a thick sequence of clay-rich deposits across central Saskatchewan (Hayes et al., 1996). The Cretaceous claystone in the Williston Basin experienced considerably thicker overlying sediment than currently present (1 to 3 km of Upper Cretaceous shales and Tertiary sediment). This overlying sediment eroded in the middle to late Tertiary and left the underlying formations over-consolidated, resulting in a regional unconformity with the Quaternary glacial deposits above the claystone (Nurkowski, 1984; Bustin, 1992; Dawson et al., 2008).

3.4.1 Location of Study Site

Our study was conducted 1 km west of the Mosaic Esterhazy K2 mine site in Saskatchewan, Canada (Figure 3.1). Selection of the site was based on several factors. First, the

claystone aquitard is part of a low-K stratum extending more than 2000 km from northwest New Mexico into Alberta and Saskatchewan (Garavito et al., 2007). Second, laboratory-determined hydraulic properties (K_v, m_v, S_S) of the aquitard have been reported in previous works (Bredehoeft et al., 1983; Corbet and Bethke, 1992; Neuzil, 1982, 1993, and 1994) and can be compared to the results of our study. Third, the claystone at this location is closer to ground surface than at other locations in the Western Sedimentary Basin in Canada, thereby somewhat reducing the cost and difficulty of drilling and installing the transducers. The ground surface elevation at the site is estimated to be 510.3 m asl. Eight open piezometers installed by Mosaic at shallow depths in the surficial till within a 1 km radius of the borehole indicate that the water table fluctuates between less than one to three m BG.

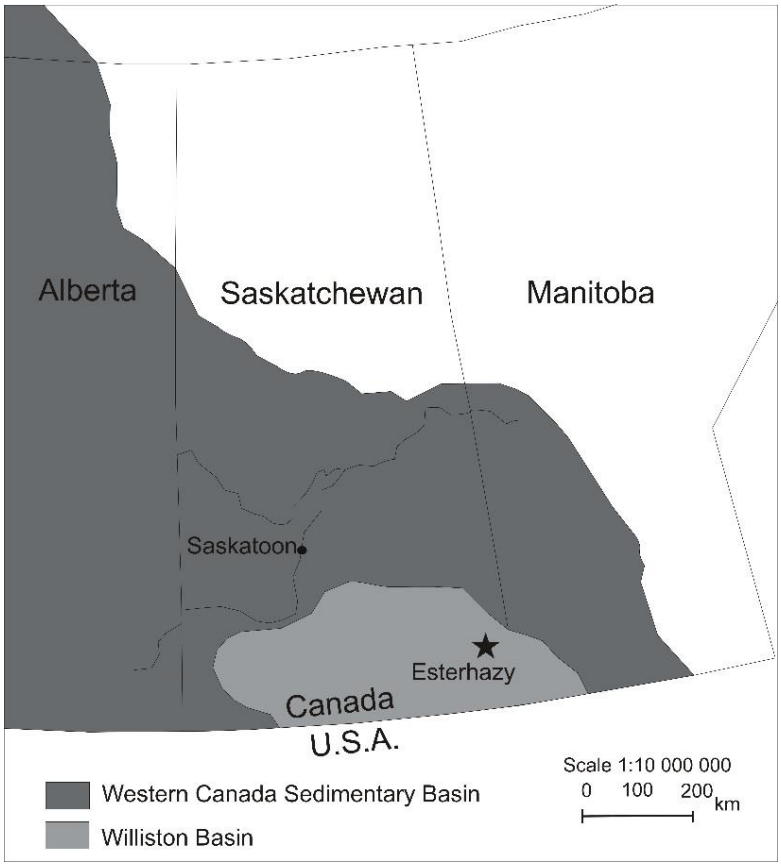

Figure 3.1: Map of west-central Canada showing the location of the borehole (star) in the Williston Basin (N5617477.62 E295357.89).

3.5 MATERIALS AND METHODS

3.5.1 Drilling and Installation of Transducers

Drilling and instrument installation was carried out in October 2009. A Failing CF-15 Top Drive rotary drill rig was used to drill through the Saskatoon Group Till (Floral and Battleford Formation; 11 m), the Pierre Shale Formation (173 m), the 1st (72 m) and 2nd Speckled Shale (25 m) Formations, and 42 m into the Belle Fourche Formation (Figure 3.2). Drilling was terminated at 323 m BG after the drill rig encountered a hard (concretion) layer located approximately 70 m above the Lower Cretaceous Mannville Formation (based on geologic logs from the K2 potash mine), which was the intended base of exploration.

Once the drill stem was removed from the 140 mm diameter borehole, 10 vibrating wire transducers (Geokon; model 4500S; ranges: -0.1 to 0.35, 0.7, 1, 2, 3 MPa, with absolute accuracy of ± 0.1% of Full Scale (F.S.) and resolution of ± 0.025% of F.S.) were installed at depths of 25 (J), 49 (I), 75 (H), 125 (G), 175 (F), 185 (E), 225 (D), 255 (C), 275 (B), and 325 (A) m BG (Figure 3.2). The transducers measure absolute fluid pressure. Depths for installation were selected based on the geological and geophysical logs and the proximity to formation contacts. Each transducer was wrapped in a lightweight non-woven geotextile fabric, fixed to the outside of a 25.40 mm OD steel tremie pipe, and lowered into the borehole. Once in place, a 4% bentonite - 96% cement grout mixture was pumped down the pipe until it returned to surface, indicating the entire hole was filled with grout and the transducers were secured in place. Samples of the grout were taken every 10 batches mixed (1 batch = two 80 kg bags of cement), with each sample collected in a 1 L glass jar, allowed to set, and then stored at room temperature (21°C) until analysis for consolidation testing and K_v testing. The grout mixture was prepared following guidelines provided by the Saskatchewan Potash Producers Association (SPPA) for groundwater monitoring at potash mine sites in Saskatchewan (SRC, 1994). The properties of both the grout and surrounding shale need to be considered for appropriate installation and are discussed further in §3.7.

Once in place, the transducers were immediately connected to an automated data acquisition system (Argus Monitoring Software, Version: 2.6.0.1) and programmed to measure pressure and temperature (T) every 30 min. A 3001 LT Solinst barologger (accuracy of ± 0.05% F.S. and resolution of 0.002% F.S.) was installed at ground surface (510.3 m asl) to measure barometric changes at surface every 30 min with the same time-stamp as the transducers.

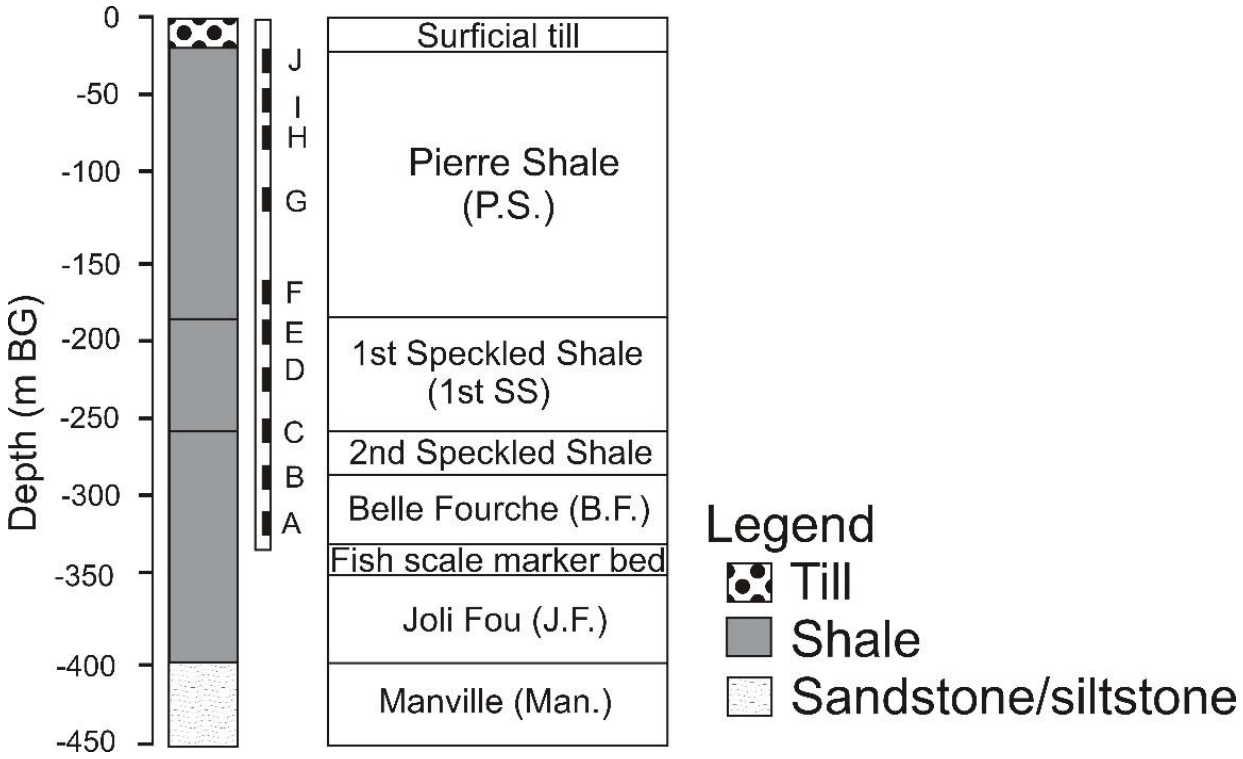

Figure 3.2: Stratigraphy of the borehole based on geological and geophysical logging. The completion depths of the 10 transducers (A to J) are presented relative to the stratigraphy.

3.5.2 Evaluation of Barometric Response in Pore-pressure Data

Porewater pressure responses to fluctuations in atmospheric pressure are well established: open stand pipe piezometers respond inversely to barometric fluctuations while shut-in (sealed, non-vented) piezometers respond directly. For a laterally homogenous formation, horizontal displacement due to atmospheric pressure change is negligible, and the stress change acting on the claystone aquitard will be essentially vertical and equal to the atmospheric pressure change at ground surface (van der Kamp and Gale, 1983). As an independent check of proper transducer function, the pore-water pressure should increase and decrease with atmospheric pressure changes to some degree, depending on γ of the formation.

For porewater pressure records obtained by means of absolute pressure transducers, such as the ones used in this study, barometric pressure effects are typically removed from porewater records in two steps. First the porewater absolute pressure records are converted to "gauge pressure" by subtracting the atmospheric pressure (B_0) at the site of the time of installation (T=0) (ie. the transducers are "zeroed" at surface before installation). The atmospheric pressure changes are then removed using a formula (dictated by the instrument used) to subtract the

change in barometric pressure B-B_0 (where B_0 and B are the barometric pressures at T=0 and at all times after T=0, respectively) from the porewater pressure. This method requires two assumptions: 1) the barometric pressure at T=0 is representative of the average barometric pressure at site, and 2) the γ is consistently 1 (i.e., the water bears 100% of the applied load), regardless of formation geology.

For this study, the load associated with atmospheric pressure changes (P_a) was removed from the porewater records following the method described by van der Kamp and Schmidt (1997) and Barr et al. (2000), which avoids the assumptions mentioned above. The first assumption was addressed by taking the time average of all the barometric pressure measurements and replacing B_0 with the resulting value (B_{ave}). B_0 is representative of the pressure system moving through the area at the time of installation, while B_{ave} is representative of the barometric pressure at this site for the duration of data collection. It is important to note that regardless of the barometric pressure datum chosen (either B_0 or B); the resulting γ will not change as we are looking at the pore pressure response to barometric pressure fluctuation at concurrent time intervals. It can, however, have a marked effect on the resulting corrected pressure head (up to 0.62 m in this study).

The second assumption was evaluated by determining the γ at the depth of each transducer. The instantaneous pore-pressure response to barometric pressure changes (which are measured and logged simultaneously) provides a means to assess how much the pore pressure varied with a known applied load. Therefore, to determine the γ at the location of each transducer, the change in barometric pressure (B-B_{ave}) was systematically multiplied by a number varying between 0 and 1.0 (γ) and subtracted from the raw porewater pressure data, already adjusted to gauge pressure, with the same time-stamp. The resulting trends were superimposed to visually determine the γ that is judged to produce the 'smoothest' corrected pressure record with the least variation between precipitation events. The equation used for the barometric correction can be written as follows:

[3.6] $$p* = [p_t - B_{ave}] - \gamma\,(B - B_{ave})$$

where p* is the corrected porewater pressure, and p_t is the uncorrected absolute pore pressure. This methodology has been used to estimate *in situ* γ, resulting in estimates for *in situ* m_v and S_S (van der Kamp and Schmidt, 1997; Barr et al., 2000) using Equations 3.3 and 3.4 (Table 3.1).

More rigorous methods of analysis are available and have been used for analysis of barometric responses (e.g. Cutillo and Bredehoeft, 2011; Butler et al., 2011). The results of such analyses are influenced to an unknown extent by other poorly characterized pressure transients, such as those due to moisture loading at the ground surface caused by precipitation, evapotranspiration and lateral flows. Such effects were identified in the records for the grouted-in transducers and therefore the simple analysis using visual judgment was preferred for the present case.

Pore pressure fluctuations due to earth tides appear in the pore pressure records, with maximum changes varying from 1 mm for the shallowest transducer to about 10 mm for the deepest one. Earth tide gravitational acceleration was computed using TSOFT software for the location of the borehole using the latitude, longitude, elevation and the same timestamp as the barometer and pressure transducers. The earth tide response was removed from the pore pressure record by determining a multiplication factor that smoothes the pore pressure trends, similar to the process of determining γ from barometric changes. This correction was successful in reducing the amplitude of the earth tide effects; however, it did not completely remove the earth tides in most cases, indicating that the observed earth tide fluctuations differed in phase from the theoretical (and approximate) gravity tide. The deviation of earth tide responses from the theoretical expectations precludes straightforward analysis for comparison with the observed barometric responses. While it is certainly possible to perform rigorous mathematical corrections to better characterize the earth tide signals (e.g. Cutillo and Bredehoeft, 2011), analysis of earth tide responses would not give a fully independent values for S_S as the calculation depends on an assumed value for Poisson's Ratio of the formation near each transducer. Therefore, the earth tide responses are not further dealt with since the results of the analysis cannot be compared directly with the results of the barometric analysis and would not contribute significantly to the objectives of this paper.

Table 3.1: Summary of calculated properties at the location of each transducer using the loading efficiency method

Transducer	Depth (m BG)	γ	m_v (kPa^{-1})	Ss* (m^{-1})	Porosity (*n*)
A (Belle Fourche Fm.)	325	0.60	2.5×10^{-7}	5.4×10^{-6}	0.36
B (2^{nd} Speckled Shale Fm.)	275	0.72	3.6×10^{-7}	6.7×10^{-6}	0.30
C (2^{nd} Speckled Shale Fm.)	255	0.70	3.2×10^{-7}	6.1×10^{-6}	0.30
D (1^{st} Speckled Shale Fm.)	225	0.70	3.3×10^{-7}	6.3×10^{-6}	0.31
E (1^{st} Speckled Shale Fm.)	185	0.72	4.1×10^{-7}	7.7×10^{-6}	0.35
F (Pierre Fm.)	175	0.80	6.4×10^{-7}	1.1×10^{-5}	0.35
G (Pierre Fm.)	125	0.84	8.2×10^{-7}	1.4×10^{-5}	0.34
H (Pierre Fm.)	75	0.87	9.5×10^{-7}	1.5×10^{-5}	0.31
I (Pierre Fm.)	49	0.92	2.4×10^{-6}	3.9×10^{-5}	0.45
J (Pierre Fm.)	25	0.93	2.2×10^{-6}	3.4×10^{-5}	0.36

* Calculated using α where an assumed value of Poisson's ratio was used (0.33)

3.5.3 Laboratory Testing

3.5.3.1 1-D Consolidation Testing

Standard oedometer tests in accordance with ASTM D2435-04 (ASTM, 2011) were conducted on individual samples from depths of 47.4, 87, and 128.4 m (Pierre Shale), 174.1, 184.9, 212 and 249 m (1^{st} Speckled Shale), 283.6 (2^{nd} Speckled Shale) and 307 m (Belle Fourche Shale) to compare with the m_v determined using the γ correction method described above (Section 4.2). After collection, the samples were immediately vacuum sealed at site and stored at 12°C prior to analysis. Each specimen was 63.3 to 63.5 mm in diameter and 12.5 to 13 mm in height. Incremental loading stages (n=13) lasting 10-12 hr were applied to each specimen, increasing from approximately 0.06 to 31 MPa. The same oedometer test was conducted on a sample of grout collected at site during the installation of the transducers from grout batch 24 (approximate depth of 140 m). Incremental loading stages (n=13) for the grout sample ranged from 0.01 to 5 MPa. Total porosity was determined using the calculated dry bulk density using

the method outlined in ASTM D 4531-86 (ASTM, 2008) and specific gravity of samples obtained every 10 m through the entire borehole (n=33).

[3.7] $$\text{Porosity } (n_T) = \left(1 - \frac{\rho_d}{\text{Sp.gr.}}\right) * 100$$

Where ρ_d is dry bulk density (m/cc) and sp.gr. (kg/m^3) is specific gravity.

3.5.3.2 Triaxial Permeameters for K_v

The K_v of core samples (n=10) recovered from the Cretaceous aquitard were determined using a fixed wall triaxial system in the laboratory of MDH Engineered Solutions, Saskatoon. Samples were taken from the Pierre Shale (20, 74, 111 m BG), the 1st Speckled Shale (207 and 257 m BG), the 2nd Speckled Shale (278 m BG), and the Belle Fourche Fm (311 m BG). Once the core was brought to surface, samples were trimmed of any drill mud, then wrapped in cellophane wrap and masking tape before being coated repeatedly (5-6 times) in paraffin wax. Samples were stored between 10 and 15°C until analysis. Once in the lab, core samples were trimmed to achieve a height of approximately 25 mm and a core diameter of approximately 74 mm before being placed in a clear plastic casing in the triaxial apparatus. The pressure difference across the sample was kept constant at 15.8 kPa for all samples resulting in a gradient between 50 and 90 m/m, depending on the sample. Average back pressure and effective confining pressure were both maintained at 200 kPa. Samples of the grout used to fill the borehole were collected during grouting of the borehole and samples corresponding to the approximate depths of 46, 182 and 317 ±10 m BG were selected for laboratory determination of K_v using the same method described above.

3.6 RESULTS AND DISCUSSION

3.6.1 Loading Efficiency and Compressibility

Values for γ were determined from pore-pressure responses to barometric pressure changes using the methods described above (Figure 3.3 and 3.4). The results show that loading efficiencies decrease with depth, suggesting that the porous matrix becomes increasingly less compressible with increasing depth (Table 3.1, Figure 3.5). While the general trend of γ decreased with depth (Figure 5a), at 325 m BG (location of transducer A) the determined γ was unexpectedly low (0.60) compared with the γ determined for depths of 255 and 275 m BG (transducers C and B, respectively). This particular measurement might be an outlier, indicating

the transducer was not functioning properly; however, more likely is that transducer A was simply installed at a depth where the claystone has a very low compressibility. This may also signify the possibility of formation heterogeneity, implying that the estimates of m_v and S_S are representative of the localized area, and not the entire formation as a whole.

The m_v and S_S of the aquitard at the locations of each transducer were calculated using Equations 3.3 and 3.4. Uncertainty in the m_v value was estimated based on the relative uncertainty of γ (assumed to be ~0.02) and propagated to S_S. These uncertainties are illustrated by error bars in Figure 3.5. A detailed description of the method is presented in Appendix A. The transducers installed below the Pierre Shale (A, B, C, D, and E) yield m_v estimates comparable to the compressibility of water (4.7×10^{-7} kPa^{-1}). Compressibility was also determined from the rebound portion of the compression-rebound curve obtained from the laboratory consolidation (oedometer) tests (Figure 3.5). Compressibility was determined to be between 2.5×10^{-5} and 1.7×10^{-6} kPa^{-1} and comparable to those reported by Corbet and Bethke (1992) and Neuzil (1982), who used porosity versus effective stress relationships to estimate the vertical m_v for Pierre Formation and Colorado claystone (subunits of the Colorado Group include the 1st and 2nd Speckled Shale in southern SK) to be between 8.5×10^{-6} and 3.1×10^{-5} kPa^{-1}. Compressibility could not be accurately determined for the 307 m BG sample using the oedometer tests because the total deflection was too small to be reliably measured. During the rebound portion of the oedometer test, the e of the sample continued to decrease rather than increase while stress was being released, indicating the oedometer test was not an appropriate test to determine compressibility or specific storage of this particular sample. The *n* of the Cretaceous shale through the aquitard sequence (0.33 ± 0.05) is greater than expected based on reports for overconsolidated shale in the literature ($n = 0.10 – 0.20$) (Freeze and Cherry, 1979), yet is consistent with previous reports for *n* of the Pierre Shale (Nichols et al., 1985; Neuzil, 1993).

Our *in situ* estimates for m_v using the γ method range from 2.5×10^{-7} (325 m BG) to 2.2×10^{-6} kPa^{-1} (25 m BG), as much as one order of magnitude less than previously published estimates and our laboratory values, depending on the depth of the samples and transducer placement (Figure 3.5). Earlier, we state that the γ determined for the depth where transducer A is installed (325 m BG) is low (0.60), indicating the claystone has a very low compressibility at this depth. The oedometer results for the claystone sample collected at 307 m BG (only 18 m

from transducer A) support this conclusion. The m_v of the grout was determined to be 1.2×10^{-5} kPa^{-1} (Figure 3.5).

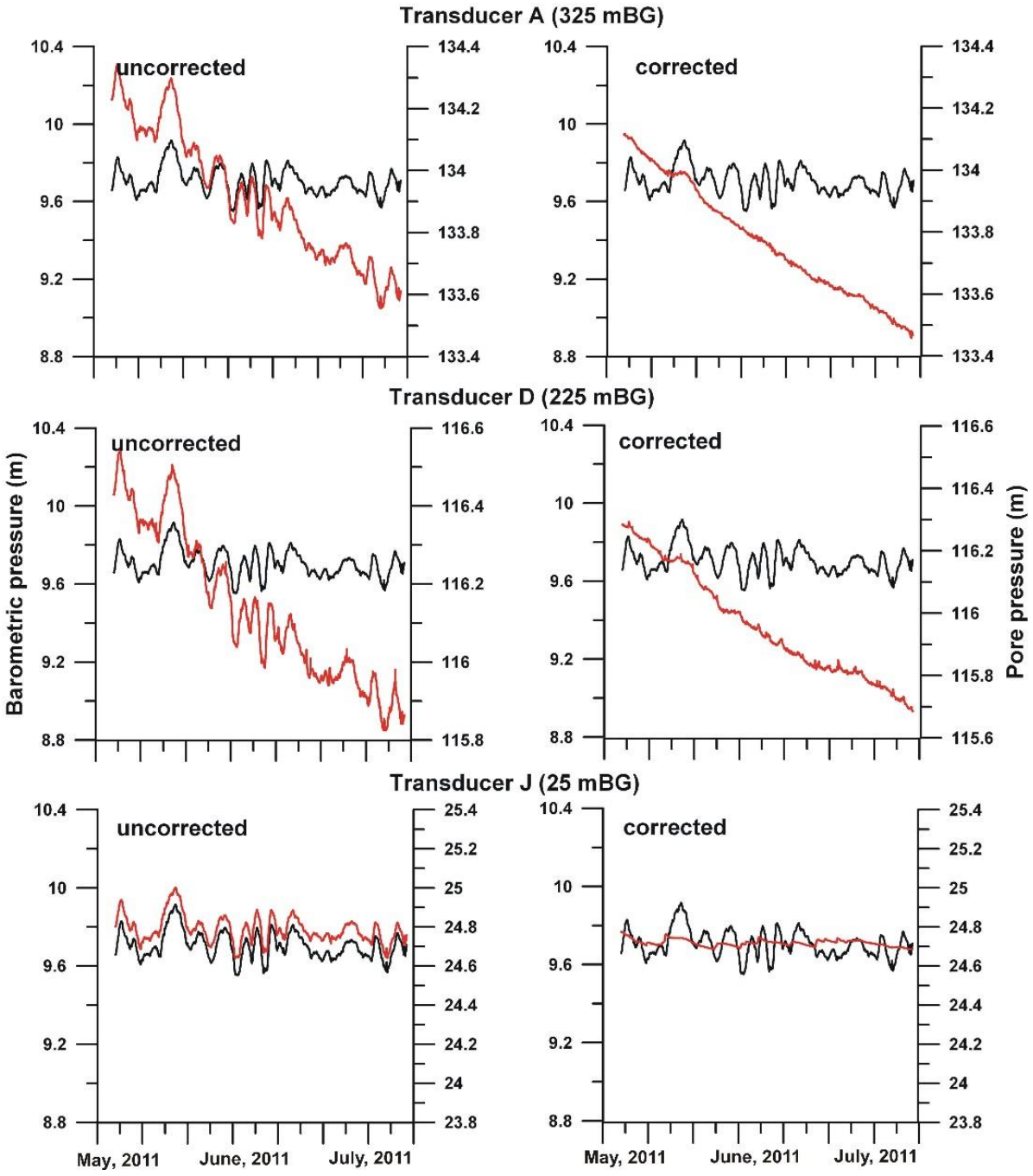

Figure 3.3: Pore pressure (—) from representative transducers A, D, and J, before and after the application of the barometric correction. The response to barometric pressure (—) in the uncorrected graphs provides confidence that the transducers are functioning properly. Pressure are reported as m of water equivalent.

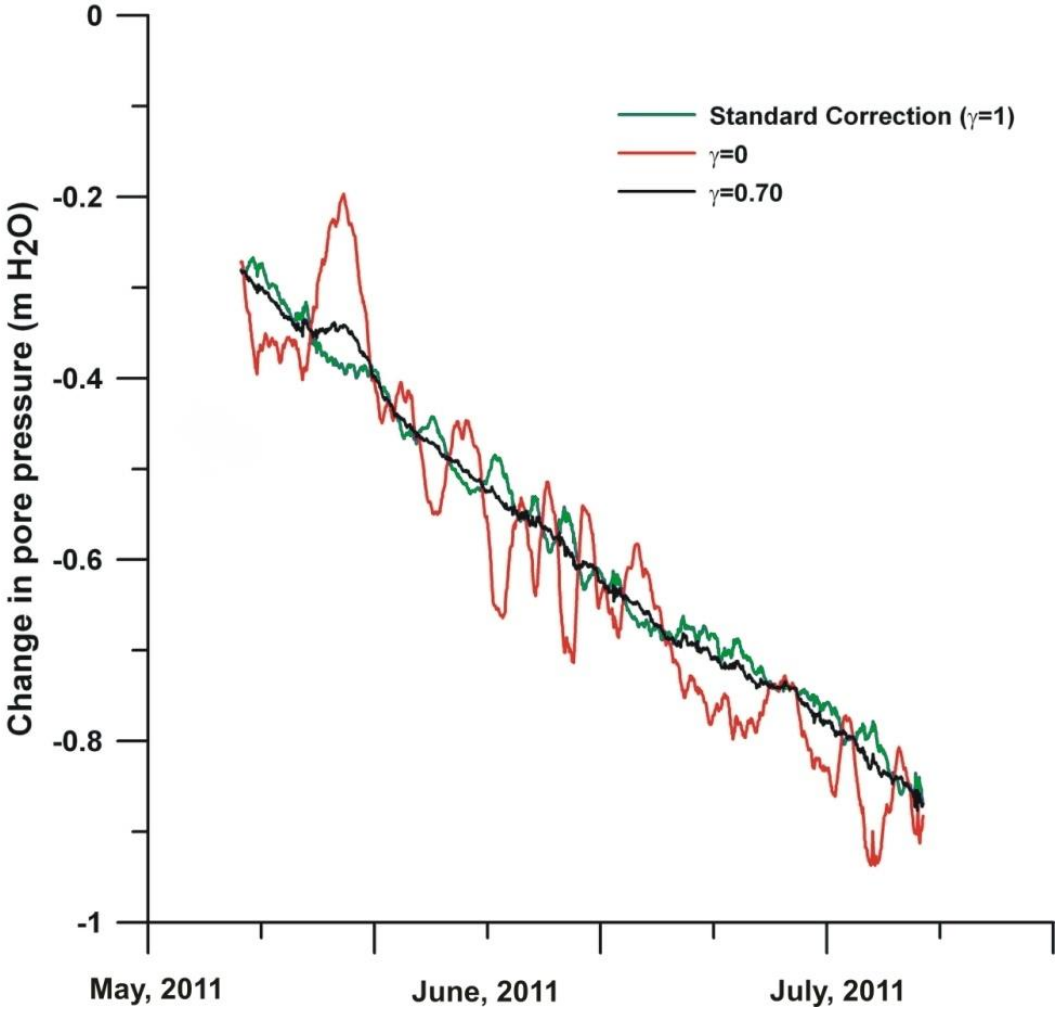

Figure 3.4: Comparison of no correction (γ=0), standard correction (γ=1), and the visual best fit (γ =0.70) for transducer A (325 m BG). Data presented as change in pore pressure relative to average pore pressure.

3.6.2 Specific Storage

Specific storage can be calculated using both field and laboratory methods and the literature contains S_S estimates for low K_v material using both approaches (Table 3.2). S_S values determined using pressure transducers in this study (γ method) were comparable to estimates determined using other *in situ* methods (pump tests and numerical modeling) for other clay aquitards (typically 10^{-5} to 10^{-6} m^{-1}), but were consistently lower than estimates based on laboratory methods (typically 10^{-4} m^{-1}). The S_S values calculated from the m_v determined from the oedometer tests in this study were compared with the S_S values calculated from the γ method.

Laboratory estimates from depths corresponding to the transducers are in all cases greater than the S_S estimated using the γ method.

Table 3.2: Laboratory and *in situ* determinations of specific storage for argillaceous tills and shale.

Study	**Method**	**Material**	**Specific storage (m^{-1})**
Grisak and Cherry (1975)	Pump tests and numerical modeling Laboratory tests	Clay loam till	$1.5– 3.1\times10^{-5}$ 1.1×10^{-2}
Neuman and Witherspoon (1972)	Laboratory tests	Clay aquitard	$7.9\times10^{-4} – 3.3\times10^{-6}$
Keller et al. (1986) *Keller et al.* (1989) *van der Kamp and Schmidt* (1997)	Laboratory tests Laboratory tests γ method	Glacial till Glacial till Glacial till	$1.2 – 3.1\times10^{-4}$ $2.1 – 3.3\times10^{-4}$ 1.8×10^{-5}
Riley (1970)	Borehole extensometer data	Clay aquitard	9.3×10^{-6}
Shaver (1997)	Laboratory tests	Glacial till (North Dakota)	$2.0\times10^{-4} – 1.1\times10^{-3}$
Konikow and Neuzil (2007)	Regional groundwater model	Claystone Aquitard (Pierre shale)	1.6×10^{-4}
Current study	γ method Laboratory tests	Claystone aquitard	$4.1\times10^{-6} – 2.6\times10^{-5}$ $1.7\times10^{-5}– 2.4\times10^{-4}$

Konikow and Neuzil (2007) compiled data for normally consolidated and overconsolidated argillaceous confining layers by plotting S_S versus *n* using results from multiple studies and predominantly from laboratory testing (Figure 3.6). According to their results, the primary consideration for estimating S_S is determining if the confining layer is overconsolidated or normally consolidated. Overconsolidated formations are frequently thought to be in the elastic deformation range, while normally consolidated formations are considered to be in the plastic deformation range. Typically, compressibilities and S_S values in the elastic range are smaller than those in the plastic range (Konikow and Neuzil, 2007). The Cretaceous shales in the Williston Basin experienced considerably thicker overburden in the past and are commonly

referred to as overconsolidated. However, Konikow and Neuzil (2007) provide an estimate of S_S for the Pierre Shale of 1.6×10^{-4} m^{-1}; which falls into the normally consolidated area of Figure 3.6, despite the fact that the Cretaceous shales are overconsolidated. The apparent disparity is thought to be due to unusually high smectite content, causing the Pierre Shale to deform viscoelastically. Interestingly, the average S_S of the Pierre Shale determined using laboratory methods in this study produce a value consistent with Konikow and Neuzil (2007), of 1.0×10^{-4} m^{-1}. In fact, all the S_S values determined using laboratory tests fit well within the range between consolidated and overconsolidated, suggesting Konikow and Neuzil (2007) have identified a fitting relationship between *n* and S_S when the S_S is determined using laboratory methods. However, nearly all the *in situ* estimates determined using the γ method plot near or above the top of the overconsolidated limit towards the water compressibility only curve (Figure 3.6) which suggests that the upper boundary of the overconsolidated range may need to be extended to include *in situ* estimates of S_S. It is also important to note that if the Pierre Shales are behaving in a viscoelastic nature (as suggested by Konikow and Neuzil, 2007); the stress response of the formations would exhibit time dependent strain. Therefore, the resulting S_S of the Pierre Shale determined over longer durations of stress change (multiple years) and larger stress changes (tens of m of pore pressure) would result in much larger S_S compared to the S_S determined using small stress changes (mm of pore pressure) over a short duration (hours to days) as we do using the γ method.

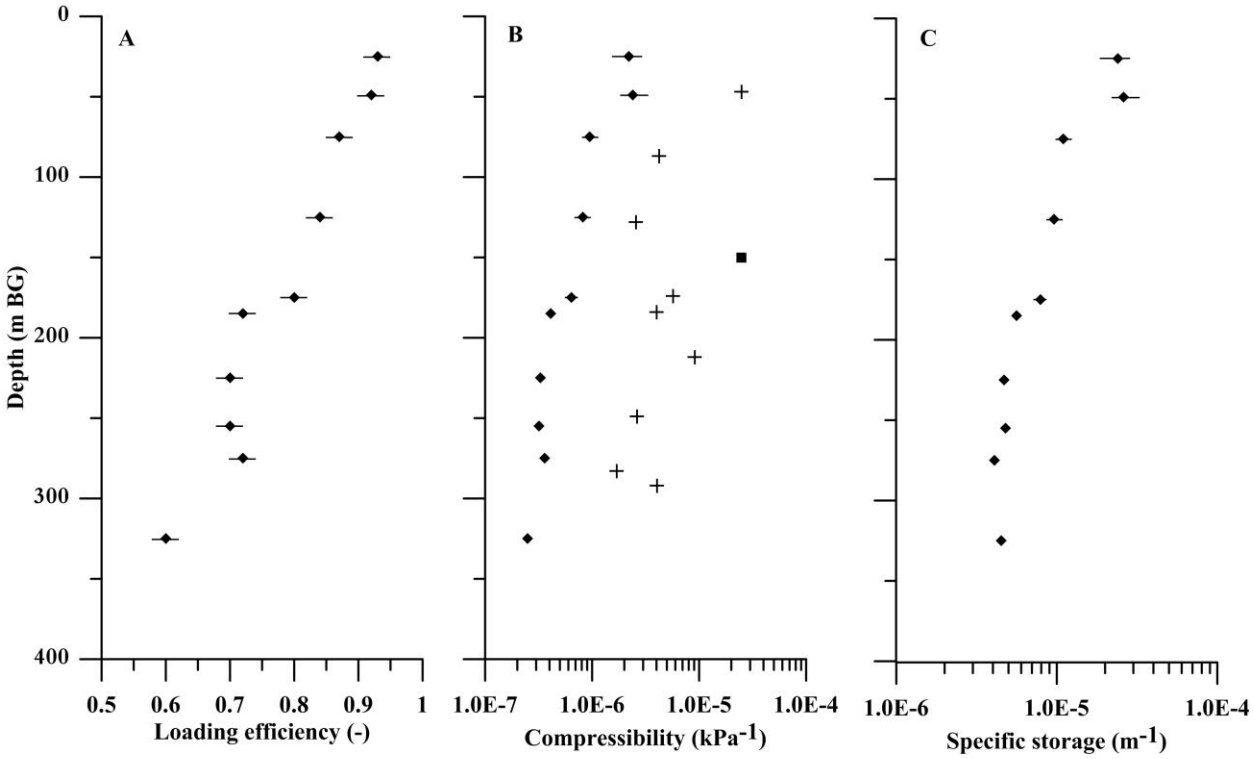

Figure 3.5: Loading efficiency determined at the depth of each transducer (A) and the resulting depth profiles for *in situ* m_v (B) and S_S (C). Laboratory consolidation tests for the shale (+) and the grout (■) are presented in B in relation to the transducer results (♦). Error bars not present are smaller than the symbol.

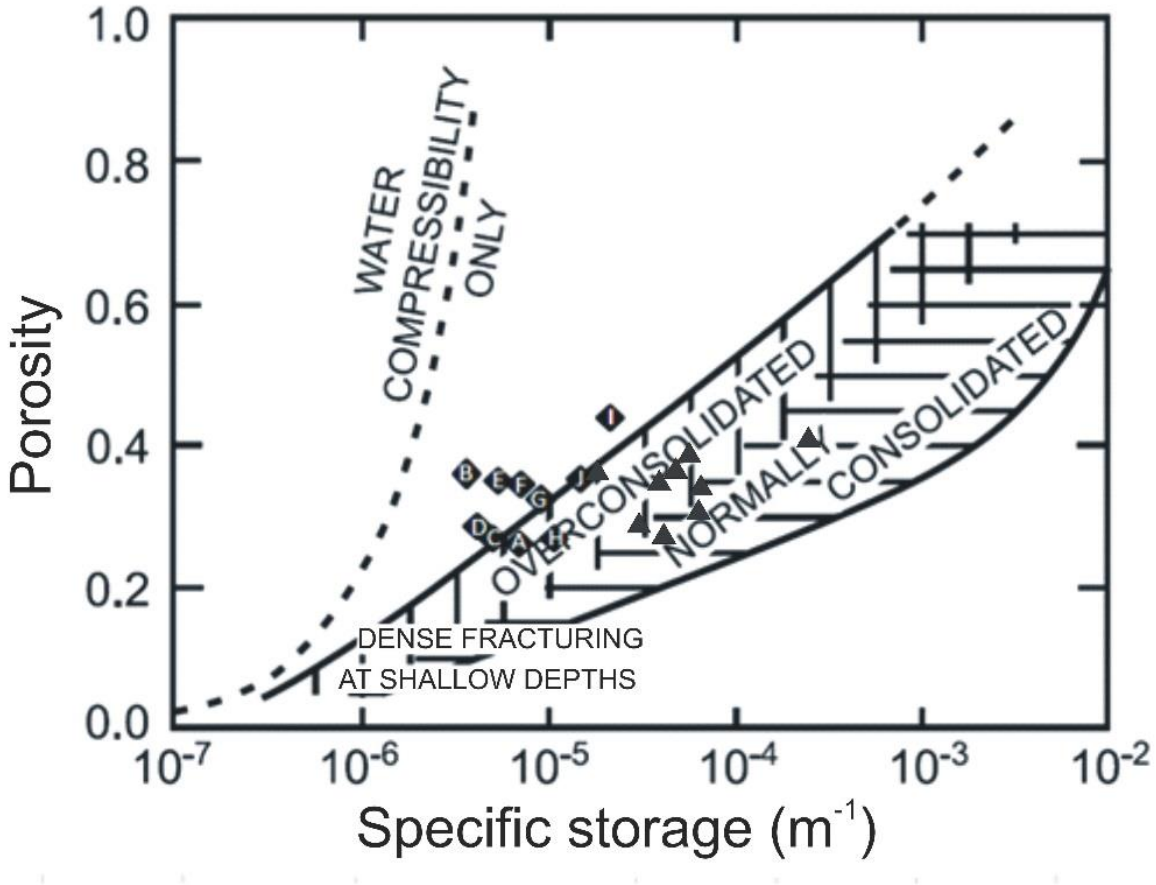

Figure 3.6: Relationship between porosity and specific storage (Konikow and Neuzil, 2007), with current study data included (identified by transducer ID, ♦) and laboratory testing results (▲). Modified by permission of American Geophysical Union.

3.6.3 Hydraulic Heads and Gradient

As illustrated in Figure 3.3, transducers A and D show about a 1 m pore pressure loss over 2 months in the presented data, while transducer J does not appear to show the same trend. It is highly unlikely that this decline of pressure for A and D could be due to net loss of soil moisture because such changes rarely exceed a few tenths of a meter in southern Saskatchewan (Marin et al., 2010) and in any case J would be most sensitive to such changes and the corresponding decline of the water table. Select transducers (particularly the ones near the Pierre and 1st Speckled Shale contact) continue to adjust since installation. The effect this has on the determination of γ (and subsequently m_v and S_S) is negligible as we are focused on how the pore pressure responds to a known surface load, i.e. barometric pressure. Therefore, the slow changes over long periods of time (months to years) can be ignored. In addition, the corrected data show varying degrees of "noise" that cannot be corrected with γ alone. This noise is inferred to be

primarily due to the remaining influence of Earth tides and moisture loading effects, but other as yet unidentified stress transients may also be playing a role.

The calculation of the hydraulic gradients from these 'stabilized' heads is largely unaffected (within 0.01-0.03 variation) regardless of when they are determined (from a few months after installation to March 2012). These head measurements were used to calculate a downward gradient of 0.22 through the Pierre Shale, 0.03 through the 1st and 2nd Speckled Shale, and an overall gradient of 0.63 through the entire 325 m of Cretaceous Shale. Errors associated with the hydraulic head calculated from pore pressure measurements can accumulate from a few sources (Neuzil, 1993). The absolute accuracy of the transducers is high (0.1 % F.S) and errors are likely insignificant compared to the corrected total head for each transducer. The elevation of each transducer is only approximately known (±1 m), leading to an error of <1 m of head. Neuzil (1993) suggests that instabilities in the borehole can cause fluctuations as much as 4 m in pressure head; however, long-term monitoring of the transducers indicates this may not be case for the present study. Further analysis and interpretation of the more than 200 m decrease of hydraulic head across the aquitard is in progress.

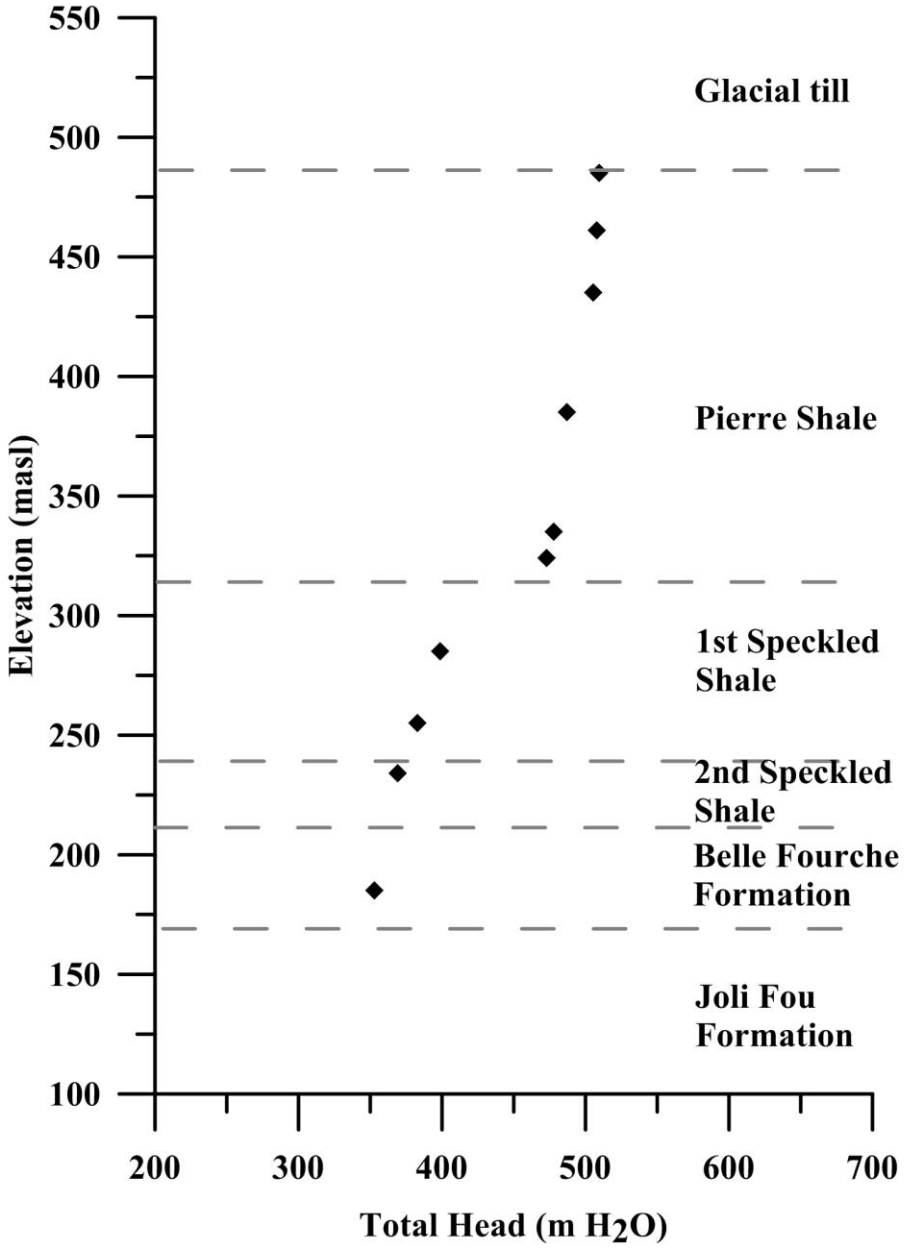

Figure 3.7: Hydraulic head distribution as a function of depth from the vibrating wire pressure transducers (♦), March 2012.

3.6.4 Vertical Hydraulic Conductivity

The K_v determined from triaxial laboratory testing on the claystone samples above the Belle Fourche Formation ranged from (2 to 10) × 10^{-12} m s^{-1}, and was relatively constant through the upper aquitard (Figure 3.8). Previous estimates of the K_v of Pierre Shale using laboratory permeability tests are consistent with our K_v for the claystone samples above the Belle Fourche Fm. *Neuzil* (1986) estimated K_v to be on the order of 10^{-13} to 10^{-11} m s^{-1} for the Pierre Fm in

North Dakota. Bredehoeft et al. (1983) measured K_v using a shut-in slug test in the Pierre Shale in South Dakota and determined it to be on the order of 4×10^{-12} to 10^{-11} m s^{-1}. Laboratory determined estimations of K_v for the three grout samples collected during transducer installation ranged from $(0.001 \text{ to } 2.0) \times 10^{-12}$ m s^{-1}. The K_v decreases with depth, which may be a result of mixing inconsistencies during grouting of the borehole; however, the low K_v in the two deep samples (182 and 317 m BG) indicates a sufficiently low K_v comparable to that of the adjoining claystone formations (Figure 3.8). It is however, important to note that since the triaxial tests could not be loaded to *in situ* effective stresses, but were conducted at a confining pressure of 20 kPa (corresponding to the *in situ* effective stress at a depth of about 20 m), the K_v of both the shale samples and grout samples may be overestimated by up to an order of magnitude.

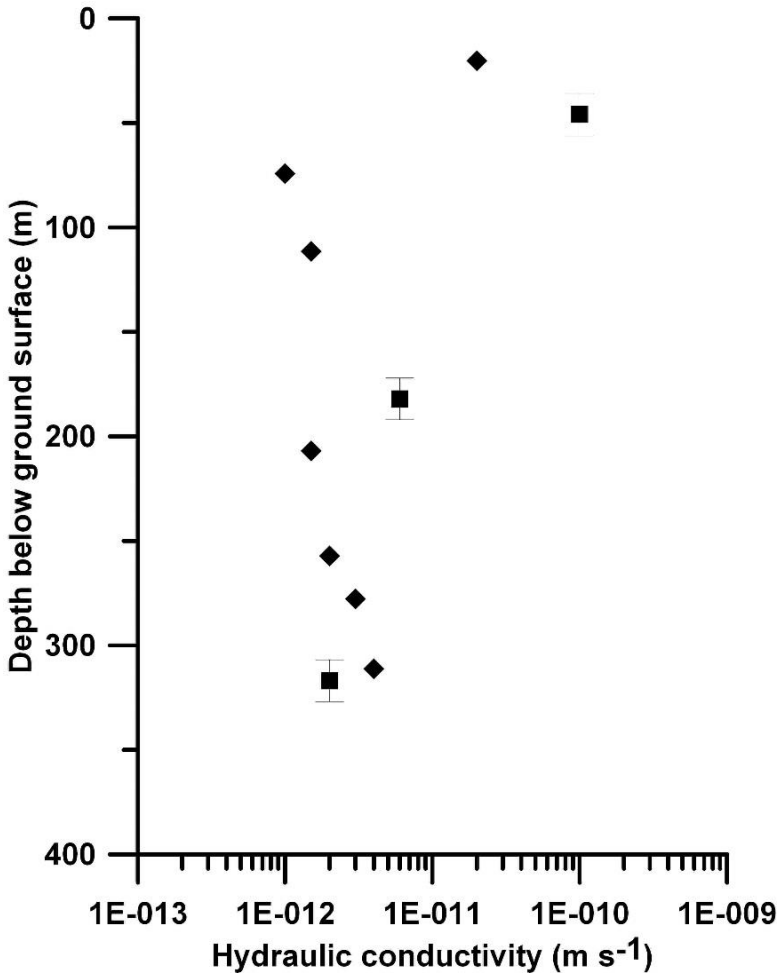

Figure 3.8: The K_v determined from laboratory triaxial permeameters for core samples (♦) and grout samples (■). Error bars (± 10 m) for grout samples reflect accuracy in the location of the grout sample.

3.7 RELIABILITY OF PORE PRESSURE MEASUREMENTS

The issues associated with using the fully grouted method for piezometer installation to measure pore pressures at depth primarily center around the interaction between the grout and surrounding ground material, and the potential for the measured pore pressures to be affected by "short-circuiting" of vertical flow through the grout to the transducers. These issues have been discussed in previous literature (Vaughn, 1969; McKenna, 1995; Mikkelsen, 2002; Mikkelsen and Green, 2003; Contreras et al., 2008), and all confirm that as long as certain criteria are met, the method can provide a cost effective, reliable and fairly simple alternative to traditional installation methods.

A piezometer must meet two main criteria to obtain accurate and reliable pore pressure measurements (McKenna, 1995): 1) the pressure measurement error must be small, and 2) the hydrodynamic time lag must be short. The development of diaphragm-type pressure transducers and their ability to measure very small fluid volume changes (0.001 cm^3 for full scale pressure equalization) over short distances allows the fully-grouted method to satisfy these requirements in a fully grouted borehole and allow for the complete elimination of the need for a highly permeable material (often a sand pack) around the piezometer.

To investigate the problem analytically, Vaughn (1969) developed closed-form steady-state solutions to estimate the error associated in the measured total pore pressure in a fully grouted piezometer installation. His work resulted in two important conclusions: 1) if the permeability of the grout is lower than the permeability of the adjacent formation, the measured pore pressure will be without error; and 2) if the permeability of the grout is within two orders of magnitude greater than the permeability of the adjacent formation, the error associated with the pore pressure measurement is not significant. To further investigate this claim, Contreras et al. (2008) developed a finite element computer model simulating seepage conditions around a fully grouted piezometer using SEEP/W, a computer modeling program developed by GEO-Slope International. An axisymmetric flow model was created to include a 70 mm radius, cement-bentonite-grout column surrounded by a soil of constant permeability. It was run at various K_{grout}/K_{soil} ratios (between 1 and 10^7) with both upward and downward flow conditions using two sets of imposed total head conditions (10 and 20 m) to induce flow at steady state conditions. The results show the error (defined as the difference in computed pore-water pressure between the soil and grout) is essentially zero when the permeability of the cement bentonite-grout mix is

within three orders of magnitude greater than the permeability of the surrounding ground for all flow conditions. These results can be understood in terms of the expected flow paths for vertical flow in the formation and through the grouted borehole, since the diameter of the area available for vertical flow through the formation is commensurate with the depth under consideration. The hydraulic resistance to vertical flow of the small-diameter grout-filled borehole is much larger than that of the surrounding formation unless the permeability of the grout is much larger than that of the formation. "Short-circuiting" of vertical flow through a more permeable grouted borehole might be significant only at very shallow depth.

As is always the case when using sealed-in instruments to measure *in situ* parameters, questions arise about what the instrument is actually measuring. It is unrealistic to fundamentally state that the long-term total pore pressure responses we are seeing are implicitly the responses of the surrounding formation. However, for the present case with a borehole diameter of 0.140 m, and given that the K of the grout was determined to be at most one to two orders of magnitude greater than the K of the surrounding formation, the error due to short-circuiting flow through the grout is almost certainly insignificant even for the shallowest observation point at 25 m depth.

The above considerations of the possible disturbing effect of vertical flow through the grout pertain to long-term more-or-less steady state pressure records obtained by means of the grouted-in transducers. For the short-term hours-to-days transients the question is whether the contrasting K and S_S of the grout and of the formation may result in delayed and damped responses of the pressure transducers to the pore pressure and stress transients in the formation. Such short-term transients include responses to barometric pressure changes, earth tides or moisture loading by high intensity rainfall events. For these cases inspection and analysis of the barometric responses can serve to detect any lag effects because the stress changes that induce the transients were measured at the site. Significant time lags were not detected in the data, as seen by the fact that the barometric pressure effects could be almost entirely removed by simple subtraction without any consideration of time lags. Similarly, short intense rainfall events were evidenced by simultaneous step-like increases of the observed pore pressures at all depths (data not shown), reflecting the change of stress due to the sudden change of total moisture mass at the ground surface (van der Kamp and Schmidt, 1997; Anochikwa et al., 2012). These moisture loading events indicate that if there is any lag time between pore pressure changes in the

formation and response of the transducers it is not much larger than about one hour. Therefore, we conclude that while there may be some influence from the grout annulus acting on the pore pressure responses, it is insignificant or very small given the method of installation and the properties of both the grout and the host formation.

3.8 IMPLICATIONS

The intrinsic difficulties in estimating *in situ* m_v values of sedimentary rock are defined by previous authors (Neuzil, 1986; Corbet and Bethke, 1992; van der Kamp, 2001). Historically, laboratory tests overestimate m_v, resulting in S_S values orders of magnitude greater than the actual *in situ* values. The alternative method presented in this paper calculates *in situ* parameters using grouted-in vibrating wire pressure transducers (installed here at depths from 25 to 325 m BG). By analyzing pore-pressure responses to barometric fluctuations, γ of the formations were determined and used to calculate m_v and S_S with depth. When the results were compared to laboratory tests and previous works in similar materials, the laboratory analysis yielded S_S estimates greater than those determined from *in situ* tests in all cases.

The results of this study demonstrate how the fully-grouted method can provide accurate and reliable *in situ* parameters of low-K materials (aquitards) at depth. This is a feat which has not yet been achieved using the laboratory or field methods currently employed, and makes this method an advantageous step towards fully understanding complex low-K flow at depth. The pore pressure records obtained by means of the grouted-in transducers as evidenced by responses to barometric pressure fluctuations, earth tides and moisture loading yielded a resolution of better than one part in 10^4 of the total pressure equivalent to cm of hydraulic head change. These observations indicate that such transducer installations can be used to monitor very small natural pore water pressure fluctuations in the formations. Furthermore, installing multiple pressure transducers in a single borehole to continuously monitor pore pressure responses to known barometric fluctuations produces a depth profile that can otherwise only be attained by drilling multiple boreholes. The ability of grouted-in pressure transducers to potentially record pore pressure changes in response to regional stress changes, such as those that might be induced by seismic activity, may provide new insight into how formations respond to sudden or transient stress and structural changes. Future work could be directed towards using pressure transducers

to monitor and track the effects of mechanical disturbances such as mining and fluid injection on the pore water pressure and stress in surrounding low-permeability geologic formations.

3.9 REFERENCES

Agnew, D.C. (2007) Earth Tides in: Treatise on Geophysics: Geodesy, T.A. Herring, Ed., Elsevier, New York. 3.06, 163-195.

American Society for Testing and Materials (ASTM) International D2435-04 (2011): Standard test methods for one-dimensional consolidation properties of soils using incremental loading. West Conshohocken, PA. USA. DOI: 10.1520/D2435_D2435M-11

American Society for Testing and Materials (ASTM) International D4531-86 (2008): Standard test methods for bulk density of peat and peat products. West Conshohocken, PA. USA.

Anochikwa, C.I., G. van der Kamp and S.L. Barbour, (2012). Interpreting pore-water pressure changes induced by water table fluctuations and mechanical loading due to soil moisture changes. *Canadian Geotechnical J., 49*, 357-366.

Bachu, S. (2002), Suitability of the subsurface in Saskatchewan and Manitoba for Geological Sequestration of Anthropogenic Carbon Dioxide. Alberta Geological Survey, Alberta Energy and Utilities Board.

Bachu, S. and B. Hitchon (1996), Regional-scale flow in formation waters in the Williston Basin. *AAPG Bull.*, 80 (2), 248–264.

Bardsley, W. E. and D. I. Campbell (1994), A new method for measuring near-surface moisture budgets in hydrological systems. *J. Hydrol., 154*, 245–254.

Bardsley, W. E. and D. I. Campbell (2007), An expression for land surface water storage monitoring using a two-formation geological weighing lysimeter. *J. Hydrol., 335*, 240–246.

Barr, A. G., G. van der Kamp, R. Schmidt, and A. Black (2000), Monitoring the moisture balance of a boreal aspen forest using a deep groundwater piezometer. *Agr. Forest Meteorol., 102*, 12–24.

Bishop, A. W. (1973), Influence of an undrained change in stress on the pore pressure in porous media of low compressibility. *Geotechnique, 23* (3), 435–442.

Black, D. K. and L. L. Lee (1973), Saturated laboratory samples by back pressure. *J. Soil Mech. Found. Div.*, 75–93.

Bredehoeft, J.D. (1967), Response of well aquifer systems to earth tides. *J. Geophys. Res*., 72 (12), 3075-3078.

Bredehoeft, J. D., C. E. Neuzil, and P. D. Milly (1983), *Regional flow in the Dakota Aquifer: A study of the role of confining layers.* U.S. Geological Survey Water Supply Paper.

Bustin, R. M. (1992) Organic maturation of the Western Canadian Sedimentary Basin. *Int. J. Coal Geol.*, *19*, 319–358.

Butler, J.J. Jr., W. Jin, G.A. Mohammed, and E.C. Reboulet (2011). New insights from well responses to fluctuations in barometric pressure. *Ground Water*, 49, 525-533.

Cherry, J. and B. Parker, (2004), *Role of Aquitards in the Protection of Aquifers from Contamination: A "State of the Science" Report.* Denver, Colorado: AWWA Research Foundation.

Clark, J. I. (1998), The settlement and bearing capacity of very large foundations on strong soils. *Can. Geotech. J. 35*, 131–145.

Clayton, C.R.I., M.C. Matthews, N.E. Simons (1995), *Site Investigation* (second edition). Wiley-Blackwell, pp. 25-29.

Contreras, I., A.T. Grosser, R.H. Ver Strate, 2008. The use of the fully- grouted method for piezometer installation, Part 1. *Geotech. News.* June, 2008

Corbet, T. F. and C. M. Bethke (1992), Disequilibrium fluid pressures and groundwater flow in the Western Canada sedimentary basin. *J. Geophys. Res., 97* (B5), 7203–7217.

Cutillo, P.A., J.D. Bredehoeft (2011), Estimating aquifer properties from the water level response to earth tides. *Ground water* 49 (4), 600-610.

Dawson, F.M., C.G. Evans, R. Marsh, R. Richardson (2008), Uppermost Cretaceous and Tertiary Strata of the Western Canada Sedimentary Basin, In: Geological Atlas of the Western Canada Sedimentary Basin. G.D. Mossop and I. Shetsen (comp.). Canadian Society of Petroleum Geologists and Alberta Research Council, Special Report 4.
URL <http://www.ags.gov.ab.ca/publications/wcsb_atlas/atlas.html>, (August 1, 2012).

Duncan, J. M., and A. Bursey (2013), Soil Modulus Correlations. Foundation Engineering in the Face of Uncertainty, in 2013 GeoCongress, San Diego, CA, March 3-7, 2013; pp. 321-336. doi: 10.1061/9780784412763.026

Freeze, R. A. and J. Cherry (1979), *Groundwater*, Prentice Hall, Englewood Cliffs, NJ, pp. 37, 158.

Garavito, A. M., H. Kooi, and C. E. Neuzil (2007), Numerical modeling of a long-term in situ chemical osmosis experiment in the Pierre Shale, South Dakota. *Adv. Water Resour.*, *29*, 481-492.

Gercek, H. (2007), Poisson's ratio values for rocks, *Rock Mechanics and Mining Sciences*, 44, 1-13.

Grisak, G. E. and J.A. Cherry (1975), Hydrologic characteristics of response of fractured till and clay confining a shallow aquifer. *Can. Geotech J.*, *12*, 23–43.

Hayes, B. J. R., J. E., Christopher, L. Rosenthal, G. Los, B. McKercher, D. Minkin, Y. M. Tremblay and J. Fennel (1996), Cretaceous Mannville Group of the Western Canada Sedimentary Basin. In: Geological Atlas of the Western Canada Sedimentary Basin. G.D.

Marin, S., G. van der Kamp, A. Pietroniro, B. Davison and B. Toth (2010), Use of geological weighing lysimeters to calibrate a distributed hydrological model for the simulation of land-atmosphere moisture exchange. *J of Hydrology*, 383, 179-185.

Mossop and I Shetsen (comps.). Calgary, Canadian Society of Petroleum Geologists and Alberta Research Council, pp. 317–363.

Hsieh, P.A. (1987), Determination of aquifer transmissivity from earth tide analysis. *Water. Resour. Res.* 23 (10), 1824-1987.

Jacob, C. (1940), On the flow of water in an artesian aquifer. *Trans. Am. Geophys.Union, 21*, 574-586.

Keller, C. K., G. van der Kamp, and J. A. Cherry (1986), Fracture permeability and groundwater flow in a clayey till near Saskatoon, Saskatchewan. *Can. Geotech. J., 23*, 229–240.

Keller, C. K., G. van der Kamp, and J. A. Cherry (1989), A multi-scale study of permeability of thick clayey till. *Water Resour. Res., 25* (11), 2299-2317.

Klohn, E. J. (1965), The elastic properties of a dense glacial till deposit. *Can. Geotech. J., 11* (2), 116–128.

Konikow, L. F. and C. E. Neuzil (2007), A method to estimate groundwater depletion from confining layers. *Water Resour. Res., 43* (W07417).

McKenna, G. T. (1995), Grouted-in installation of peizometers in boreholes. *Can. Geotech. J., 32*, 355-363.

Mikkelsen, P. E. (2002), Cement-bentonite grout backfill for borehole instruments. *Geotech. News.* December 2002.

Mikkelsen, P.E., G.E. Green (2003), Piezometers in fully grouted boreholes. *Symposium on Field Measurements in Geomechanics, FMGM.* Oslo, Norway, September.

Neuman, S. and P. Witherspoon (1972), Field determination of the hydraulic properties of leaky multiple aquifer systems. *Water Resour. Res., 8* (5), 1284–1298.

Neuzil, C. E. (1982), On conducting the modified 'slug' test in tight formations. *Water Resour. Res., 18* (2), 439–441.

Neuzil, C. E. (1986), Groundwater flow in low-permeability environments. *Water Resour. Res., 22* (8), 1163–1195.

Neuzil, C. E. (1993), Low fluid pressure within the Pierre Shale: A transient response to erosion. *Water Resour. Res., 29*, 2007–2020.

Neuzil, C. E. (1994), How permeable are clays and shales? *Water Resour. Res., 30*, 145–150.

Neuzil, C. and Pollock, D. (1983), Erosional unloading and fluid pressures in hydraulically 'tight' rocks. *J. Geo*., 91, 179-193.

Nichols, T.C., D.S. Collins, R.R. Davidson (1985), *In situ* and laboratory geotechnical tests of the Pierre Shale near Hayes, South Dakota - A characterization of engineering behavior. *Can. Geotech. J.*, 23, 181–194.

Nurkowski, J. R. (1984), Coal quality, coal rank variation and its relation to reconstructed overburden, Upper Cretaceous and Tertiary plains coals, Alberta, Canada. *AAPG Bulletin* (68), 285-295.

Radhakrishna, H. S. and T. W. Klym (1974), Geotechnical properties of very dense glacial till. *Can. Geotech. J., 11*, 396–408.

Riley, F. S. (1970), Analysis of borehole extensometer data from central California. In: Proc Tokyo Symp on Land Subsidence, Sept 1969. International Association of Scientific Hydrology, Gentbrugge, Belgium, pp. 423–430. As referenced by van der Kamp, G. (2001).

Rojstaczer, S. (1988), Determination of fluid flow properties from the response of water levels in wells to atmospheric loading. *Water Resour. Res.*, *24* (11), 1927–1938.

Rojstaczer, S., D. Carr Agnew (1989), The influence of formation material properties on the response of water levels in wells to Earth tides and atmospheric loading. *J. Geophys. Res.*, *94*, 12403-12411.

Saskatchewan Research Council (SRC) (1994), Guidelines for Groundwater Monitoring at Potash Mines in Saskatchewan, SRC Publication No. R-1220-3-E-94, p. 141.

Shaver, R. B. (1997), The determination of glacial till specific storage in North Dakota. *Ground Water, 36* (4), 552–557.

Skempton, A. W. (1954), The pore-pressure coefficients A and B. *Geotechnique, 4*, 146–147.

Smith, L. A., S. L. Barbour, M. J. Hendry, K. Novakowski, G. van der Kamp (2016), A multiscale approach to determine hydraulic conductivity in thick claystone aquitards using field, laboratory and numerical modeling methods. *Water Resour. Res.* (DOI: 10.1002/2015WR018448).

Sophocleous, M., E. Bardsley, and J. Healey (2006), A rainfall loading response recorded at 300 meters depth: Implications for geological weighing lysimeters. *J. Hydrol., 319*, 237–244.

Terzaghi, K. (1923), Die Berechnung der Durchlässigkeitsziffer des Tones aus dem Verlauf der hydrodynamischen Spannungserscheinungen. *Sitz. Akad. Wissen. Wien d. matem.-naturw.Kl., part IIa, 132*, pp. 125–138. [English translation by C. R. I. Clayton and H. Müller Seinhagen: A method of calculating the coefficient of permeability of clay from the variation of hydrodynamic stress with time. As cited in Clayton, C. R. I., H. M. Steinhagen, and W. Prowrie (1995), Terzaghi's theory of consolidation, and the discovery of effective stress. Proceedings of the Institution of Civil Engineers. *Geotech. Engin. 113* (4), 191–205.]

Terzaghi, K. and K. O. Frohlich (1936), Theorie der Setzung von Tonshichten: eine einfuhrung in die analytische Tonmechanil, Leipzig, Franz Deuticke. [As cited in Terzaghi, K., R.B. Peck and G. Mesri (1996), Soil mechanics in egineering practice (third edition), John Wiley and Sons, New York. NY, USA.]

Terzaghi, K., R. B. Peck, and G. Mesri (1996), *Soil mechanics in engineering practice* (third ed.). New York, NY, USA: John Wiley and Sons.

Toll, N., T.C. Rasmussen (2007), Removal of barometric pressure effects and Earth tides from observed water levels. *Ground water*, 45(1), 101-105.

van der Kamp, G. (2001), Methods for determining the in situ hydraulic conductivity of shallow aquitards - an overview. *Hydrogeol. J., 9*, 5–16.

van der Kamp, G. and J. E. Gale (1983), Theory of Earth tide and barometric effects in porous formations with compressible grains. *Water Resour. Res., 19* (2), 538–544.

van der Kamp, G. and R. Schmidt (1997), Monitoring of total soil moisture on a scale of hectares using groundwater piezometers. *Geophys. Res. Lett., 24* (6), 719–722.

Vaughan, P.R. (1969), A note on sealing piezometers in boreholes. *Geotechnique, 19* (3), 405-413.

Vigrass, L. (2006), Williston Basin. Encyclopedia of Saskatchewan. http://esask.uregina.ca/entry/williston_basin.html Last Accessed Jan 23, 2011.

4.0 A MULTISCALE APPROACH TO DETERMINE HYDRAULIC CONDUCTIVITY IN THICK CLAYSTONE AQUITARDS USING FIELD, LABORATORY, AND NUMERICAL MODELING METHODS

PREFACE

This chapter addresses Objective 2 of the thesis: to characterize the K of argillaceous aquitards using laboratory, *in situ*, and numerical modeling and compare the multi-scale results to each other and previous work in the literature. In this chapter, the parameters determined in the previous chapter using the grouted-in VWPs (α and S_S) were used in this chapter as input parameters in the numerical modeling developed to determine K_h, and to simulate the hydraulic head distribution through the aquitard.

In addition to the editorial and formatting changes, reference to Appendix material (geophysical logging, Appendix F) was added to § 4.3.1 as evidence of the presence of the bentonite layer at Site 1.

4.1 SUMMARY

Characterizing the hydraulic conductivity (K) of aquitards is difficult due to technical and logistical difficulties associated with field-based methods as well as the cost and challenge of collecting representative and competent core samples for laboratory analysis. The objective of this study was to produce a multi-scale comparison of vertical and horizontal hydraulic conductivity (K_v and K_h, respectively) of a regionally extensive Cretaceous argillaceous aquitard in southern Saskatchewan. Ten vibrating wire pressure transducers were lowered into place at depths between 25 and 325 m, then the annular was space was filled with a cement-bentonite grout. The *in situ* K_h was estimated at the location of each transducer by simulating the early-time pore pressure measurements following setting of the grout using a 2D axisymmetric, finite element, numerical model. Core samples were collected during drilling for conventional laboratory testing for K_v to compare with the transducer-determined *in situ* K_h. Results highlight the importance of scale and consideration of the presence of possible secondary features (e.g. fractures) in the aquitard. The proximity of the transducers to an active potash mine (~1 km) where depressurization of an underlying aquifer resulted in drawdown through the aquitard provided a unique opportunity to model the current hydraulic head profile using both the K_h and K_v estimates. Results indicate that the transducer-determined K_h estimates would allow for the development of the current hydraulic head distribution, and that simulating the pore pressure recovery can be used to estimate moderately low *in situ* K_h ($<10^{-11}$ ms^{-1}).

4.2 INTRODUCTION

Aquitards are geologic deposits with low values of hydraulic conductivity (K; $\leq 10^{-8}$ ms^{-1}) and of sufficient regional extent (i.e., thickness and areal continuity) and integrity to impede groundwater flow (Cherry and Parker, 2004). Claystone aquitards, commonly referred to as shales, can also act as caprock formations, trapping or concentrating oil, gas, injected fluid wastes, or water and preventing migration into overlying shallow aquifers. The design of *in situ* methods for the recovery of unconventional petroleum products (e.g., Steam-Assisted Gravity Drainage and Cyclic Steam Stimulation) requires characterization of the hydraulic properties of caprock formations. In addition, aquitards in sedimentary basins have been considered as host formations for the sequestration of hazardous wastes (e.g. Mazurek et al., 2011; Neuzil, 2013; Hendry et al., 2015). In spite of the additional focus over the last 30 years on groundwater flow and contaminant transport through aquitards (e.g. Batlle-Aguilar et al., 2016), they remain a

poorly understood area of hydrogeology. This lack of understanding can be attributed to a historical lack of study, complicated behaviour due to coupled flow or local deformation effects, along with the slow response of field-based measurements in low-K material, and the cost and challenge of collecting representative and competent core samples for laboratory analysis.

Characterization of K in aquitards is a particular challenge (Neuzil, 1986; van der Kamp, 2001), and few studies exist that use multiple methods to determine aquitard K (Keller et al., 1989). Traditional methods to determine *in situ* K include aquifer pumping tests with piezometers in the aquitard in addition to observation wells in the aquifer, measurements of seasonal fluctuations of pore pressure, measurement of pore pressure changes and settlement due to surface loading, and numerical analysis of field observations of local and regional pressure changes (van der Kamp, 2001). Although laboratory consolidation or triaxial permeameter tests can be used to measure K, testing is often limited to the direction of the core (e.g., vertical or K_v) and to small sample volumes ($<1.0\times10^{-3}$ m^3). *In situ* effective stresses and fluid pressures are not routinely used in laboratory testing and to obtain measurements in a reasonable amount of time the applied hydraulic gradients are typically orders of magnitude greater than *in situ* gradients. Samples are also susceptible to mechanical disturbance as a result of the sampling method and the associated stress release following coring, which can significantly influence the compressibility (e.g. Smith et al. 2013). While laboratory tests can provide an approximate range of small-scale K, they cannot be used to assess the impact of heterogeneity or secondary features such as fractures. For these reasons, a large discrepancy often exists between the results of field and laboratory testing of the same materials (Bredehoeft et al., 1983). While some researchers have ascribed the differences between laboratory-determined K_v and field-determined K_h of the same formation to the existence of heterogeneities or fractures in the formation (Neuzil, 1994), K is not always scale dependent in low permeable materials (Keller et al., 1989; Hendry and Wassenaar, 1999; Neuzil, 1994). *In situ* K measurements influenced by larger scale features such as anisotropy, heterogeneity, and secondary structures (i.e., fractures) are not captured by laboratory testing and consequently can result in large differences between laboratory- and field-based K measurements. In most cases, the best approach to estimating *in situ* K in aquitards may be a combination of both laboratory and *in situ* methods, and large-scale inverse analyses.

Pore water pressure measurements in both aquifers and aquitards are routinely made using pressure transducers. The installation of transducers to measure pore pressure by grouting

them in place is not new, and many papers have discussed related advantages and disadvantages (Vaughan, 1969; McKenna, 1995; Mikkelsen, 2002; Mikkelsen and Green, 2003; Conteras et al., 2008; Smith et al., 2013). These studies highlight that, given appropriate instrumentation and installation techniques, grouting transducers in place is cost-effective and reliable with respect to measuring pore pressures. Arguably, the most crucial element of the fully-grouted transducer installation is the cement/bentonite grout. The temporal variations in pore pressures are influenced by the hydraulic properties of the grout (i.e., compressibility and K), and the longevity and integrity of the borehole relies on proper grout mixing and installation. Measurement errors associated with transducers grouted in place include 'short circuiting' of vertical flow through the grout and time lags or damped responses (Smith et al., 2013). Provided the K of the grout is within two to three orders of magnitude of the K of the adjacent formation, the error associated with pore pressure measurements is not significant (Mikkelsen, 2002). Recent advances in analyzing the pore pressure record of grouted-in pressure transducers suggest that more information can be garnered about the host formations (e.g. compressibility, m_v). Smith et al. (2013) describe how fully-grouted pressure transducers at equilibrium with the adjacent formation can sometimes be used to determine *in situ* parameters (i.e., compressibility) in addition to monitoring the pore pressure. Examination of the long-term stabilized pore pressure record for a set of ten grouted-in piezometers over a depth of approximately 325 m showed no evidence of 'short circuiting' through the grout, and short-term (i.e., hours-to-days) transients such as earth tides, barometric pressure changes, and the pore pressure changes due to mechanical loading by short term rain fall events were all identifiable in the pore pressure record with little or no time lag (Smith et al., 2013).

The objective of this study was to use multiple methods to determine the hydraulic properties (K_v and K_h) of a thick (400 m), regionally extensive aquitard studied by Smith et al. (2013), to compare K_h and K_v at multiple scales, and, in so doing, assess the viability of analyzing the pore pressure recovery of pressure transducers after installation to determine *in situ* K_h. This objective was met by comparing and contrasting the results from three methods: one dimensional (1-D) consolidation and triaxial permeameter laboratory scale tests (K_v), simulations of early time (installation to stabilization) observations from pressure transducers (*in situ* K_h) which are responding to predominantly radial and horizontal flow, and 1-D transient simulations

of the evolution of the current head profile through the aquitard in response to nearly 35 years of nearby depressurization due to mining activities (*in situ* bulk K_v).

To the best of our knowledge, only one study has used numerical modeling to simulate the transient pore pressure recovery from grouted-in pressure transducers and it focused on evaluating the hydraulic diffusivity of thick Cretaceous shale aquitards in the Great Artesian Basin, Australia (Smerdon et al., 2014). No attempt was made to evaluate the reliability of these estimates using other methods. In the current study, the transducers are proximal to an active mine where dewatering activities have led to drawdown below the Cretaceous shale. This provides a unique opportunity to simulate the response of the aquitard to these head changes as a way to estimate its properties at a large scale. The estimated *in situ* parameters (using pressure transducers) were incorporated in numerical analyses to determine if the parameters could be used to reproduce the current hydraulic head profile.

4.2.1 Study area and hydrogeologic setting

The study was conducted in the north east portion of the Williston Basin (WB), approximately 1 km west of the Mosaic Esterhazy K2 mine site in southern Saskatchewan, Canada (Figure 4.1a). The WB is a structural-sedimentary basin that lies within the larger Western Canada Sedimentary Basin (WCSB) and underlies approximately 250,000 km^2 of North Dakota, South Dakota, Montana, Manitoba, and Saskatchewan. The WB contains a near-continuous sedimentary record from the Middle Cambrian to the Cretaceous (Hendry et al., 2013). Due to the occurrence of regressive and transgressive successions during the Upper Cretaceous period, a thick (up to 900 m) argillaceous deposit (or aquitard) was deposited across central Saskatchewan (Hayes et al., 1994). Extensive volcanic activity in the Western Cordillera during the Cretaceous period resulted in large quantities of volcanic ash blown eastwards by the prevailing winds. The ash settled in the brackish sea present in the northwestern areas (including what is now southern Saskatchewan) and was later buried and consolidated by marine sediments. Many of these ash layers were later altered to bentonite (Pusch, 2001).

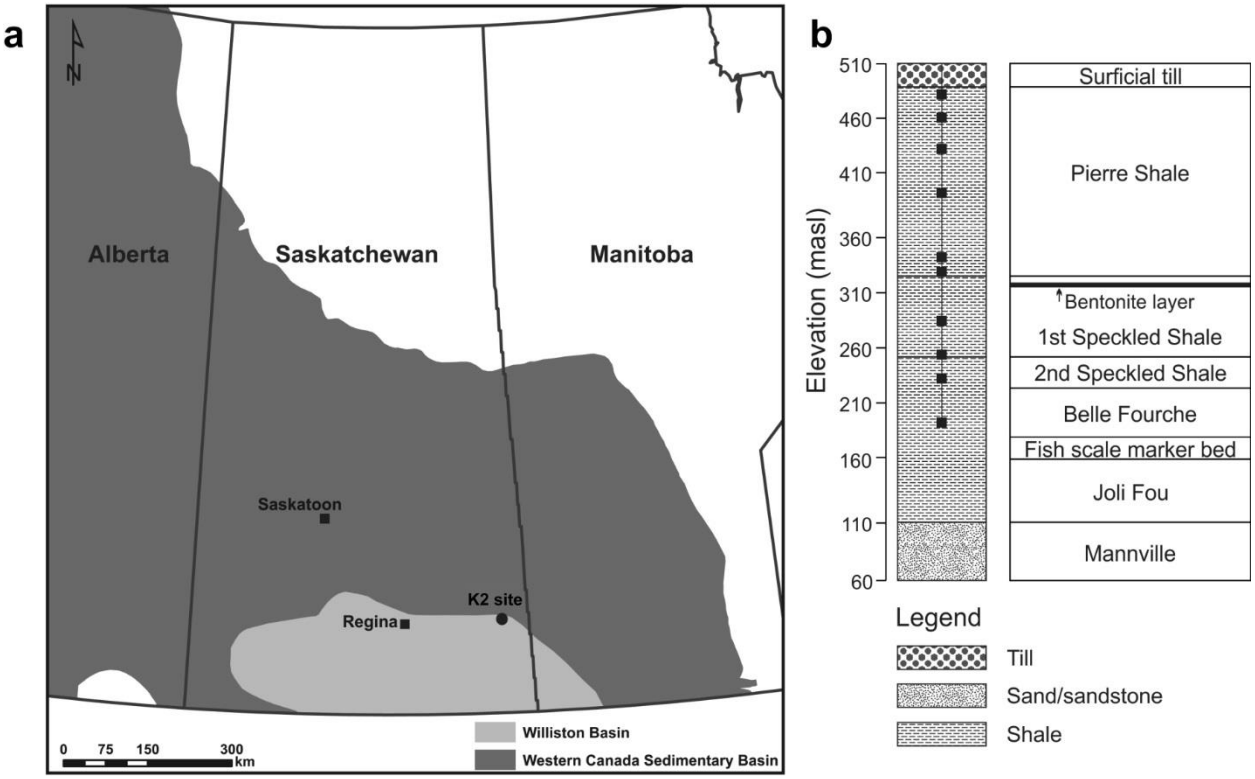

Figure 4.1: Map of west-central Canada illustrating the location of the current study in the Williston Basin (K2 site: N5617477.62 E295357.89) (a); and the stratigraphy of the borehole based on geological and geophysical logging, as well as the regional geological information that extends below the borehole (b).

The Cretaceous deposits present today were previously overlain by thicker sediments (1 to 3 km of Upper Cretaceous Shales and Tertiary sediment) that were eroded in the middle to late Tertiary (Nurkowski, 1984; Bustin, 1992; Dawson et al., 2008), as well as the Laurentide ice sheets (up to 3 km thick) during the Quaternary. These loading events resulted in the claystone (or shales) becoming overconsolidated. The shales in this area are widespread, extending more than 2,000 km from northwest New Mexico into Alberta and Saskatchewan (Garavito et al., 2007). Current understanding of groundwater flow in the WB indicates that the dominant driving force behind basin-scale flow is topography (Bachu and Hitchon, 1996; Bachu, 2002), with recharge areas at high elevations in Montana and South Dakota to discharge areas at low elevation areas at outcrop locations along the Canadian Shield in Manitoba and the Dakotas (Bachu and Hitchon, 1996). Drill stem tests (DSTs) conducted on the Mannville Group (underlying the Cretaceous Shales) indicate the same regional northeastward flow with hydraulic heads ranging from more than 1,000 masl in the south west to less than 400 masl at the Manitoba escarpment in the northeast (Bachu and Hitchon, 1996).

4.3 MATERIALS AND METHODS

4.3.1 Drilling, sampling and instrument installation

A rotary drill rig was used to continuously core a single borehole (K2 site) to a depth of 325 m below ground (BG). The initial base of exploration at the onset of the study was the Mannville Group; however, at approximately 325 m a hard concretion layer prevented the drill bit from advancing further. Core samples (~75 mm diameter × 150 mm long) were collected every 10 m. Selected samples were immediately trimmed to remove any drill fluid and then wrapped in plastic wrap and waxed in the field. The samples were stored in a cooler at ambient surface temperature (~5-10 °C) until transport to the University of Saskatchewan (UofS) where they were stored at room temperature for 30-60 d until testing. All samples were evaluated in the laboratory for geotechnical properties (detailed in §4.3.2) and subjected to 1-D consolidation (oedometer) tests and triaxial hydraulic conductivity permeameter tests (K_v).

The stratigraphy (Figure 4.1b) was determined based on geological and geophysical logging, as well as the regional geological information that extends below the borehole. Cretaceous shale (11-392 m BG) is overlain by an argillaceous Quaternary aged glacial till (0-11 m BG). The underlying Mannville Group (aquifer) consists of alternating sand/shale from 392 to 485 m BG. The Cretaceous aquitard consists of the Pierre Shale (11-184 m BG), the 1st (184 to 256 m BG) and 2nd (256 to 281 m BG) White Speckled Shales, the Belle Fourche (281 to 336 m BG), and the Joli Fou (336 to 392 m BG) formations. One thick (5 m) and three thin (< 0.1-0.2 m) bentonite layers were identified during drilling. The thin layers are not homogenous, but rather a mix of shale and bentonite and unlikely to be continuous or regionally extensive. The 5 m thick bentonite layer present at about 191-196 m BG (top of the 1st Speckled Shale) was observed during drilling/coring, and was a light grey/greenish soft clay that expanded when in contact with water.

Geophysical logging (natural gamma, single point resistance, and spontaneous potential (self-potential) was completed following drilling to 215.8 m BG. The logging tool could not be advanced below this depth, possibly due to an obstruction or the combination of buoyancy produced by drilling mud combined with some restriction in the borehole. However, the results of the gamma ray log confirmed a sharp increase and decrease over an approximate thickness of 5 m near 190 m BG (Appendix F). Following geophysical logging, a series of 10 vibrating wire absolute pressure transducers (VWPs) were installed. The pressure transducers (Geokon model

4500S) had a minimum measurement pressure of -0.1 MPa and a maximum range of 0.35, 0.7, 1, 2, and 3 MPa (absolute accuracy of ± 0.1% full scale (FS) and resolution of ± 0.025% FS). The VWPs were grouted in at depths of 25 (J), 49 (I), 75 (H), 125 (G), 175 (F), 185 (E), 225 (D), 255 (C), 275 (B), and 325 (A) m BG (Figure 4.1b) using a 4% bentonite-96% Portland cement mixture. Samples of the grout were tested regularly to ensure a density of 1700 kg/m^3, and collected in 1 L glass jars to be stored (allowed to set up under room temperature, 21°C) until subjected to oedometer and triaxial (K_v) tests. The transducers were connected to a datalogger and programmed to record pressure and temperature at 30 min increments starting about 1 d after installation. Stabilized hydraulic heads were corrected for barometric pressure following the method described in Smith et al. (2013), in which the loading efficiency (γ) for the formation at the location of each transducer was determined and pore pressure records corrected accordingly to define hydraulic head. No adjustment was made for pore fluid density since the pore water total dissolved solids ranged from 1000-2000 mg L^{-1}. The equilibrium head profile indicates an average downward gradient of 0.52 through the entire 325 m of Cretaceous Shale. Shallow monitoring wells (n=8) completed in the till formation within 1 km of the K2 mine indicate that the water table at the site fluctuates seasonally between 1 and 3 m BG (Hendry et al., 2013). Monitoring wells (n=12) were also installed in the underlying Mannville aquifer within a 90 km^2 area of the K2 mine by the Mosaic Company. The wells are located between 100 to 8000 m from the study site and were screened at either the top (n=5; 407-425 m BG) or the base (n=7; 463-491 m BG) of the Mannville Group.

4.3.2 Laboratory testing

Gravimetric water content (ω) was measured on core samples using the method outlined in ASTM D2216-10 (2010), and dry bulk density (ρ_d) was determined following the method in ASTM D7263-09 (2009) (n=46). The ω and ρ_d were used to determine volumetric water content (θ) of the core samples, which is equivalent to the total porosity (*n*) if saturation of the sample is assumed. *n* was also determined using the calculated dry bulk density (ρ_d, kg m^{-3}) and particle density (ρ_p) on 46 core samples in accordance with ASTM D4531-86 and D854-92, respectively. Atterberg limits were determined on core samples (n=33) in accordance with ASTM D4318-95 (1996). Atterberg Limits can be used along with particle size information to calculate soil activity (i.e. plasticity index/clay sized particles), an indicator of the tendency of the soil to undergo volume change (e.g. swelling/shrinking) as a result of changes in stress or chemistry. A

sample obtained from the bentonite horizon at 191-196 m BG was sent to the Advanced Microanalysis Centre at the Saskatchewan Research Council for X-ray diffraction (XRD) analysis. Clay abundance was calculated based on the intensity of characteristic peaks using the intensity of the illite (003) reflection as a reference, with an estimated error of 5%.

Standard oedometer tests (ASTM D2435-04, 2004) were conducted on individual samples collected from the Pierre Shale (47.4, 87, and 128 m BG), the 1st Speckled Shale (174.1, 184.9, 212, and 249 m BG), the 2nd Speckled Shale (283.6 m), and the Belle Fourche Fm (292 m BG). The same oedometer test was conducted on one sample of grout collected during the installation of the transducers from about 140 m BG. K_v was calculated from the calculated from the coefficient of consolidation (C_v) estimated from the sample deflection verses elapsed time data during each loading increment of the oedometer test as described by Terzaghi (1943). The co-efficient of volume compressibility (m_v, kPa^{-1}) calculated from the load-deflection data collected during oedometer testing was converted to a bulk compressibility (α) based on the relationships described by Duncan and Bursey (2013). A Poisson's ratio (υ) of 0.33 for shales and 0.2 for the grout were chosen based on a range of literature values for claystones and cement, respectively (Gercek, 2007).

K_v was also measured on nine core samples using a steady-flow fixed wall triaxial system on core samples collected from the Pierre Shale (20, 74, and 111 m BG), the 1st Speckled Shale (207 and 257 m BG), the 2nd Speckled Shale (278 m BG), and the Belle Fourche Fm (311 m BG) (Smith et al., 2013). Grout samples collected at depths of 46, 182 and 317 m BG during grouting of the borehole were subjected to the same testing, resulting in K_v estimates of (2-100) $\times 10^{-12}$ ms^{-1} (Smith et al., 2013). All grout K_v estimates were within three orders of magnitude of the adjacent formation and therefore satisfy the requirements of fully-grouted pressure transducers (Smith et al., 2013). Further information regarding the oedometer and triaxial tests are presented in Smith et al. (2013).

4.3.3 Simulation of transducer recovery

In situ K_h was estimated from the transducer data by simulating the pore-pressure measurements following setting of the grout (after about 48 h), using a commercial 2D, axisymmetric, finite element numerical model (SEEP/W) (GEO-SLOPE International Ltd., 2007). The model simulated the equilibration of pore pressure in the grouted borehole (140 mm radius) with the pore pressure in the adjacent aquitard (30 m radius) over 365 d, similar to

Smerdon et al. (2014). The simulation was repeated using varying radial distances to the far field boundary to establish the location of the assumed 'fixed head' boundary condition (determined to be 30 m). The mesh size within a 30 m radius of the borehole was 0.1 m. The simulation was run for 365 d because all transducers approached equilibrium within one year.

The initial pressure within the grout was defined by the measured pore pressure following setting of the grout, determined using the minimum pore pressure prior to recovery. The hydraulic head in the formation was defined from the pore pressure following recovery (t=365 d). The *n* and α values for the grout established from laboratory measurements (Smith et al., 2013) were assumed to characterize the entire grouted volume. The α values for the aquitard were measured *in situ* based on barometric loading efficiency (Smith et al., 2013). The *n* of the formation was determined from laboratory measurements (Smith et al., 2013). The values of specific storage (S_S) used in the modelling were calculated using a compressibility of water (β) of 4.7×10^{-7} kPa^{-1} along with the measured *n* and α values. Using these parameters, K was varied systematically until an optimum visual fit to the transducer data was achieved. The rate of pore pressure recovery is also dependent on the α of the grout and the formation. While the formation α was determined *in situ*, the grout α was determined in the laboratory under effective stresses that were much less than *in situ*. For this reason, additional simulations were conducted to assess the sensitivity of the simulated pore pressure recovery to the α value of the grout by varying it ± one order of magnitude from the laboratory determined value (4.8×10^{-5} kPa^{-1}).

To determine the accuracy of the simulations, 'best fit' simulations were compared to observed data using the root mean square error model verification equation:

[4.1] $$RMSE = \sqrt{\frac{\sum_{i-1}^{n}(O-P)^2}{n}}$$

where *O* is the observed hydraulic head (masl), *P* is the simulated hydraulic head (masl), and *n* is the number of observations.

4.3.4 Simulation of the formation head distribution (bulk K_v)

Finite element modeling of vertical transient flow through the aquitard was performed using the same commercial finite element model as for the recovery simulations; however, in this case, a single column of elements was used to create a 1-D domain. The models simulate the current head distribution observed from the stabilized pressure transducers from 25 to 325 m BG based on the known formation S_S (Smith et al., 2013) and estimated initial conditions. The

objective was to estimate the overall K required to develop the current head distribution through the aquitard given assumed initial conditions and the relatively rapid drop of head in the underlying Mannville due to the ingress of water into the mine, which began approximately 35 years ago. The conceptual model is analogous to a large, continuous pumping test where observation 'wells' (pressure transducers) are installed in the overlying aquitard formations. The initial conditions for the stratigraphic sequence including the Mannville were chosen based on DST pressures recorded in the Mannville prior to mining inflow in the vicinity of the study site (Palombi, 2008). Similar downward gradients to those assigned were observed through the Pierre Shale at other sites in southern Saskatchewan with no mining. The initial conditions consisted of an overall downward gradient of 0.20. A lower boundary head of 340 masl was chosen to be consistent with the measured pressure head of the deepest transducer (A), the observed water level measured in the Mannville wells in the area, along with measurements reported in previous work (Palombi, 2008) (discussed further in §4.4.4). Given the limited data on the hydraulic head distribution within the Mannville local to the monitoring site over the past 35 years, a range of possible changes in head within the Mannville over this time frame are used to define the lower boundary condition within the model. This analysis assumes that the primary control on the transient changes in hydraulic head through the aquitard at this location are in response to a drop in head within the Mannville. Changes in pressure may have also occurred throughout the aquitard in response to strains created as a result of subsidence associated with mining of the Prairie Evaporite Fm. For these analyses, we assume that the subsidence-induced pore pressure changes are minimal but note that this assumption may need to be reconsidered in the future. However, given this assumption, modeling the drawdown-only interpretation may also serve to demonstrate certain limitations or anomalies not addressed by this scenario and highlight areas of future research (discussed further in §4.4.6).

Three separate transient scenarios were conducted in which the present-day head profile was simulated. All of the models were comprised of a single column of 1 m wide elements over the 400 m depth with a vertical element size of 1 m. For the first model (defined as the uniform model), we assumed a 400 m thick homogeneous aquitard over which depth weighted average values (weighting by the thickness of each layer) of n (from core samples) and α (from transducer analysis) (Smith et al., 2013) were applied to the entire aquitard (Figure 4.2a). These values were used along with an assumed value of β to calculate the S_S used in the model. The

second model (defined as the complex A model) was divided into layers. The boundaries of the layers were equidistant between transducer depths. If a layer extended over more than one formation, the contact was defined as the formation contact and only represented the formation in which the transducer was installed. The values of α determined at each transducer and the *n* values from the core samples from the same location were utilized to calculate the Ss of each layer (Figure 4.2b). The final scenario (defined as the complex B model) was used to determine the impact of a thick bentonite layer on the simulated hydraulic head profiles (Figure 4.2c). It was identical to the complex A model, but with the addition of the 5 m bentonite layer located 191-196 m BG. Formation parameters (α: 3.0×10^{-5} kPa^{-1}, *n*: 0.45, K: 1.0×10^{-14} ms^{-1}) obtained from the literature were assigned to the bentonite layer (Mondol et al., 2007; Pusch, 2001).

The initial modeling effort was to systematically and uniformly vary the K in the uniform model to obtain a visual best fit to the hydraulic head data to determine the required 'bulk K_v' to fit the observed head data. To increase the complexity of the scenario, the same process was conducted in both the complex A and complex B models which use individually determined *n* and α values to calculate the S_S of each layer. Finally, the model was repeated once more using either the laboratory determined K_v or the transducer determined K_h to determine if these estimates could produce a similar trend to the observed pore pressure data.

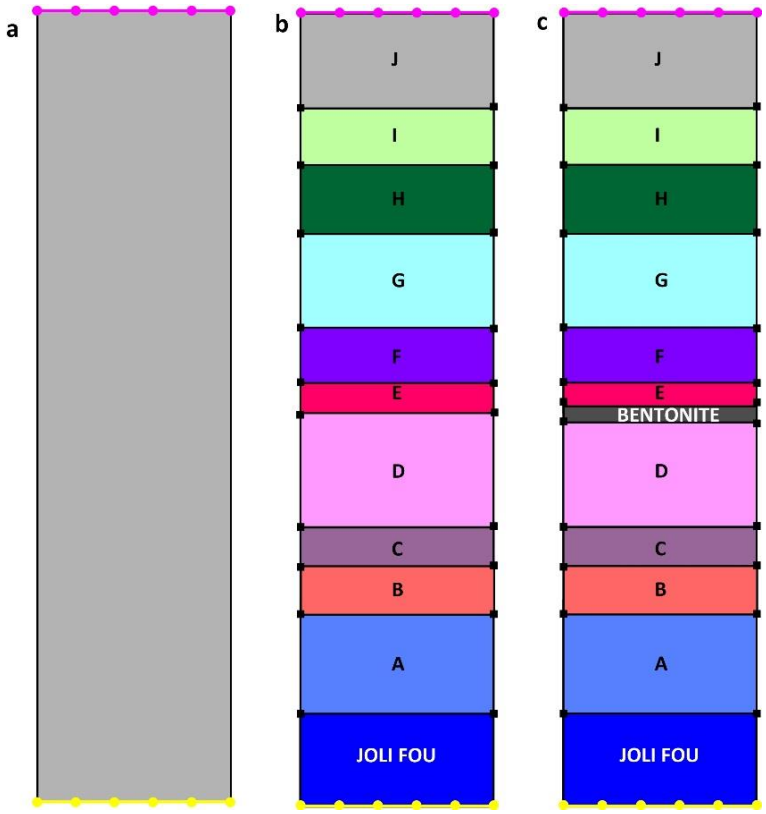

Figure 4.2: Conceptual diagram illustrating the 'uniform' (a), 'complex A' (b), and 'complex B' (c) numerical models. The complex A model is identical to the complex B model, only without the bentonite layer. The simple model assumed homogeneous shale with a weighted average porosity and S_S determined from data generated from the 10 transducers. Each layer in the complex models was assigned the porosity and S_S based on individual analyses.

4.4 RESULTS AND DISCUSSION

4.4.1 Hydrogeologic and mineralogical characterization

Laboratory-determined index parameters (ρ, θ, ω, Atterberg limits, and particle density) are plotted in Figure 4.3. The measured ρ_d and ρ_b are fairly uniform through the aquitard profile, with mean values of 2.1±0.09 and 1.8±0.1 g cc^{-1}, respectively (n=45). The ω of the shale was 18.3±3.9% (n=45) and the *n* estimated from the ω was 32.6±5.4 (n=45). The mean *n* values estimated from the core samples has a mean of 0.33±0.04 (n=45) (Smith et al., 2013).

The mean liquid limit (LL) and plasticity index (PI) varied between 60 and 140 % through the Pierre Shale and were comparatively greater than values in the underlying 1st and 2nd Speckled Shales. The LL and PI in the formations below the Pierre Shale are uniform with depth, with intermittently higher values (102-152 %) measured at 260, 270, and 290 m BG. The higher (>30%) PI values at these defined depths, as well as through the Pierre Fm, indicate the shale is

highly plastic. The plastic limits (PLs) throughout the aquitard formations are consistently lower than the ω, which is typical of highly overconsolidated clay. The activity of the soil (PI divided by % clay-sized particles) ranges from 1.2-2.3 (average 1.6±0.64) through the Pierre Shale. High activity values (e.g., > 1.25) signify that the soil contains clay minerals which make the soil more susceptible to volume change (e.g. swelling/shrinkage) in response to changes in effective stress or pore-fluid chemistry. The aquitard formations below the Pierre Shale has a consistently lower activity (< 0.75), with the exception of intermittently higher values corresponding to the high LL and PI depths mentioned earlier (260, 270, 290 m BG). With the exception of these three depths, the shale would be considered to be comprised of lower activity clays.

XRD (< 2 μm) of the bentonite sample submitted for bulk rock and clay fraction analysis show that 95% of the bulk sample is composed of clay and this clay fraction is smectite. No other clay minerals were observed in the < 2 μm fraction and, therefore, it is assumed that the remaining clay particles (> 2 μm) are also smectite.

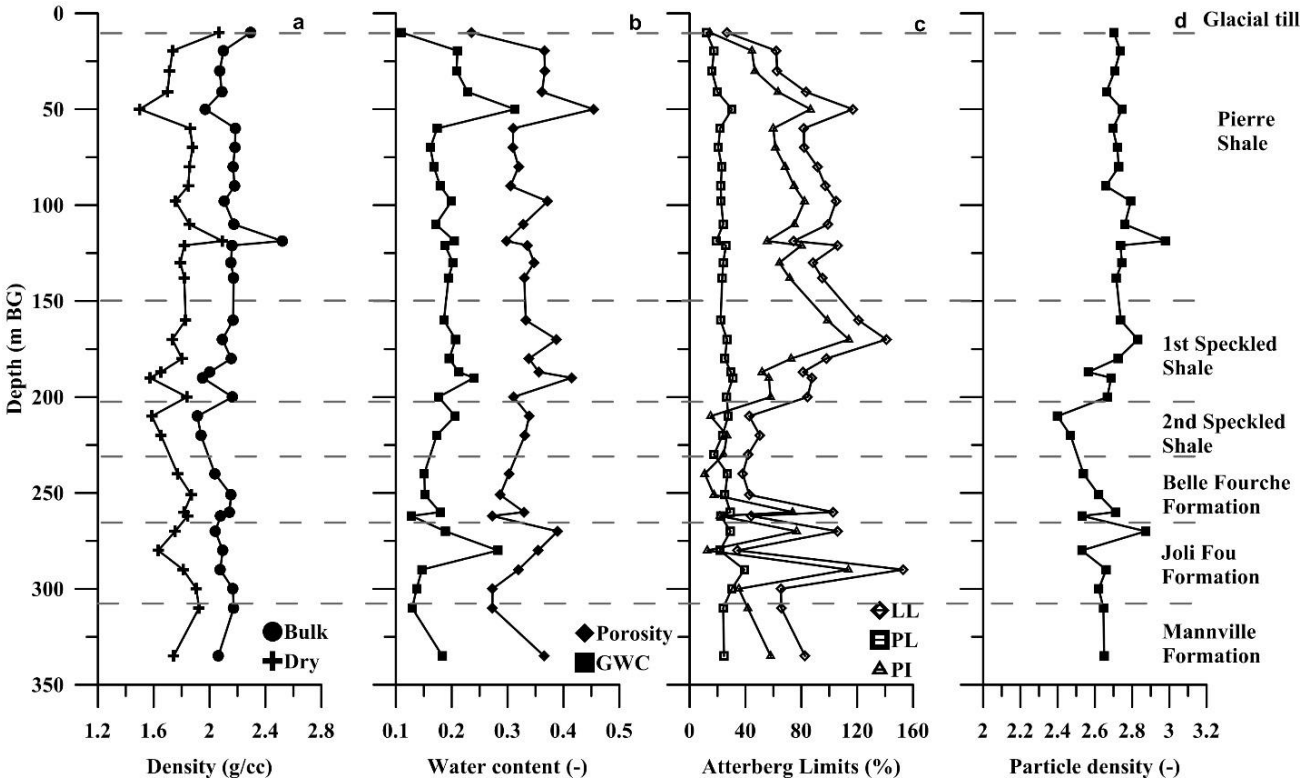

Figure 4.3: Depth profiles of index properties determined on core samples. (a) Density profile: bulk and dry; (b) Water content profile: gravimetric and volumetric water content; (c) Atterberg limit profile: liquid limit (LL), plastic limit (PL), and plasticity index (PI); (d) particle density.

4.4.2 Laboratory estimates of K_v

K_v was calculated from the odeometer test data (n=9) at the effective stress interval closest to the *in situ* effective stress where the samples were collected (Figure 4.4a). With the exception of the shallowest sample (47 m BG), the K_v values calculated from the oedometer tests were relatively uniform with depth, ranging from (0.6-2.5) × 10^{-12} ms^{-1}. The K_v of the shallowest sample from the Pierre Fm is about one order of magnitude greater than the deeper samples (2.0 × 10^{-11} ms^{-1}). K_v values determined from triaxial laboratory testing on the core samples obtained between 20 and 311 m BG ranged from (0.1-2.0) × 10^{-11} ms^{-1} (Smith et al., 2013). The Joli Fou Fm samples obtained from 352 and 384 m BG yielded K_v estimates of 1.5 and 8.2 × 10^{-11} ms^{-1}, respectively, which are approximately one order of magnitude greater than the results from shallower formations. Due to equipment limitations, these triaxial tests were conducted on samples that were not loaded to *in situ* stresses. However, given the observed laboratory and field values of compressibility and the stress changes applied during laboratory testing, a decrease in K of up to one order of magnitude appears to be consistent with conventional clay behaviour (empirical relationships between e and K) (Mitchell and Soga, 1993).

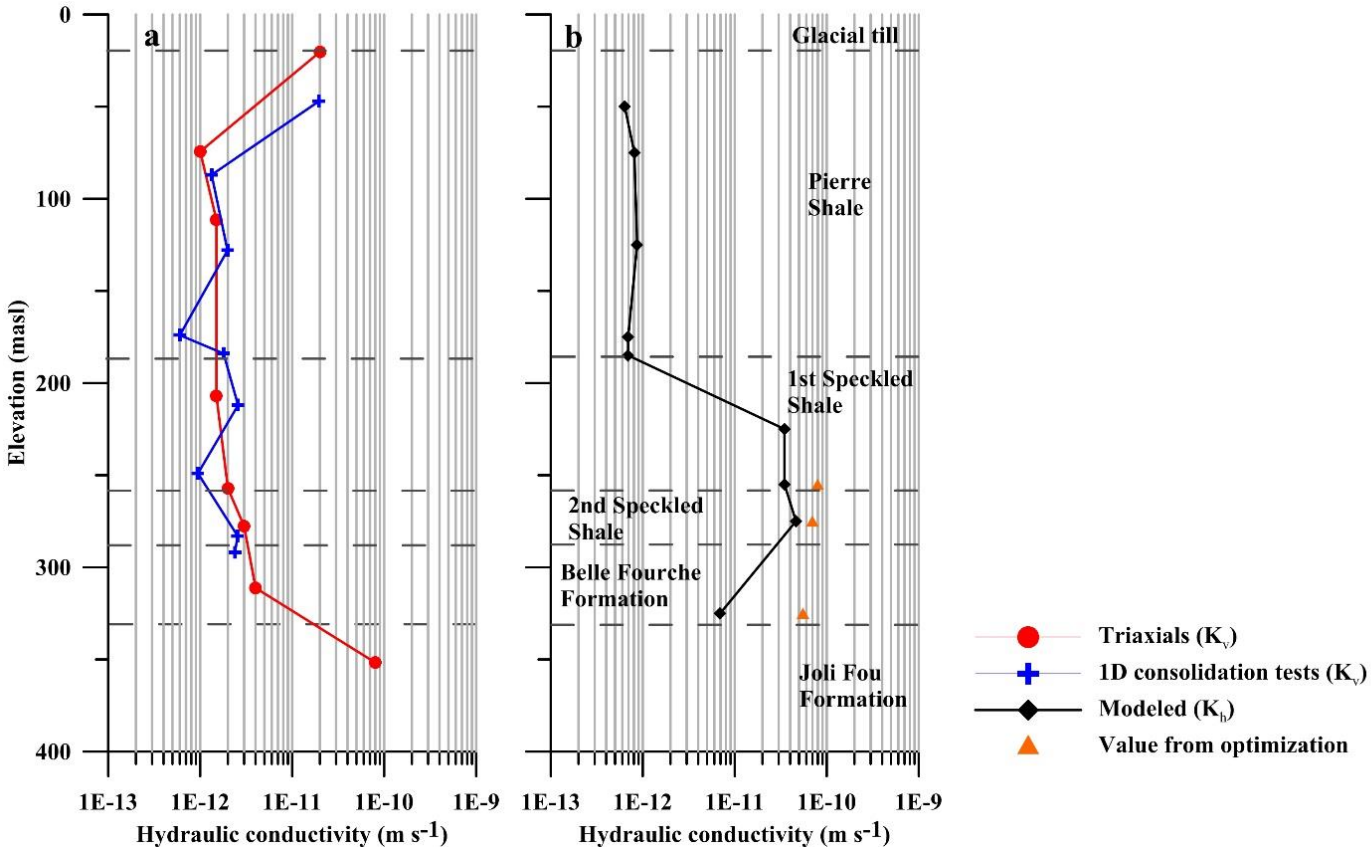

Figure 4.4: Summary of laboratory determined K_v values (a) and transducer determined K_h (b). Error bars for the laboratory determined tests were smaller than the width of the data point. The triaxial matrix K_v values were reported in Smith et al. (2013).

The K_v values obtained from the oedometer tests were similar to those from triaxial testing (Figure 4.4a). The triaxial K_v of the shallowest Pierre Shale sample (20 m BG) was the same as the shallowest oedometer sample (2.0×10^{-11} ms^{-1}) and the two methods resulted in similar estimates from the Pierre Shale through to the 2nd Speckled Shale. Although no samples for oedometer tests were collected in the Joli Fou Fm, the triaxial K_v results are consistent with the results of triaxial permeameter tests conducted through the lower Colorado Group shales (equivalent to the Joli Fou Fm) in central Saskatchewan (Schmeling, 2014). The results of the oedometer tests for K_v were consistent with the range of K_v estimates determined from laboratory consolidation tests reported by Bredehoeft et al. (1983), Misfeldt (1988), and Hendry and Schwartz (1988) (10^{-14} to 10^{-10} ms^{-1}), and the K_v estimates from triaxial permeameters were in keeping with K_v estimates reported by Neuzil (1986), Misfeldt (1988), and Schmeling (2014) (10^{-13} to 10^{-10} ms^{-1}). A comparison of the results from the two laboratory methods indicates that the aquitard matrix is relatively uniform when analyzing samples at a small scale (1.0×10^{-5} m^3).

4.4.3 Transducer recovery modeling for *in situ* K_h

Early time pore pressure measurements (installation to stabilization) generally follow a characteristic recovery trend (Figure 4.5). As grout is pumped down the tremmie pipe to fill the borehole, the pore pressure increases rapidly until grouting is stopped. The peak pore pressure corresponds to both the density of the grout (1700kg/m^3) and the depth of the transducers. Generally, the peak pore pressure is approximately 60% greater than the pore pressure of the adjacent formation. As the grout cures, free water in the system is consumed in an exothermic chemical reaction that results in a decrease in pore pressure and an increase in temperature (heat of hydration). As curing slows, temperature stabilizes and formation water flows toward the grouted annulus, causing the pore pressure to gradually increase until it recovers to equilibrium with the adjacent formation. Theoretically, this rate of recovery is dependent on the α and K of the formation and the grout. However, it is important to recognize that grout evolution during curing (thermal or chemical inconsistencies) and/or stress changes in the borehole due to drilling and curing of the grout could pose complications. Pore pressure changes caused by these complications would affect the very early time recovery (first 10 d) but to a lesser extent the later pore pressure measurements (once the grout was fully cured and induced stresses had redistributed). Since any pore pressure variances caused by grout or borehole stabilization in the early days would be overshadowed by the pore pressure recovery (up to 150 m of pressure head), simulating the overall pore pressure recovery should still provide a trend that is primarily dependent on the hydrogeologic parameters of the adjacent formation.

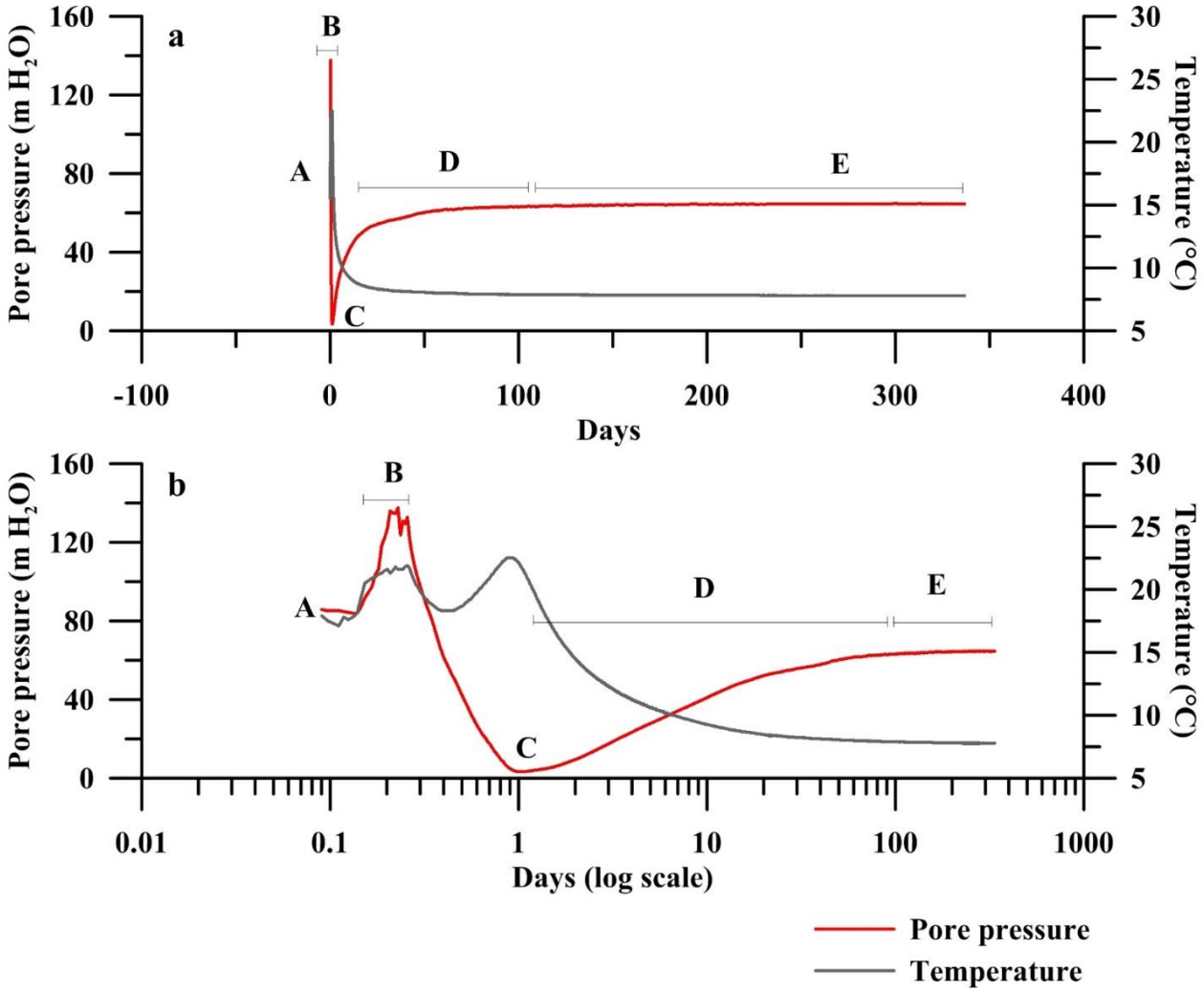

Figure 4.5: Characteristic pore pressure recovery trend of a grouted-in pressure transducer in the Pierre Shale in Southern Saskatchewan (80 m BG; unpublished data) vs time (presented on arithmetic scale (a) and logarithmic scale (b). The pore pressure recorded once once the transducers are lowered to installation depth in the borehole (A), Once in place, the cement bentonite grout is pumped down the borehole and increases pore pressure (B), followed by curing of the grout in an exothermic reaction that results in a decrease in pore pressure and an increase in temperature (heat of hydration) (C), formation water then flows towards the borehole and pore pressure gradually increases (D), until it reaches steady state with the adjacent formation (E).

The patterns of recovery for the ten transducers were characterized into one of three groups (Figure 4.6). Transducers in Group I reached equilibrium with the adjacent formation over a period of approximately 300 d. Group I included the transducers from 50 (I), 75 (H), 125 (G), 175 (F), and 185 (E) m BG in the Pierre Shale. For some transducers in Group I (transducers G, H, and I), the start of recovery was delayed until 10 to 24 d after the grout had cured. The cause of this delay is not clear, but it could be due to skin effects or the relatively greater activity

of the clays at these depths. Water introduced to the borehole during drilling or grouting could be absorbed by clays prone to swelling (high activity) and restrict water from entering the borehole until the excess water introduced to the borehole was redistributed in the formation. Once water began to flow into the borehole, Group I recovery followed the anticipated pore pressure trend (C-E in Figure 4.5). The Group II transducers exhibited a rapid recovery, reaching equilibrium in < 30 d. Group II included the deepest transducers at 225 (D), 255 (C), 275 (B), and 325 (A) m BG installed in the 1st and 2nd Speckled Shale and Belle Fourche Formations. Group III included only the shallowest transducer (J, 25 m BG) and attained equilibrium with the adjacent formation before the transducers were programmed to record (approximately 24 h) and, as a result, did not exhibit the anticipated pore pressure recovery (J; Figure 4.6).

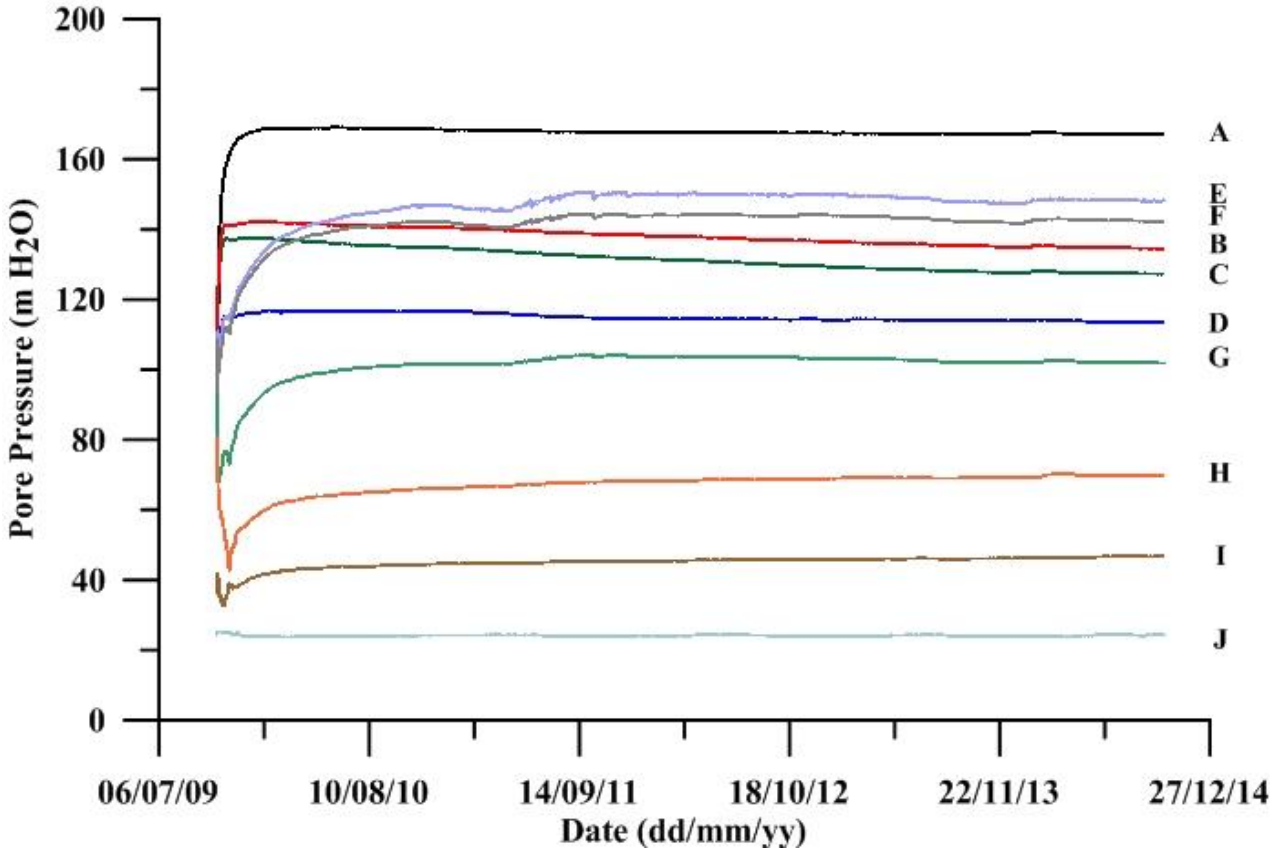

Figure 4.6: Transducer pore pressure recovery for the ten transducers installed at the K2 site from grout curing to t=1400 days.

The numerical modelling exercise to simulate the pore pressure recovery after transducer installation also resulted in two groupings of K_h that coincided with the previously defined groups. The Group II transducers (225-325 m BG) yielded K_h values approximately one order of

magnitude greater than those from the Group I transducers (50-185 m BG), as expected from their response times differing by about an order of magnitude. Representative transducers from each group (E from Group I and B from Group II) are presented to illustrate the distinctive recovery of each group (red trend), along with the modeled best fit K (black trend) bracketed by the best fit ± 50% (dashed lines) (Figure 4.7). Because the Group I transducers took longer to stabilize than the Group II transducers, these data intuitively suggest that the K_h of the formation hosting the shallow transducers (50-185m BG; Group I) is less than the K_h of the formations hosting the deeper transducers (225-325 m BG; Group II). The results of the numerical model support this assumption. The simulated pore pressure recovery from the Group I transducers yield a K_h ranging from (6.3-8.7) × 10^{-13} ms^{-1} (RMSE 0.96 – 2.0), while the K_h values for the Group II transducers were over an order of magnitude greater, ranging from (0.35-8.0) × 10^{-11} ms^{-1} (RMSE 1.38-1.77) (Figure 4.4b).

The results of the Group I transducer data (Pierre Shale) compared well with *in situ* estimates of K_h reported in the literature for the Pierre Shale. Bredehoeft et al. (1983) estimated a range of K_h of (0.5-3.5) × 10^{-11} ms^{-1} for the Pierre Shale in South Dakota using slug tests but note that leakage during the tests may have resulted in overestimates. van der Kamp et al. (1986) determined the K_h of the Pierre Shale in Southern Saskatchewan to be 1.4 × 10^{-12} ms^{-1} based on the initial water-level rise after installation of a small-diameter open piezometer; while Neuzil (1993) determined a K_h between 10^{-13} to 10^{-14} ms^{-1} in the Pierre Shale in South Dakota using recovery tests. While the range of reported K_h values for the Pierre Shale is quite large (10^{-11}-10^{-14} ms^{-1}), the K_h values determined from the pressure transducers in the current study fit in the middle of this range.

Few studies have determined *in situ* K_h for the lower Colorado Group shales. Neuzil et al. (1984) compiled data from Gries et al. (1976) to analyze pump tests conducted in the Mowry-Belle Fourche Shales and determined a K_h between (0.1 - 1.0) × 10^{-11} m s^{-1}. Neuzil et al. (1984) subsequently estimated K_v using a regional numerical model, resulting in an estimate of 5.0 × 10^{-12}. The estimated K_h of the deeper transducers (Speckled Shale and Belle Fourche Fm) were consistent with these estimates, ranging from (5.0-11.0) × 10^{-12} m s^{-1}.

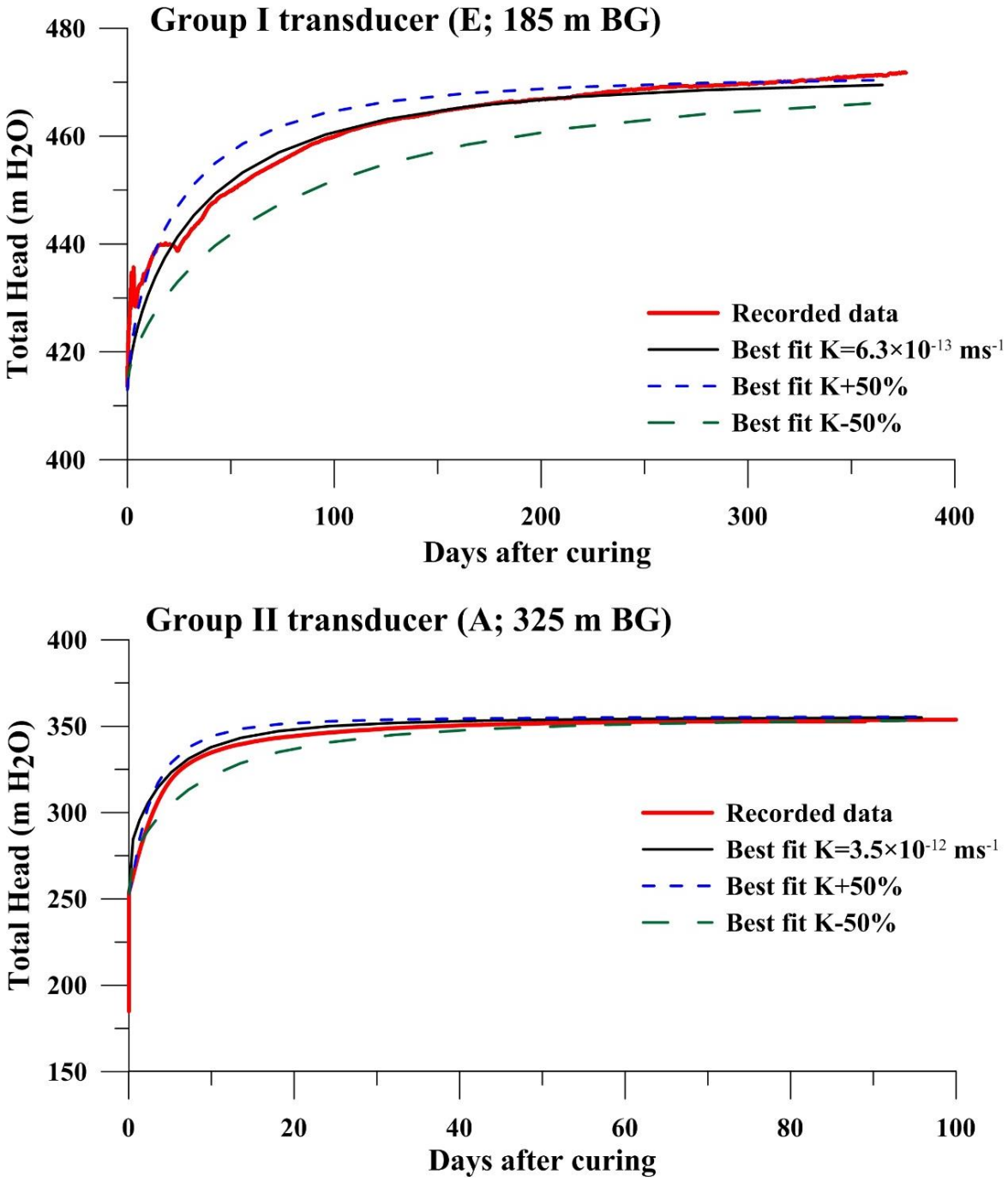

Figure 4.7: Measured and simulated total hydraulic head recovery for two transducers (B and E). Transducer E illustrates the characteristic recovery trend of transducers installed between 50-185 m BG (Group I) and transducer B illustrates the characteristic recovery trend of the transducers installed between 225-325 m BG (Group II). A sensitivity analysis is presented by bracketing the best fit K with ±50% (dashed lines).

4.4.3.1 Sensitivity studies

Simulations conducted to assess the sensitivity of both the grout and formation parameters on the pore pressure recovery showed that the α of the grout had the greatest influence on the simulated recovery. Increasing or decreasing the grout α by one order of magnitude generally increases or decreases, respectively, the determined formation K by up to one order of magnitude. For a given value of grout α (laboratory-determined), and a known value of formation α (transducer-determined), the formation K_h was unique. If, however, the formation α (and subsequently S_S) was not known, identical values of the hydraulic diffusivity (K/S_S) will provide the same solution (i.e. multiple combinations of formation S_S and K_h can produce the same fit). Similarly, if the grout S_S is not known, identical values of the hydraulic diffusivity can produce the same pore pressure recovery. Because the grout has a finite volume, the volume of water that must be transferred from the formation to the grout during pore pressure recovery will depend not only on the α of the grout but also the volume of the borehole ($V_T=\pi \cdot r^2 \cdot h$). The change in the mass of water in the borehole depends on α, V_T, and the change in pore water pressure (Δu). Uncertainties with respect to the grout (α and V_T) affect the analysis of the early time recovery, but likely not the later time recovery (once cured), meaning the overall recovery trend would not be significantly affected. To investigate this further, additional simulations were conducted to assess how variability in the borehole diameter (and, as a result, V_T) would affect the simulated results. The borehole diameter (140 mm) was uniformly increased or decreased by 10% (to 154 or 126 mm, respectively), and the formation K_h was again modified to optimize its fit. The results show that increasing the borehole diameter increased the estimated K_h while decreasing the borehole diameter decreased the estimated K_h. In all cases, the error was between 5-11%. It is likely that the borehole diameter was not consistently 140 mm with depth; however, the maximum error of 11% (if the entire borehole diameter was 10% larger or smaller than initially estimated), suggests that sporadic variances in diameter of the borehole only result in small associated errors (<5%). For future projects, a caliper log would help provide a more accurate estimate of V_T as well as reveal portions of the borehole with varying radii.

4.4.4 Modeling head distribution for bulk K_v

The present-day hydraulic head distribution through the Cretaceous shale at the K2 site was determined from the grouted-in pressure transducers. The hydraulic head in the Mannville aquifer was determined from the 12 monitoring wells in the K2 area. The head in wells screened

near the top and bottom of the Mannville ranged from 364-378 and 235-304 masl, respectively. However, the Mannville head has been evolving since drawdown began and has been particularly dynamic over the last four years. A boundary condition of 340 masl at the bottom of the shale was chosen primarily because it is consistent with the head measured in the lowest transducer (A, 325 m BG) and with measurements recorded in previous work (Palombi, 2008). Assigning a constant-head boundary condition at the bottom of the Joli Fou Shale (top of Mannville Group) is a limitation of this model and will introduce some uncertainty in the results. Because the lower boundary is dynamic and likely fluctuates with time, it is a fitting parameter and representative of only one scenario. Additional scenarios were conducted with a lower boundary condition ranging from 235-370 masl.

Three numerical modeling scenarios were examined to determine the bulk K_v required to develop the current head profile through the aquitard over the last 35 years. The bulk K_v required to produce the best fit for all the models (uniform model as well as the complex A and B models) was 4.0×10^{-10} ms^{-1}. The uniform and complex A models resulted in identical trends, while that for the complex B model was slightly different (Figure 4.8a). The complex B scenario with the same K_v was repeated with a lower head boundary of 300 or 370 m and a bulk K_v of 4×10^{-10} ms^{-1} (Figure 4.8b). By using a boundary condition with the lowest of the Mannville Group head measurements (235 masl), similar fits could be obtained with a bulk K_v of 1.0×10^{-10} ms^{-1} (not illustrated in Figure 4.8b).

4.4.4.1 Simulated head distribution using modeled K_h values and laboratory K_v values

The complex models were modified to include either the laboratory-determined K_v values or the transducer-determined K_h values (Figure 4.9) to assess if the current hydraulic head distribution could be produced with these estimates. The remaining parameters (*n* and S_S) were not altered. For a natural, mechanically undisturbed clay with a smectite content of about 70%, K was estimated to be about 10^{-14} ms^{-1} (Pusch, 2001). Because the bentonite layer at the test site is dominated by smectite, a K value of 10^{-14} ms^{-1} was assigned to the bentonite layer in the complex B scenario. A comparison of the complex A and complex B scenarios shows that the bentonite layer can play a significant role in the hydraulic head distribution through the aquitard. While none of the simulations for either the complex A or complex B scenarios completely fit the observed data points, the complex B scenario using the calculated K_h values obtained from pore pressure recovery fits all but four of the data points (located in the 1st and 2nd Speckled Shale,

below the bentonite layer). The complex B K_h model was substantially improved by increasing the K value at the location of transducer A by approximately one order of magnitude (determined using trial and error), and that at the location of transducers B and C by less than half an order of magnitude (complex B, K_h optimized) above the value of K_h as determined from the recovery analysis. Secondary structures present below the bentonite layer (discussed further in §4.4.5) are likely contributing to higher large-scale K_h values. Therefore, increasing the K_h at these three locations to optimize this model is within both the associated error of the K_h values (within one order of magnitude) as well as the conceptual understanding of the geology in the deeper formations of the aquitard.

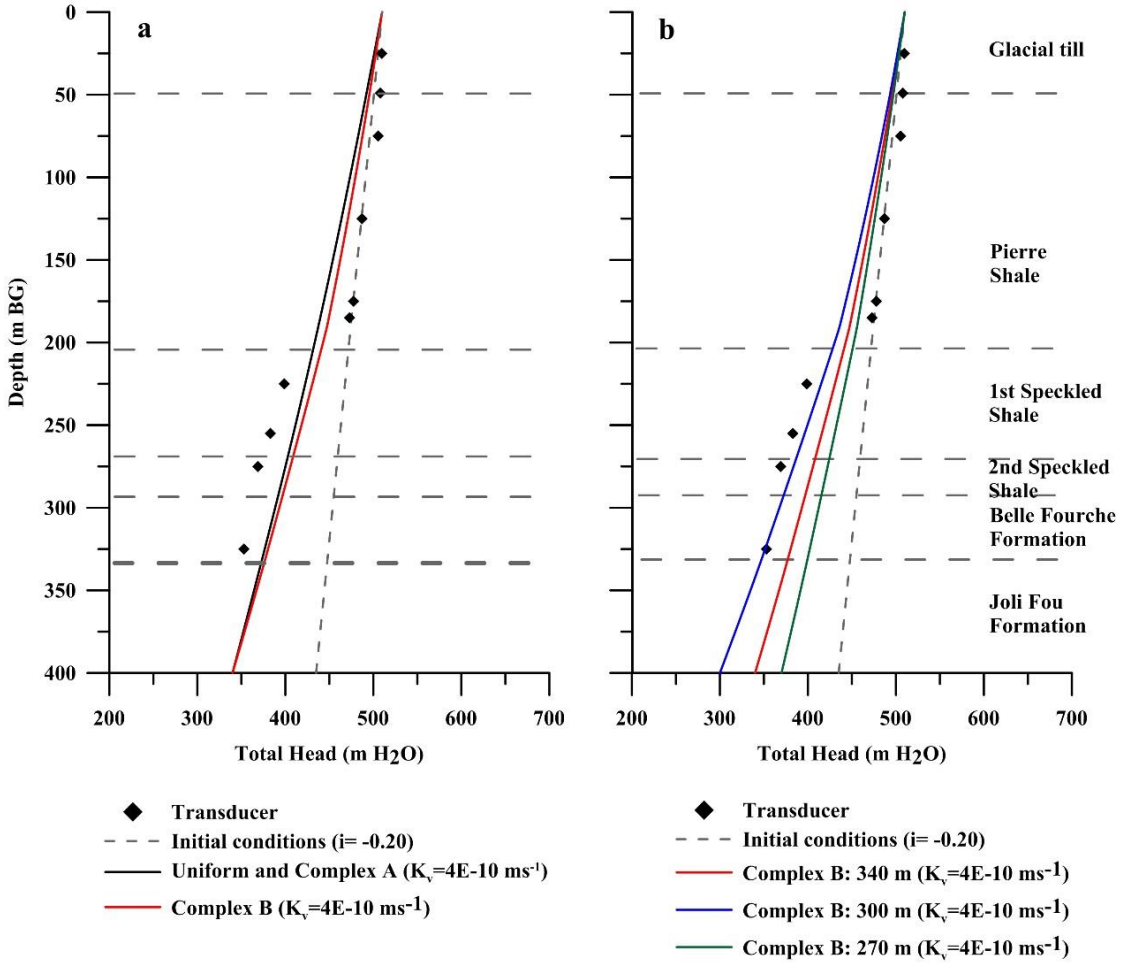

Figure 4.8: Current (November 2015) total hydraulic heads determined from the pressure transducer data (♦). (a) Simulated hydraulic head distribution for bulk Kv using an expected Mannville head (lower boundary) condition of 340 m resulted in the same trend for the uniform as well as the Complex A model (K_v = 4E-10 ms^{-1}). (b) The complex B simulation was repeated for a lower boundary condition of 300 and 370 m. Initial conditions (downward 0.20 gradient) are represented by the grey dashed line.

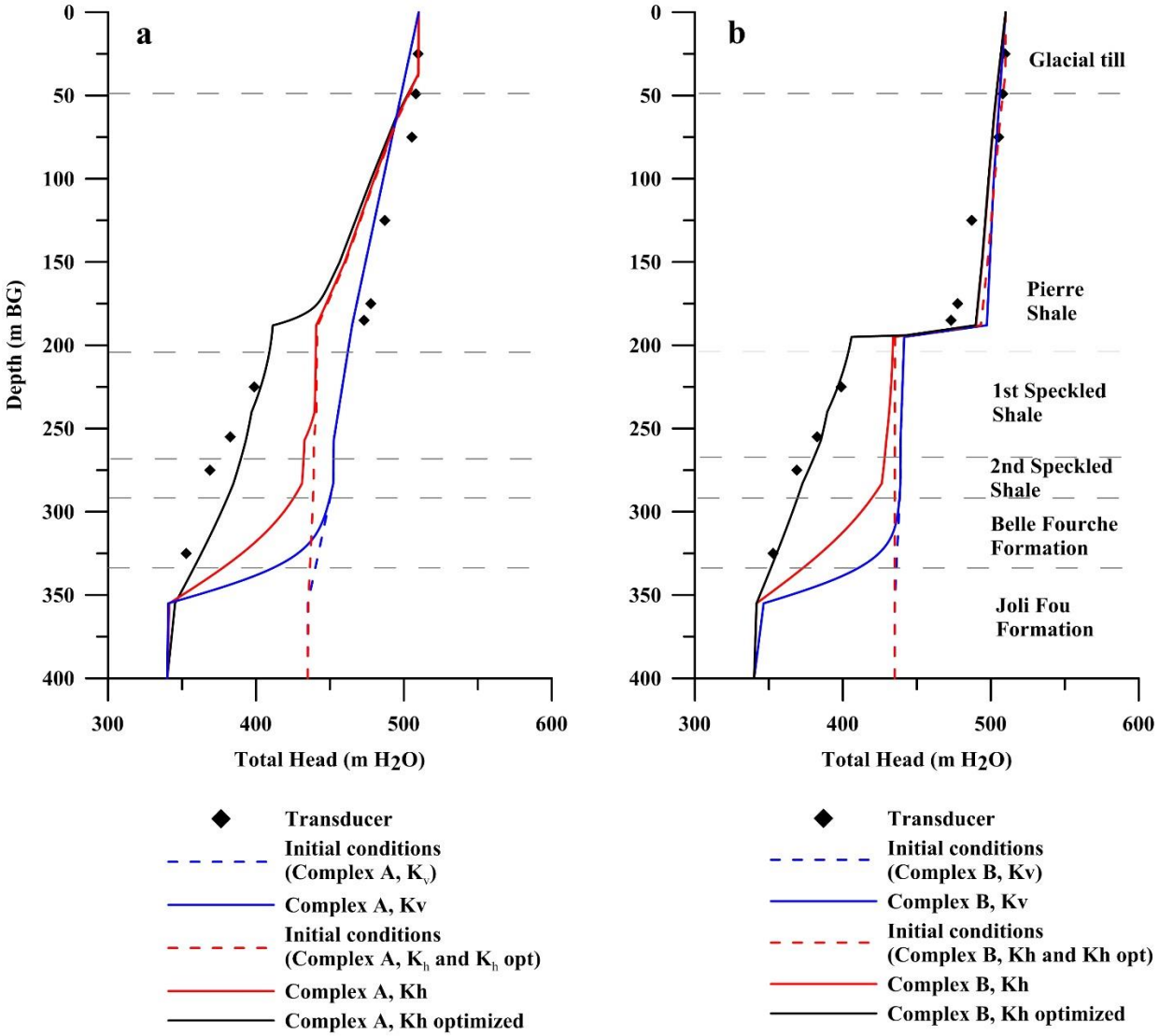

Figure 4.9: Current (November 2015) hydraulic heads determined from the pressure transducer data (♦) and the simulated total hydraulic head distribution determined from the complex A (a) and the complex B numerical models (b). Simulations were conducted using the Kh determined from recovery modeling (red), the K_v determined from triaxial laboratory tests (blue), and the K_h optimized (black) values for the lower three transducers (A, B and C). Initial conditions (downward 0.20 gradient) of the various complex A and B scenarios are represented by the red and blue dashed lines.

The significance of the thick bentonite layer is not limited to the overall trend of the head distribution. Such a thick, low-K material in the aquitard sequence could act as a barrier by hydraulically isolating the aquitards located above and below the bentonite layer. The effect of such a layer would delay the propagation of head changes in the underlying Mannville Group

into the aquitard overlying the bentonite layer. To illustrate this, the optimized complex B model (using the transducer-determined K_h) was re-graphed to include 12 time steps from 0 to 35 years (Figure 4.10; only 8 time steps presented). T=0 was established prior to mining with a downward gradient of 0.20, or a total head drop across the entire aquitard of 75 m (initial conditions). It is apparent in the simulation results that there are no head changes at locations above the bentonite layer. Consequently, the assumed initial conditions (i.e. initial downward gradient) and the presence of the bentonite layer were determined to be the primary factors controlling the hydraulic head distribution in the Pierre Shale, whereas the formation properties of the Speckled Shale, Belle Fourche Fm, and Joli Fou Fm, along with the drawdown, are the primary factors controlling the hydraulic head distribution below the bentonite layer. To further investigate the significance of the bentonite layer, the optimized complex B model was repeated with an increased induced gradient (Mannville head boundary lowered to 0 masl) and the model duration was increased to 100 years. Neither modification induced any change in the hydraulic head distribution of the transducers installed above the bentonite layer. In addition, the observed heads in the four transducers installed below the bentonite layer (transducers A, B, C and D) are decreasing (approximately 0.3, 1.5, 1.7 and 0.7 m/a, respectively), while the heads in the transducers above the bentonite layer are all increasing except for the shallowest transducer (J), which is stable. This further suggests that the formations above and below the bentonite layer are hydraulically isolated. The continuity and thickness of the bentonite layer and estimated bentonite K are key factors. The transducer determined parameter are summarized in Table 4.1.

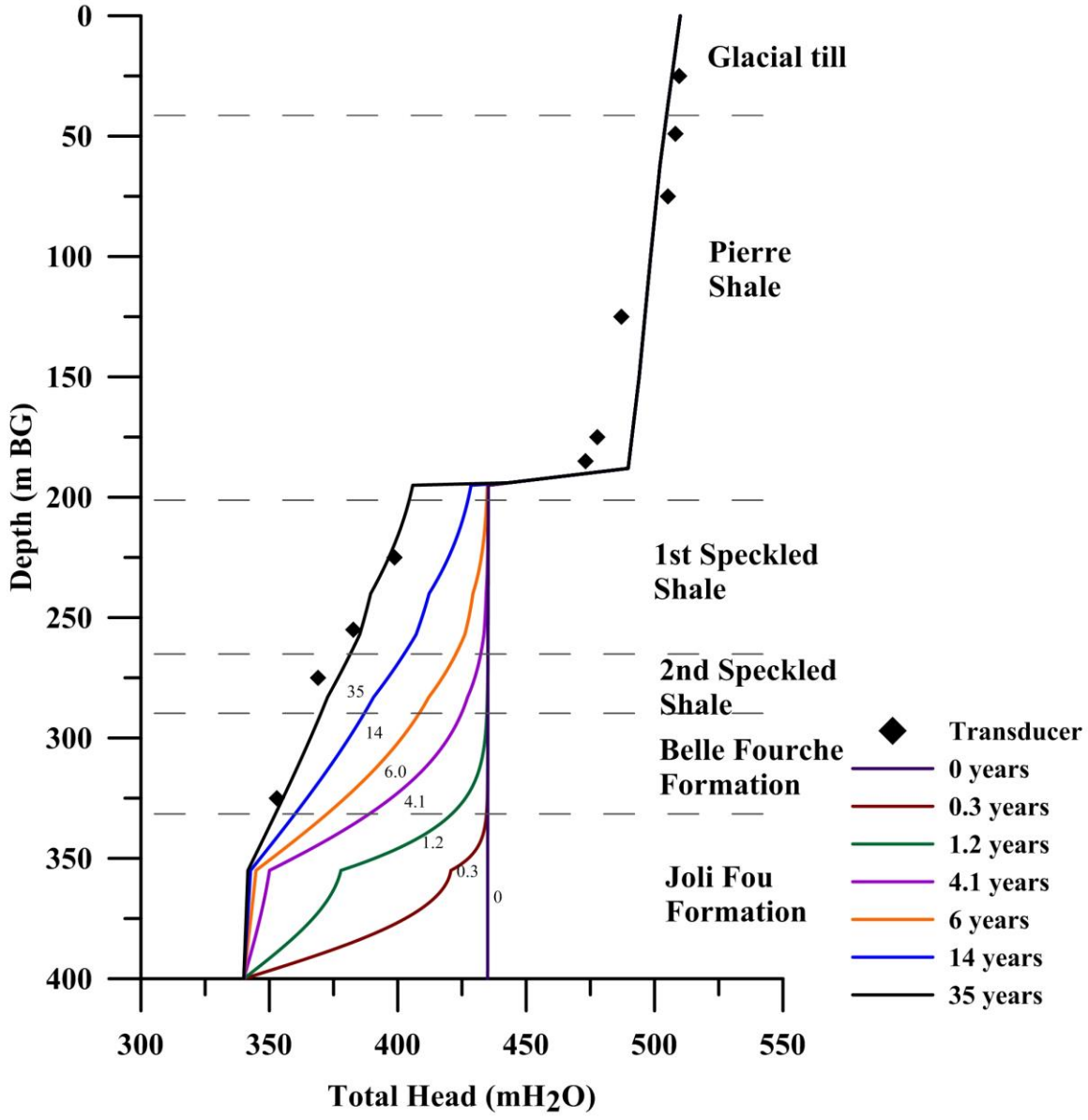

Figure 4.10: Transient response in the complex B optimized model (with the bentonite layer at 191-196 m BG) with depth, illustrating that the head change only occurs in the lower 200 m over a 30-year time period.

Table 4.1: Summary of transducer determined properties

Fm	VWP	Installation Depth (m BG)	Elevation (masl)	Total head* (m H_2O)	Modeled K_h (ms^{-1})	Optimized K_h (ms^{-1})	m_v (kPa^{-1})	α ** (MPa^{-1})
Pierre Shale	J	25	485	509.6	n.d	5.0 E-13	2.2E-06	3.2E-06
Pierre Shale	I	49	461	508.0	6.3E-13	6.3E-13	2.4E-06	3.8E-06
Pierre Shale	H	75	435	505.3	8.1E-13	8.1E-13	9.5E-07	1.4E-06
Pierre Shale	G	125	385	487.2	8.6E-13	8.6E-13	8.2E-07	1.2E-06
Pierre Shale	F	175	335	477.7	6.9E-13	6.9E-13	6.4E-07	9.6E-07
Pierre Shale	E	185	324	473.1	6.9E-13	6.9E-13	4.1E-07	6.2E-07
1st Speckled Shale	D	225	285	398.8	3.5E-11	3.5E-11	3.3E-07	5.0E-07
2nd Speckled Shale	C	255	255	382.7	3.5E-12	8.0E-11	3.2E-07	4.8E-07
2nd Speckled Shale	B	275	234	368.9	4.6E-11	7.0E-11	3.6E-07	5.4E-07
Belle Fourche	A	325	185	352.9	6.9E-12	5.5E-11	2.5E-07	3.8E-07

*Far field head boundary
** Calculated from the bulk modulus (α=1/B)
n.d. not determined

4.4.5 Comparison of K_h and K_v

The transducer determined K_h and laboratory K_v values determined in this study were $3.5 \times 10^{-11} – 6.3 \times 10^{-13}$ ms^{-1} and $2.0 \times 10^{-11} – 9.3 \times 10^{-13}$ ms^{-1}, respectively. The results of laboratory tests (K_v) and transducer analyses (K_h) compared well with K_h and K_v values reported in the literature for Cretaceous shales in the WB (Table 4.2). Comparing K_h and K_v is not always straightforward because normal and parallel bedding in shales can sometimes cause the K_h to be greater than K_v by a factor of about two (Neuzil and Pollock, 1983; Neuzil, 1984). Regardless, the laboratory-determined K_v and transducer determined K_h, are relatively uniform with depth (Figure 4.4a) until reaching the 1st Speckled Shale. K_h clearly increases between the transducers

at the base of the Pierre Shale (185 m BG) and the middle of the 1st Speckled Shale by nearly two orders of magnitude (Figure 4.4b). Given the larger scale of the transducer-determined K_h, secondary structures (e.g., fractures) in the formation may be contributing to the pore pressure recovery and thereby increasing the estimated K_h at the location of each transducer. In other words, fractures present in the formation are likely not present in the small-scale laboratory tests and therefore are not contributing to vertical flow through the core sample resulting in a K_v only representative of the aquitard matrix. Further, samples with fractures are often unsuitable for laboratory testing, so there could be selective bias towards intact core samples. This may explain why the increase in the laboratory K_v from the Pierre to the 1st Speckled Shale is modest, while the transducer-determined K_h increase is so large. A related study conducted 3D seismic modeling at three separate horizons in the aquitard sequence in the K2 region: The Pierre Shale, the 1st Speckled Shale, and the Mannville Group. The results indicate extensive polygonal fracturing in the 1st Speckled Shale but no fracturing in either the Pierre Shale or the Mannville Group (Figure 4.11). Given the greater plasticity of the Pierre Shale (based on Atterberg Limit profile) it would be expected that changes in formation-scale K due to fracturing would have a greater influence on the K of the less plastic 1st and 2nd Speckled Shale than the Pierre Shale. The presence of polygonal fracturing currently active below the Pierre Shale (i.e., not filled in, or 'healed') would help explain why the pore pressure recoveries of the Group I transducers are much slower than the Group II transducers.

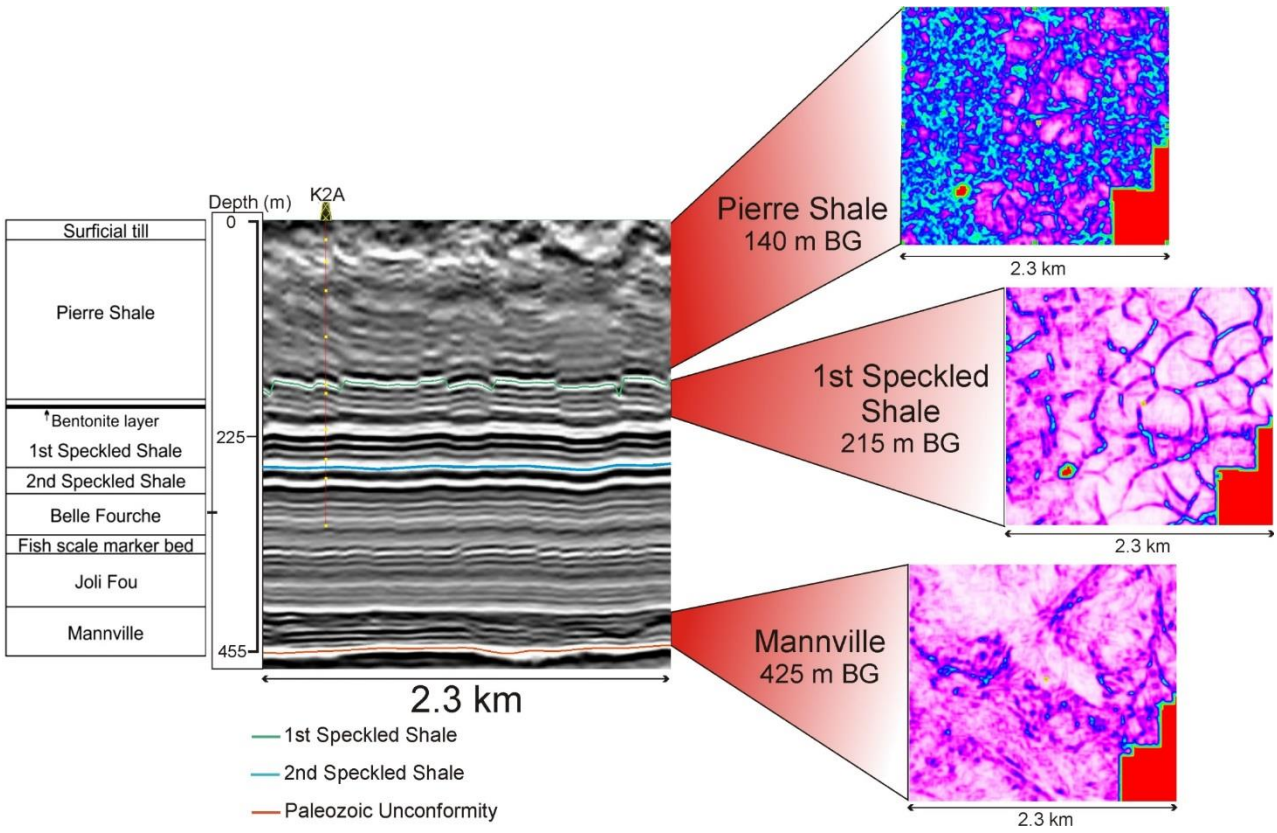

Figure 4.11: Vertical and horizontal structure in the vicinity of the K2 site determined using 3D seismic mapping of the Pierre Shale, 1st Speckled Shale, and the Mannville Group. Yellow dots in the vertical profile represent the location of pressure transducers.

Theoretically, for flow perpendicular to the layers, the bulk K_v (or equivalent K_v) should be the harmonic mean of the K_v for each unit (Freeze and Cherry, 1979) and consequently is biased towards the lowest K_v values (in this case, the bentonite layer). If we apply this theory to the aquitard using the laboratory determined K_v for the formations and an assumed K_v for the bentonite of 1.0×10^{-14} ms^{-1}, the theoretical equivalent bulk K_v is 5.8×10^{-13} ms^{-1}. The bulk K_v through the aquitard determined by modeling the current hydraulic head distribution (described in §4.4.4), was 1.0-4.0 $\times 10^{-10}$ ms^{-1} for all scenarios (uniform, as well as the uniform K but complex A and complex B storage properties). This estimated bulk K_v value is greater than both the laboratory determined K_v and transducer determined K_h estimates, as well as the theoretical equivalent K_v through the entire aquitard by up to three orders of magnitude. However, the bulk K_v simulations provided a poor match to the measured data (Figure 4.8). No combinations of bulk K_v or changes in the assumed drawdown within the Mannville head increased the quality of the fit, presumably because the formations are hydraulically isolated above and below the

bentonite layer and all head changes through the aquitard are occurring below the bentonite. Given this, the theoretical bulk K_v was calculated for only the formations below the bentonite layer. Using the laboratory determined K_v estimates, the theoretical equivalent bulk K_v is 3.2×10^{-12} ms^{-1}. If the field determined K_h (from pore pressure recovery) values are used, the theoretical equivalent bulk K_v is 1.2×10^{-11} ms^{-1}. The equivalent bulk K_v obtained from the optimized K_h values is 6.1×10^{-11} ms^{-1}, less than half an order of magnitude lower than the modeled equivalent K_v.

Vertical fracturing in the lower formations (below the bentonite layer) and the expected high K_v in the Joli Fou Fm (10^{-10} ms^{-1}) may be the underlying cause of the higher K_v values from optimization. Fractures would allow the water to drain faster in response to drawdown of head in the Mannville, resulting in decreasing head measurements with time. While modeling the hydraulic head distribution through the aquitard may provide an approximate estimate of *in situ* K_v, a section of the aquitard with a high (relative) K or low storage parameter (S_S) (such as the Joli Fou) would likely skew the bulk K_v considerably and may only provide a general estimate of K_v through the aquitard sequence. Further evidence to the presence of a high K_v formation (Joli Fou) would be the rate of pore pressure change in the deepest four transducers (A, B, C, and D). While the detailed drawdown history at the top of the Mannville is unknown (e.g., instantaneous change vs. increasing rates of drawdown with time), assuming that the Joli Fou Fm has a high K_v implies that a transducer near this formation would likely have changed very little in recent years as most of the change would have occurred shortly after drawdown began. According to the rate of change illustrated in Figure 4.10, the head measured by transducer A should be decreasing by less than 0.3 m/a while transducers B, C, and D should be decreasing by 0.6 m/a. The observed data indicates that the head in transducer A is decreasing by ~0.45 m/a, while B, C, and D are decreasing by ~1 m/a.

Table 4.2: Summary of reported hydraulic conductivities in the Cretaceous shales and similar formations

Fm	Porosity (*n*)	K (ms^{-1})	Direction	Method	Reference
Pierre Shale (Saskatchewan)	Not reported	1.4×10^{-12}	K_h	Slug tests	van der Kamp (1986)
Pierre Shale (South Dakota)	Not reported	$0.003 - 3.0 \times 10^{-12}$ $0.3 - 3 \times 10^{-13}$	K_h K_v	Slug tests Consolidation tests	Bredehoeft et al. (1983)
Pierre Shale (South Dakota)	0.30	$0.1 - 1 \times 10^{-13}$	K_h	Recovery tests	Neuzil (1993)
Pierre Shale (North Dakota)	0.32	$0.01 - 1 \times 10^{-11}$	K_v	Permeameter tests	Neuzil (1986)
Pierre Shale (South Dakota)	Not reported	$10^{-14} - 10^{-12}$ $10^{-12} - 10^{-11}$ 10^{-9}	K_v	Consolidation tests Pump test Regional model	Neuzil (1984)
Pierre Shale (Saskatchewan)	Not reported	$3.8 - 7.6 \times 10^{-12}$ $0.38 - 2.5 \times 10^{-10}$ 3.8×10^{-10}	K_h K_v K_v	Permeameter tests Permeameter tests Consolidation tests	Misfeldt (1988)
Colorado Group (Alberta)	0.07*	$0.1 - 1 \times 10^{-10}$	K_v	Consolidation tests	Hendry and Shwartz (1988)
Lower Colorado (Saskatchewan)	0.34±0.04	$0.1 - 1 \times 10^{-10}$	K_v	Permeameter tests	Schmeling et al. (2014)
Pierre Shale (Saskatchewan)	0.34±0.04	$6.3 - 8.7 \times 10^{-13}$ $0.1 - 2 \times 10^{-11}$ $0.6 - 2 \times 10^{-11}$	K_h K_v K_v	Recovery modeling Permeameter tests Consolidation tests	Current study
Speckled Shale and Belle Fourche (Saskatchewan)	0.31±0.06	$3.5 - 8.0 \times 10^{-11}$ $1.5 - 4 \times 10^{-12}$ $0.93 - 2.5 \times 10^{-12}$	K_h K_v K_v	Recovery modeling Permeameter tests Consolidation tests	Current study
Joli Fou (Saskatchewan)	0.32±0.02	$1.5 - 8.2 \times 10^{-11}$	K_v	Permeameter tests	Current study
Cretaceous Shales (Saskatchewan)	0.33±0.04	$1 - 5 \times 10^{-10}$	Bulk K_v	Numerical modeling	Current study

4.4.6 Other Considerations

Total stress loading of the aquitard (e.g. glaciation) can cause a change in total volume and subsequent volumetric strain that causes formation pressures to increase (Neuzil, 2012). In a similar manner, bending or flexure of the aquitard can produce changes in lateral unloading that are likely to result in an induced pore pressure. For example, lateral stresses increase under the weight of a glacier as the lithosphere is depressed and thereby increases fluid pressure (Khader and Novakowski, 2014; Johnston et al. 1998). Neuzil (2012) suggests that pressure effects due to

flexural loading should be considered when defining basinal groundwater systems during glacial loading. Strains created by subsidence due to mining may cause similar flexural loading. For this reason, it is necessary to acknowledge that mining of the Prairie Evaporite Fm in the K2 region may influence pore pressures through the aquitard. While the exact amount of subsidence is not reported, the borehole is located on the flank of the subsidence where lateral strains would be much less than at the center. However, strain induced on the flanks could still influence the measured pore pressures and should be addressed.

A few indications in the pore pressure record indicate that some type of slip/strain behaviour may be influencing pore pressures at the K2 site. The analysis presented in this paper assumes that the primary control on the transient changes in hydraulic head through the aquitard at this location is a response to a laterally extensive drop in the head in the Mannville. The slowly decreasing heads measured by the deeper transducers (A-D; 0.3-1.8 m/a) are consistent with this behavior; however, the same trend is not observed in the shallower transducers (E-J). Transducer J (25 m BG) is nearly constant, which is expected because its pore pressure response is controlled primarily by the water table. Pore pressures measured by Transducers I and H (50 and 75 m BG, respectively) increase with time (0.8-1.3 m/a), which is contrary to what would be expected given the drawdown in the Mannville but likely what might be seen in the upper portion of the formation for subsidence-induced strain. Transducers G, F, and E (at 125, 175, and 185 m BG, respectively) measure multiple instances of anomalous falling and rising behaviour that are suggestive of creep-slip events, which are possibly due to subsidence (Figure 4.12). An interesting observation for these three transducers is their location relative to the prominent 5 m thick bentonite layer (191-196 m BG). The magnitude of the responses gradually dampen with vertical distance from the bentonite (i.e., the transients observed for transducer E are most prominent, while G is the least prominent), and no such response is observed in the transducers directly below the bentonite. This suggests that creep-slip events could be occurring in the weak, highly plastic bentonite and affecting pore pressures above the layer, as measured by transducers G, F, and E. Further work on these pressure anomalies or other possible effects due to subsidence is warranted.

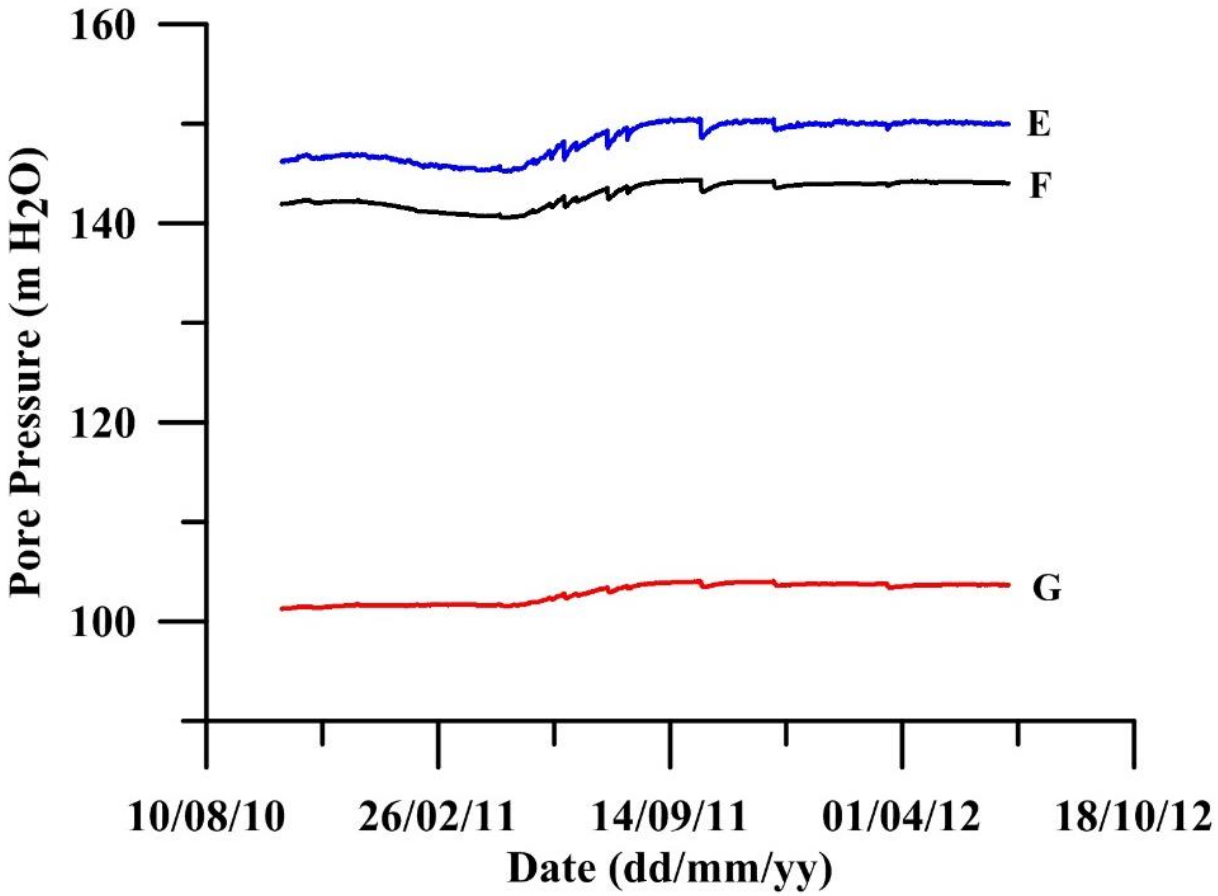

Figure 4.12: Pore pressure transients possibly due to creep-slip events recorded above the bentonite layer (191-196 m BG) by transducers E (185 m BG), F (175 m BG) and G (125 m BG).

4.5 SUMMARY AND CONCLUSIONS

This study demonstrates different methods to estimate both K_v and K_h of a thick clay rich aquitard at various scales in a sedimentary basin: (1) laboratory consolidation tests (matrix K_v), (2) laboratory triaxial permeameters, (3) numerical modeling of borehole pressure recovery (*in situ* K_h), and (4) numerical modeling of the head distribution (bulk *in situ* K_v). The results provide a valuable and rare set of data obtained from grouted-in pressure transducers; however, the significance of this study may lie primarily in extending applications of grouted-in pressure transducers to determine *in situ* hydrogeologic parameters of aquitard formations (Smith et al., 2013; Smerdon et al., 2014). The results of this study indicate that the K_h estimates determined from the transducers (within their associated error, and evidence of vertical fracturing) would allow for the development of the current hydraulic head distribution. This study focuses

primarily on determining the hydraulic parameters of aquitard formations and the consequences of a large-scale drawdown in the underlying aquifer on the head distribution in the aquitard. While acknowledging that further work is warranted to investigate the possible influence of subsidence induced stress and its effect on pore pressures through the aquitard, simulating the pore pressure recovery appears to be an attractive method for estimating *in situ* K_h. This, in turn, suggests that installing grouted-in pressure transducers could prove to be a useful tool for acquiring hydraulic data for materials that are historically difficult to characterize.

4.6 REFERENCES

ASTM D854-92 (1992), Standard Test Methods for Specific Gravity of Soils, ASTM International, West Conshohocken, PA.

ASTM D4318-95 (1995), Standard Test Methods Liquid Limit, Plastic Limit, and Plasticity Index of Soils, ASTM International, West Conshohocken, PA.

ASTM D2435-04 (2004), Standard Test Methods for One-Dimensional Consolidation Properties of Soils Using Incremental Loading, ASTM International, West Conshohocken, PA.

ASTM D7263-09 (2009), Standard Test Methods for Laboratory Determination of Density (Unit Weight) of Soil Specimens, ASTM International, West Conshohocken, PA.

ASTM D2216-10 (2010), Standard Test Methods for Laboratory Determination of Water (Moisture) Content of Soil and Rock by Mass, ASTM International, West Conshohocken, PA.

Bachu, S. (2002), Suitability of the subsurface in Saskatchewan and Manitoba for Geological Sequestration of Anthropogenic Carbon Dioxide. Alberta Geological Survey, Alberta Energy and Utilities Board.

Bachu, S., and B. Hitchon (1996), Regional-scale flow in formation waters in the Williston Basin, *AAPG Bull*., 80 (2), 248–264.

Batlle-Aguilar, J., P.G. Cook, G.A. Harrington (2016), Comparison of hydraulic and chemical methods for determining hydraulic conductivity and leakage rates in argillaceous aquitards, *J. Hydrol.*, 532, 102-121.

Bredehoeft, J. D., C. E. Neuzil, and P. D. Milly (1983), Regional flow in the Dakota Aquifer: A study of the role of confining layers. U.S. Geological Survey Water Supply Paper.

Bustin, R. M. (1992), Organic maturation of the Western Canadian Sedimentary Basin, *Int. J. Coal Geol.*, 19, 319–358.

Cherry, J., and B. Parker (2004), Role of Aquitards in the Protection of Aquifers from Contamination: A "State of the Science" Report. AWWA Research Foundation, Denver, CO.

Conteras, I., A. T. Grosser, R. H. Ver Strate (2008), The use of the fully- grouted method for piezometer installation, Part 1, *Geotech. News*. June, 2008.

Dawson, F.M., C.G. Evans, R. Marsh, R. Richardson (2008), Uppermost Cretaceous and Tertiary Strata of the Western Canada Sedimentary Basin, In: Geological Atlas of the Western Canada Sedimentary Basin. G.D. Mossop and I. Shetsen (comp.). Canadian Society of Petroleum Geologists and Alberta Research Council, Special Report 4.
URL <http://www.ags.gov.ab.ca/publications/wcsb_atlas/atlas.html>, [August 1, 2012].

Duncan, J. M., and A. Bursey (2013), Soil Modulus Correlations. Foundation Engineering in the Face of Uncertainty, in 2013 GeoCongress, San Diego, CA, March 3-7, 2013; pp. 321-336. doi: 10.1061/9780784412763.026

Freeze, R.A., and J.A. Cherry (1979), Groundwater. New Jersey: Prentice Hall.

Garavito, A. M., H. Kooi, and C. E. Neuzil (2007), Numerical modeling of a long-term *in situ* chemical osmosis experiment in the Pierre Shale, South Dakota, Adv. *Water Resour*. *Res*., 29, 481-492.

GEO-SLOPE International Ltd. (2007) Seepage modeling with SEEP/W. An Engineering Methodology 2nd Edition. Calgary, AB.

Gercek, H. (2007), Poisson's ratio values for rocks, *Rock Mechanics and Mining Sciences*, 44, 1-13.

Gries, J. P., P. H. Rahn, and R. K. Baker (1976), A pump test in the Dakota sandstone at Wall, South Dakota. *South Dakota Geol. Survey, Circ*. 43, p. 9.

Hayes, B. J. R., J. E., Christopher, L. Rosenthal, G. Los, B. McKercher, D. Minkin, Y. M. Tremblay, and J. Fennel (1994), Cretaceous Mannville Group of the Western Canada Sedimentary Basin, in Geological Atlas of the Western Canada Sedimentary Basin. G.D. Mossop

and I. Shetsen (comp.), Canadian Society of Petroleum Geologists and Alberta Research Council, Available at http://www.ags.gov.ab.ca/publications/wcsb_atlas/atlas.html.

Hendry, M. J., and F. W. Schwartz (1988), An alternate view on the origin of chemical and isotopic patterns in groundwater for the Milk River aquifer, Canada, *Water Resour. Res*. 24, 1747-1763.

Hendry, M. J., and L. I. Wassenaar (1999), Controls on the distribution of major ions in pore waters of a thick surficial aquitard, *Water Resour. Res*., 36 (2), 503-513.

Hendry, M. J., S. L. Barbour, K. Novakowski, and L. I. Wassenaar (2013), Palaeo-hydrogeology of the Cretaeous sediments of the Williston Basin using stable isotopes of water, *Water Resour. Res*., 49, 4580-4592, doi: 10.1002/wrcr.20321.

Hendry, M.J., D.K. Solomon, M. Person, L.I. Wassenaar, W.P. Gardner, I.D. Clark, K.U. Mayer, T. Kunimaru, K. Nakata, and T. Hasegawa. 2015. Can argillaceous formation isolate nuclear waste? Insights from isotopic, noble gas, and geochemical profiles. *Geofluids* 15(3): 381-386. DOI: 10.1111/gfl.12132.

Hendry, M.J., D.K. Solomon, M. Person, L.I. Wassenaar, W.P. Gardner, I.D. Clark, K.U. Mayer, T. Kunimaru, K. Nakata, and T. Hasegawa (2015), Can argillaceous formation isolate nuclear waste? Insights from isotopic, noble gas, and geochemical profiles. *Geofluids* 15(3): 381-386. DOI: 10.1111/gfl.12132.

Johnston, P, P. Wu, and K. Lambeck (1998), Dependence of horizontal stress magnitude on load dimension in glacial rebound models, *Geophysical Journal International*, **132**, 41-60.

Khader, O. and K. Novakowski (2014), Impacts of Pleistocene glacial loading on abnormal pore-water pressure in the eastern Michigan Basin, *Geofluids*, 14(2), 200-220.

Mazurek, M., P. Alt-Epping, A. Bath, T. Gimmi, H. Niklaus Waber, S. Buschaert, P. De Cannière, M. De Craen, A. Gautschi, S. Savoye, A. Vinsot, I. Wemaere, and L. Wouters (2011), Natural tracer profiles across argillaceous formations, *Appl. Geochem*., 26, 1035-1064.

McKenna, G. T. (1995), Grouted-in installation of piezometers in boreholes, *Can. Geotech. J.*, 32, 355-363.

Mikkelsen, P. E. (2002), Cement-bentonite grout backfill for borehole instruments, *Geotech. News.* December 2002.

Mikkelsen, P. E., and G. E. Green (2003), Piezometers in fully grouted boreholes, in Symposium on Field Measurements in Geomechanics, FMGM. Oslo, Norway, September 2003.

Misfeldt, G. A. (1988), An interactive slope stability and groundwater flow analysis in the Hepburn landslide. M.Sc. Thesis, University of Saskatchewan.

Mitchell, J. K., and K. Soga (1993), Fundamentals of Soil Behavior 3rd Edition. John Wiley & Sons Inc., Hoboken, NJ.

Mondol, N. H., K. Bjorlykke, J. Jahren, and K. Hoeg (2007), Experimental mechanical compaction of clay mineral aggregates- Changes in physical properties of mudstones during burial, *Marine Petrol. Geol.,* 24, 289-311.

Neuzil, C.E., J.D. Bredehoeft, and R. G. Wolff (1984), Leakage and fracture permeability in the Cretaceous shales confining the Dakota Aquifer in South Dakota, *in* Proc. of the First C. V. Theis Conf. on Geohydrology, Oct. 5 - 6, 1982, Lincoln, NB, ed. by D. G. Jorgenson and D. C. Signor, National Water Well Assoc., Worthington OH

Neuzil, C. E. (1986), Groundwater flow in low-permeability environments. *Water Resour. Res.,* 22 (8), 1163–1195.

Neuzil, C. E. (1993), Low fluid pressure within the Pierre Shale: A transient response to erosion. *Water Resour. Res*., 29, 2007–2020.

Neuzil, C. E. (1994), How permeable are clays and shales? *Water Resour. Res*., 30, 145–150.

Neuzil, C.E. (2012), Hydromechanical effects of continental glaciation on groundwater systems. *Geofluids*, 12, 22-37.

Neuzil, C., and D. Pollock (1983), Erosional unloading and fluid pressures in hydraulically ‘tight’ rocks. *J. Geol*., 91, 179-193.

Nurkowski, J. R. (1984), Coal quality, coal rank variation and its relation to reconstructed overburden, Upper Cretaceous and Tertiary plains coals, Alberta, Canada. *AAPG Bull.*, 68, 285-295.

Palombi, D. (2008), Regional Hydrogeological Characterization of the Northeastern Margin in the Williston Basin. M.Sc. Thesis, University of Alberta.

Pusch, R. (2001), The Buffer and Backfill Handbook: Part 2: Materials and techniques. Technical Report TR-02-12. Svensk Kärnbränslehantering AB. Swedish Nuclear Fuel and Waste Management Co., Stockholm, Sweden.

Schmeling E. E. (2014), Characterization of the hydrogeology and solute transport in a geologically complex, fractured, late-Cretaceous shale, Fort a la Corne Kimberlite Field, Saskatchewan, Canada. M.Sc. Thesis, University of Saskatchewan.

Smerdon, B. D., L. A. Smith, G. A. Harrington, W. P. Gardner, C. Delle Piane, and J. Sarout (2014), Estimating the hydraulic properties of an aquitard from *in situ* pore pressure measurements, *Hydrogeol. J.*, 22(8), 1875-1887, DOI: 10.1007/s10040-014-1161-x.

Smith L. A., G. van der Kamp, and M. J. Hendry (2013), A new technique for obtaining high-resolution pore pressure records in thick claystone aquitards and its use to determine *in situ* compressibility, *Water Resour. Res.*, 49, 732-743, DOI:10.1002/wcwr.20084.

Terzaghi, K. (1943), Theoretical Soil Mechanics. John Wiley & Sons, New York, pp. 265-290.

van der Kamp, G., H. Maathuis, W.A. Meneley (1986), Bulk permeability of a thick till overlying a buried-valley aquifer near Weyburn, Saskatchewan. Proceedings of the Third Canadian Hydrogeological Conference, Saskatoon, April 20 - 23, IAH Canadian National Chapter, pp. 94-99.

van der Kamp, G. (2001), Methods for determining the *in situ* hydraulic conductivity of shallow aquitards - an overview. Hydrogeol. J., 9, 5–16.

Vaughan, P. R. (1969), A note on sealing piezometers in boreholes. Geotechnique, 19 (3), 405-413.

5.0 *IN SITU* HYDROGEOLOGIC PROPERTIES OF ARGILLACEOUS FORMATIONS IN THE WILLISTON BASIN DETERMINED FROM GROUTED-IN PRESSURE TRANSDUCERS

PREFACE

This chapter addresses Objective 3 of the thesis: to generate a detailed data set of hydrogeologic parameters of argillaceous aquitards in the WB to evaluate the potential of grouted-in VWPs for determining *in situ* parameters (m_v and K_h) of aquitards. The methods developed in the previous two chapters were applied to an additional 27 transducers installed at a second site (Site 2) in the Williston Basin for the purposes of determining the consistency of the methods between sites and to develop a database of *in situ* parameters of argillaceous aquitards.

The chapter is intended for submission as a journal article to Hydrogeology Journal.

5.1 SUMMARY

Determining the *in situ* hydrogeologic parameters of aquitard formations is difficult due to various challenges associated with studying formations with low hydraulic conductivity (K). Recently, fully-grouted vibrating wire pressure transducers (VWPs) were used to characterize the *in situ* horizontal hydraulic (K_h) and geotechnical (compressibility) properties of overconsolidated aquitard formations by analyzing the pore pressure responses after installation, and responses due to barometric pressure fluctuations. To date, the VWP methods yielded promising results, but the application of the method has been limited. Here we present the results from 27 VWPs installed in overconsolidated argillaceous glacial till and claystone formations located near the center of the Williston Basin (Site 2) to augment the results obtained from 10 VWPs installed at a previously studied site near the north eastern portion of the Williston Basin (Site 1). The results of the VWPs installed at Site 2 were consistent with the results obtained from Site 1, and indicate the method could be a useful tool to characterize the hydrogeology of aquitard formations. In addition, installing multiple VWPs in the same borehole provides a natural analogue to a laboratory consolidation test. For this reason, it was possible to evaluate if the pattern of decreasing 1-D constrained compressibility (m_v) with depth in the field could be reconciled to the stress behaviour observed in the laboratory. Using the laboratory determined compression (Cc) and recompression (or swell, Cr) indices during conventional 1-D

consolidation tests, the m_v was calculated at multiple effective stresses (σ`). A sensitivity study showed that relative to Cr, varying the values of Pc', Cc or e had a minor influence on these profiles, and provided the Cr was adjusted accordingly, the stress behaviour was consistent with *in situ* observations.

5.2 INTRODUCTION

Low-hydraulic conductivity ($K \leq 10^{-8}$ ms^{-1}) argillaceous sediments (clay-rich aquitards) are globally widespread, making up 2/3 of all sedimentary rocks on Earth. Characterizing the hydrogeologic properties of these aquitards is important to understand the sources and distribution of natural resources in sedimentary basins, which contain the largest repositories for oil and gas in the world, as well as contain extensive evaporite deposits (potash, anhydrite, halite, etc.). These claystone aquitards (commonly referred to as shales) can also act as caprock formations restricting oil or gas migration to surface or into overlying shallow aquifers during unconventional resource extraction processes (e.g., steam-assisted gravity drainage and cyclic steam stimulation). Moreover, the low-K and high sorption capacity of thick basinal aquitards make them possible host formations for the sequestration of hazardous wastes (Hendry et al., 2015; Neuzil, et al. 2013; Mazurek et al., 2011).

Groundwater flow and contaminant transport through high-K units (aquifers) in sedimentary basins have been characterized using both hydraulic and chemical analysis, but few studies have investigated flow and transport through aquitards. The difficulties associated with estimating *in situ* hydrogeologic parameters of low-K argillaceous formations is discussed by several authors (Neuzil, 1986; Corbet and Bethke, 1992; van der Kamp, 2001; Smith et al., 2013; Smith et al., 2016). Conventional laboratory testing of core samples generally overestimates the one dimensional (1-D) constrained compressibility (m_v), and underestimates K by orders of magnitude (e.g. van der Kamp and Schmidt, 1997; Smith et al., 2013). Traditional field based methods, such as pumping or slug tests to determine K in low-K formations require long time periods to perform, making these conventional *in situ* tests impractical in aquitards. For this reason, various field based methods with faster response times have been developed, all of which have advantages and disadvantages. A summary of these methods is presented in Batlle-Aguilar et al. (2016). These field based methods include the use of multi-port packers (Beauheim et al., 2014; Roberts et al., 2011), piezometers embedded in sand packs (Neuzil, 1993) and fully-

grouted vibrating wire piezometers (VWPs) (Smerdon et al., 2014; Smith et al., 2016). A particular advantage of using fully-grouted VWPs is their ease of installation. Provided the K of the grout mixture is within three orders of magnitude greater than that of the adjacent aquitard (Vaughn, 1969, Contreras, 2008), installation of several VWPs within a drill hole can be carried out in a few hours. Further, fully-grouted VWPs can also be used to determine *in situ* bulk compressibility (i.e. α) from measured values of m_v, if a Poisson's ratio is assumed. To date, the VWP methods have yielded promising results, but has been limited to few sites. Fully-grouted VWPs have the potential to become a widely used method to determine *in situ* m_v and K_h of low-K aquitards, but application of these methods in various geomedia is required to determine the success and consistency of the method.

The goal of the current study was to improve upon our understanding of geotechnical and hydraulic properties of argillaceous aquitards by using VWPs to determine *in situ* m_v and K_h values from argillites in the Williston Basin (WB). The specific objectives of this study were to: (1) determine K_h and m_v using pore pressure recoveries and barometric loading efficiencies (respectively) from 27 VWPs installed in overconsolidated till and shale at a site near the center of the WB (referred to as Site 2) to augment the results obtained from 10 VWPs installed at a previously studied site near the north eastern portion of the WB (Site 1, Smith et al., 2013; Smith et al., 2016), to assessing the consistency of the results obtained by these methods through argillaceous glacial till and shale; (2) evaluate how m_v for similar lithologies can be related to stress history and current *in situ* stress levels to determine if the stress behaviour observed during laboratory testing can be applied to *in situ* observations; and (3) evaluate how the *in situ* results from Objective 1 compare to previous work summarizing values of m_v and K of argillaceous formations. The transducers at Site 1 were used to develop *in situ* methods to obtain *in situ* m_v, and K_h measurements at the location of each transducer (Smith et al., 2013; Smith et al., 2016). As such, m_v and K_h data from Site 1 are published, although the impact of *in situ* stress on m_v has not been presented previously, and neither has the data obtained from the 27 transducers at Site 2. The findings of this study have widespread implications because the data sets collected using these methods could help constrain aquitard parameters through similar deposits in other sedimentary basins worldwide.

5.3 MATERIALS AND METHODS

The following section provides a description of the materials and methods used to produce the data sets in §5.4. Sections 5.3.3-5.3.6 present a cursory overview of the methods either developed or described in Smith et al., 2013 and Smith et al., 2016) for Site 1. As such, the methods used to collect the data for Site 1 (transducer installation and core sampling, analysis of pore pressure data for m_v, pore pressure recovery for K_h and 1-D consolidation testing) were published in Smith et al. (2013) and Smith et al (2016). Further information and description of these methods can be found in these publications.

5.3.1 Geologic Setting

The WB is a sedimentary basin within the Western Canada Sedimentary Basin (WCSB) (Figure 5.1a). The WCSB is essentially a wedge of sub-horizontal sedimentary rock that progressively thins from 5,500 m under the Rocky Mountains to 0 m near the eastern margins. The WB underlies approximately 250,000 km^2 of North Dakota, South Dakota, Montana, Manitoba, and Saskatchewan (Vigrass, 2006). The sedimentary rocks in the WB range from Cambrian to late Tertiary and can be divided into two main divisions: a lower succession of Cambrian to Jurassic age formations that are predominantly carbonate rocks and formed before the major uplift of the Canadian Cordillera; and an upper succession of mid-Jurassic to Tertiary aged rocks of predominantly shale and sandstone deposited following the uplift in the Cordillera. The upper succession is typically covered by glacial drift deposited during the Pleistocene Epoch (2 Ma- 11,000 years BP). The carbonate rocks in the lower succession make Canada the world's leading producer of evaporite minerals (anhydrite, halite and potash) (Jasinski, 2010), while the upper succession contains one of the world's richest reserves of petroleum and natural gas.

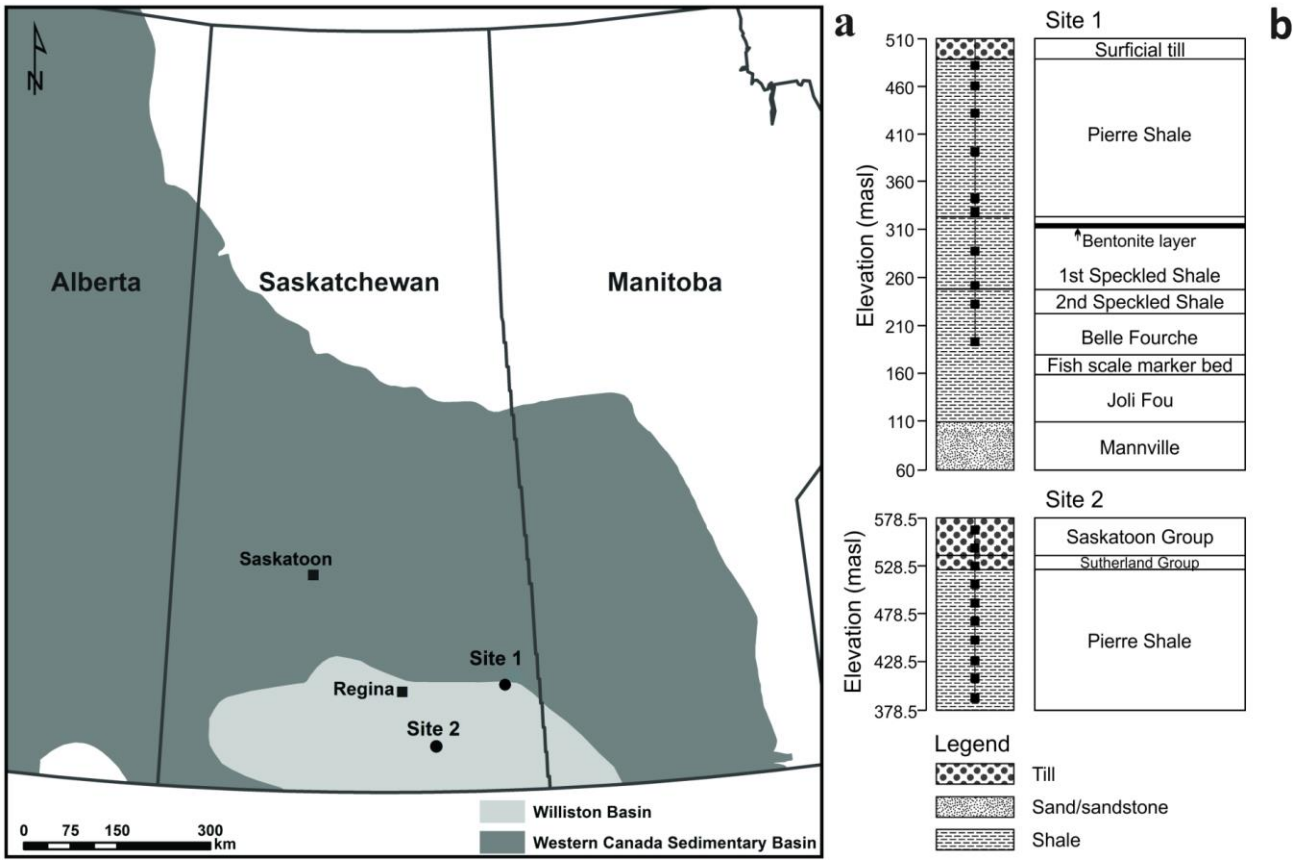

Figure 5.1: Map of the eastern portion of the WCSB through Saskatchewan and Manitoba, as well as the Canadian portion of the WB (a). The locations of Site 1 and Site 2 are shown on the map and the corresponding stratigraphic sections of each borehole are illustrated with transducer locations identified by a black square (■) (b). Only one of the five boreholes from Site 2 is presented here and although the till/shale contact varies from 35-70 m BG at Site 2, this profile is intended to illustrate the high frequency of VWP installations through both the till and the Pierre Shale.

5.3.2 Study sites

Site 1 is located on the northeast edge of the WB where the surficial till is thin (<10 m) relative to other regions in the basin (Figure 5.1a). This site was the focus of multiple publications dedicated to understanding the hydrogeology and paleohydrogeology of the extensive Cretaceous Shales in the WB (Hendry et al., 2013; Hendry and Harrington, 2014), and to develop alternative methods to characterize the hydrogeologic parameters (m_v and K_h) of thick aquitard sequences (Smith et al., 2013; Smith et al., 2016). The latter publications provide rare data sets of high resolution *in situ* m_v (and subsequently, bulk compressibility, α) and K_h measurements obtained from deep (25-325 m BG) grouted-in pressure transducers. Site 2 is located approximately 350 km southwest of Site 1 closer to the center of the basin (Figure 5.1a),

where both the surficial till and underlying Pierre Shale are considerably thicker (Figure 5.1b). The Mannville Group is a regionally extensive aquifer and a convenient stratigraphic reference to correlate the two sites (and other formations) across the WB. In addition, it can also play a central role in the hydraulic head distribution through the shale (Smith et al., 2016).

5.3.3 Drilling, sampling, and transducer installation

A single borehole was continuously cored at Site 1 in 2009 (total depth: 325m BG) and five boreholes were continuously cored at Site 2 between 2012-2014 (total depth: 100-200 m BG). The five boreholes at Site 2 were within a 180 km^2 area and although the formations were the same, the depth to the till/shale contact varied from 35-75 m BG. The porosity of core samples collected at the depth of each VWP were measured according to ASTM D4531-86 (n=10 from Site 1; n=27 from Site 2). Porosity values are required to calculate m_v and K_h and is a parameter often used in the literature to correlate with K and α. Additional core samples were collected for 1-D consolidation testing (ASTM D2435-04, n=9 from Site 1). Samples were trimmed in the field to remove drill mud and then either vacuum sealed at site, or wrapped in cellophane and masking tape before being coated repeatedly (5-6 times) in paraffin wax. Core samples were stored between 10 and 15ºC until analysis.

Nested Geokon VWPs (n=3-10) were installed in 5 boreholes at the two sites (Figure 5.1b) to measure absolute fluid pressure. The scale of the Geokon VWPs ranged from -0.1 to 0.35, 0.7, 1, 2, and 3 MPa (absolute accuracy of ± 0.1% full scale (FS) and resolution of ± 0.025% FS). At both sites, the transducers were attached to the outside of a steel tremie pipe and lowered into the borehole. A bentonite/cement grout mixture was pumped down the tremie pipe until grout returned to surface, indicating the entire borehole was filled with grout and the transducers were secured in place. The grout used at both sites was a mixture of 4% bentonite-96% cement. It was regularly tested during installation to ensure the specific gravity was approximately 1.7 (density of 1700 kg m^{-3}). Samples of the grout were collected as the VWPs were installed at both sites for triaxial testing at both sites for K_v. Once in place, the transducers were connected to an automated data acquisition systems and programmed to measure pressure and temperature at intervals between 10 and 60 min. A barologger was installed at ground surface at each site to measure barometric changes at surface with the same time stamp as the transducers.

5.3.4 Analysis of pore pressure data

The γ of the aquitard was determined by analyzing the pore pressure responses to known barometric fluctuation as described in Smith et al. (2013). Values of m_v, α, and specific storage (S_S) were then calculated for each VWP location at Site 1 and Site 2. For example, m_v was calculated using (van der Kamp and Gale, 1983):

[5.1] $$m_v = \frac{\gamma n \beta}{1-\gamma}$$

where *n* is porosity, and β is the bulk compressibility of water (4.6×10^{-7} kPa^{-1}). The value of m_v can then be converted to a constrained modulus ($M=1/m_v$) and then to a bulk modulus (B) by assuming a Poisson's ratio of 0.33 (based on published estimates for shales) and the following relationship (Duncan and Bursey, 2013):

[5.2] $$B = \frac{M}{3}\frac{(1+v)}{(1-v)}$$

where *v* is Poisson's ratio. The inverse of B is bulk compressibility (α, kPa^{-1}). A Poisson's ratio (υ) of 0.33 for shales was chosen based on a range of literature values for claystones (Gercek, 2007). Specific storage (S_S) was then calculated using:

[5.3] $$S_S = \rho g(n\beta + \alpha)$$

where ρg is the unit weight of water (9.8 kN m^{-3}).

5.3.5 Recovery modeling for K_h

A commercial, 2D axisymmetric, finite element model (SEEP/W, Geo-Slope International, 2012) was used to simulate the pore pressure recovery recorded by each transducer. The initial pore pressure was defined by the measured pore pressure following setting of the grout, and the far field head boundary was defined from the pore pressure following recovery (t=365 days). The α of the grout (n=1) was determined on core/grout samples in the laboratory assuming a Poisson's ratio of 0.21. The α of the aquitards were determined from the pore pressure analysis described in § 5.3.4, assuming a Poisson's ratio of 0.33. The *in situ* K_h was determined by varying the K systematically until an optimum visual fit to the transducer data was achieved. Because the grout was not loaded to *in situ* pressures during laboratory testing and only two samples were analyzed, simulations were conducted to assess the sensitivity of the pore pressure recovery to the compressibility of the grout by varying α by over

one order of magnitude from the laboratory determined value (4.8×10^{-5} kPa^{-1}). Additional information regarding sensitivity and calibration of the model is discussed in Smith et al. (2016).

5.3.6 1-D consolidation tests

Core samples collected from Site 1 were submitted for 1-D consolidation tests in 2010. These tests were conducted on samples obtained from depths of 47.4, 87, and 128.4 m (Pierre Shale), 174.1, 184.9, 212 and 249 m (1st Speckled Shale), 283.6 (2nd Speckled Shale) and 307 m (Belle Fourche Shale) [ASTM D2435-04, ASTM, 2011]. After collection, the samples were immediately vacuum sealed at site and stored at 12°C prior to analysis. Each specimen was 63.3 to 63.5 mm in diameter and 12.5 to 13 mm in height. Incremental loading stages (n=13) lasting 10-12 hr were applied to each specimen, increasing from approximately 0.06 to 31 MPa. The m_v calculated from the load-deflection data collected during oedometer testing was converted to α based on the relationships described by Duncan and Bursey [2013]. A value of 0.33 for Poisson's ratio was used to calculate the α.

5.4 RESULTS AND DISCUSSION

The thickness of the glacial till and Pierre Shale Fm at the two sites vary from 10-54 and 175-500 m, respectively. The Mannville Group is about 600 m deeper at Site 2 than at Site 1. As such, the m_v and K_h data collected from the transducers installed at Sites 1 and 2 are plotted in Figure 5.2 as distance above the Mannville Group and as depth (m) below ground. These data are also summarized in Table 5.1. The compiled data provides a profile of the various *in situ* hydrogeologic parameters of till and shale aquitards above the Mannville.

5.4.1 Lithology

The glacial till present at both sites is often referred to as Quaternary drift. The Quaternary drift is composed of the Sutherland Group and the Saskatoon Group, which are difficult to differentiate using only lithology. Both groups are composed of overconsolidated silt and clay with various accumulations of coarser and finer fractions. Generally, the two groups are differentiated based on laboratory testing (e.g. carbonate content, Atterberg limits, preconsolidation pressure) and geophysical signatures (c.f. Christensen, 1968a and b; Christensen, 1970; Christensen, 1992). The Pierre Shale at both sites was primarily grey-dark grey, non-calcareous, over consolidated silt and clay. Shell fragments, fossils, and pyrite mineralization were observed at various horizons. Thin layers (< 5 cm) of bentonite are common

throughout the Pierre Shale. Both the 1st and 2nd Speckled Shale are calcareous mudstone with abundant coccoliths and coccospheres producing a 'speckled' appearance. There are also minor amounts of bentonite, fossils, and concretions in both formations, and are often only distinguished by the high total carbon content and hydrogen indices of the 2nd Speckled Shale. Both the Belle Fourche and Joli Fou Formations are composed of greyish black shale, and are separated by a marker bed at the base of the Belle Fourche known as the 'fish scales zone'. The Mannville Group is generally divided into an upper and lower portion. The upper zone is composed of interbedded marine shale and sandstone and the lower zone is composed of interbedded continental sand and shale.

The total porosity (*n*) values estimated from the core samples at Sites 1 and 2 are consistent, albeit decreasing slightly, with depth (Figure 5.2 and 5.3). The mean *n* of Site 1 and Site 2 are 0.33±0.04 (n=45), and 0.33±0.02 (n=28), respectively. Both estimates are consistent with measured values from the Lower Colorado shales near the Fort ala Corne forest 160 km north of Saskatoon (mean=0.33±0.05; Schmeling, 2013), a value of 0.34 for the Pierre Shale in South Dakota (Neuzil, 1993), and an approximate value of 0.31 for the Pierre Shale in South Dakota (Bredehoeft, 1983). In geotechnical engineering α and K are often related to e (i.e. volume of voids / volume of solids). The *n* values were converted to void ratio (e), and the mean e of Site 1 and Site 2 are 0.49±0.1 (n=45), and 0.49±0.05 (n=28), respectively (Figure 5.3). The bulk density of the shales from both sites are consistent with one another with averages of 1.79±0.1 and 1.77±0.05 from Site 1 and Site 2, respectively. The liquid limits (LL) determined for the Pierre Shales at both Site 1 and Site 2 are also presented in Figure 5.3. While there is some variance between sites, they follow a similar trend with depth, and would suggest that the shales at the two sites are similar, though not identical. The LL at Site 1 ranges from 38-152%, and the LL at Site 2 ranges from 58-144%.

Table 5.1: Transducer determined ranges of hydrogeologic parameters from Site 1 and 2 in the WB

Material	Porosity * (-)	Loading efficiency (-)	Compressibility (kPa^{-1})	Specific Storage (m^{-1})	Hydraulic Conductivity (ms^{-1})
Glacial Till (n=11)	0.27 - 0.37	0.45 - 0.92	0.31 - 1.9 E-06	0.27- 2.0 E-05	1.2 - 6.9 E-12
Shale (n=26)	0.24 - 0.36	0.53 - 0.93	0.16 - 2.5 E-06	0.30 - 2.6 E-05	0.035 - 4.6 E-11

* Laboratory determined total porosity

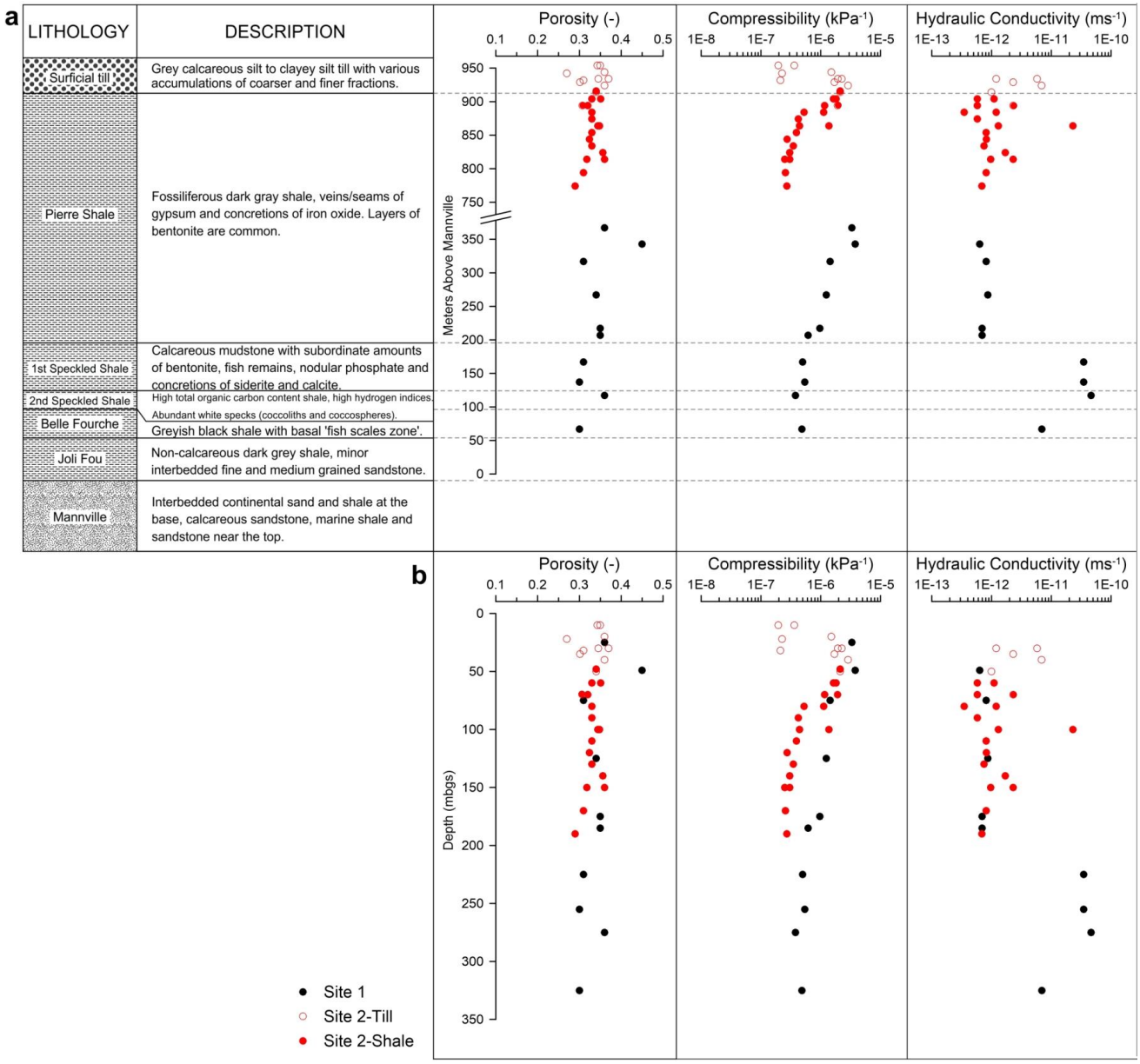

Figure 5.2: Stratigraphy and description of each formation compiled from the geologic logs from Site 1 and 2, along with the laboratory determined porosity, and transducer determined results (α, S_S, and Kh) plotted by depth relative to the Mannville Group (a) and depth below ground (b). A break in the vertical axis removes 400 m of Pierre Shale where no transducers were installed (a).

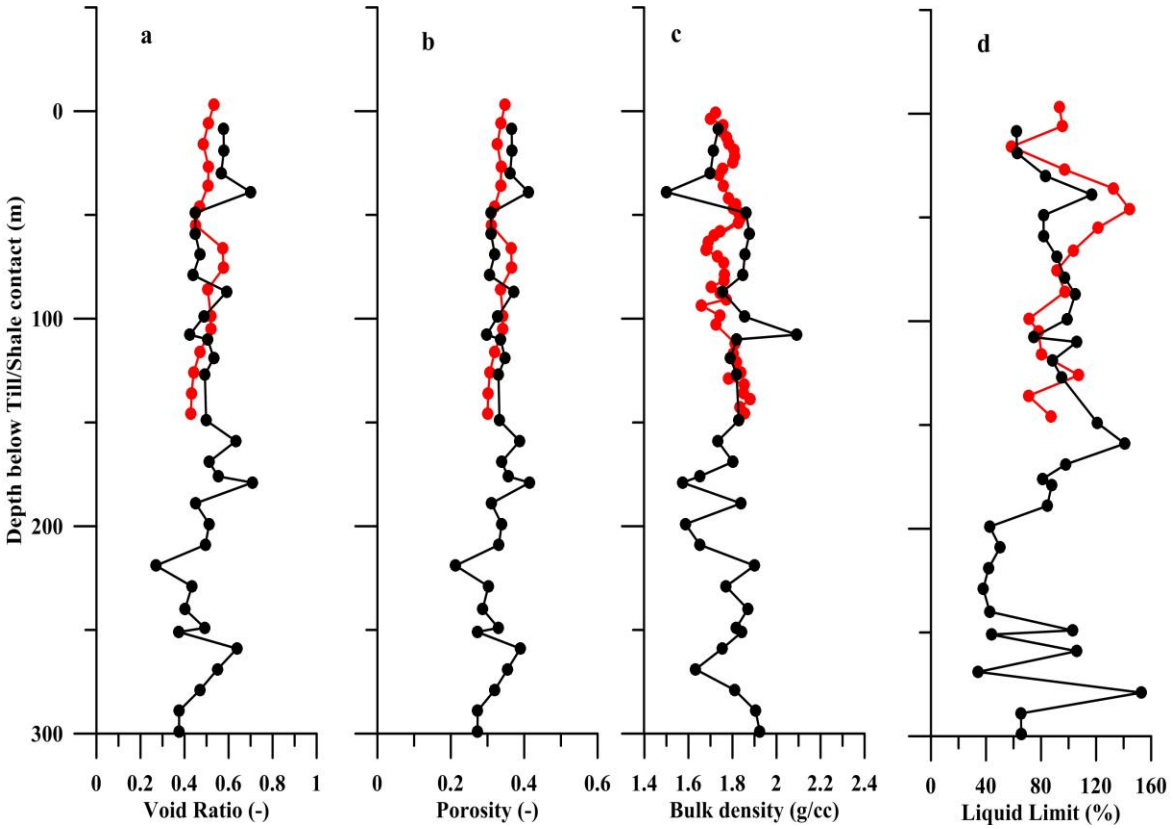

Figure 5.3: Void ratio, total porosity (*n*), bulk density, and liquid limit of the Cretaceous Shale at Site 1 (black circles) and Site 2 (red circles) plotted by depth below the till/shale contact.

5.4.2 Compressibility

With the exception of the shallow transducers installed in the Saskatoon Group till at Site 2, α generally decreases with increasing depth at both sites (Figure 5.2). Given the similar lithology and geotechnical parameters with depth (Figure 5.3), this trend is attributed to the increasing effective stresses (σ') with depth. Some of the transducers within the till at Site 2 yielded low values of α that could be the result of weathering and consolidation of the material. The *in situ* α for the shale from Site 1 and 2 span about one order of magnitude, ranging from 3.0×10^{-6} to 2.0×10^{-7} kPa^{-1}. The *in situ* α for the till at Site 2 ranged from 3.1×10^{-7} to 1.9×10^{-6} kPa^{-1}. The results also indicate that the Pierre Shale at Site 2 is less compressible then the Pierre Shales at Site 1 by about half an order of magnitude. The two sites are separated by approximately 350 km and Site 2 is located near the center of the WB, while Site 1 is located on the edge of the basin. It is possible that slight differences in the evolution of the basin at each site (i.e. thicknesses of the overburden, glacial loading/unloading) could have some affect on the current *in situ* m_v.

The laboratory determined α for Site 1, taken at stress levels similar to those associated with the same depth, were about one order of magnitude greater than the observed *in situ* α values, ranging from 2.5×10^{-5} to 1.2×10^{-6} kPa^{-1}. Determining α from core samples using traditional laboratory methods introduces multiple sources of error that cannot always be accounted for in the results and likely contributes to underestimating stiffness. Core samples removed from the subsurface undergo unavoidable disturbance as a result of stress changes during collection, and possible damage due to moisture loss or sample transport (Clayton et al., 1995). Even if there is no damage to the sample after collection, structural disturbances during drilling can increase the α of the sample (Klohn, 1965; Radhakrishna and Klym, 1974).

5.4.2.1 Laboratory compression indices (Cc and Cr)

As illustrated by 1-D consolidation tests, the m_v of a sample will decrease with increasing stress levels and is also dependent on the stress history of the sediments (Terzaghi, 1943). Because soils are not perfectly elastic, the deformation behaviour observed during the sequential incremental loading of a sample to levels that exceed the expected *in situ* σ', depends on the stress history of the material. These tests provide information needed to calculate two compression indices. The compression index (Cc) is the slope of the e-log(σ') curve during the first loading of the sample or the slope when the sample is re-loaded to stresses higher than it has previously experienced in its stress history. The recompression (or swell) index (Cr) is obtained from the slope of the e-log(σ') during unloading (or reloading at stress less than the preconsolidation stress). The preconsolidation pressure (P_C') is estimated using a curve fitting method (Casagrande, 1936) and represents the maximum vertical σ' the sample has experienced prior to sampling. If the *in situ* σ' is less than the P_C' then the sample is considered to be overconsolidated, the degree of which can be described using the overconsolidation ratio ($OCR=P_C'/\sigma'$). An OCR > 1 would indicate an overconsolidated sediment, such as might occur due to glacial loading then unloading, or as a result of removal of overlying sediments following deposition as a result of erosion. The OCR's calculated for the laboratory consolidation tests range from 1.05-8.08 (average=3.0±2.1) and indicate they are all overconsolidated. Generally, the OCR's increase with depth.

Theoretically, core samples of similar texture collected from the same borehole (or location) should follow a similar loading curve if they've experienced the same stress history. The results of a representative consolidation test conducted on a core sample of the Pierre Shale

(185 m BG) obtained from Site 1 is illustrated in Figure 5.4. The slope of the compression line and the recompression line are identified, as well as the process of determining the P_C' using Cassegrande's method. The C_C calculated for each test ranged from 0.1 to 0.5 with an average of 0.27±0.1. The Cr for all of the samples except 212 m ranged from 0.03 to 0.07 with an average of 0.04±0.02, and approximately 10% of the estimated Cc for each test. Although it is unknown why the recompression curve of the sample from 212 m BG did not follow an expected trend, it is possible that testing errors, differences in material, or damage to the sample were the cause. No corrections were applied to account for sample disturbance. The Cc and Cr compression indices are consistent with those measured by Smith (1978) for undisturbed core samples of Pierre Shale in Colorado of 0.34 and 0.026, respectively; and by Peterson (1958) for similar hard shale samples from the Bearpaw Fm in southern Saskatchewan of approximately 0.68 and 0.06, respectively.

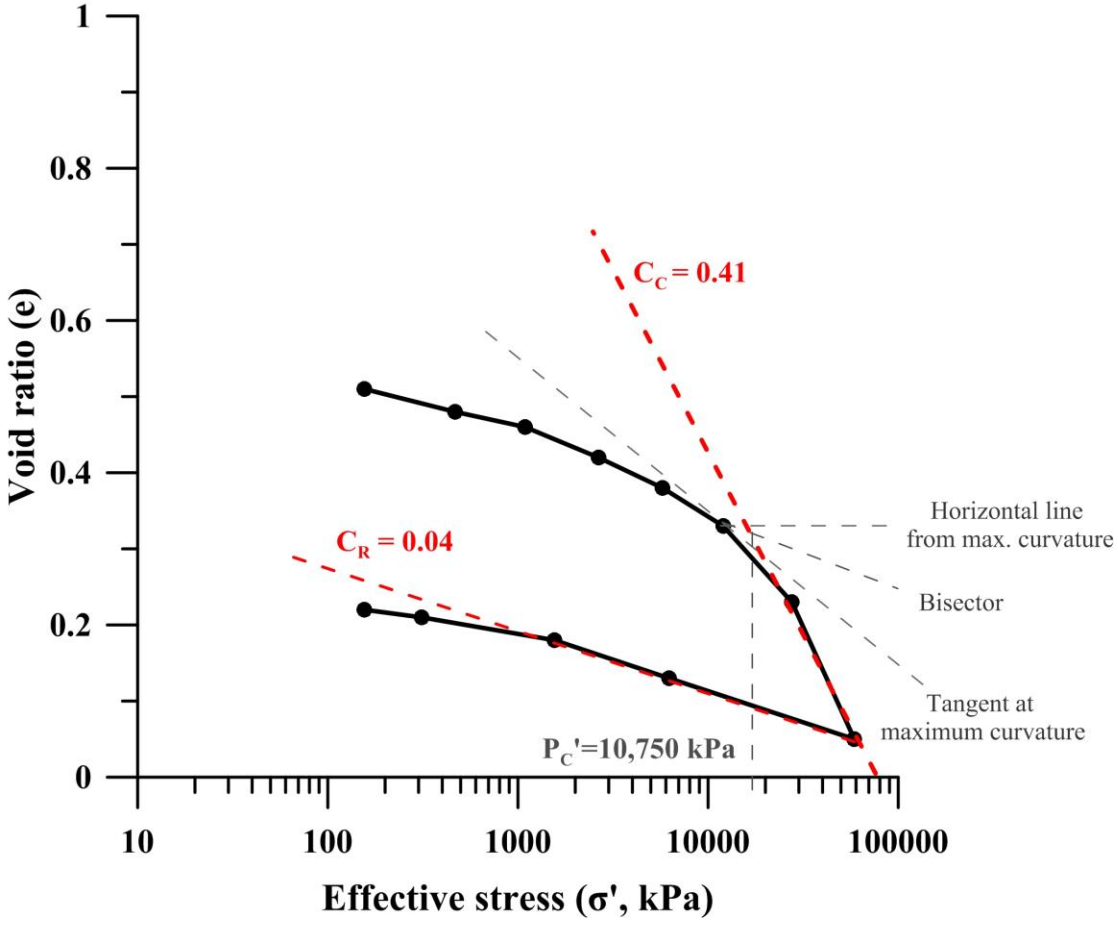

Figure 5.4: 1-D consolidation test results of a core sample obtained from the Pierre Shale at Site 1 (185 m BG) (black solid line). The slope of the compression line (Cc) and recompression line

(Cr) are identified by dashed red lines. Cassegrande's method to determine preconsolidation pressure (Pc') is illustrated in grey dashed lines (Cassegrande, 1936).

5.4.2.2 Applying laboratory stress behaviour to *in situ* stress behaviour

Even though the values of m_v and the compression indices are known to be different between laboratory tests and *in situ* observations, it should still be possible to evaluate whether the pattern of decreasing m_v with depth as observed in both laboratory tests and the *in situ* m_v measurements can be reconciled. The installation of multiple VWPs in the same borehole provides a natural analogue to a laboratory consolidation test in which the samples from different depths are loaded to pre-consolidation conditions and then allowed to rebound during unloading to stress levels representative of the *in situ* conditions for the sample. A comparison between the stress behaviour observed *in situ* vs the laboratory can provide insight as to whether the pattern of m_v with depth, as observed from the *in situ* measurements, is consistent with the known dependency of compressibility on *in situ* stress level and stress history.

This comparison was undertaken by calculating the *in situ* m_v of the laboratory and *in situ* samples using the following procedure. The observed pre-consolidation pressures from the laboratory samples were used to estimate a profile of pre-consolidation pressures increasing linearly with depth. This pre-consolidation profile would represent a stress history in which sediment previously present at the site was removed. The e of the samples at a range of depths when loaded to the Pc' value were calculated using a single value of Cc and an initially assumed e and σ'. The value of Cc assumed in this analysis was 0.27. The e of each of these samples under their current effective stress were then be calculated based on an assumed value of Cr. The values of Cr were selected to ensure that the final void ratios were in the range observed for both the field and laboratory data sets. For example, using e similar to those determined from core samples, the average Cr (0.04) determined from the laboratory tests was superimposed on a plot of field e vs. σ' as shown in Figure 5.5. Because the void ratios are uniform with depth through the Pierre Shale at both sites, the Cr slope will be shallow; however, the transposed Cr slope determined from the laboratory tests is reasonably consistent with the *in situ* data.

The compressibility at the *in situ* (or final laboratory) stress levels were then be estimated by calculating the coefficient of compressibility (A_v, kPa^{-1}):

[5.4] $$A_v = 0.434\frac{C_r}{\sigma'}, \text{ and}$$

[5.5] $$m_v = \frac{A_v}{1+e_o}$$

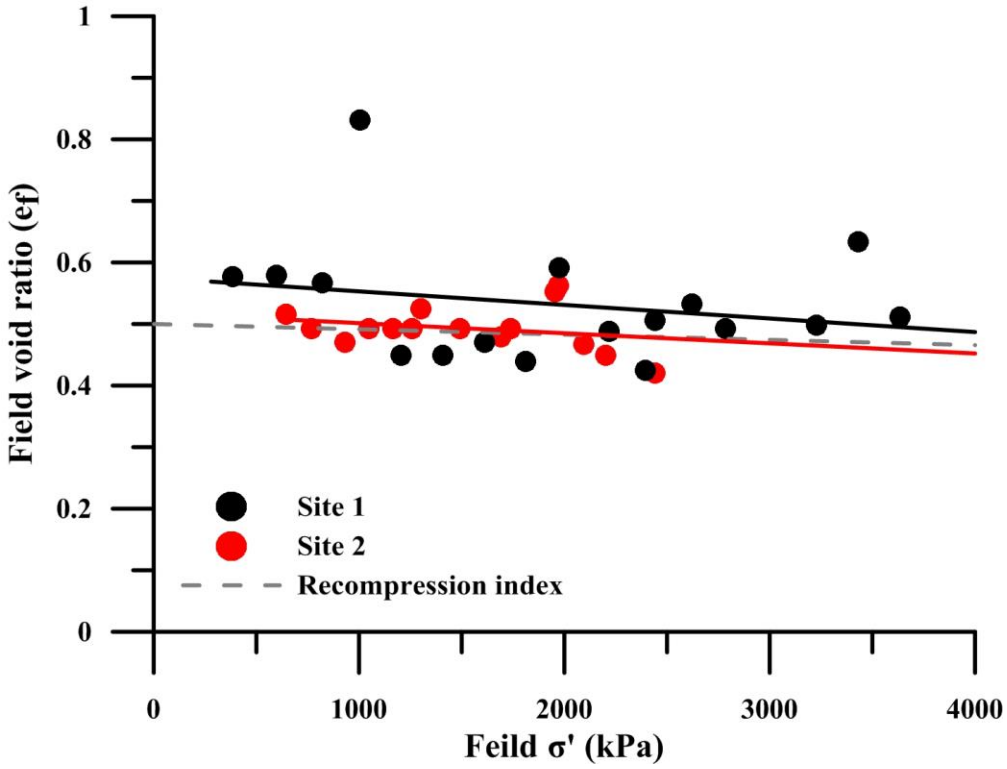

Figure 5.5: Field e vs field σ' for the Pierre Shale at Site 1 (red) and Site 2 (black) and linear relationships illustrated by solid red and black lines, respectively. The recompression trend (Cr) from the consolidation tests was superimposed using e's consistent with the field (grey dashed line).

The calculated values of compressibility are plotted along with the measured field and laboratory values in Figure 5.6. The shaded envelope of calculated values was obtained by varying the value of Cr over a relatively small range for each site and the laboratory data. The values of Cr assumed for the laboratory tests (0.02-0.06) were in the same range as observed in the laboratory testing. However, the range of Cr values for each of the sites was much lower than the laboratory values; specifically, 0.005 - 0.01 for Site 1 and 0.001-0.003 for Site 2. A sensitivity study highlighted that varying the values of Pc', Cc or e have relatively minor influence on these profiles relative to Cr.

The reason why such a low range of Cr is required to fit the *in situ* data is not known; however, Peterson and Peters (1963) observed that laboratory tests on clay shale in southern Saskatchewan did not provide good correlation with observed field behaviour. Clay structure and diagenetic bonds appear to be an important factor to consider regarding the swell behaviour of the material (Bjerrum, 1967; Smith 1978). Smith (1978) measured Cc and Cr of undisturbed and remoulded core samples from various shale formations in the UK and North America. The Cc

and Cr of the undisturbed samples were consistently lower than the remoulded core samples. The author suggests that when an undisturbed sample is consolidated, the diagenetic bonds are destroyed in proportion to their strength and the applied pressure, where as the bonding in a remoulded sample is already destroyed (Smith, 1978). Therefore, it would follow that samples that have undergone some amount of disturbance would result in the breaking of diagenetic bonds or clay structure, resulting in a larger Cc and Cr. Further, the LL at both sites vary by up to 120% with depth, which may play an important role. Typically, Cc and Cr both increase with increasing LL. Applying laboratory determined compression indices to *in situ* observations assumes that the Cr in the field is representative of the Cr calculated in the laboratory. It is possible that the Cr in the field is much lower due to a lower overall LL, that was not captured in the small core samples.

The advantage of having both field and laboratory m_v (α) data is the ability to compare not only the results of the two methods, but to determine if the deformation behaviour is similar for comparable materials. It is important to note that all of the laboratory samples used to constrain Cr were obtained from the Cretaceous Shales at Site 1, and while similar to the shales at Site 2, they do differ slightly in lithology (i.e. LL, mineralogy, etc.). Regardless, the primary goal was to determine if the stress behaviour observed from the laboratory tests would highlight a pattern (predicted m_v with depth) that could be applied to the *in situ* results at both sites. Admittedly, it is a challenge to definitively state why the Cr required to produce a range of m_v values consistent with the *in situ* observations. However, it appears that the stress behaviour (and resulting trend) determined in the laboratory can be applied to both Site 1 and Site 2.

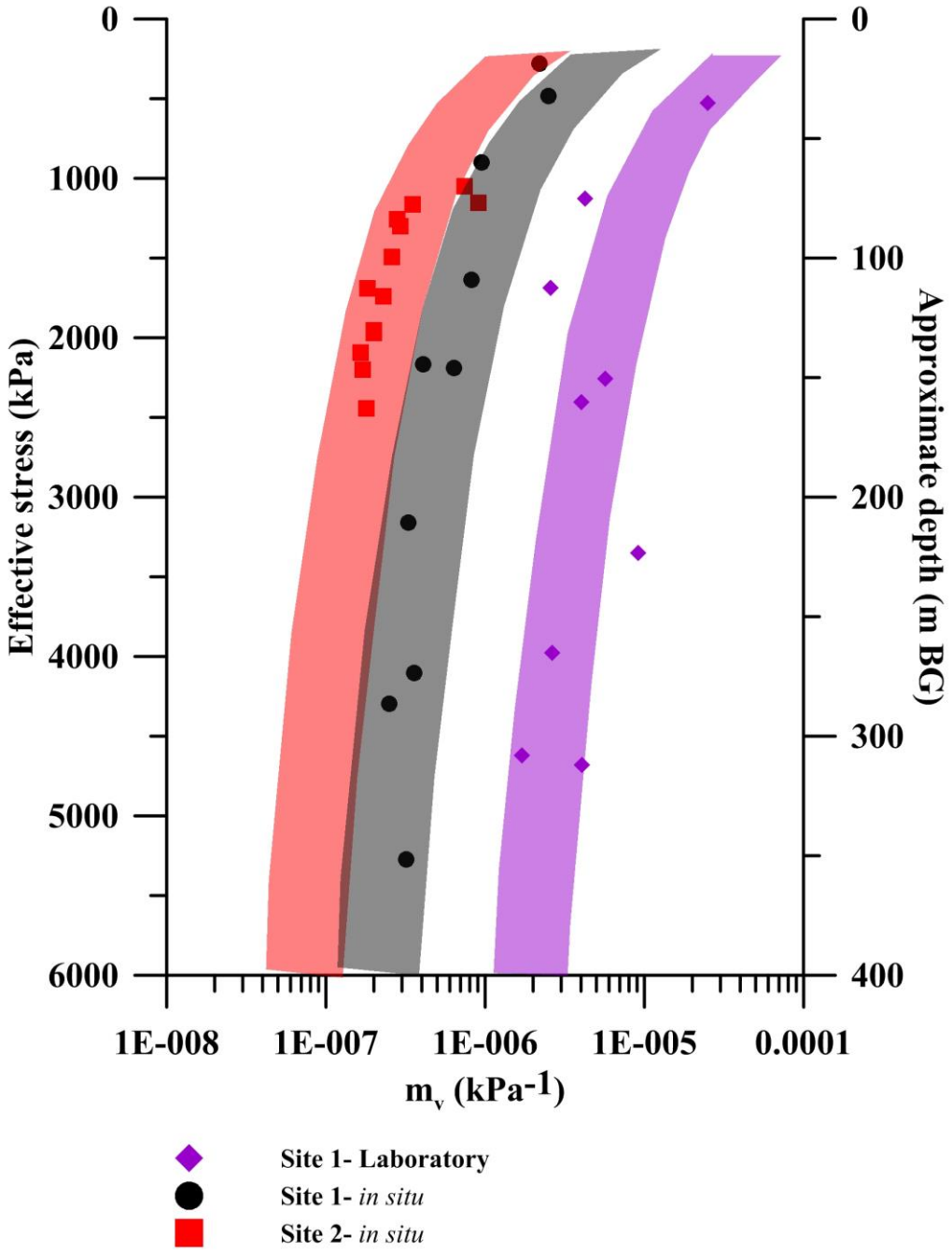

Figure 5.6: Depth profile of σ' and m_v of both Site 1 (red squares) and Site 2 (black circles), along with the laboratory estimates at *in situ* σ' (purple diamonds). The shaded regions represent a range of calculated m_v from the laboratory determined Cc and Cr. The purple shaded region was produced using Cc and Cr consistent with the laboratory tests (0.27 and 0.2-0.06, respectively). The black and red shaded regions were produced using Cc consistent with laboratory testing (0.27) but Cr estimates of 0.005-0.01 and 0.001-0.003, respectively.

5.4.3 Specific Storage

Specific storage is largely dependent on compressibility, and as such, follows a similar trend with depth. The *in situ* S_S for the shale at Site 1 and 2 range from approximately 3.0×10^{-6} to 2.6×10^{-5} m^{-1}. A general relationship between *n* and S_S for normally to overconsolidated argillaceous media was defined by Konikow and Neuzil (2007) using results from laboratory tests of various formations reported in the literature (Domenico and Mifflin; 1965; Skempton, 1970; Cripps and Taylor, 1981; Tellam and Lloyd, 1981; and Neuzil, 1993) (cross hatch region, Figure 5.7). Because the majority of the S_S data used to define this relationship was determined from laboratory determined m_v values, it is reasonable to conclude that S_S would decrease with decreasing *n* because it is related to a decrease in porous matrix m_v with compaction (Konikow and Neuzil, 2007). Smith et al. (2013) revisited this relationship and added the results of the transducer determined S_S data from Site 1. A portion of the transducer determined S_S results plotted above the overconsolidated boundary, which is consistent with the OCR's calculated in the previous section, and indicate that the upper boundary should be extended to include *in situ* estimates of S_S. Consistent with the Site 1 data, the *in situ* S_S estimates from Site 2 plot both within and outside the cross hatch region defined by Konikow and Neuzil (2007). The majority of the transducers that plotted within the region were installed in the till formations or the shallow shale and the transducers installed >75 m BG generally plotted outside the region.

All loading and unloading intervals for each of the consolidation tests were plotted on Figure 5.7, and while some intervals plot outside the normally consolidated region, the S_S estimates determined for the expected σ' of each sample plotted entirely within the expected region defined by Konikow and Neuzil (2007). A comparison of the laboratory S_S estimates with the *in situ* values determined using pressure transducers of the same formations at Site 1 illustrate the differences between laboratory and *in situ* results (Figure 5.7). Laboratory tests can be useful to determine an estimate of formation m_v (and α), but as discussed in §3.3, it is important to be aware that results determined from samples removed from *in situ* conditions could have an error exceeding one order of magnitude.

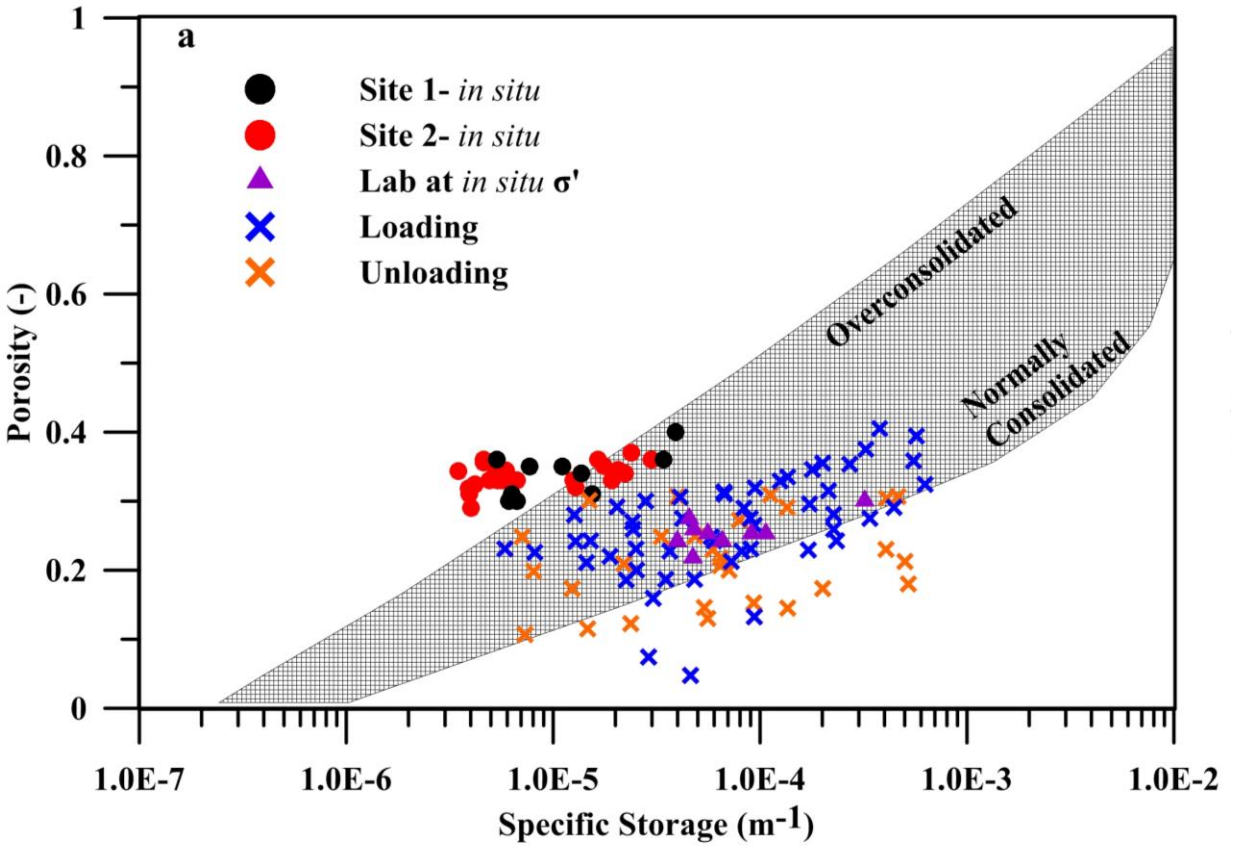

Figure 5.7: Cross plot of specific storage determined from transducers installed at Sites 1 and 2 vs. measured porosity (a) along with the calculated S_S of each loading and unloading interval. The predicted area for overconsolidated formations and range of laboratory determined values of argillaceous formations reported in the literature (Konikow and Neuzil, 2007) is defined by the cross-hatch zone.

5.4.4 Hydraulic conductivity

Generally, the relationship between e and K for argillaceous materials is well defined; as e (or *n*) decreases, K usually decreases (Neuzil, 1994; Mazurek, 2011; Smerdon et al. 2014). Mitchell (2005) highlights that these relationships often follow a form in which K varies as e^2 or $e^3/(1+e_o)$ where e_o is an initial reference e. The majority of the measured K values in the literature have been determined from laboratory testing. Damaged or disturbed core samples will likely introduce some amount of error, but the foremost concern regarding laboratory determined K are scale effects. If the core samples selected for testing are not representative of the formation features (e.g. heterogeneities, or fractures), the test is essentially measuring the matrix K. This is a possible explanation as to why there is often a large discrepancy between field and laboratory testing for the same materials (Bredehoeft et al., 1983). Typically, the best approach

to characterize a formation K is a combination of both laboratory and field methods, along with basin scale numerical modeling.

The results of the transducer based method to determine K_h at Sites 1 and 2 and the results of laboratory tests to determine K_v from both sites are plotted vs e (Figure 5.8a). Due to different formations and methods used to compile this data, there is no discernable pattern in the results; however, general trends of $e^3/1+e_o$ highlighted on the graph show that within a particular formation these trends are followed, albeit loosely. The *in situ* results obtained from the same formation (Pierre Shale) for Site 1 and Site 2 are plotted separately in Figure 5.8b. While a greater range in e would be helpful to determine if a pattern can be identified, K_h generally increases with increasing e according to the empirical relationship $K=e^3/(1+e_o)$ (Mitchell, 2005) (Figure 5.8b). These findings are consistent with results from previous work in the WCSB and in sedimentary basins world wide as shown in (Figure 5.9a and b) and summarized in Table 5.2. A comprehensive summary of K for argillaceous formations around the world is presented by Batlle-Aguilar et al. (2016). The transducer determined results from Site 2 are consistent with estimates from Site 1. Although consistency does not inherently imply the estimates are correct, it does provide some confidence that the transducer based method is a viable option for determining *in situ* K_h in argillaceous aquitards.

The significance of using VWPs to determine *in situ* parameters does not lie entirely in the ability to avoid laboratory testing. A comparison of laboratory and *in situ* results provides additional information about the heterogeneity of the formation. If the laboratory results and the transducer based results are not consistent (e.g., the transducer results are 1-2 orders of magnitude greater than the laboratory results), it could indicate that the laboratory scale tests are measuring only the matrix K and any secondary features (e.g., fractures) are not accounted for. As such, a comparison of both methods could help determine if any heterogeneities exist in the formation (Smith et al., 2016).

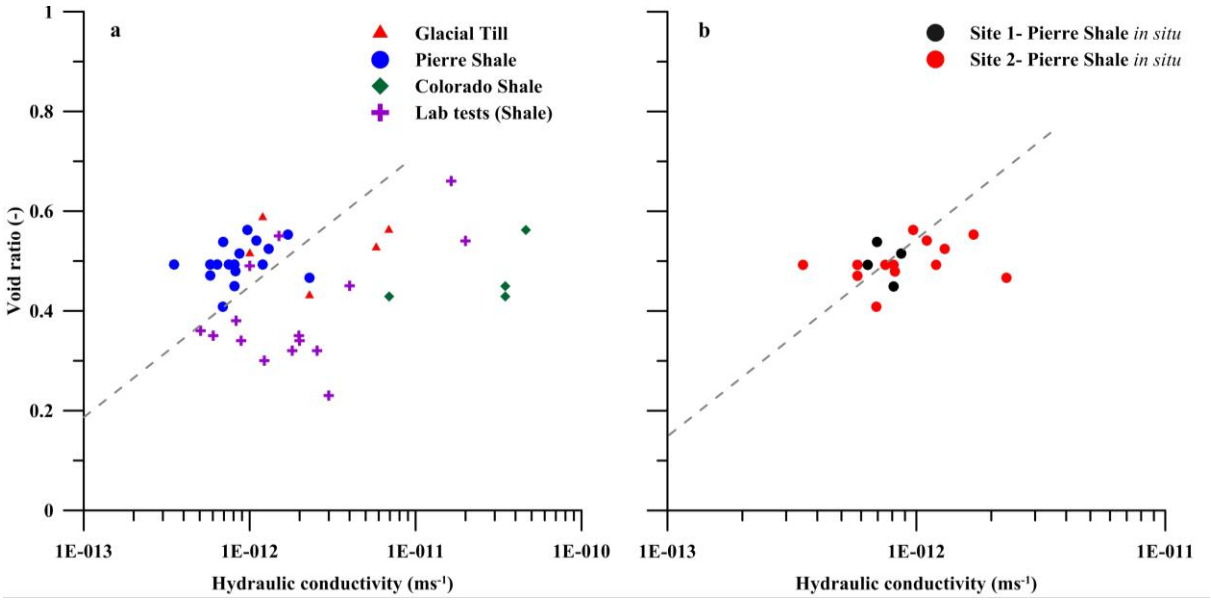

Figure 5.8: Results of the transducer determined hydraulic conductivity from the glacial till, Pierre Shale and Colorado Shale from Sites 1 and 2, along with the laboratory determined hydraulic conductivity from core samples obtained from Site 1, plotted against e (a). Results of similar material in the Pierre Shale obtained from Site 1 and 2 (b) generally showing how hydraulic conductivity increases with e. K generally increases with increasing e according to the empirical relationship $K=e^3/(1+e_o)$ (grey dashed line).

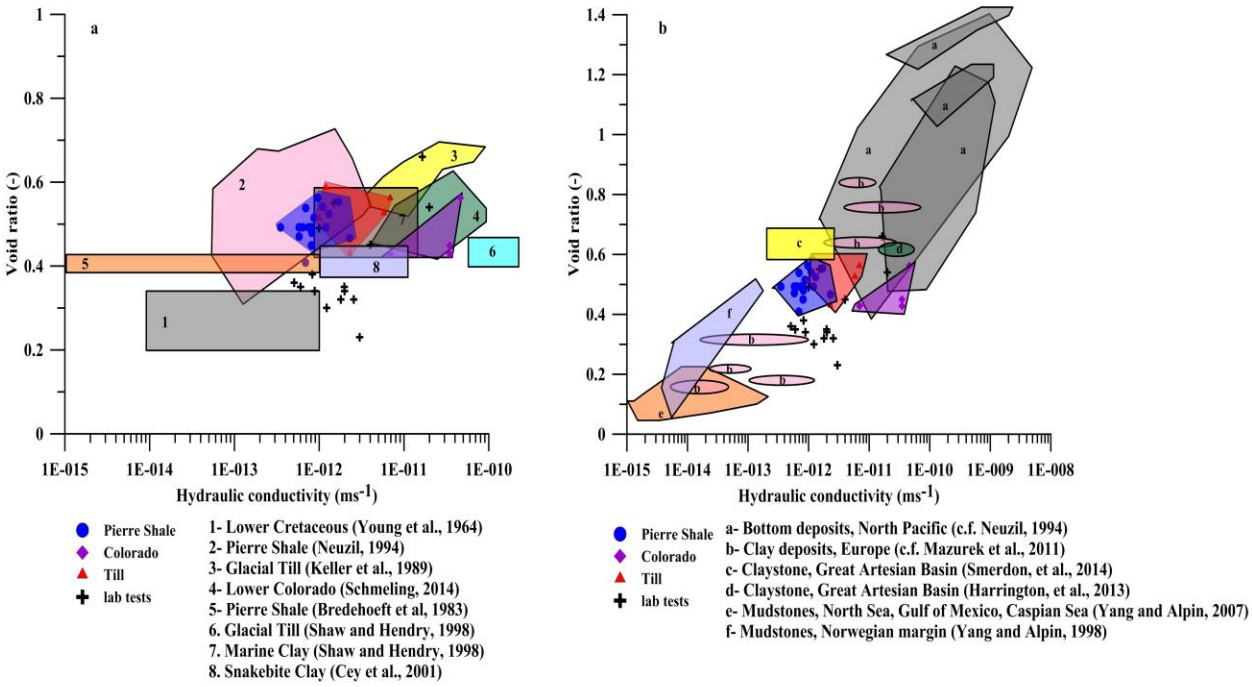

Figure 5.9: Cross plot of e vs. hydraulic conductivity in argillaceous deposits from previous work in the WCSB (a) and similar argillaceous deposits in sedimentary basins world wide (b). The extent of transducer and laboratory determined K values for geologic media from this study are presented.

Table 5.2: Hydraulic conductivity data from studies of argillaceous aquitards (plotted in Figure 9a and b).

Region in Figure 9a	Location	Formation	Lithology	Type of test	Source
1	Western Canada	Lower Cretaceous	Clayey silt/sandstone	Steady flow laboratory test	Young et al. (1964)
2	South Dakota	Pierre Shale	Claystone	Mechanical, and hydraulic transient, Steady flow	Neuzil (1994)
3	Saskatchewan	Sutherland Group	Glacial Till	Mechanical transient and steady flow	Keller et al. (1989)
4	Fort a la Corne	Lower Colorado	Claystone	*In situ* γ method	Schmeling (2014)
5	South Dakota	Pierre Shale	Claystone	Regional groundwater model	Bredehoeft (1983)
6	Saskatchewan	Battleford and Saskatoon Group Till	Glacial Till	Laboratory and slug tests	Shaw and Hendry (1998)
7	Saskatchewan	Bearpaw Fm	Marine Clay	Laboratory tests	Shaw and Hendry (1998)
8	Saskatchewan	Bearpaw Fm	Marine Clay	Laboratory tests	Cey et al. (2001)
Region in Figure 9b	**Location**	**Formation**	**Lithology**	**Type of test**	**Source**
a	North Pacific	Various	Bottom deposits	Laboratory tests	c.f. Neuzil, (1994)
b	Europe	Various	Claystone	Laboratory tests	c.f. Mazurek et al. (2011)
c	Australia	GAB	Claystone	Laboratory and *in situ* tests	Smerdon et al. (2014)
d	Australia	GAB	Claystone	Numerical modeling	Harrington et al. (2013)
e	North Sea, Gulf of Mexico, Caspian Sea	Various	Mudstone	Laboratory tests	Yang and Alpin (2007)
f	Norwegian margin		Mudstone	Numerical modeling	Yang and Alpin (1998)

5.5 CONCLUSIONS

Ten VWPs were installed in argillaceous aquitard formations in the north east portion of the WB, and used to determine m_v (α) and K_h (Site 1) (Smith et al., 2013; Smith et al., 2016). However, with only a few *in situ* estimates of S_S in the literature, and limited use of VWPs to determine *in situ* α and K_h of aquitard formations, further work was required to determine the consistency of the method. Twenty-seven additional VWP`s were installed in similar argillaceous till and shale formations at a second site (Site 2) approximately 350 km southwest of Site 1. The results obtained from Site 2 were consistent with the results from Site 1. As such, these data suggest that VWPs have the potential to provide an alternative method to determine *in situ* hydrogeologic parameters of argillaceous aquitards. The data presented in this paper strengthens the position of using grouted-in pressure transducers to further our understanding of complex low-K argillaceous deposits at depth; but the best approach to characterize aquitard formations remains a combination of laboratory and field-based methods.

Laboratory consolidation tests provide an indication of the stress history experienced by the shales. Sample disturbance generally tends to underestimate the stiffness of a sample and overestimate Cr, presumably due to breaking of diagenetic bonds or rearranging clay structure. However, the general trend of the stress behaviour (e relationship to σ') observed in the laboratory was consistent, though offset by about an order of magnitude, with *in situ* observations. Current work is focused on applying the transducer based methods to other geologic media (e.g. carbonate formations, heterogeneous deposits, and dynamic environments) and continue to build the database for transducer determined parameters.

5.6 REFERENCES

American Society for Testing and Materials (ASTM) International D2435-04 (2011): Standard test methods for one-dimensional consolidation properties of soils using incremental loading. West Conshohocken, PA. USA. DOI: 10.1520/D2435_D2435M-11

American Society for Testing and Materials (ASTM) International D4531-86 (2008): Standard test methods for bulk density of peat and peat products. West Conshohocken, PA. USA.

Batlle-Aguilar, J., P.G. Cook, G.A. Harrington (2016), Comparison of hydraulic and chemical methods for determining hydraulic conductivity and leakage rates in argillaceous aquitards, *J. Hydrol.* 532, 102-121.

Bredehoeft, J.D. (1965), The drill-stem test: The petroleum industry's deep-well pumping test, *Ground Water*, 3(3), 31-36.

Bredehoeft, J. D., C. E. Neuzil, and P. D. Milly (1983), *Regional flow in the Dakota Aquifer: A study of the role of confining layers.* U.S. Geological Survey Water Supply Paper.

Casagrande, A. (1936), The determination of the pre-consolidation load and its practical significance. Proceedings of the international conference on soil mechanics and foundation engineering. Harvard University Cambridge. 60-64.

Cey, B.D., S.L. Barbour, M. J. Hendry (2001), Osmotic flow through a Cretaceous clay in southern Saskatchewan, *Canada, Can. Geotech. J*. 38, 1025-1033.

Conteras, I., A. T. Grosser, R. H. Ver Strate (2008), The use of the fully- grouted method for piezometer installation, Part 1, *Geotech. News*. June, 2008.

Clark, J. I. (1998), The settlement and bearing capacity of very large foundations on strong soils. *Can. Geotech. J. 35*, 131–145.

Clayton, C.R.I., M.C. Matthews, N.E. Simons (1995), *Site Investigation* (second edition). Wiley-Blackwell, pp. 25-29.

Cripps, J. C., and R. K. Taylor (1981), The engineering properties of mudrocks, *Q. J. Eng. Geol.*, 14(4), 325– 346

Christensen, E.A. (1968a), Pleistocene stratigraphy of the Saskatoon area, Saskatchewan, Canada, *Can. J. Earth Sci*., v.5, 1167-1173.

Christensen, E.A. (1968b), A thin till in west-central Saskatchewan Canada, *Can. J. Earth Sci*, v.5, 329-336.

Christensen, E.A. (1992), Pleistocene stratigraphy of the Saskatoon area, Saskatchewan, Canada: an update: *Can. J. Earth Sci*, v.29, 117-145.

Domenico, P. A., and M. D. Mifflin (1965), Water from low-permeability sediments and land subsidence, *Water Resour. Res*., 1, 563– 576.

Duncan, J. M., and A. Bursey (2013), Soil Modulus Correlations. Foundation Engineering in the Face of Uncertainty, in 2013 GeoCongress, San Diego, CA, March 3-7, 2013; pp. 321-336. doi: 10.1061/9780784412763.026

Grisak, G., J. F. Pickens, J. D. Avis, D. W. Belanger, M. Thury, A. Schneider (1985), Principles of hydrogeologic investigations at depth in crystalline rock, Int. Congr. *Int. Assoc. Hydrogeol*., 17, 52-71.

Harrington, G. A., W. P. Gardner, B.D. Smerdon, M. J. Hendry (2013), Palaeohydrogeological insights from natural traer profiles in aquitard porewater, Great Artesian Basin, Australia, *Water Resour. Res*. 49, 4054-4070.

Hendry, M. J., S. L. Barbour, K. Novakowski, and L. I. Wassenaar (2013), Palaeo-hydrogeology of the Cretaeous sediments of the Williston Basin using stable isotopes of water, *Water Resour. Res*., 49, 4580-4592, doi: 10.1002/wrcr.20321.

Hendry, M.J., G.A. Harrington (2014), Comparing vertical profiles of natural tracers in the Williston Basin to estimate the onset of deep aquifer activation. *Water Resour. Res*., 50 (8), 6496-6506.

Hendry, M.J., D.K. Solomon, M. Person, L.I. Wassenaar, W.P. Gardner, I.D. Clark, K.U. Mayer, T. Kunimaru, K. Nakata, and T. Hasegawa (2015), Can argillaceous formation isolate nuclear waste? Insights from isotopic, noble gas, and geochemical profiles. *Geofluids* 15(3): 381-386. DOI: 10.1111/gfl.12132.

Hendry, M. T., M.J. Hendry, L.A. Smith, (in review), Analysis of the measured pore pressure response to atmospheric pressure changes to evaluate small strain moduli: Methodology and case studies. Submitted to *Geotechnique.*

Jasinski, S.M. (2010), Potash, *Mining Engineering*, 69-70.

Keller, C. K., G. van der Kamp, and J. A. Cherry (1986), Fracture permeability and groundwater flow in a clayey till near Saskatoon, Saskatchewan. *Can. Geotech. J., 23*, 229–240.

Keller, C. K., G. van der Kamp, and J. A. Cherry (1989), A multi-scale study of permeability of thick clayey till. *Water Resour. Res., 25* (11), 2299-2317.

Klohn, E. J. (1965), The elastic properties of a dense glacial till deposit, *Can. Geotech. J*., 11(2), 116–128.

Mazurek, M., P. Alt-Epping, A. Bath, T. Gimmi, H. Niklaus Waber, S. Buschaert, P. De Cannière, M. De Craen, A. Gautschi, S. Savoye, A. Vinsot, I. Wemaere, and L. Wouters (2011), Natural tracer profiles across argillaceous formations, *Appl. Geochem*., 26, 1035-1064.

McKenna, G. T. (1995), Grouted-in installation of piezometers in boreholes, *Can. Geotech. J.*, 32, 355-363.

Mikkelsen, P. E. (2002), Cement-bentonite grout backfill for borehole instruments, *Geotech. News*. December 2002.

Mikkelsen, P. E., and G. E. Green (2003), Piezometers in fully grouted boreholes, in Symposium on Field Measurements in Geomechanics, FMGM. Oslo, Norway, September 2003.

Neuzil, C. E. (1993), Low fluid pressure within the Pierre Shale: A transient response to erosion, *Water Resour. Res*., 29, 2007–2020.

Neuzil, C. E. (1994), How permeable are clays and shales? *Water Resour. Res.*, 30, 145– 150.

Peterson, R. (1958), Rebound in Bearpaw Shale, Western Canada, Bull. Geol. Soc. Am., 69, 1113-1124.

Peterson, R and N. Peters (1963), Heave of spillway structures on clay shales. Can. Geotech. J. 1(1), 5-15.

Keller, C. K., G. van der Kamp, and J. A. Cherry (1989), A multi-scale study of permeability of thick clayey till. *Water Resour. Res., 25* (11), 2299-2317.

Konikow, L. F., and E. Kendy (2005), Groundwater depletion: A global problem, *Hydrogeol. J.*, 13(1), 317– 320.

Radhakrishna, H. S., and T. W. Klym (1974), Geotechnical properties of very dense glacial till, *Can. Geotech. J*., 11, 396–408.

Schmeling E. E. (2014), Characterization of the hydrogeology and solute transport in a geologically complex, fractured, late-Cretaceous shale, Fort a la Corne Kimberlite Field, Saskatchewan, Canada. M.Sc. Thesis, University of Saskatchewan.

Shaw, R.J. and M. J. Hendry (1998), Hydrogeology of a thick clay till and Cretaceous clay sequence, Saskatchewan, Canada, *Can. Geotech. J.* 35, 1041-1052.

Skempton, A. W. (1970), The consolidation of clays by gravitational compaction, *Q. J. Geol. Soc. London*, 125, 373– 411.

Smerdon, B. D., L. A. Smith, G. A. Harrington, W. P. Gardner, C. Delle Piane, and J. Sarout (2014), Estimating the hydraulic properties of an aquitard from *in situ* pore pressure measurements, *Hydrogeol. J.*, 22(8), 1875-1887, DOI: 10.1007/s10040-014-1161-x.

Smith L. A., G. van der Kamp, and M. J. Hendry (2013), A new technique for obtaining high-resolution pore pressure records in thick claystone aquitards and its use to determine *in situ* compressibility, *Water Resour. Res.*, 49, 732-743, DOI:10.1002/wcwr.20084.

Smith L. A., Barbour, S.L. and M. J. Hendry (in prep), *In situ* hydrogeologic properties of argillaceous formations in the Williston Basin determined from grouted-in pressure transducers.

Smith, L. A., S. L. Barbour, M. J. Hendry, K. Novakowski, G. van der Kamp (2016), A multiscale approach to determine hydraulic conductivity in thick claystone aquitards using field, laboratory and numerical modeling methods. *Water Resour. Res.* (DOI: 10.1002/2015WR018448).

Smith T.J. (1978), Consolidation and other geotechnical properties of shales with respect t age and composition. PhD Thesis, University of Durham.

Tellam, J. H., and J.W. Lloyd (1981), A review of the hydrogeology of British onshore non-carbonate mudrocks, *Q. J. Eng. Geol*., 14(4), 347–355.

van der Kamp, G., and J. E. Gale (1983), Theory of Earth tide and barometric effects in porous formations with compressible grains, *Water Resour. Res.*, 19(2), 538–544.

Vaughan, P. R. (1969), A note on sealing piezometers in boreholes. *Geotechnique*, 19 (3), 405-413.

Vigrass, L. (2006), Williston Basin. Encyclopedia of Saskatchewan [Available at http://esask.uregina.ca/entry/williston_basin.html, accessed 23 Nov. 2015].

Yang, Y. and A.C. Alpin (1998), Influence of lithology and compaction on the pore size distribution and modelled permeability of some mudstones from the Norweigian margin, *Marine and Petroleum Geology*, 15 (2), 163-175.

Yang, Y. and A.C. Alpin (2007), Permeability and petrophysical properties of 30 natural mudstones, *J. Geophys. Res*., 112, B03206, doi:10.1029/2005JB004243.

Young, A., P.F. Low, A.S. McLatchie (1964), Permeability studies of argillaceous rocks, *J. Geophys. Res*., 69(20), 4237-4245.

6.0 SUMMARY OF CONCLUSIONS AND RECOMMENDATIONS

The challenges associated with estimating *in situ* hydrogeologic parameters of low-K (aquitard) formations are well documented in the literature. Conventional field and laboratory methods typically result in an overestimation of 1-D compressibility (m_v) and underestimation of K, both of which are commonly used in numerical modeling to predict groundwater flow and contaminant transport. Even small errors in m_v and K can have a large impact on the results of such models. Due to challenges associated with slow pore pressure response times in the field, and in obtaining competent and representative core samples, aquitard research is often slow and yields a lack of data on *in situ* parameters for aquitards.

The goal of this thesis was to develop and apply alternative methods to characterize the hydrogeological properties of low-K formations and increase our understanding of deep (up to 400 m) aquitard systems in the Williston Basin (WB). The main objectives of the research were to: (1) determine the *in situ* m_v through argillaceous aquitards at one site in the WB by analyzing pore pressure responses from grouted-in VWPs; (2) characterize the K of these argillaceous aquitards using laboratory, *in situ,* and numerical modeling methods, and compare and contrast the multi-scale results with previous work in the literature; and (3) generate a detailed data set of hydrogeologic parameters of argillaceous aquitards in the WB to evaluate the potential of grouted-in VWPs for determining *in situ* parameters (m_v and K_h) of aquitards. Objectives (1) and (2) were met by studying core samples and a nest of VWPs (n=10) installed at Site 1 located near the north east portion of the WB, while Objective (3) was met by studying an additional 27 VWPs at a new site near the center of the WB (Site 2).

A summary of conclusions from each of the three objectives are presented below.

6.1 Objective 1: Determine the *in situ* compressibility through argillaceous aquitards in the WB by analyzing pore pressure responses from grouted-in VWPs (Chapter 3, Manuscript #1)

An alternative method to determine the *in situ* m_v (and subsequently α and S_S) of thick Cretaceous claystone aquitards using grouted-in VWPs (n=10) was presented in Chapter 3. Ten VWPs were installed in a single borehole near the north east portion of the WB, and programmed to record pressure and temperature every 30 minutes, in conjunction with a surface barometer. Analysis of pore-pressure responses to barometric fluctuations reveal the γ at the

location of each transducer, which then enabled the calculation of α and S_S with depth, with an assumed Poisson's ratio. The results of conventional laboratory tests conducted on core samples obtained near the VWPs yielded m_v estimates greater than those determined by the VWP method in all cases (2.5×10^{-7}-2.4×10^{-6} kPa^{-1} and 1.7×10^{-6}-2.5×10^{-5} kPa^{-1}, respectively). These results suggest that the results from laboratory testing may not be representative of the formation *in situ.*

Determining the *in situ* parameters of aquitard formations at a depth up to 325 m has not yet been achieved using laboratory or field methods currently employed, thus making fully-grouted VWPs a potentially useful tool to characterize low-K formations at depth. In addition, the easy installation process and the ability to install multiple VWPs in a single borehole are attractive features of this method, resulting in depth profiles that can otherwise only be achieved by drilling multiple boreholes. Finally, the ability of grouted-in VWPs to constantly measure and record pore pressure changes could provide new insight into how formations respond to sudden or transient stress and structural changes, such as those that might be induced by seismic activity, glacial rebound, or subsidence due to mining activity.

6.2 Objective 2: Characterize the K of argillaceous aquitards using laboratory, *in situ*, and numerical modeling and compare the multi-scale results to each other and previous work (Chapter 4, Manuscript #2)

Multiple methods were used to estimate both K_v and K_h of Cretaceous claystone aquitards at various scales in the WB at Site 1 using core samples obtained during drilling, and the installed VWPs: (1) laboratory consolidation tests (matrix K_v) (n=9; $2.0 \times 10^{-11} – 9.3 \times 10^{-13}$ ms^{-1}), (2) laboratory triaxial permeameters (n=7; $2.0 \times 10^{-11} – 1.5 \times 10^{-12}$ ms^{-1}), (3) numerical modeling of borehole pressure recovery (*in situ* K_h) (n=9; $3.5 \times 10^{-11} – 6.3 \times 10^{-13}$ ms^{-1}), and (4) numerical modeling of the head distribution (bulk *in situ* K_v) ($1.0\text{-}5.0 \times10^{-10}$ ms^{-1}). The results of these methods, on their own, provide a valuable and rare set of data for aquitard formations. On a larger scale, the results could be used to better understand aquitard formations not only in the WB, but in similar sedimentary basins around the world. Further, comparing large-scale *in situ* results to lab-scale results can provide insight into heterogeneities through the formation that may not be observed in small samples (e.g. fracture systems, differences in mineralogy). However, the significance of this study lies primarily on evaluating the applications of grouted-in VWPs to determine *in situ* K. The proximity of the study site to an active potash mine that has caused drawdown through the aquitard since production has been likened to a large continuous

pumping test. The results of this study indicate that the K_h estimates determined from the transducers (within their associated error, and evidence of vertical fracturing) could be used to simulate the current hydraulic head distribution that resulted from drawdown due to mining. This, in turn, reiterates that installing grouted-in pressure transducers could prove to be a useful tool for acquiring hydraulic data for materials that are historically difficult to characterize.

6.3 Objective 3: Generate a detailed data set of hydrogeologic parameters of argillaceous aquitards in the WB to evaluate the potential of grouted-in VWPs for determining *in situ* parameters (m_v and K_h) of aquitards (Chapter 5, Manuscript #3)

The VWP methods described and conducted at one site (Site 1) in the WB in Chapters 3 and 4 were repeated at a second site (Site 2) in the WB. Site 2 was located near the town of Weyburn, Saskatchewan, approximately 350 km south west of Site 1. Twenty-seven VWPs were installed at Site 2 to augment the results obtained from the 10 VWPs installed at Site 1. The results from both sites demonstrate the consistency of the methods through argillaceous glacial till and shale. The α and K_h values determined from the transducers at Site 2 ($2.4 \times 10^{-7} – 1.0 \times 10^{-6}$ kPa^{-1} and $3.5 \times 10^{-13} – 6.9 \times 10^{-12}$ ms^{-1}, respectively) were consistent with the results from Site 1 and further strengthens the methodology of using VWPs to increase our understanding of how to define the hydrogeologic parameters of complex low-K argillaceous deposits at depths up to 325 m BG. However, given the relatively small data set for grouted-in VWPs, the best approach to characterize aquitard formations remains a combination of laboratory and field-based methods.

A secondary aspect of this Chapter was to evaluate if the pattern of decreasing compressibility with increasing σ' in the laboratory could be applied to decreasing compressibility with depth *in situ*. The general trend of the stress behaviour (e relationship to σ') observed in the laboratory was consistent for similar materials and though offset by about an order of magnitude, with the *in situ* observations.

6.4 Global Conclusions

A common theme in this thesis is whether or not fully-grouted VWPs can be used to determine *in situ* parameters (m_v and K_h) of argillaceous aquitards. The logistical and technical difficulties in accurately estimating geotechnical and hydraulic properties of aquitards make it challenging to fully understand groundwater flow through such formations. This is particularly

troublesome because the low-K and high sorption capacity of clay-rich aquitards make them attractive host formations to sequester hazardous materials. Many countries around the world are currently investigating the potential of these aquitards to dispose of nuclear waste. With nuclear energy rapidly becoming a leading source of energy around the world, the success of such an project would solve one of the biggest problems facing the nuclear energy sector. The fully-grouted method provides an additional tool to help understand the geotechnical and hydraulic properties of potential host formations, and ultimately help protect and manage groundwater and future generations from harmful contaminants.

6.5 Recommendations for Future Work

During the course of this research, several aspects were identified as avenues for future work. Areas both directly related to the sites discussed in this thesis (e.g. continued monitoring of pore pressures at both active sites and interpretations for observed slip-strain behaviour) as well as more global perspectives (e.g. applying the methods to a variety of sites to build a data base of *in situ* parameters) were recognized as important topics for future work. In addition, questions raised about the importance of drilling methods and grout stiffness/permeability should also be addressed to increase our understanding of the advantages and limitations of the fully-grouted VWP methods. The following specific recommendations are made to help identify areas of this research that could be improved with continued work:

1) The VWPs at both Site 1 and Site 2 should continue to be monitored to evaluate whether disturbance of the formation as a result of mechanical disturbances due to mining (e.g. subsidence) (Site 1) and fluid/gas injection (e.g. pore pressure change) (Site 2). In addition, the pore pressure could be monitored in conjunction with a seismograph located on site to determine if natural or induced seismic activity can affect the pore pressure in low-K formations.
2) There are a few indications in the pore pressure record at Site 1 that indicate slip/strain behaviour may be occurring at the base of the Pierre Shale. Multiple instances of anomalous falling and rising behavior were measured at depths of 125 (G), 175 (F) and 185 (E) m BG, just above a thick bentonite layer (191-196 m BG). The magnitude of the responses gradually dampen with vertical distance from the bentonite and no such response is observed in the transducers directly below the bentonite, suggesting that these

events could be occurring in the weak, highly plastic bentonite. The reason these events are occurring is unknown. Possible explanations include: subsidence induced strain due to mining; deformation caused by drawdown in the underlying Mannville (i.e. the Noordbergum effect'); glacial rebound; or seismic events. Further work should be conducted to determine if any (or all) of the effects of these processes could produce the observed anomalies.

3) The findings of the research presented in this thesis were obtained from VWPs installed in boreholes that were continuously cored. In our experience, when boreholes are continuously cored, the pore pressure recovery follows the anticipated recovery trend, making it possible to model the pore pressure recovery and determine K_h. However, when transducers are installed in boreholes that have been tri-coned, the pore pressure takes substantially longer to recover and does not follow the characteristic recovery trend. It should be noted, however, that once the pore pressure is fully recovered, the γ method to determine m_v (α) and S_S remains successful. The impact of the two drilling methods on the pore pressure recovery and the cause of the recovery delay should be investigated further.
4) The application of the VWP methods should be applied at multiple sites with various formations/geologic material to continue building a database of *in situ* hydrogeologic parameters (m_v, α, K_h) for aquitards and help constrain the limitations of the method in a range of geomedia (i.e. minimum/maximum stiffness, highest/lowest K, dynamic groundwater/stress environments).
5) The grout in the 'fully-grouted' installation is a crucial component to the success of this method, as well as the associated methods to determine the *in situ* parameters described in this study (m_v, K_h). Additional laboratory and field tests should be conducted to constrain both the hydrogeological and geotechnical parameters of various grout mixtures, as well as the impact the grout has on determining these parameters from the pore pressure responses of the host formation.
6) Differences between laboratory and *in situ* measurements of m_v are well documented in the literature. Applying the grouted-in VWP method to determine m_v at several sites in conjunction with conventional laboratory testing may provide a greater understanding of the overall error associated with lab scale methods and help develop a relationship to

estimate the actual *in situ* m_v from laboratory samples where installation of VWPs is not possible.

APPENDIX A: Uncertainty of m_v

Uncertainty in m_v was estimated based on the error associated with determination of loading efficiency (γ). The m_v is a function of γ and can be graphed both linearly and in semi-log (Figures 1a and b, respectively), using Equation A1. The results illustrate that very large and very small values of γ can result in large associated uncertainty, while values between 0.25 and 0.8 have a relatively small range of uncertainty. Further, m_v is be very sensitive to the value of porosity, as shown in Figure A1.

[A1] $$m_v = \frac{\gamma n \beta}{1-\gamma},$$

where m_v is the 1-D constrained compressibility of the formation, β is the compressibility of water at 20°C (4.6×10^{-7} kPa^{-1}), and *n* is the porosity of the formation.

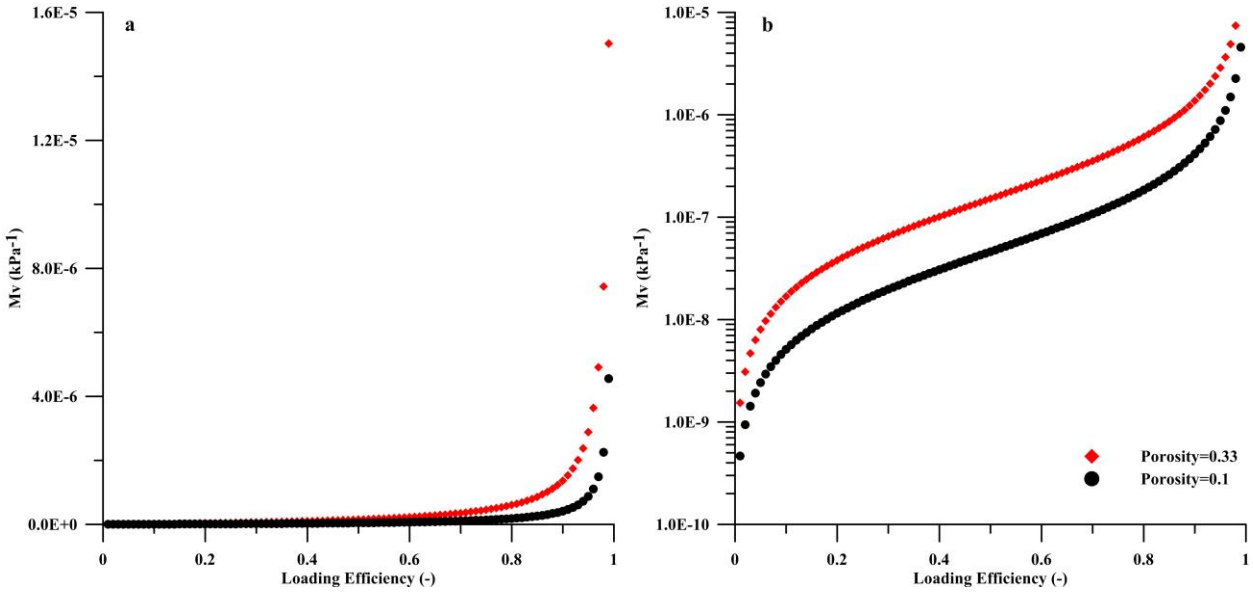

Figure A1: m_v as a function of γ on a linear scale (a) and semi-log scale (b) for a material with a porosity of 0.33 and 0.1, calculated from Equation A1.

The uncertainty in m_v can be determined by the following derivative:

[A2] $$\partial m_v = n\beta\left(\left(\frac{1}{1-\gamma}\right) + \left(\frac{\gamma}{1-\gamma}\right)^2\right)\partial\gamma$$

According to Figure 1, intuitively, the uncertainty at the highest value of γ at Site 1 (0.93) should be large relative to the lowest value of γ at Site 1 (0.6). Figure 2 illustrates the differences in the

uncertainty of m_v with a *n* of 0.33. m_v was calculated at a γ of 0.93 and 0.60. The uncertainty at 0.60 is very low, ranging from 2.3-2.7×10^{-07} kPa^{-1} and could not be illustrated in Figure A2, because the uncertainty was smaller than the size of the symbol. The uncertainty at 0.93 was much larger, ranging from 1.5-2.9×10^{-06}, and is well illustrated in Figure 2 by the vertical blue line.

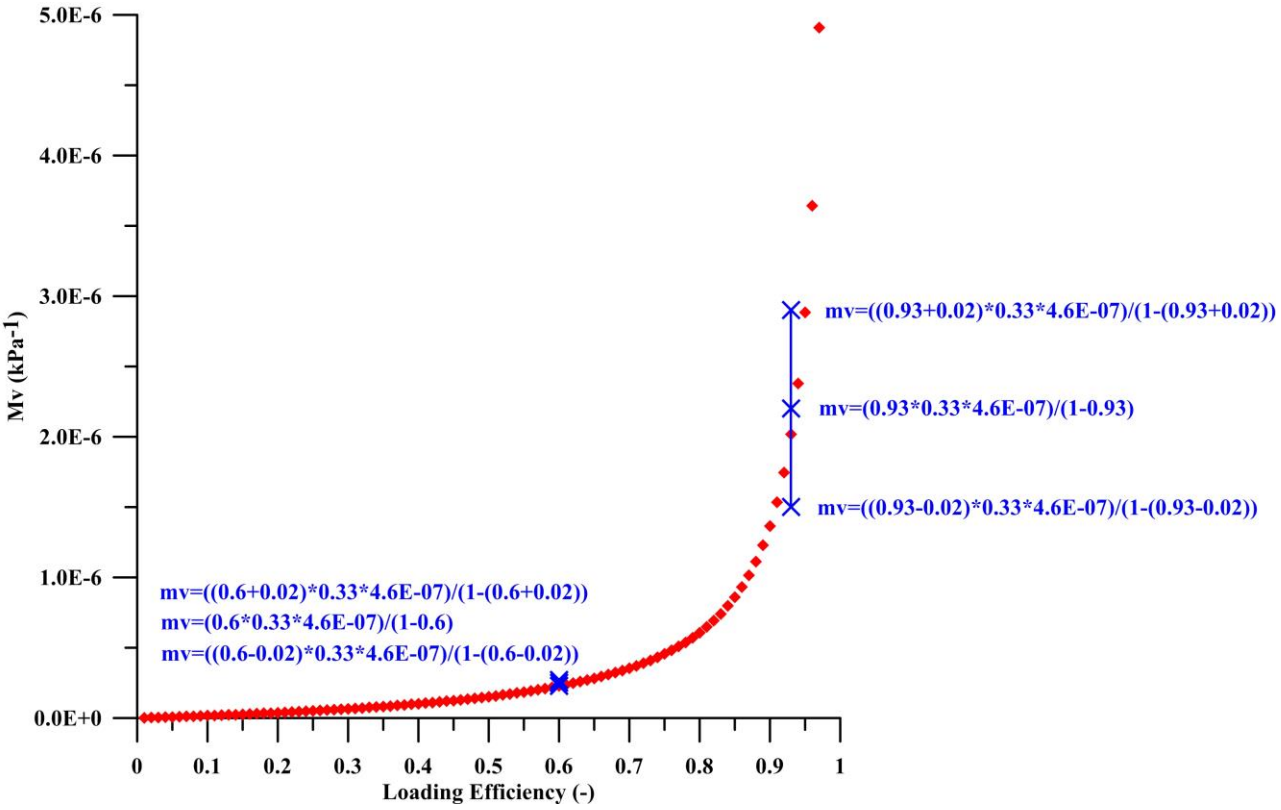

Figure A2: A graphical illustration of the differences in uncertainty calculated for a material with a porosity of 0.33 (the average porosity of the aquitard at Site 1), with a γ consistent with the shallowest transducer (J; γ= 0.93) and deepest transducer (A; γ=0.60). The range of calculated m_v at a γ of 0.60 was smaller than the size of the symbol.

APPENDIX B: Transducer completion logs

Appendix B1: Site 1- Borehole 1 completion log

Appendix B2: Site 2- Borehole 1 completion log

Appendix B3: Site 2- Borehole 2 completion log

Appendix B4: Site 2- Borehole 3 completion log

Appendix B5: Site 2- Borehole 4 completion log

Appendix B6: Site 2- Borehole 5 completion log

Appendix B1: Site 1- Borehole 1 completion log

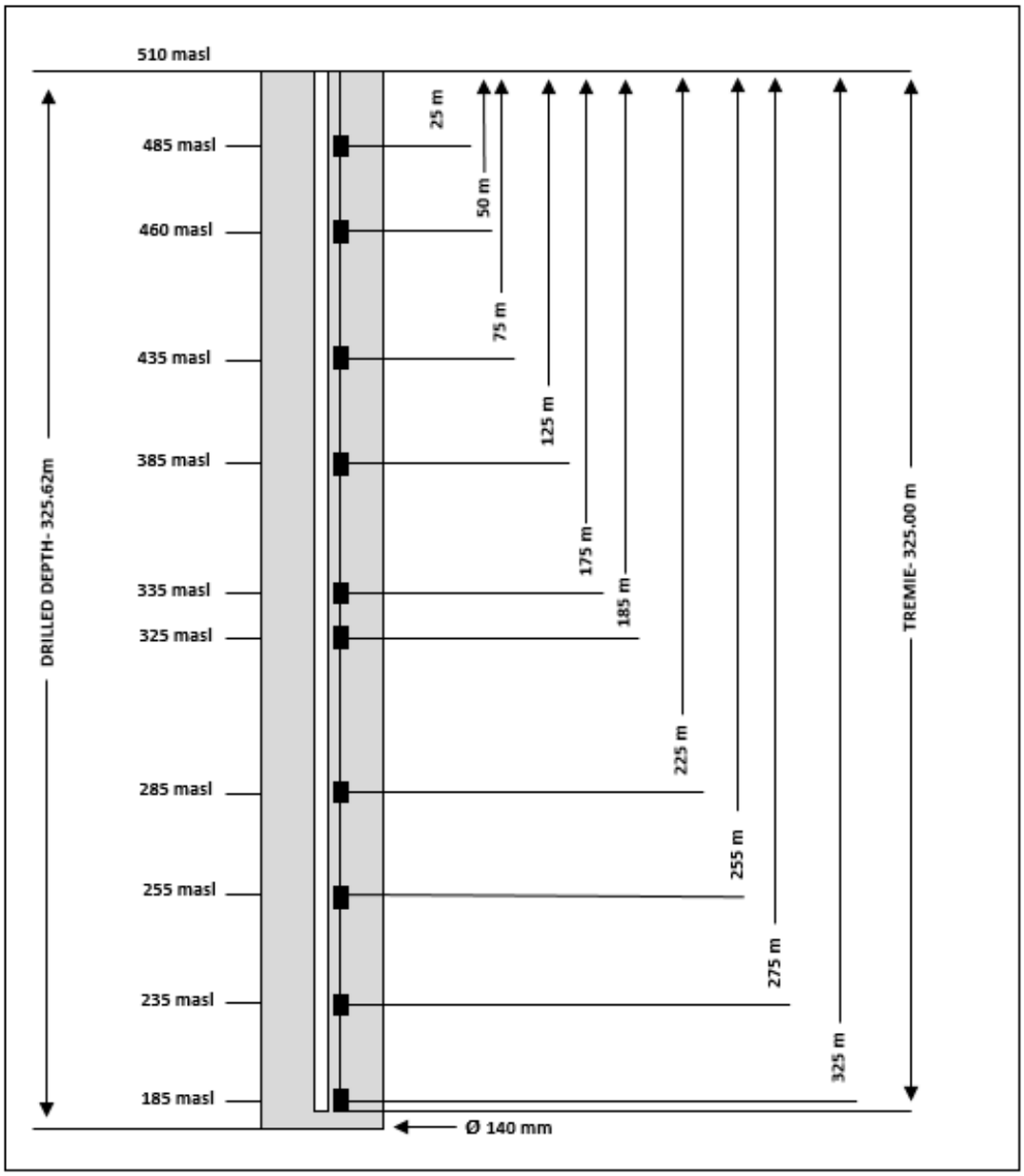

Appendix B2: Site 2- Borehole 1 completion log

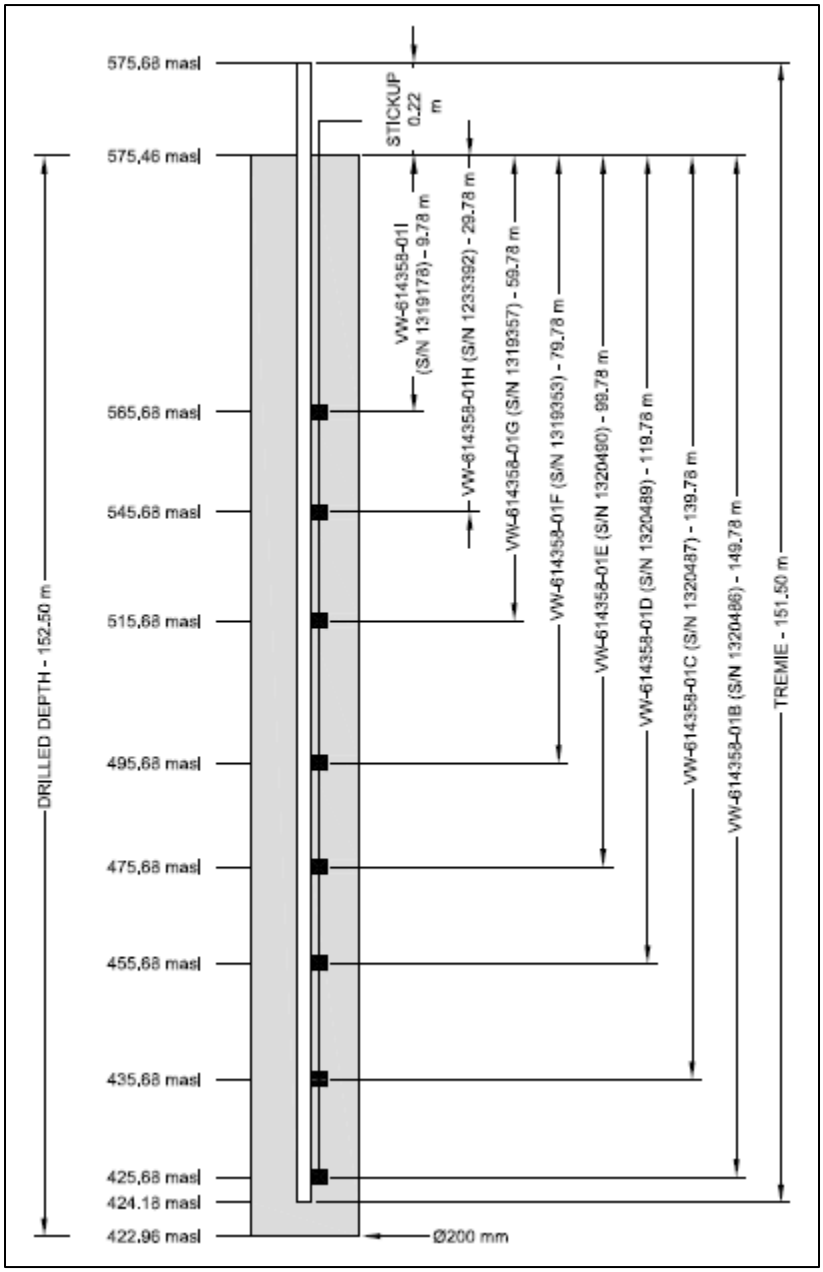

Appendix B3: Site 2- Borehole 2 completion log

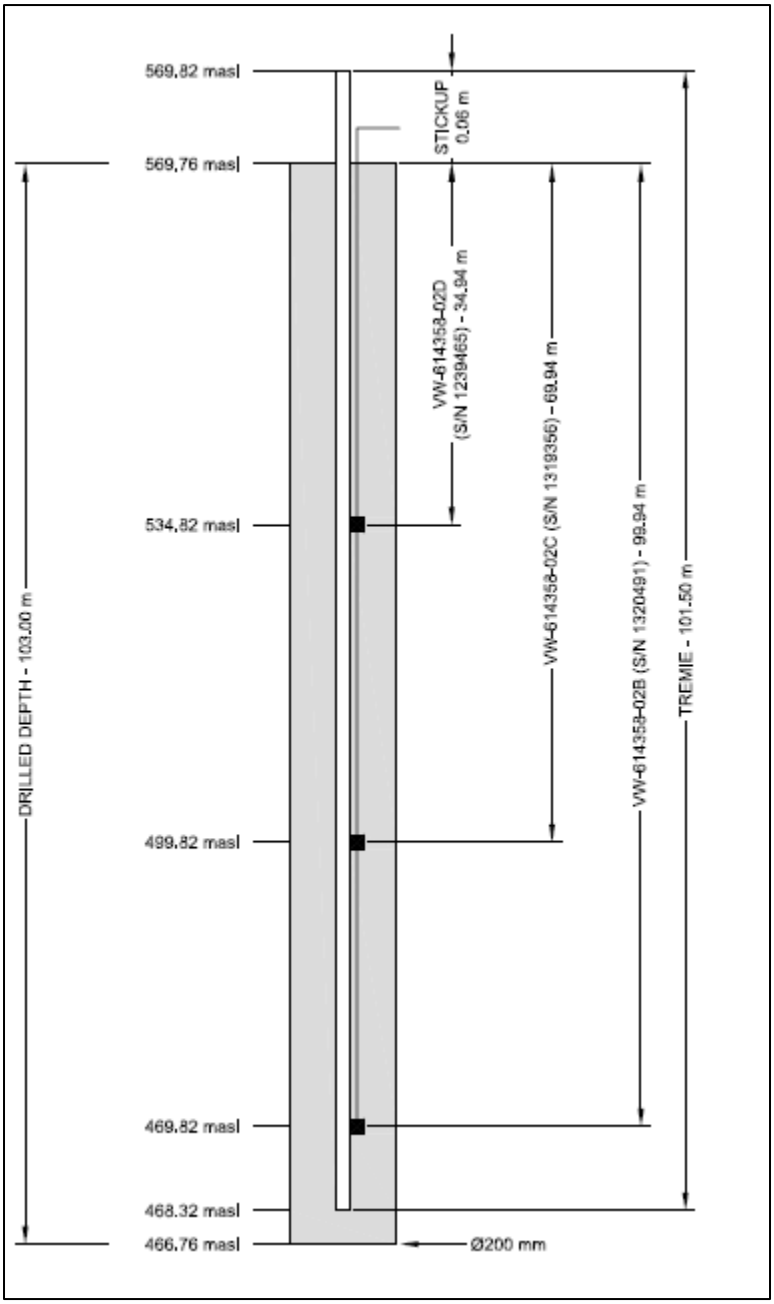

Appendix B4: Site 2- Borehole 3 completion log

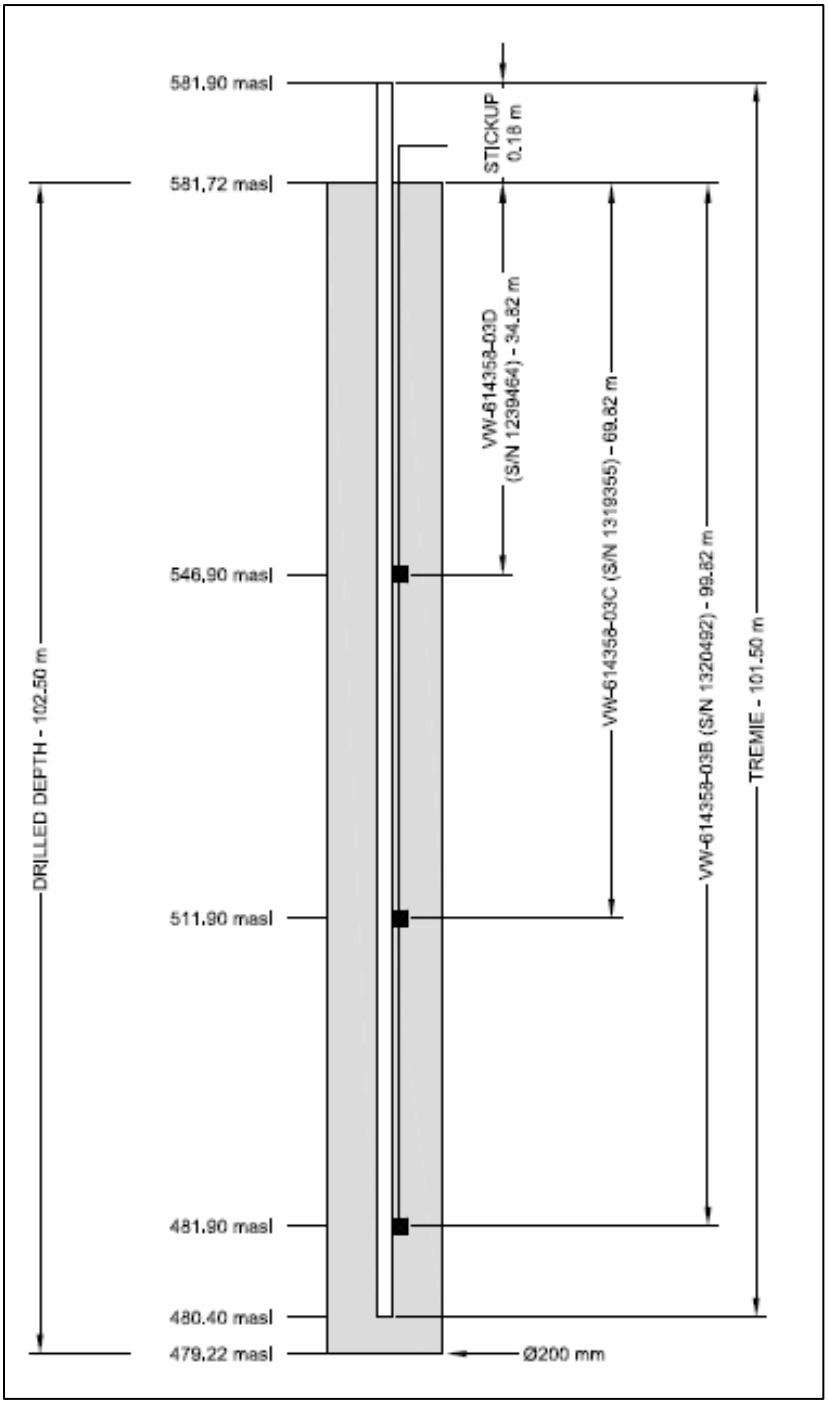

Appendix B5: Site 2- Borehole 4 completion log

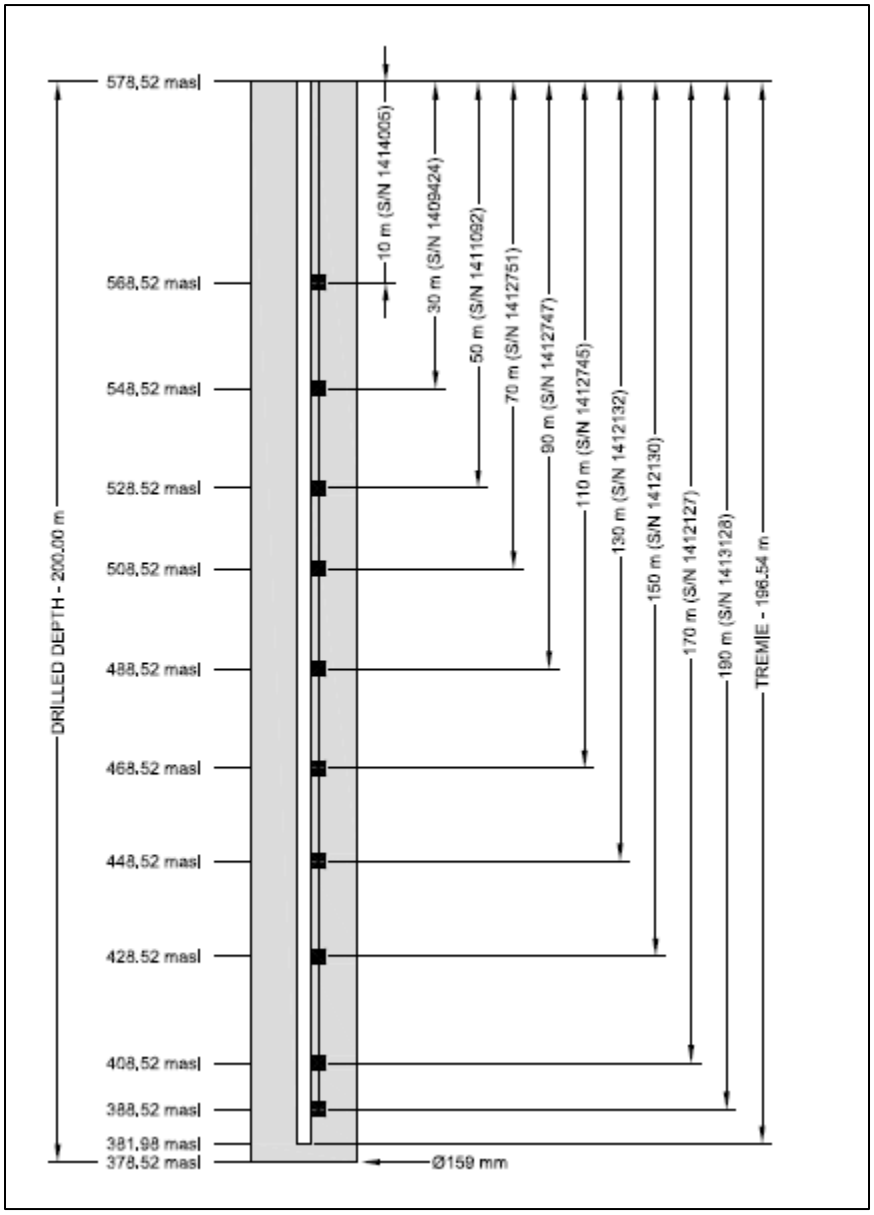

Appendix B6: Site 2- Borehole 5 completion log

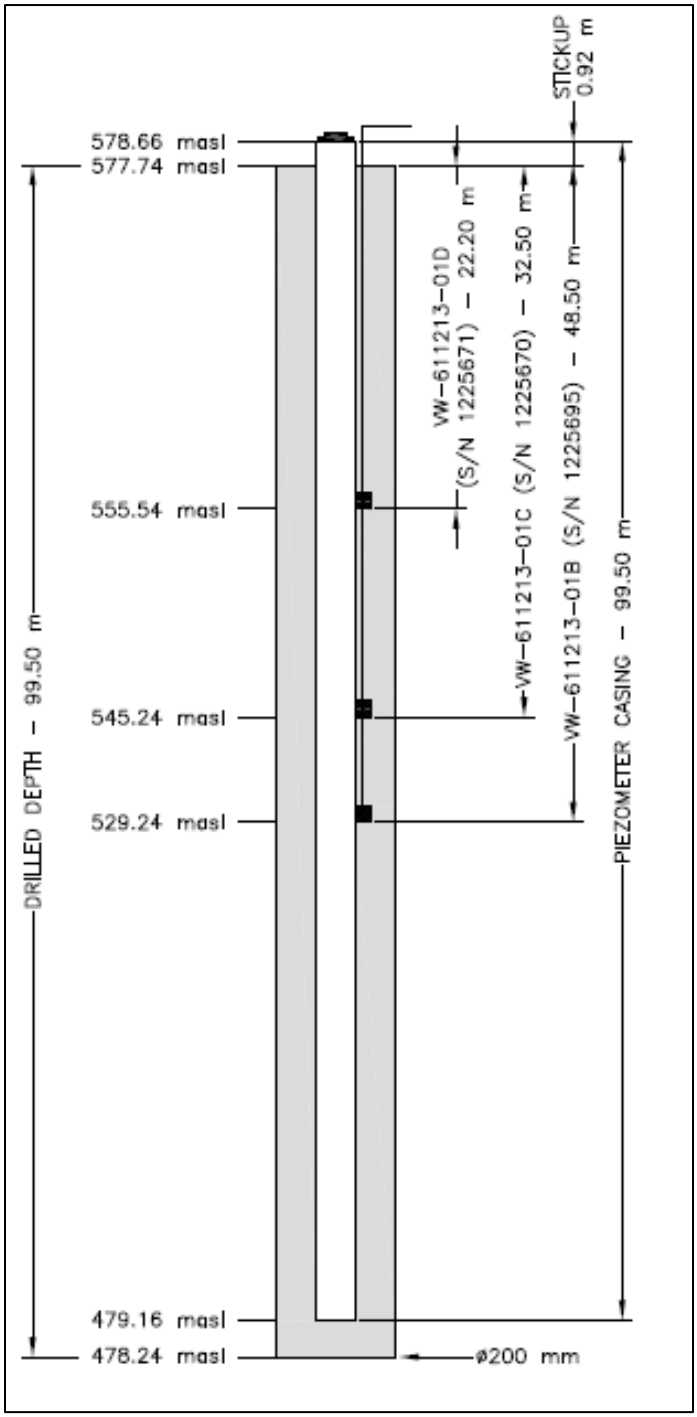

APPENDIX C: Geotechnical characterization of core samples

Appendix C1: Geotechnical characterization summary from core samples (Site 1)

Appendix C2: Geotechnical characterization summary from core samples (Site 2)

Appendix C3: Atterberg limits from core samples (Site 2)

Appendix C1: Geotechnical characterization summary from core samples (Site 1)

Borehole depth below ground surface (m)	**Core Diameter (mm)**	**Core length (mm)**	**Specific Gravity Gs**	**In-situ Bulk Density ρb (g/cc)**	***in situ* bulk density (kg/m3)**	**Specific weight (N/m3)**	**Specific weight (kN/m3)**	**Gravimetric water content (%)**
10	61.23	16.57	2.70	2.29	2294.21	22483.22	22.48	11.01
19.5	70.26	15.30	2.74	2.10	2100.36	20583.55	20.58	21.02
30	68.95	9.82	2.71	2.07	2071.51	20300.81	20.30	20.87
41	67.56	16.38	2.66	2.09	2087.59	20458.40	20.46	22.85
50	72.32	10.12	2.75	1.97	1969.85	19304.52	19.30	31.30
60	71.56	11.68	2.70	2.18	2184.53	21408.42	21.41	17.38
70	71.95	14.33	2.72	2.18	2181.33	21377.06	21.38	16.18
80	71.85	9.35	2.73	2.17	2168.03	21246.73	21.25	16.80
90	71.24	7.05	2.66	2.18	2179.21	21356.29	21.36	17.95
98	71.09	10.59	2.79	2.11	2105.35	20632.39	20.63	19.95
110	72.12	7.56	2.76	2.17	2173.82	21303.42	21.30	17.17
118.7	70.23	9.52	2.98	2.52	2520.91	24704.91	24.70	20.51
121	71.51	14.49	2.74	2.16	2160.85	21176.35	21.18	18.82
130	72.29	9.89	2.75	2.15	2152.62	21095.66	21.10	20.20
138	72.48	7.62	2.71	2.17	2172.33	21288.82	21.29	19.43
160	71.09	10.24	2.74	2.17	2168.22	21248.56	21.25	18.60
170	70.25	13.13	2.83	2.09	2091.89	20500.50	20.50	20.70
180	70.98	7.95	2.72	2.15	2154.55	21114.63	21.11	19.55
187	71.95	10.30	2.56	2.00	2001.78	19617.48	19.62	21.24
190	72.05	10.69	2.69	1.95	1950.05	19110.50	19.11	23.98
200	69.56	15.34	2.67	2.16	2163.73	21204.51	21.20	17.66
210	71.86	16.34	2.40	1.91	1913.49	18752.20	18.75	20.60
220	71.38	19.55	2.47	1.94	1938.04	18992.82	18.99	17.31
230	71.45	12.18	2.78	2.41	2405.63	23575.16	23.58	9.88
240	72.44	17.39	2.54	2.04	2038.12	19973.53	19.97	15.09
251	71.56	10.58	2.62	2.15	2153.49	21104.17	21.10	15.20
260	70.24	13.78	2.71	2.14	2142.92	21000.66	21.00	17.91
262	71.95	14.33	2.53	2.08	2078.86	20372.86	20.37	12.82
270	72.23	11.02	2.87	2.08	2084.31	20426.22	20.43	18.85
280	72.15	11.31	2.53	2.09	2094.33	20524.41	20.52	28.30
290	72.88	14.11	2.66	2.08	2076.12	20345.93	20.35	14.66
300	72.45	11.61	2.62	2.17	2166.50	21231.65	21.23	13.72
310	72.54	11.65	2.65	2.17	2172.48	21290.33	21.29	12.92

Appendix C1 con't: Geotechnical characterization summary from core samples (Site 1)

	Particle size distribution				Atterberg limits		
Borehole depth below ground surface (m)	Clay (<0.002 mm) (%)	Silt (0.075-0.002mm) (%)	Sand (4.75-0.075mm) (%)	Gravel (>4.75mm) (%)	LL (%)	PL (%)	PI (%)
10	16.8	25.6	39.9	17.7	26.65	12.04	14.61
19.5	39	61	0	0	62.1	17.53	44.57
30	39	61	0	0	62.6	15.92	46.68
41	35	65	0	0	83.3	19.94	63.36
50	38.5	62.5	0	0	116.8	30.27	86.53
60	41	59	0	0	81.8	21.83	59.97
70	34	66	0	0	81.88	20.48	61.4
80	49	51	0	0	91.5	23.03	68.47
90	46	54	0	0	97.2	22.34	74.86
98	46.5	53.5	0	0	104.8	22.56	82.24
110	57	43	0	0	99.1	24.09	75.01
118.7	39.8	60.2	0	0	74.6	19.11	55.49
121	49.2	50.8	0	0	106	26.01	79.99
130	45.8	54.2	0	0	88.3	24.05	64.25
138	39.3	60.7	0	0	95	23.39	71.61
160	48.7	51.3	0	0	120.9	22.15	98.75
170	49.5	50.5	0	0	140.8	26.79	114
180	49.7	50.3	0	0	97.9	25.23	72.67
187	40.5	59.5	0	0	81.2	29.47	51.73
190	42.3	57.7	0	0	87.7	30.97	56.73
200	53.5	46.5	0	0	84.5	26.53	57.97
210	35.8	64.2	0	0	42.7	27.63	15.07
220	36.1	63.9	0	0	50.3	23.54	26.76
230	43.2	56.8	0	0	41.9	17.47	24.43
240	28.7	71.3	0	0	38	27.17	10.83
251	29.8	70.2	0	0	42.7	25.3	17.4
260	42.6	57.4	0	0	102.9	29.18	73.72
262	33.3	66.7	0	0	44	22.3	21.7
270	40.2	59.8	0	0	105.9	29.26	76.64
280	47.9	52.1	0	0	34.3	21.65	12.65
290	46.5	53.5	0	0	152.8	39.19	113.6
300	37.6	62.4	0	0	65.4	30.15	35.25
310	37.2	62.8	0	0	65.6	24.01	41.59

Appendix C1 con't: Geotechnical characterization summary from core samples (Site 1)

Borehole depth below ground surface (m)	Dry Bulk Density ρd (g/cc)	Volumetric water content (%)	Void ratio, e	Porosity, n	Degree of Saturation, Sr (%)
10	2.07	22.76	0.308	0.235	96.7
19.5	1.74	36.47	0.577	0.366	99.7
30	1.71	35.76	0.579	0.367	97.5
41	1.70	38.83	0.566	0.362	107.4
50	1.50	46.96	0.831	0.454	103.5
60	1.86	32.35	0.449	0.310	104.4
70	1.88	30.38	0.449	0.310	98.1
80	1.86	31.18	0.470	0.320	97.5
90	1.85	33.16	0.439	0.305	108.7
98	1.76	35.02	0.591	0.372	94.2
110	1.86	31.85	0.488	0.328	97.1
118.7	2.09	42.90	0.424	0.298	144.0
121	1.82	34.23	0.505	0.336	102.0
130	1.79	36.18	0.533	0.348	104.1
138	1.82	35.34	0.493	0.330	107.1
160	1.83	34.00	0.498	0.333	102.3
170	1.73	35.87	0.633	0.388	92.5
180	1.80	35.24	0.511	0.338	104.2
187	1.65	35.07	0.553	0.356	98.5
190	1.57	37.72	0.708	0.415	91.0
200	1.84	32.47	0.450	0.310	104.6
210	1.59	32.69	0.512	0.339	96.5
220	1.65	28.59	0.495	0.331	86.4
230	2.19	21.63	0.271	0.213	101.6
240	1.77	26.72	0.434	0.302	88.4
251	1.87	28.41	0.402	0.287	99.1
260	1.82	32.55	0.491	0.330	98.8
262	1.84	23.62	0.374	0.272	86.7
270	1.75	33.06	0.638	0.389	84.9
280	1.63	46.19	0.550	0.355	130.2
290	1.81	26.55	0.470	0.320	83.1
300	1.91	26.14	0.376	0.273	95.7
310	1.92	24.85	0.375	0.273	91.1

Appendix C2: Geotechnical characterization summary from core samples (Site 2)

Borehole depth below ground surface (m)	Gravimetric water content (%)	Degree of Saturation (%)	Bulk Density (kg/m3)	Porosity, n	Void ratio, e
3.00	16.40	102.56	1861.13	0.2976858	0.4238641
8.90	27.07	101.87	1554.90	0.4132466	0.7042935
11.90	22.47	105.47	1693.68	0.3608756	0.5646407
17.90	28.28	101.20	1522.41	0.4255063	0.7406631
20.90	23.18	100.44	1644.34	0.3794943	0.6115887
23.90	26.58	100.67	1559.06	0.411674	0.699738
26.90	23.50	102.27	1647.15	0.3784336	0.6088387
29.90	24.42	101.96	1621.15	0.388244	0.6346386
32.90	25.35	99.70	1583.28	0.4025347	0.6737374
35.90	24.72	102.48	1616.72	0.3899188	0.6391262
38.90	20.69	98.99	1705.43	0.3564429	0.5538636
41.90	21.68	98.11	1671.22	0.3693503	0.5856664
44.70	22.58	102.70	1674.33	0.3681783	0.582725
48.70	21.71	105.32	1713.83	0.3532726	0.5462465
51.70	21.17	105.26	1728.69	0.3476641	0.5329526
54.70	20.82	102.52	1722.82	0.3498792	0.5381757
57.70	21.75	103.25	1700.67	0.358238	0.5582101
60.70	20.03	104.49	1757.36	0.3368437	0.50794
63.70	20.27	104.33	1749.41	0.3398449	0.5147955
66.70	18.71	100.30	1773.47	0.3307645	0.4942422
69.70	18.76	102.45	1784.22	0.3267089	0.4852416
72.70	18.96	107.56	1806.39	0.3183438	0.4670151
75.70	21.84	124.59	1809.50	0.3171685	0.4644902
78.70	18.99	106.91	1801.81	0.3200725	0.470745
81.70	20.23	105.21	1755.64	0.3374943	0.5094209
84.60	20.74	104.84	1738.68	0.3438934	0.5241425
89.90	20.59	107.72	1759.03	0.3362166	0.5065155
95.90	19.69	107.05	1781.53	0.3277227	0.4874815
98.90	19.19	110.64	1815.40	0.3149439	0.4597344
100.90	18.73	105.70	1803.38	0.3194804	0.4694653
102.80	17.95	105.42	1826.20	0.3108678	0.4511004
105.90	17.81	106.44	1835.95	0.3071874	0.4433918
116.90	22.68	105.95	1690.83	0.3619509	0.5672776
107.90	18.34	107.80	1826.60	0.3107175	0.4507839
111.90	20.99	106.90	1742.93	0.342289	0.5204246
113.90	22.37	109.02	1716.65	0.3522068	0.5437025

Appendix C2 con't: Geotechnical characterization summary from core samples (Site 2)

Borehole depth below ground surface (m)	Gravimetric water content (%)	Degree of saturation (%)	Bulk Density (kg/m^3)	Porosity, n	Void ratio, e
119.90	23.56	108.92	1684.38	0.3643851	0.5732796
120.90	22.74	104.42	1680.22	0.3659555	0.5771764
123.90	20.59	103.04	1732.51	0.3462238	0.5295754
127.10	20.09	105.43	1760.81	0.3355442	0.5049911
132.70	19.95	105.02	1762.79	0.3347976	0.5033018
135.70	19.82	104.05	1761.17	0.3354078	0.504682
138.70	21.43	102.34	1704.25	0.3568868	0.5549363
141.70	20.40	103.97	1743.56	0.342051	0.5198747
144.70	19.69	105.26	1771.71	0.3314294	0.4957283
147.70	25.80	114.48	1659.18	0.373896	0.5971787
152.60	20.94	106.75	1743.58	0.3420463	0.5198638
156.90	20.09	99.38	1725.60	0.3488314	0.5357006
165.90	18.24	104.59	1812.34	0.3160962	0.462194
170.90	18.29	103.12	1802.77	0.31971	0.4699613
174.90	17.55	101.75	1818.77	0.3136727	0.4570307
179.90	17.72	106.43	1838.78	0.3061204	0.4411723
182.90	18.98	103.24	1781.85	0.3276043	0.4872196
185.90	15.81	97.39	1852.83	0.3008198	0.4302464
189.90	16.40	100.52	1850.03	0.3018742	0.4324066
192.90	15.64	101.23	1880.24	0.2904761	0.4093957
196.70	17.22	102.58	1834.28	0.3078176	0.4447058
199.70	16.66	102.94	1854.58	0.3001594	0.4288967

Appendix C3: Atterberg limits from core samples (Site 2)

	Atterberg Limits		
Depth	**PL (%)**	**LL (%)**	**PI (%)**
50.9	20.6	93.4	72.8
59.9	20.5	95.6	75.1
69.9	17.6	58.5	40.9
80.9	20.9	97	76.1
90	20.6	132.7	112.1
100	19.2	144.3	125.1
109	18.6	121.3	102.7
120	25.5	103.4	77.9
129.5	21.7	91.5	69.8
139.9	20.9	97.3	76.4
152.8	23.9	71.2	47.3
159	23.1	78.1	55
170	28.3	80.4	52.1
180	24.2	107.3	83.1
190	22	70.9	48.9
199.9	21.7	87.2	65.5

APPENDIX D: Results of 1-D consolidation tests

Appendix D1: Site 1, Pierre Shale- 47 m BG

Appendix D2: Site 1, Pierre Shale- 87 m BG

Appendix D3: Site 1, Pierre Shale- 128 m BG

Appendix D4: Site 1, Pierre Shale- 174 m BG

Appendix D5: Site 1, Pierre Shale- 185 m BG

Appendix D6: Site 1, 1st Speckled Shale- 212 m BG

Appendix D7: Site 1, Pierre Shale- 1st Speckled Shale m BG

Appendix D8: Site 1, 2nd Speckled Shale- 283 m BG

Appendix D9: Site 1, Belle Fourche Shale- 307 m BG

Appendix D10: Site 1, Grout sample- Batch 32

Appendix D1: Site 1, Pierre Shale- 47 m BG

MDH ENGINEERED SOLUTIONS

One-Dimensional Consolidation Test - ASTM D 2435

Project No:	610598	Project Name	U of S
Date:	4-Jun-12	Tech:	JH
Sample No:	GDC-02	Checked by:	JG
Test Procedure:	Trimmed from shelby specimen		
Method of testing:	Method B	Condition of test:	Natural moisture

Input:

Diameter of ring:	63.76	mm
Height of sample:	18.19	mm
Specific gravity:	2.65	(assumed)
Initial wet sample mass:	103.97	g
Initial water content:	20.7	%
Initial LVDT reading:	9.0960	mm
Final dry mass of sample:	86.14	g
Mechanical Advantage:	1.00	

Calculations:

Cross-sectional area:	31.93	cm^2	3.2E-03 m^2
Volume of solids:	32.51	cc	3.3E-05 m^3
Total volume:	58.08	cc (prior to loading)	
Volume of voids:	25.57	cc (prior to loading)	
Initial void ratio:	0.79	(prior to loading)	
Dry mass of solids:	86.14	g	
Initial wet density:	1790	kg/m^3 (prior to loading)	
Initial dry density:	1483	kg/m^3 (prior to loading)	
Initial LVDT reading:	9.10	mm	

		At End of Primary Consolidation							Coefficient of Consolidation						
Loading Increment	Pressure (kPa)	R_{100} (mm)	Uncorrected Sample Height (mm)	Equipment Compressibility (mm)	Corrected Sample Height (mm)	Volume of Sample (cc)	Volume of Voids (cc)	Void Ratio	Average Void Ratio	R_{50} (mm)	Corrected Sample Height at R_{50} (mm)	$H_{0/50}$ (mm)	time50 (sec)	Coefficient of Consolidation c_v (cm^2/s)	coefficient of compressibility a_v (per kPa)
	0							0.79							
1	153.6	8.1220	17.2160	0.0020	17.2180	54.98	22.47	0.69	0.74	8.15	17.25	8.62	360	4.07E-04	
2	460.9	7.9550	17.0490	0.0080	17.0570	54.46	21.96	0.68	0.68	7.98	17.08	8.54	240	5.99E-04	5.15E-05
3	1075.4	7.6900	16.7840	0.0180	16.8020	53.65	21.14	0.65	0.66	7.74	16.86	8.43	300	4.66E-04	4.08E-05
4	2611.6	7.1700	16.2640	0.0320	16.2960	52.03	19.53	0.60	0.63	7.28	16.40	8.20	240	5.52E-04	3.24E-05
5	5684.0	6.6400	15.7340	0.0560	15.7900	50.42	17.91	0.55	0.58	6.79	15.94	7.97	420	2.98E-04	1.62E-05
6	11828.9	6.0300	15.1240	0.0840	15.2080	48.56	16.05	0.49	0.52	6.24	15.42	7.71	1200	9.75E-05	9.30E-06
7	27191.0	4.6200	13.7140	0.1160	13.8300	44.16	11.65	0.36	0.43	4.98	14.19	7.09	2400	4.13E-05	8.81E-06

MDH ENGINEERED SOLUTIONS

One-Dimensional Consolidation Test - ASTM D 2435

Project No:	610598	Project Name	U of S
Date:	4-Jun-12	Tech:	JH
Sample No:	GDC-02	Checked by:	JG
Test Procedure:	Trimmed from shelby specimen		
Method of testing:	Method B	Condition of test:	Natural moisture

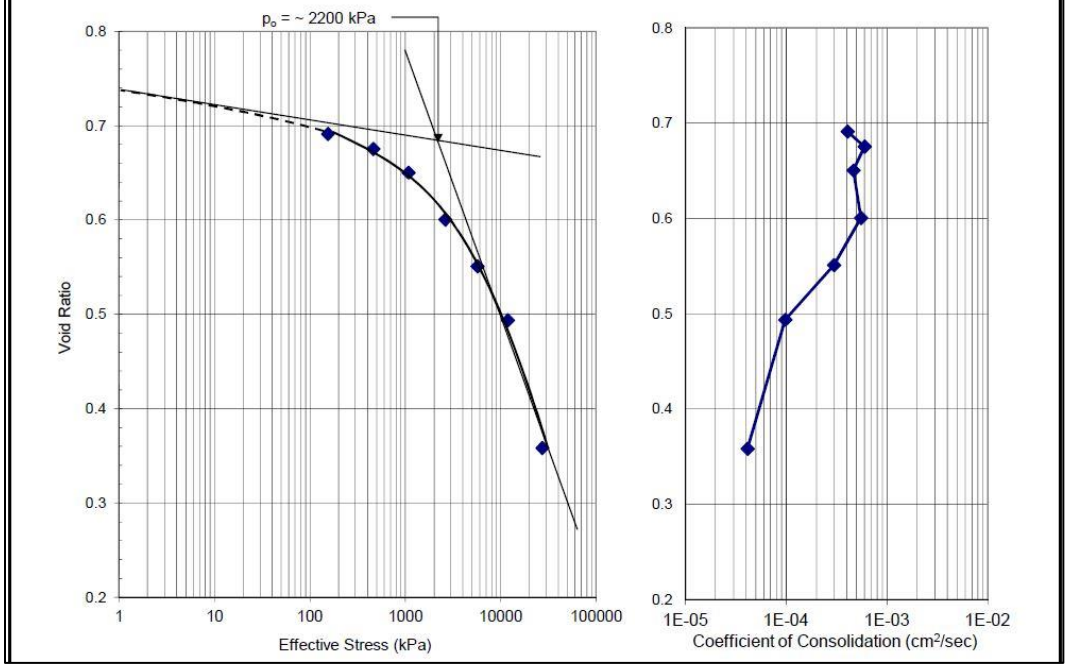

Appendix D2: Site 1, Pierre Shale- 87 m BG

MDH ENGINEERED SOLUTIONS

One-Dimensional Consolidation Test - ASTM D 2435

Project No:	L2981	Project Name	U of S - 2011 K2 Project
Date:	11-Oct-11	Tech:	TH
Sample No:	GDC-06 Core Run	Checked by:	JG
Test Procedure:	Trimmed from core specimen		
Method of testing:	Method B	Condition of test:	inundated

Input:

Diameter of ring:	63.51	mm
Height of sample:	12.56	mm
Specific gravity:	2.60	assumed
Initial wet sample mass:	85.48	g
Initial water content:	8.6	%
Initial LVDT reading:	3.566	mm
Mechanical Advantage:	1.00	

Calculations:

Cross-sectional area:	31.68	cm^2	3.2E-03 m^2
Total volume:	39.79	cc (prior to loading)	
Dry mass of solids:	78.71	g	m^3
Volume of solids:	30.27	cc	3.0E-05
Volume of voids:	9.52	cc (prior to loading)	
Initial void ratio:	0.31	(prior to loading)	
Initial deg. of saturation	0.71		
Initial wet density:	2148	kg/m^3 (prior to loading)	
Initial dry density:	1978	kg/m^3 (prior to loading)	

		At End of Primary Consolidation							Coefficient of Consolidation						
Loading Increment	Pressure (kPa)	R_{100} (mm)	Uncorrected Sample Height (mm)	Equipment Compressibility (mm)	Corrected Sample Height (mm)	Volume of Sample (cc)	Volume of Voids (cc)	Void Ratio	Average Void Ratio	R_{50} (mm)	Corrected Sample Height at R_{50} (mm)	$H_{0.50}$ (mm)	time50 (sec)	Coefficient of Consolidation c_v (cm^2/s)	coefficient of compressibility a_v (per kPa)
swelling	66.3							0.314							
1	132.6	3.782	12.344	0.084	12.428	39.37	9.10	0.301	0.31	3.77	12.85	6.43	900	9.04E-05	
2	265.2	3.876	12.250	0.150	12.400	39.28	9.01	0.298	0.30	3.87	13.02	6.51	510	1.64E-04	2.21E-05
3	530.4	3.952	12.174	0.218	12.392	39.26	8.98	0.297	0.30	3.95	13.16	6.58	360	2.37E-04	3.16E-06
4	1060.8	4.048	12.078	0.312	12.390	39.25	8.98	0.297	0.30	4.04	13.35	6.67	660	1.33E-04	3.95E-07
5	2121.6	4.154	11.972	0.398	12.370	39.19	8.91	0.294	0.30	4.15	13.54	6.77	210	4.30E-04	1.97E-06
6	4243.2	4.328	11.798	0.544	12.342	39.10	8.83	0.292	0.29	4.32	13.86	6.93	660	1.43E-04	1.38E-06
7	8486.4	4.606	11.520	0.728	12.248	38.80	8.53	0.282	0.29	4.59	14.32	7.16	270	3.74E-04	2.32E-06
8	16972.7	5.092	11.034	1.076	12.110	38.36	8.09	0.267	0.27	5.06	15.13	7.56	420	2.68E-04	1.70E-06
9	30901.7	6.272	9.854	1.884	11.738	37.19	6.91	0.228	0.25	6.12	17.00	8.50	1200	1.19E-04	2.79E-06
10	8486.4	5.450	10.676	1.246	11.922	37.77	7.49	0.248	0.24						
11	2121.6	5.030	11.096	0.996	12.092	38.31	8.03	0.265	0.26						
12	530.4	4.840	11.286	0.930	12.216	38.70	8.43	0.278	0.27						
13	132.6	4.578	11.548	0.866	12.414	39.33	9.05	0.299	0.29						

MDH ENGINEERED SOLUTIONS

One-Dimensional Consolidation Test - ASTM D 2435

Project No:	L2981	Project Name	U of S - 2011 K2 Project
Date:	11-Oct-11	Tech:	TH
Sample No:	GDC-06 Core Run 2	Checked by:	JG
Test Procedure:	Trimmed from core specimen		
Method of testing:	Method B	Condition of test:	inundated

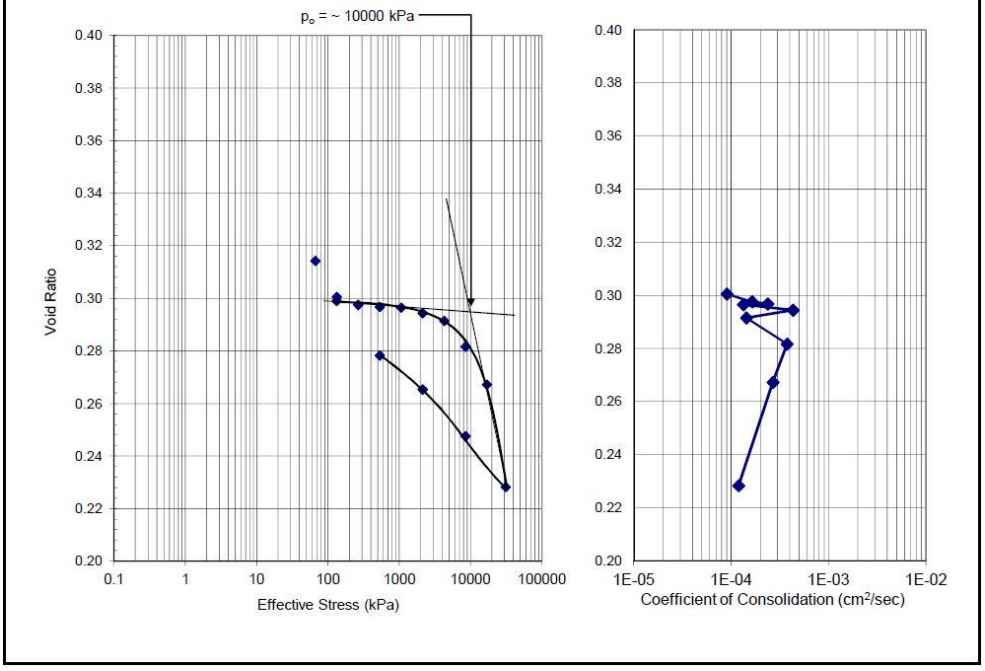

Appendix D3: Site 1, Pierre Shale- 128 m BG

MDH ENGINEERED SOLUTIONS

One-Dimensional Consolidation Test - ASTM D 2435

Project No:	610598	Project Name	U of S
Date:	5-Jun-12	Tech:	JH
Sample No:	GDC-09	Checked by:	JG
Test Procedure:	Trimmed from shelby specimen		
Method of testing:	Method B	Condition of test:	Natural moisture

Input:

Diameter of ring:	63.81	mm
Height of sample:	18.93	mm
Specific gravity:	2.65	(assumed)
Initial wet sample mass:	121.31	g
Initial water content:	10.1	%
Initial LVDT reading:	11.5300	mm
Final dry mass of sample:	110.02	g
Mechanical Advantage:	1.00	

Calculations:

Cross-sectional area:	31.98	cm^2	3.2E-03 m^2
Volume of solids:	41.52	cc	4.2E-05 m^3
Total volume:	60.54	cc (prior to loading)	
Volume of voids:	19.02	cc (prior to loading)	
Initial void ratio:	0.46	(prior to loading)	
Dry mass of solids:	110.02	g	
Initial wet density:	2004	kg/m^3 (prior to loading)	
Initial dry density:	1817	kg/m^3 (prior to loading)	
Initial LVDT reading:	11.53	mm	

		At End of Primary Consolidation							Coefficient of Consolidation						
Loading Increment	Pressure (kPa)	R_{100} (mm)	Uncorrected Sample Height (mm)	Equipment Compressibility (mm)	Corrected Sample Height (mm)	Volume of Sample (cc)	Volume of Voids (cc)	Void Ratio	Average Void Ratio	R_{50} (mm)	Corrected Sample Height at R_{50} (mm)	H_{t50} (mm)	time50 (sec)	Coefficient of Consolidation c_v (cm^2/s)	coefficient of compressibility a_v (per kPa)
swelling	0.0							0.458							
1	153.4	11.5150	18.9150	0.0300	18.9450	60.58	19.07	0.459	0.46	11.52	18.95	9.48	900	1.97E-04	
2	460.1	11.4596	18.8596	0.0400	18.8996	60.44	18.92	0.456	0.46	11.47	18.91	9.45	360	4.89E-04	1.14E-05
3	1073.7	11.3536	18.7536	0.0650	18.8186	60.18	18.66	0.450	0.45	11.37	18.84	9.42	18000	9.71E-06	1.02E-05
4	2607.5	11.2160	18.6160	0.0900	18.7060	59.82	18.30	0.441	0.45	11.22	18.71	9.36	1800	9.58E-05	5.65E-06
5	5675.1	11.0504	18.4504	0.1000	18.5504	59.32	17.81	0.429	0.43	11.07	18.57	9.28	450	3.77E-04	3.91E-06
6	11810.3	10.7608	18.1608	0.1650	18.3258	58.60	17.09	0.412	0.42	10.79	18.36	9.18	1200	1.38E-04	2.82E-06
7	2607.5	11.0700	18.4700	0.0920	18.5620	59.36	17.84	0.430	0.42						1.98E-06
8	460.1	11.2800	18.6800	0.0450	18.7250	59.88	18.36	0.442	0.44						5.85E-06
9	153.4	11.3500	18.7500	0.0330	18.7830	60.07	18.55	0.447	0.44						1.46E-05

MDH ENGINEERED SOLUTIONS

One-Dimensional Consolidation Test - ASTM D 2435

Project No:	610598	Project Name	U of S
Date:	5-Jun-12	Tech:	JH
Sample No:	GDC-09	Checked by:	JG
Test Procedure:	Trimmed from shelby specimen		
Method of testing:	Method B	Condition of test:	Natural moisture

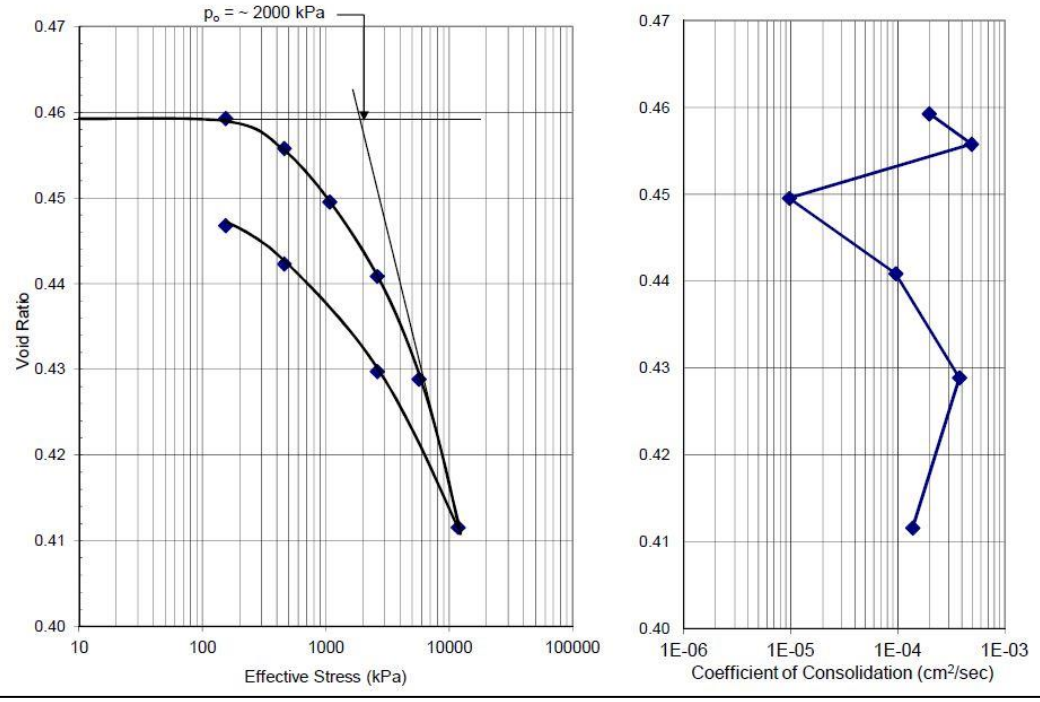

Appendix D4: Site 1, Pierre Shale- 174 m BG

MDH ENGINEERED SOLUTIONS

One-Dimensional Consolidation Test - ASTM D 2435

Project No:	610598	Project Name	U of S
Date:	24-Jul-12	Tech:	JH
Sample No:	GDC-12	Checked by:	JG
Test Procedure:	Trimmed from shelby specimen		
Method of testing:	Method B	Condition of test:	natural moisture

Input:

Diameter of ring:	63.58	mm
Height of sample:	8.7	mm
Specific gravity:	2.65	(assumed)
Initial wet sample mass:	54.52	g
Initial water content:	11.9	%
Initial LVDT reading:	8.4740	mm
Final dry mass of sample:	48.56	g
Mechanical Advantage:	1.00	

Calculations:

Cross-sectional area:	31.75	cm^2	3.2E-03 m^2
Volume of solids:	18.32	cc	1.8E-05 m^3
Total volume:	27.62	cc (prior to loading)	
Volume of voids:	9.30	cc (prior to loading)	
Initial void ratio:	0.51	(prior to loading)	
Dry mass of solids:	48.56	g	
Initial wet density:	1974	kg/m^3 (prior to loading)	
Initial dry density:	1758	kg/m^3 (prior to loading)	
Initial LVDT reading:	8.474	mm	

		At End of Primary Consolidation							Coefficient of Consolidation						
Loading Increment	Pressure (kPa)	R_{100} (mm)	Uncorrected Sample Height (mm)	Equipment Compressibility (mm)	Corrected Sample Height (mm)	Volume of Sample (cc)	Volume of Voids (cc)	Void Ratio	Average Void Ratio	R_{50} (mm)	Corrected Sample Height at R_{50} (mm)	H_{D50} (mm)	time50 (sec)	Coefficient of Consolidation c_v (cm^2/s)	coefficient of compressibility a_v (per kPa)
swelling	#REF!							0.51							
1	154.5	8.0191	8.2451	0.02	8.2651	26.24	7.92	0.43	0.47	8.03	8.27	4.14	150	2.25E-04	
2	463.5	7.8950	8.1210	0.022	8.1430	25.85	7.53	0.41	0.42	7.91	8.16	4.08	900	3.64E-05	6.85E-05
3	1081.4	7.7060	7.9320	0.03	7.9620	25.28	6.95	0.38	0.40	7.72	7.98	3.99	390	8.04E-05	5.07E-05
4	2626.4	7.4862	7.7122	0.052	7.7642	24.65	6.33	0.35	0.36	7.50	7.77	3.89	1800	1.65E-05	2.22E-05
5	5716.2	7.3580	7.5840	0.048	7.6320	24.23	5.91	0.32	0.33	7.37	7.65	3.82	606	4.75E-05	7.41E-06
6	11895.9	7.1952	7.4212	0.076	7.4972	23.80	5.48	0.30	0.31	7.21	7.51	3.76	1260	2.21E-05	3.78E-06
7	27345.2	6.6890	6.9150	0.188	7.1030	22.55	4.23	0.23	0.26	6.74	7.16	3.58	3000	8.41E-06	4.42E-06
8	58243.8	6.0950	6.3210	0.258	6.5790	20.89	2.56	0.14	0.19	6.21	6.70	3.35	2400	9.20E-06	2.94E-06
9	6179.7	6.6920	6.9180	0.092	7.0100	22.26	3.93	0.21	0.18						
10	1544.9	6.8900	7.1160	0.092	7.2080	22.88	4.56	0.25	0.23						
11	309.0	7.0160	7.2420	0.046	7.2880	23.14	4.81	0.26	0.26						
12	154.5	7.0660	7.2920	0.012	7.3040	23.19	4.86	0.27	0.26						

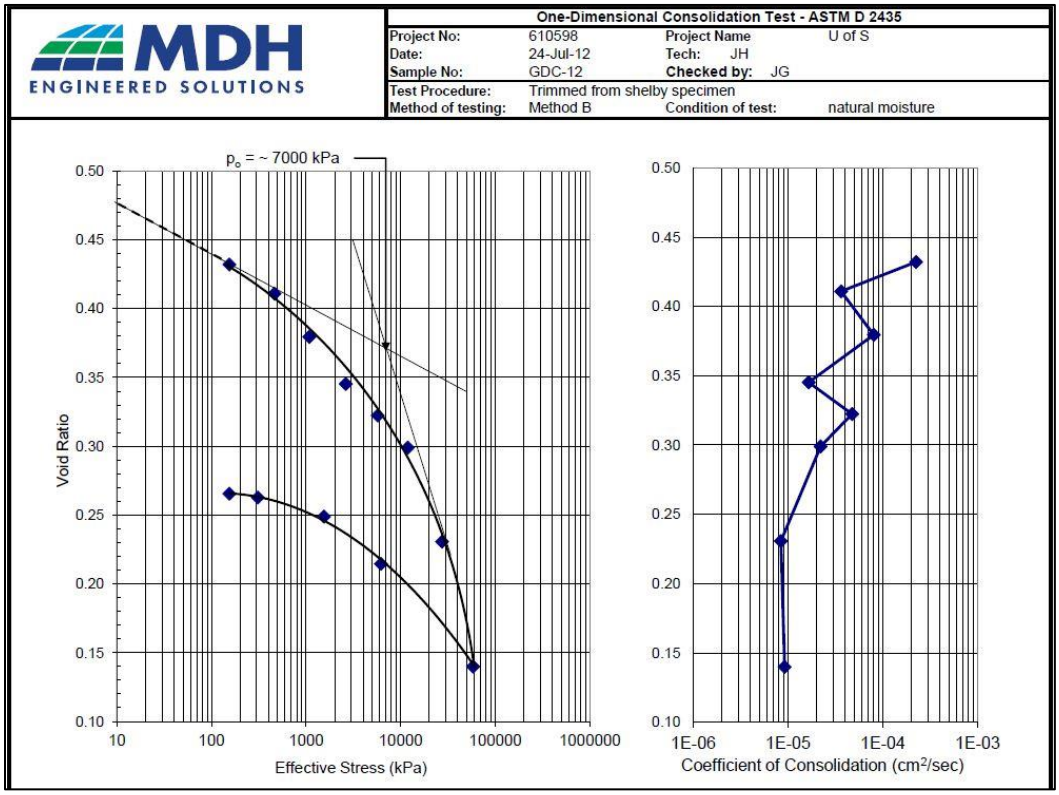

Appendix D5: Site 1, Pierre Shale- 185 m BG

MDH ENGINEERED SOLUTIONS

One-Dimensional Consolidation Test - ASTM D 2435

Project No:	610598	Project Name	U of S
Date:	25-Jul-12	Tech:	JH
Sample No:	JNC-06	Checked by:	JG
Test Procedure:	Trimmed from shelby specimen		
Method of testing:	Method B	Condition of test:	natural moisture

Input:

Diameter of ring:	50.64	mm
Height of sample:	11.93	mm
Specific gravity:	2.65	(assumed)
Initial wet sample mass:	50.16	g
Initial water content:	17.0	%
Initial LVDT reading:	12.082	mm
Final dry mass of sample:	41.97	g
Mechanical Advantage:	1.00	

Calculations:

Cross-sectional area:	20.14	cm^2	2.0E-03 m^2
Volume of solids:	15.84	cc	1.6E-05 m^3
Total volume:	24.03	cc (prior to loading)	
Volume of voids:	8.19	cc (prior to loading)	
Initial void ratio:	0.52	(prior to loading)	
Dry mass of solids:	41.97	g	
Initial wet density:	2088	kg/m^3 (prior to loading)	
Initial dry density:	1747	kg/m^3 (prior to loading)	
Initial LVDT reading:	12.08	mm	

		At End of Primary Consolidation							Coefficient of Consolidation						
Loading Increment	Pressure (kPa)	R_{100} (mm)	Uncorrected Sample Height (mm)	Equipment Compressibility (mm)	Corrected Sample Height (mm)	Volume of Sample (cc)	Volume of Voids (cc)	Void Ratio	Average Void Ratio	R_{50} (mm)	Corrected Sample Height at R_{50} (mm)	H_{D50} (mm)	time50 (sec)	Coefficient of Consolidation c_v (cm^2/s)	coefficient of compressibility a_v (per kPa)
swelling	#REF!							0.52							
1	155.9	12.0160	11.8640	0.0020	11.8660	23.90	8.06	0.51	0.51	12.04	11.89	5.94	246	2.83E-04	
2	467.6	11.7945	11.6425	0.0240	11.6665	23.50	7.66	0.48	0.50	11.81	11.69	5.84	420	1.60E-04	8.14E-05
3	1091.0	11.5850	11.4330	0.0580	11.4910	23.14	7.31	0.46	0.47	11.60	11.51	5.75	360	1.81E-04	3.58E-05
4	2649.7	11.2420	11.0900	0.1040	11.1940	22.55	6.71	0.42	0.44	11.28	11.23	5.61	606	1.02E-04	2.42E-05
5	5766.9	10.9320	10.7800	0.0840	10.8640	21.88	6.04	0.38	0.40	10.98	10.91	5.45	540	1.09E-04	1.35E-05
6	12001.4	10.4850	10.3330	0.1060	10.4390	21.03	5.19	0.33	0.35	10.55	10.50	5.25	480	1.13E-04	8.67E-06
7	27587.7	9.6110	9.4590	0.2180	9.6770	19.49	3.65	0.23	0.28	9.73	9.79	4.90	1800	2.62E-05	6.22E-06
8	58760.2	8.1000	7.9480	0.3300	8.2780	16.67	0.83	0.05	0.14	8.46	8.63	4.32	3600	1.02E-05	5.71E-06
9	6234.5	8.8540	8.7020	0.2000	8.9020	17.93	2.09	0.13	0.09						
10	1558.6	9.2900	9.1380	0.1420	9.2800	18.69	2.85	0.18	0.16						
11	311.7	9.6160	9.4640	0.0740	9.5380	19.21	3.37	0.21	0.20						
12	155.9	9.6700	9.5180	0.0040	9.5220	19.18	3.34	0.21	0.21						

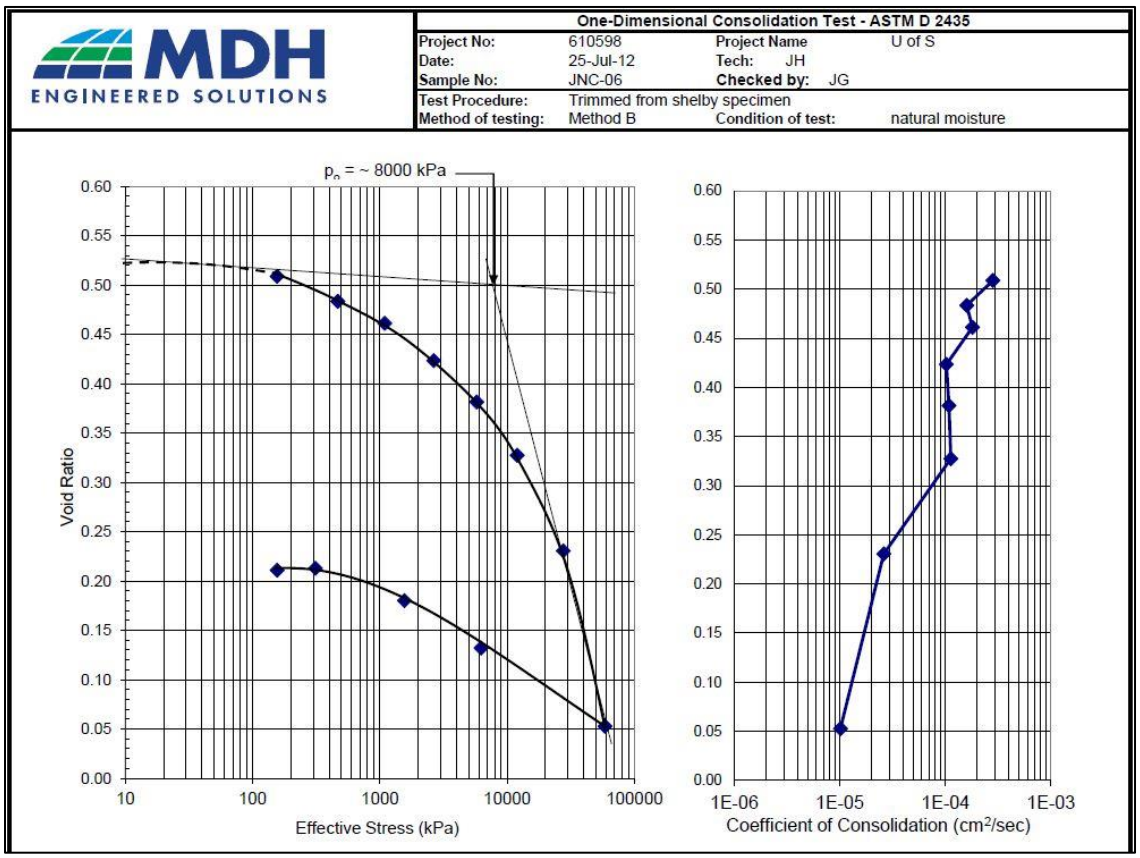

Appendix D6: Site 1, 1st Speckled Shale- 212 m BG

MDH ENGINEERED SOLUTIONS

One-Dimensional Consolidation Test - ASTM D 2435

Project No:	L2981	Project Name	U of S - 2011 K2 Project
Date:	06-Oct-11	Tech:	TH
Sample No:	GDC-14 Core Run	Checked by:	JG
Test Procedure:	Trimmed from core specimen		
Method of testing:	Method B	Condition of test	inundated

Input:

Diameter of ring:	63.3	mm
Height of sample:	13.19	mm
Specific gravity:	2.60	assumed
Initial wet sample mass:	72.81	g
Initial water content:	8.1	%
Initial LVDT reading:	4.144	mm
Mechanical Advantage:	1.00	

Calculations:

Cross-sectional area:	31.47	cm^2 3.1E-03 m^2
Total volume:	41.51	cc (prior to loading)
Dry mass of solids:	67.35	g
Volume of solids:	25.91	cc 2.6E-05 m^3
Volume of voids:	15.60	cc (prior to loading)
Initial void ratio:	0.60	(prior to loading)
Initial deg. Of saturation	0.35	
Initial wet density:	1754	kg/m^3 (prior to loading)
Initial dry density:	1623	kg/m^3 (prior to loading)

		At End of Primary Consolidation							Coefficient of Consolidation						
Loading Increment	Pressure (kPa)	R_{100} (mm)	Uncorrected Sample Height (mm)	Equipment Compressibility (mm)	Corrected Sample Height (mm)	Volume of Sample (cc)	Volume of Voids (cc)	Void Ratio	Average Void Ratio	R_{50} (mm)	Corrected Sample Height at R_{50} (mm)	H_{D50} (mm)	time50 (sec)	Coefficient of Consolidation c_v (cm^2/s)	coefficient of compressibility a_v (per kPa)
swelling	76.7							0.60							
1	153.3	4.258	13.076	0.124	12.952	40.76	14.85	0.57	0.59	4.25	13.42	6.71	600	1.48E-04	
2	306.6	4.324	13.010	0.170	12.840	40.41	14.50	0.56	0.57	4.33	13.54	6.77	24	3.76E-03	8.87E-05
3	613.2	4.400	12.934	0.202	12.732	40.07	14.16	0.55	0.55	4.39	13.64	6.82	12000	7.63E-06	4.28E-05
4	1226.5	4.500	12.834	0.246	12.588	39.61	13.71	0.53	0.54	4.49	13.78	6.89	15600	6.00E-06	2.85E-05
5	2452.9	4.652	12.682	0.302	12.380	38.96	13.05	0.50	0.52	4.65	13.99	7.00	480	2.01E-04	2.06E-05
6	4905.8	4.848	12.486	0.396	12.090	38.05	12.14	0.47	0.49	4.84	14.28	7.14	1500	6.69E-05	1.44E-05
7	9811.6	5.148	12.186	0.596	11.590	36.47	10.57	0.41	0.44	5.13	14.77	7.39	1140	9.43E-05	1.24E-05
8	19623.2	5.676	11.658	0.998	10.660	33.55	7.64	0.29	0.35	5.63	15.67	7.83	720	1.68E-04	1.15E-05
9	31107.0	6.388	10.946	1.454	9.492	29.87	3.97	0.15	0.22	6.28	16.78	8.39	1080	1.28E-04	1.24E-05
10	9811.6	5.740	11.594	0.902	10.692	33.65	7.74	0.30	0.23						
11	2452.9	5.388	11.946	0.626	11.320	35.62	9.72	0.38	0.34						
12	613.2	5.162	12.172	0.564	11.608	36.53	10.62	0.41	0.39						
13	153.3	5.010	12.324	0.494	11.830	37.23	11.32	0.44	0.42						
14	76.7	4.970	12.364	0.494	11.870	37.35	11.45	0.44	0.44						

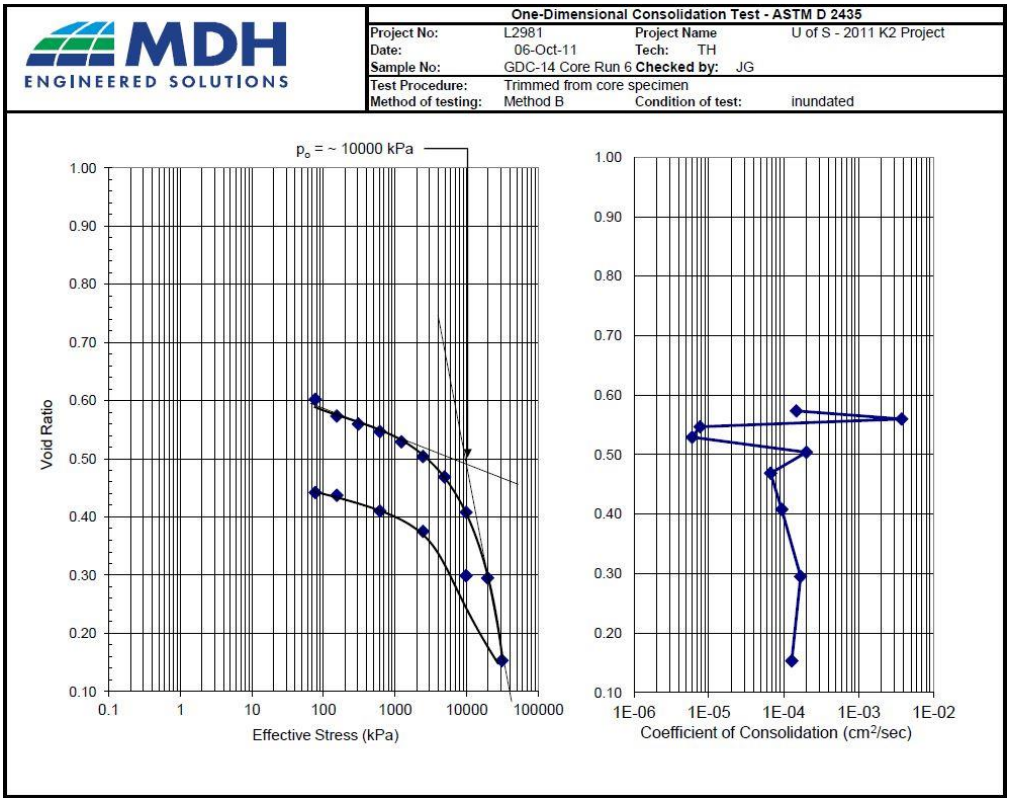

Appendix D7: Site 1, Pierre Shale- 1st Speckled Shale m BG

MDH ENGINEERED SOLUTIONS

One-Dimensional Consolidation Test - ASTM D 2435

Project No:	610598	Project Name:	U of S
Date:	26-Jul-12	Tech:	JH
Sample No:	JNC-10	Checked by:	JG
Test Procedure:	Trimmed from shelby specimen		
Method of testing:	Method B	Condition of test:	natural moisture

Input:

Diameter of ring:	62.89	mm
Height of sample:	12.08	mm
Specific gravity:	2.65	(assumed)
Initial wet sample mass:	80.66	g
Initial water content:	9.0	%
Initial LVDT reading:	14.3550	mm
Final dry mass of sample:	74.00	g
Mechanical Advantage:	1.00	

Calculations:

Cross-sectional area:	31.06	cm^2	3.1E-03 m^2
Volume of solids:	27.92	cc	2.8E-05 m^3
Total volume:	37.52	cc (prior to loading)	
Volume of voids:	9.60	cc (prior to loading)	
Initial void ratio:	0.34	(prior to loading)	
Dry mass of solids:	74.00	g	
Initial wet density:	2150	kg/m^3 (prior to loading)	
Initial dry density:	1972	kg/m^3 (prior to loading)	
Initial LVDT reading:	14.36	mm	

		At End of Primary Consolidation							Coefficient of Consolidation						
Loading Increment	Pressure (kPa)	R_{100} (mm)	Uncorrected Sample Height (mm)	Equipment Compressibility (mm)	Corrected Sample Height (mm)	Volume of Sample (cc)	Volume of Voids (cc)	Void Ratio	Average Void Ratio	R_{50} (mm)	Corrected Sample Height at R_{50} (mm)	H_{D50} (mm)	time50 (sec)	Coefficient of Consolidation c_v (cm^2/s)	coefficient of compressibility a_v (per kPa)
swelling	0.0							0.34							
1	157.9	14.1905	11.9155	0.0100	11.9255	37.05	9.12	0.33	0.34	14.20	11.93	5.97	180	3.90E-04	
2	473.7	14.1313	11.8563	0.0500	11.9063	36.99	9.06	0.32	0.33	14.13	11.91	5.95	900	7.76E-05	6.76E-06
3	1105.3	14.0718	11.7968	0.0500	11.8468	36.80	8.88	0.32	0.32	14.08	11.85	5.93	1200	5.77E-05	1.05E-05
4	2684.3	13.8685	11.5935	0.0900	11.6835	36.29	8.37	0.30	0.31	13.88	11.69	5.85	600	1.12E-04	1.15E-05
5	5842.4	13.6000	11.3250	0.1000	11.4250	35.49	7.57	0.27	0.29	13.61	11.44	5.72	540	1.19E-04	9.11E-06
6	12158.4	13.3020	11.0270	0.1750	11.2020	34.80	6.87	0.25	0.26	13.33	11.23	5.62	720	8.63E-05	3.93E-06
7	27948.5	12.5390	10.2640	0.4000	10.6640	33.13	5.20	0.19	0.22	12.58	10.71	5.35	1080	5.23E-05	3.79E-06
8	59528.8	11.2750	9.0000	0.6650	9.6650	30.02	2.10	0.08	0.13	11.34	9.73	4.87	330	1.41E-04	3.52E-06
9	6316.1	12.1850	9.9100	0.2000	10.1100	31.41	3.48	0.12	0.10						
10	1579.0	12.4900	10.2150	0.1000	10.3150	32.04	4.12	0.15	0.14						
11	315.8	12.6900	10.4150	0.0700	10.4850	32.57	4.65	0.17	0.16						
12	157.9	12.7350	10.4600	0.0250	10.4850	32.57	4.65	0.17	0.17						

MDH ENGINEERED SOLUTIONS

One-Dimensional Consolidation Test - ASTM D 2435

Project No:	610598	Project Name	U of S
Date:	26-Jul-12	Tech:	JH
Sample No:	JNC-10	Checked by:	JG
Test Procedure:	Trimmed from shelby specimen		
Method of testing:	Method B	Condition of test:	natural moisture

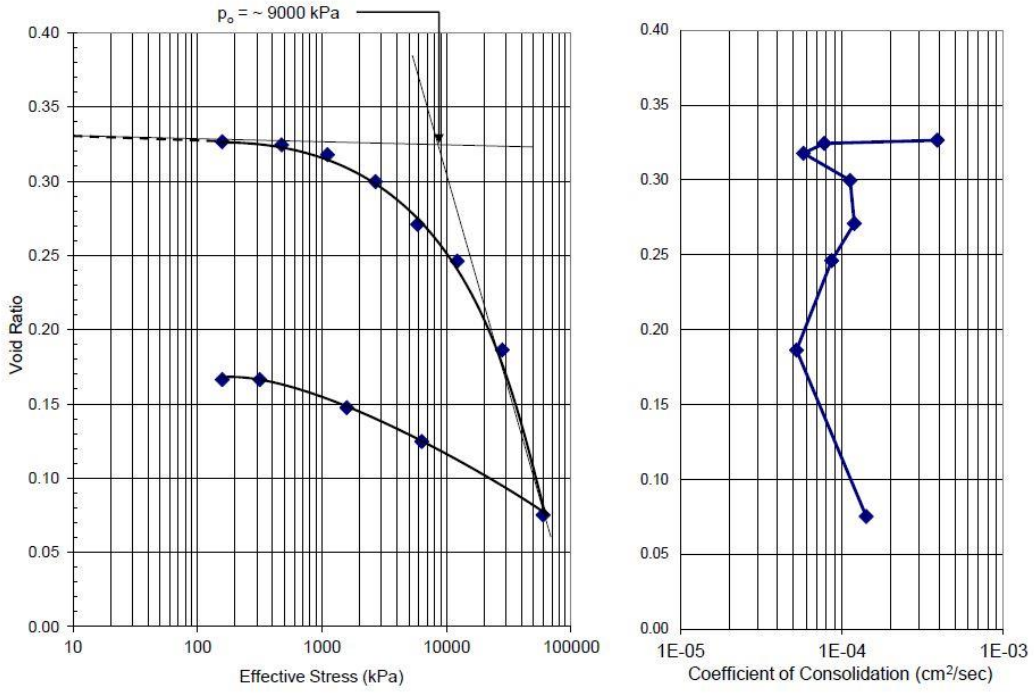

Appendix D8: Site 1, 2nd Speckled Shale- 283 m BG

MDH ENGINEERED SOLUTIONS

One-Dimensional Consolidation Test - ASTM D 2435

Project No:	610598	Project Name:	U of S
Date:	31-Jul-12	Tech:	JH
Sample No:	JNC-14	Checked by:	JG
Test Procedure:	Trimmed from shelby specimen		
Method of testing:	Method B	Condition of test:	natural moisture

Input:

Diameter of ring:	63.51	mm
Height of sample:	17.77	mm
Specific gravity:	2.65	(assumed)
Initial wet sample mass:	113.34	g
Initial water content:	5.2	%
Initial LVDT reading:	11.4340	mm
Final dry mass of sample:	104.81	g
Mechanical Advantage:	1.00	

Calculations:

Cross-sectional area:	31.68	cm^2	3.2E-03 m^2
Volume of solids:	39.55	cc	4.0E-05 m^3
Total volume:	56.29	cc (prior to loading)	
Volume of voids:	16.74	cc (prior to loading)	
Initial void ratio:	0.42	(prior to loading)	
Dry mass of solids:	104.81	g	
Initial wet density:	2013	kg/m^3 (prior to loading)	
Initial dry density:	1862	kg/m^3 (prior to loading)	
Initial LVDT reading:	11.43	mm	

		At End of Primary Consolidation							Coefficient of Consolidation						
Loading Increment	Pressure (kPa)	R_{100} (mm)	Uncorrected Sample Height (mm)	Equipment Compressibility (mm)	Corrected Sample Height (mm)	Volume of Sample (cc)	Volume of Voids (cc)	Void Ratio	Average Void Ratio	R_{50} (mm)	Corrected Sample Height at R_{50} (mm)	H_{d50} (mm)	time50 (sec)	Coefficient of Consolidation c_v (cm^2/s)	coefficient of compressibility a_v (per kPa)
swelling	0.0							0.42							
1	154.8	11.0850	17.4210	0.009	17.4300	55.22	15.67	0.40	0.41	11.09	17.44	8.72	180	8.32E-04	
2	464.5	11.0292	17.3652	0.038	17.4032	55.13	15.58	0.39	0.40	11.04	17.41	8.70	1200	1.24E-04	6.93E-06
3	1083.8	10.9788	17.3148	0.054	17.3688	55.02	15.47	0.39	0.39	10.99	17.38	8.69	360	4.13E-04	4.45E-06
4	2632.2	10.8118	17.1478	0.086	17.2338	54.60	15.04	0.38	0.39	10.82	17.25	8.62	420	3.49E-04	6.98E-06
5	5728.8	10.6430	16.9790	0.102	17.0810	54.11	14.56	0.37	0.37	10.66	17.09	8.55	240	6.00E-04	3.95E-06
6	11922.2	10.4100	16.7460	0.156	16.9020	53.54	13.99	0.35	0.36	10.43	16.92	8.46	246	5.73E-04	2.31E-06
7	27405.5	9.7920	16.1280	0.352	16.4800	52.21	12.66	0.32	0.34	9.83	16.52	8.26	540	2.49E-04	2.18E-06
8	58372.2	9.4700	15.8060	0.396	16.2020	51.33	11.78	0.30	0.31	9.56	16.29	8.15	780	1.68E-04	7.19E-07
9	6193.3	9.7300	16.0660	0.322	16.3880	51.92	12.36	0.31	0.31						
10	1548.3	10.0480	16.3840	0.192	16.5760	52.51	12.96	0.33	0.32						
11	309.7	10.2300	16.5660	0.062	16.6280	52.68	13.13	0.33	0.33						
12	154.8	10.2920	16.6280	0.02	16.6480	52.74	13.19	0.33	0.33						

MDH ENGINEERED SOLUTIONS

One-Dimensional Consolidation Test - ASTM D 2435

Project No:	610598	Project Name	U of S
Date:	31-Jul-12	Tech:	JH
Sample No:	JNC-14	Checked by:	JG
Test Procedure:	Trimmed from shelby specimen		
Method of testing:	Method B	Condition of test:	natural moisture

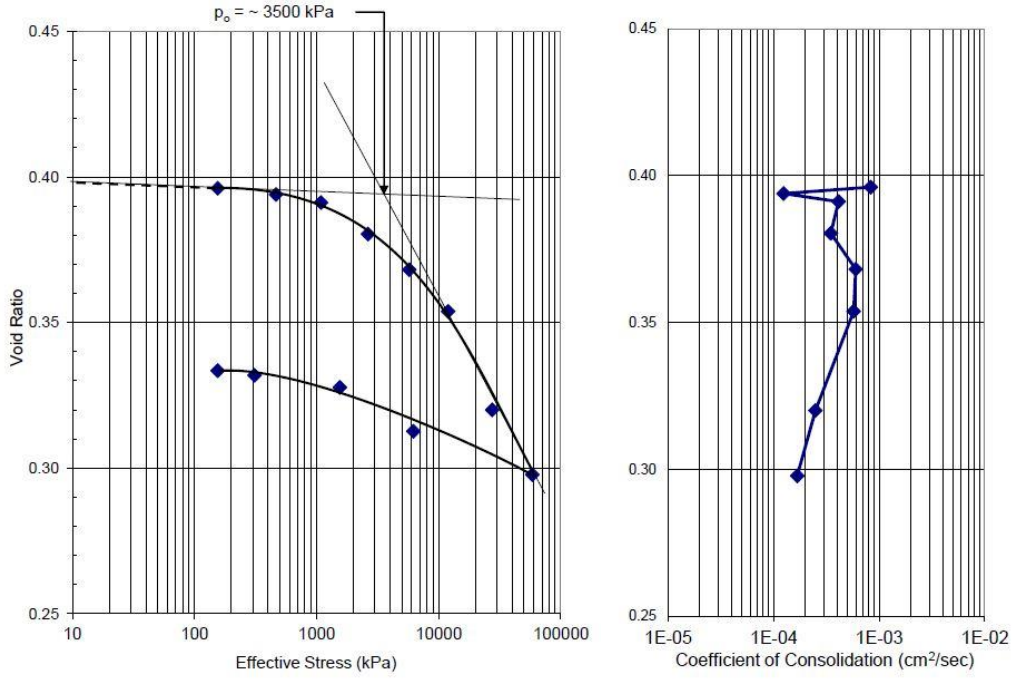

Appendix D9: Site 1, Belle Fourche Shale- 307 m BG

MDH ENGINEERED SOLUTIONS

One-Dimensional Consolidation Test - ASTM D 2435

Project No:	L2981	**Project Name**	U of S - 2011 K2 Project
Date:	06-Oct-11	**Tech:**	TH
Sample No:	KLP-18	**Checked by:**	JG
Test Procedure:	Trimmed from core specimen		
Method of testing:	Method B	**Condition of test**	inundated

Input:

Diameter of ring:	63.32	mm
Height of sample:	12.72	mm
Specific gravity:	2.61	assumed
Initial wet sample mass:	90.13	g
Initial water content:	6.2	%
Initial LVDT reading:	4.4340	mm
Mechanical Advantage:	1.00	

Calculations:

Cross-sectional area:	31.49 cm^2	3.1E-03 m^2
Total volume:	40.06 cc	(prior to loading)
Dry mass of solids:	84.87 g	
Volume of solids:	32.52 cc	3.3E-05 m^3
Volume of voids:	7.54 cc	(prior to loading)
Initial void ratio:	0.23	(prior to loading)
Initial deg. of saturation	0.698	
Initial wet density:	2250 kg/m^3	(prior to loading)
Initial dry density:	2119 kg/m^3	(prior to loading)

		At End of Primary Consolidation							Coefficient of Consolidation						
Loading Increment	Pressure (kPa)	R_{100} (mm)	Uncorrected Sample Height (mm)	Equipment Compressibility (mm)	Corrected Sample Height (mm)	Volume of Sample (cc)	Volume of Voids (cc)	Void Ratio	Average Void Ratio	R_{50} (mm)	Corrected Sample Height at R_{50} (mm)	H_{t50} (mm)	time50 (sec)	Coefficient of Consolidation c_v (cm^2/s)	coefficient of compressibility a_v (per kPa)
swelling	59.8							0.23							
2	119.6	4.452	12.702	0.084	12.786	40.26	7.75	0.24							
3	239.3	4.528	12.626	0.124	12.750	40.15	7.63	0.23							
4	478.5	4.554	12.600	0.168	12.768	40.21	7.69	0.24							
5	957.0	4.592	12.562	0.218	12.780	40.24	7.73	0.24							
6	1914.0	4.632	12.522	0.296	12.818	40.36	7.85	0.24							
7	3828.1	4.744	12.410	0.412	12.822	40.38	7.86	0.24							
8	7656.1	4.950	12.204	0.602	12.806	40.33	7.81	0.24							
9	15312.2	5.385	11.769	0.908	12.677	39.92	7.40	0.23							
10	30624.5	6.235	10.919	1.482	12.401	39.05	6.53	0.20							
11	7656.1	5.380	11.774	0.603	12.377	38.98	6.46	0.20							
12	1914.0	5.085	12.069	0.298	12.367	38.94	6.43	0.20							
13	478.5	4.850	12.304	0.169	12.473	39.28	6.76	0.21							
14	119.6	4.700	12.454	0.086	12.540	39.49	6.97	0.21							

MDH ENGINEERED SOLUTIONS

One-Dimensional Consolidation Test - ASTM D 2435

Project No:	L2981	**Project Name**	U of S - 2011 K2 Project
Date:	18-Jul-11	**Tech:**	TH
Sample No:	KLP-18	**Checked by:**	JG
Test Procedure:	Trimmed from core specimen		
Method of testing:	Method B	**Condition of test:**	inundated

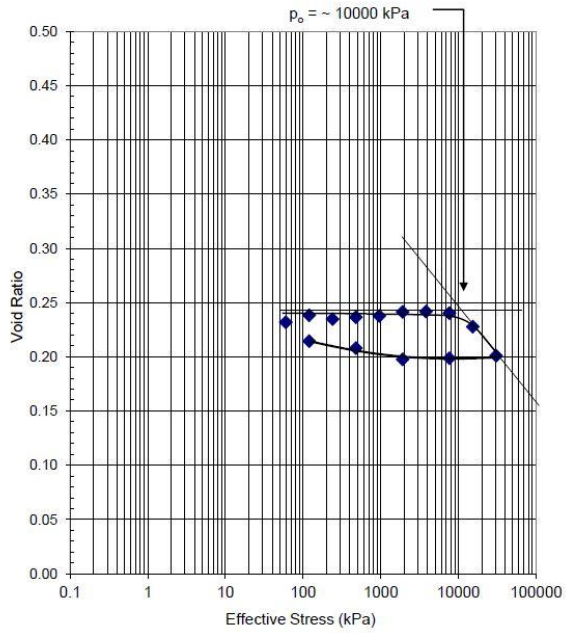

Appendix D10: Site 1, Grout sample- Batch 32

MDH ENGINEERED SOLUTIONS

One-Dimensional Consolidation Test - ASTM D 2435

Project No:	L2981	Project Name	-
Date:	03-Aug-11	Tech:	TH
Sample No:	Grout B#32	Checked by:	JG
Test Procedure:	Trimmed from core specimen		
Method of testing:	Method B	Condition of test:	inundated

Input:

Diameter of ring:	63.72	mm
Height of sample:	19.49	mm
Specific gravity:	2.70	assumed
Initial wet sample mass:	100.18	g
Initial water content:	41.3	%
Initial LVDT reading:	6.3440	mm
Mechanical Advantage:	11.00	

Calculations:

Cross-sectional area:	31.89	cm^2 3.2E-03 m^2
Total volume:	62.15	cc (prior to loading)
Dry mass of solids:	70.90	
Volume of solids:	26.26	cc 3.0E-07 m^3
Volume of voids:	35.89	cc (prior to loading)
Initial void ratio:	1.37	(prior to loading)
Initial deg. of saturation	0.8158	
Initial wet density:	1612	kg/m^3 (prior to loading)
Initial dry density:	1141	kg/m^3 (prior to loading)

		At End of Primary Consolidation							Coefficient of Consolidation						
Loading Increment	Pressure (kPa)	R_{100} (mm)	Uncorrected Sample Height (mm)	Equipment Compressibility (mm)	Corrected Sample Height (mm)	Volume of Sample (cc)	Volume of Voids (cc)	Void Ratio	Average Void Ratio	R_{50} (mm)	Corrected Sample Height at R_{50} (mm)	H_{t50} (mm)	time50 (sec)	Coefficient of Consolidation c_v (cm^2/s)	coefficient of compressibility a_v (per kPa)
swelling	10.6							1.37							
1	21.8	6.3360	19.4820	0.0000	19.4820	62.13	35.87	1.37	1.37	6.34	19.48	9.74	10200	1.83E-05	
2	44.1	6.3280	19.4740	0.0080	19.4820	62.13	35.87	1.37	1.37	6.33	19.48	9.74	12000	1.56E-05	
3	85.8	6.3260	19.4720	0.0180	19.4900	62.15	35.89	1.37	1.37	6.33	19.49	9.75	12600	1.48E-05	
4	170.4	6.2860	19.4320	0.0320	19.4640	62.07	35.81	1.36	1.37	6.30	19.47	9.74	4080	4.58E-05	3.73E-05
5	339.6	6.1840	19.3300	0.0480	19.3780	61.79	35.54	1.35	1.36	6.20	19.40	9.70	3720	4.98E-05	6.17E-05
6	680.8	6.1220	19.2680	0.0740	19.3420	61.68	35.42	1.35	1.35	6.13	19.35	9.68	960	1.92E-04	1.28E-05
7	1357.6	6.0620	19.2080	0.1060	19.3140	61.59	35.33	1.35	1.35	6.07	19.32	9.66	10800	1.70E-05	5.02E-06
8	2703.0	5.9860	19.1320	0.1460	19.2780	61.48	35.22	1.34	1.34	6.00	19.29	9.65	10800	1.70E-05	3.25E-06
9	5026.4	5.8945	19.0405	0.2000	19.2405	61.36	35.10	1.34	1.34	6.00	19.34	9.67	10800	1.71E-05	1.96E-06
10	1357.6	5.9880	19.1340	0.1260	19.2600	61.42	35.16	1.34	1.34						
11	339.6	6.0600	19.2060	0.0760	19.2820	61.49	35.23	1.34	1.34						
12	85.8	6.0960	19.2420	0.0460	19.2880	61.51	35.25	1.34	1.34						
13	10.6	6.1210	19.2670	0.0240	19.2910	61.52	35.26	1.34	1.34						

MDH ENGINEERED SOLUTIONS

One-Dimensional Consolidation Test - ASTM D 2435

Project No: L2981 Project Name -
Date: 03-Aug-11 Tech: TH
Sample No: Grout B#32 Checked by: JG
Test Procedure: Trimmed from core specimen
Method of testing: Method B Condition of test: inundated

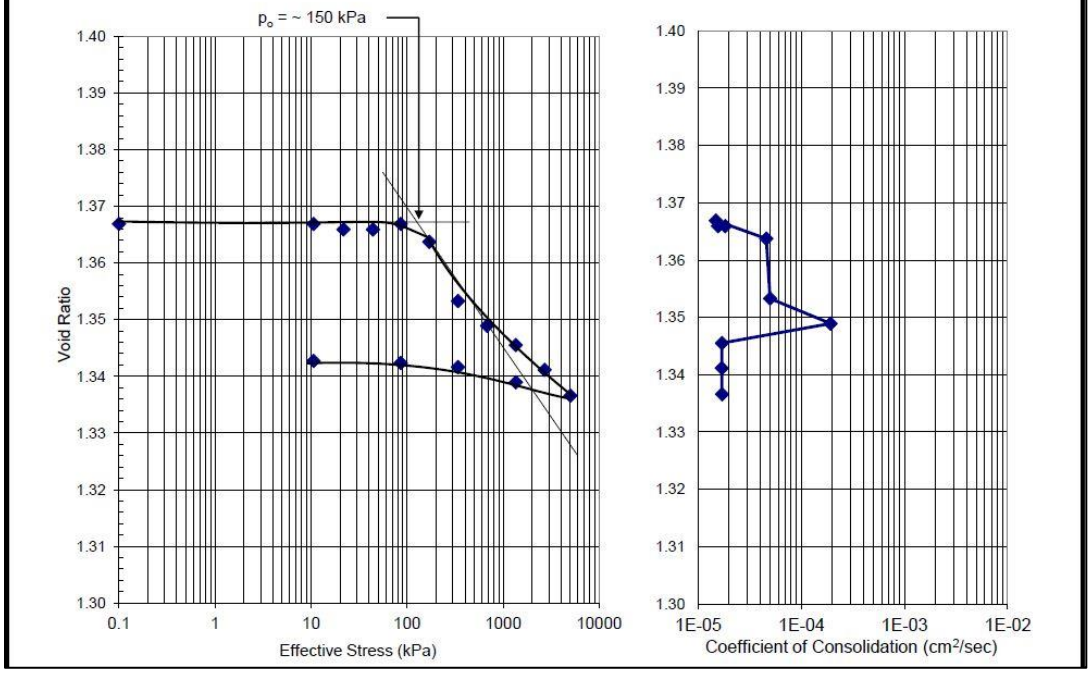

APPENDIX E: Results of the triaxial hydraulic conductivity tests

Appendix E1: Site 1, Pierre Shale- 20.7 m

Appendix E2: Site 1: Pierre Shale- 74.33 m

Appendix E3: Site 1, Pierre Shale- 111 m

Appendix E4: Site 1, 1st Speckled Shale- 207 m

Appendix E5: Site 1, 1st Speckled Shale- 257 m

Appendix E6: Site 1, 2nd Speckled Shale- 277 m

Appendix E7: Site 1, Belle Fourche- 311 m

Appendix E8: Site 1, Grout- Batch 1

Appendix E9: Site 1, Grout-Batch 24

Appendix E10: Site 1, Grout- Batch 48

Appendix E11: Site 2, Pierre Shale- 30 m

Appendix E12: Site 2, Pierre Shale- 82 m

Appendix E13: Site 2, Pierre Shale- 126.77 m

Appendix E1: Site 1, Pierre Shale- 20.7 m

TRIAXIAL HYDRAULIC CONDUCTIVITY TEST REPORT

Test reference: ASTM D 5084

MDH ENGINEERED SOLUTIONS

CLIENT:	-
PROJECT:	-
MDH Job No:	M1870
DATE:	14-Dec-10

SAMPLE: ADK-01 Core sample

Depth: 7.0m

Testing Summary:

Average back pressure =	200 kPa	**Post test condition**	
Effective confining pressure =	200 kPa	Final sample diameter =	73.85 mm
Head across sample =	15.8 kPa	Final sample height =	21.89 mm
Hydraulic gradient =	73	Final water content =	21.0 %
		Final Dry Density =	1725 kg/m^3
Specific gravity of solids =	2.55 (assumed)	Final void ratio =	0.54
Initial sample condition			
Initial sample diameter =	73.85 mm		
Initial sample height =	22.00 mm	Permeant:	de-aired tap-water
Initial Water Content =	17.5 %		
Initial Dry Density =	1775 kg/m^3	**Final Hydraulic Conductivity:**	
Initial void ratio =	0.49	k = 2.0E-11 m/s @	38,774 minutes

Comments:

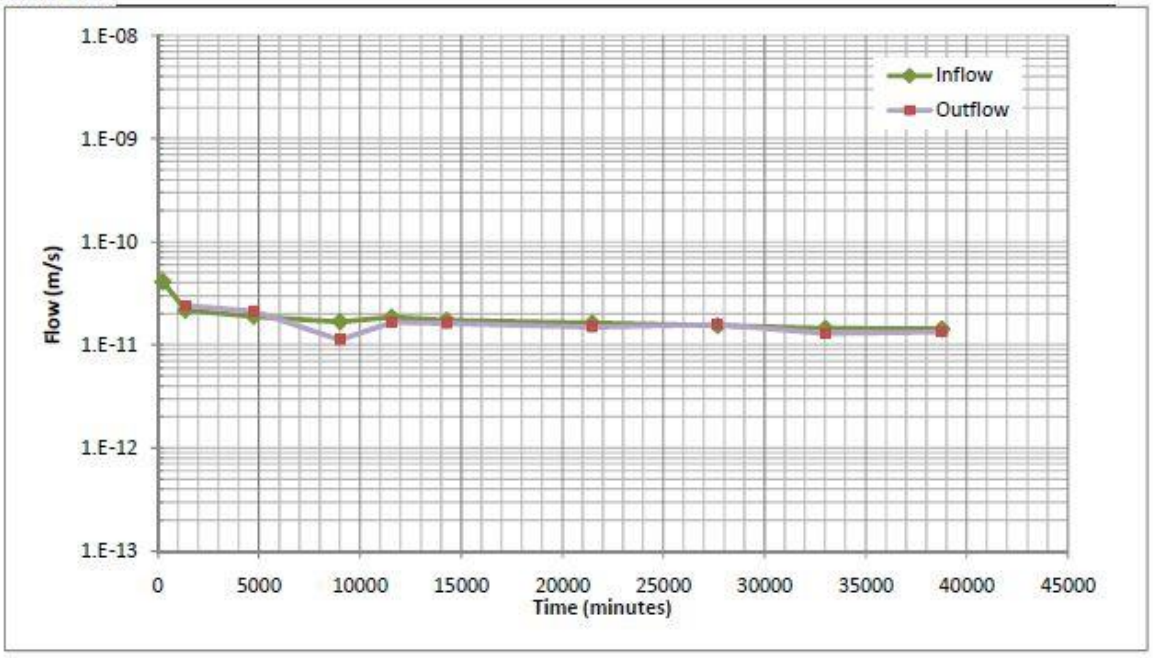

The testing services reported here have been performed in accordance with accepted local industry standards.

The results presented are for the sole use of the designated client only.

This report constitutes a testing service only. It does not represent any interpretation or opinion regarding specification compliance or material suitability.

Engineering interpretation will be provided by MDH Engineered Solutions Corp upon request.

Appendix E2: Site 1, Pierre Shale- 74.33 m

TRIAXIAL HYDRAULIC CONDUCTIVITY TEST REPORT

Test reference: ASTM D 5084

MDH ENGINEERED SOLUTIONS

CLIENT:	-
PROJECT:	-
MDH Job No:	M1870
DATE:	17-Dec-10

SAMPLE: GDC-05 Core sample

Depth: 74.33m

Testing Summary:

Average back pressure =	200 kPa	**Post test condition**	
Effective confining pressure =	200 kPa	Final sample diameter =	70.48 mm
Head across sample =	15.8 kPa	Final sample height =	33.53 mm
Hydraulic gradient =	50	Final water content =	19.7 %
		Final Dry Density =	1827 kg/m^3
Specific gravity of solids =	2.65 (assumed)	Final void ratio =	0.49
Initial sample condition			
Initial sample diameter =	70.48 mm		
Initial sample height =	32.44 mm	Permeant:	de-aired tap-water
Initial Water Content =	15.6 %		
Initial Dry Density =	1905 kg/m^3	**Final Hydraulic Conductivity:**	
Initial void ratio =	0.39	k = ~1.0E-12 m/s @	84,528 minutes

Comments:

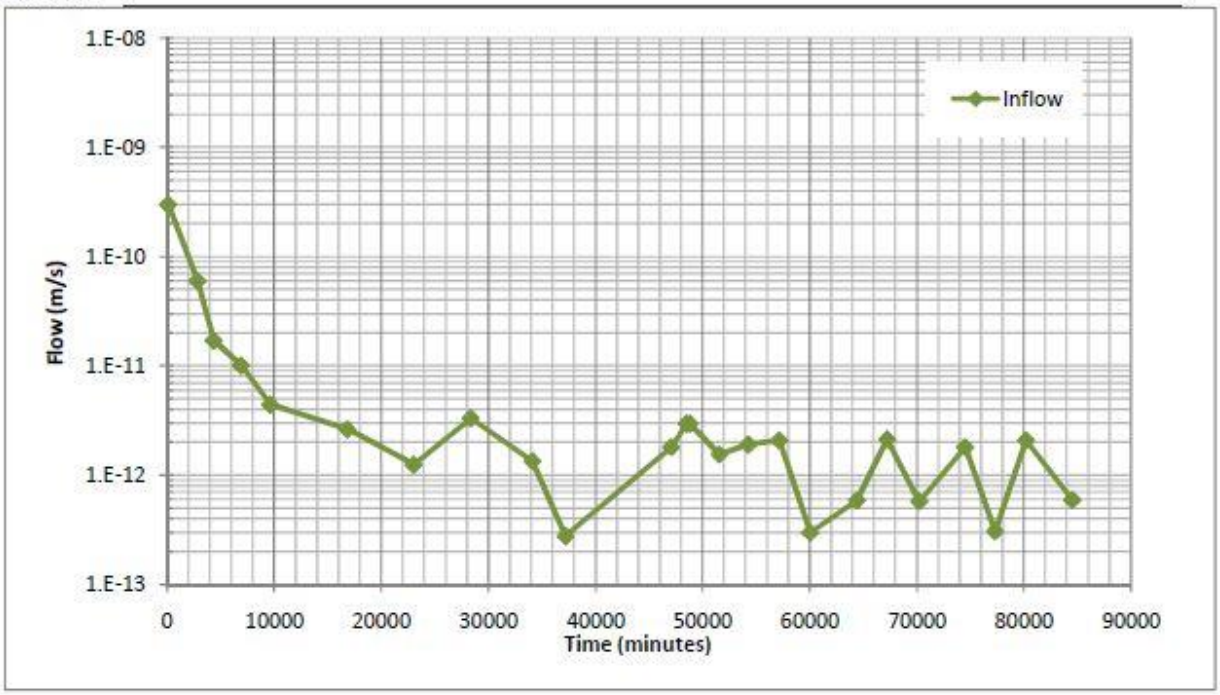

Appendix E3: Site 1, Pierre Shale- 111 m

TRIAXIAL HYDRAULIC CONDUCTIVITY TEST REPORT

Test reference: ASTM D 5084

MDH ENGINEERED SOLUTIONS

CLIENT:	-
PROJECT:	-
MDH Job No:	M1870
DATE:	17-Nov-10

SAMPLE: JNC-02 Core sample

Depth: 7.0m

Testing Summary:

Average back pressure =	200 kPa	**Post test condition**	
Effective confining pressure =	200 kPa	Final sample diameter =	73.22 mm
Head across sample =	15.8 kPa	Final sample height =	31.20 mm
Hydraulic gradient =	54	Final water content =	18.4 %
		Final Dry Density =	1783 kg/m^3
Specific gravity of solids =	2.65 (assumed)	Final void ratio =	0.49
Initial sample condition			
Initial sample diameter =	72.32 mm		
Initial sample height =	29.95 mm	Permeant:	de-aired tap-water
Initial Water Content =	12.3 %		
Initial Dry Density =	1904 kg/m^3	**Final Hydraulic Conductivity:**	
Initial void ratio =	0.39	k = 4.0 E-12 m/s @	37,309 minutes

Comments:

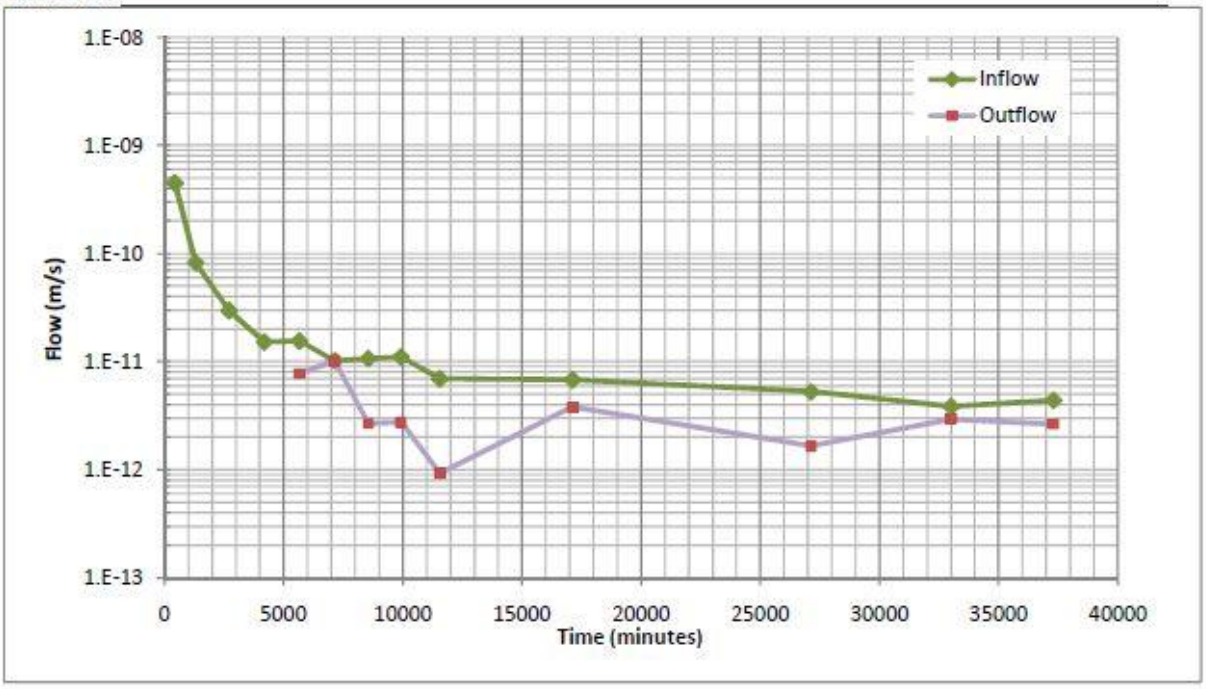

The testing services reported here have been performed in accordance with accepted local industry standards.

The results presented are for the sole use of the designated client only.

This report constitutes a testing service only. It does not represent any interpretation or opinion regarding specification compliance or material suitability.

Engineering interpretation will be provided by MDH Engineered Solutions Corp upon request.

Appendix E4: Site 1, 1st Speckled Shale- 207 m

TRIAXIAL HYDRAULIC CONDUCTIVITY TEST REPORT

Test reference: ASTM D 5084

MDH ENGINEERED SOLUTIONS

CLIENT:	-
PROJECT:	-
MDH Job No:	M1870
DATE:	17-Nov-10

SAMPLE: GDC-13 Core sample

Depth: 7.0m

Testing Summary:

Average back pressure =	200 kPa	**Post test condition**	
Effective confining pressure =	200 kPa	Final sample diameter =	73.54 mm
Head across sample =	15.8 kPa	Final sample height =	27.82 mm
Hydraulic gradient =	59	Final water content =	23.2 %
		Final Dry Density =	1566 kg/m^3
Specific gravity of solids =	2.55 (assumed)	Final void ratio =	0.55
Initial sample condition			
Initial sample diameter =	73.54 mm		
Initial sample height =	27.23 mm	Permeant:	de-aired tap-water
Initial Water Content =	19.5 %		
Initial Dry Density =	1602 kg/m^3	**Final Hydraulic Conductivity:**	
Initial void ratio =	0.52	k = 1.5E-12 m/s @	41,208 minutes

Comments:

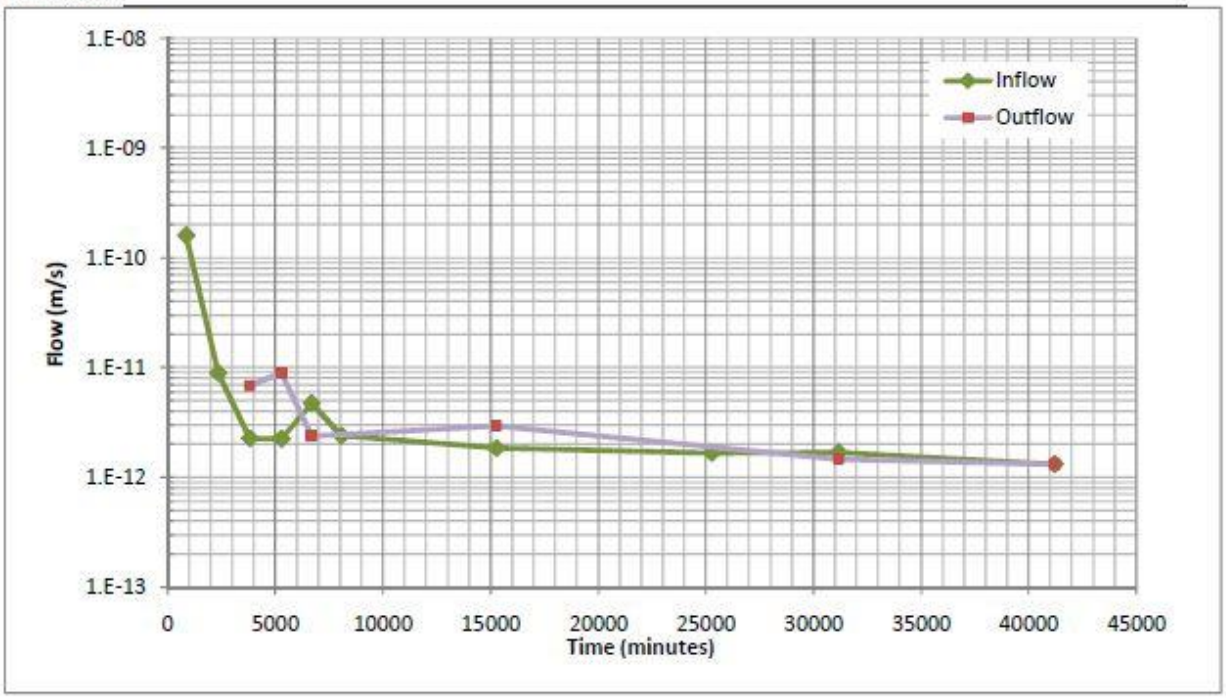

Appendix E5: Site 1, 1st Speckled Shale- 257 m

TRIAXIAL HYDRAULIC CONDUCTIVITY TEST REPORT

Test reference: ASTM D 5084

MDH ENGINEERED SOLUTIONS

CLIENT:	-
PROJECT:	-
MDH Job No:	M1870
DATE:	17-Dec-10

SAMPLE: KLP-11 Core sample

Depth: 257.2m

Testing Summary:

Average back pressure =	200 kPa	**Post test condition**	
Effective confining pressure =	200 kPa	Final sample diameter =	74.77 mm
Head across sample =	15.8 kPa	Final sample height =	26.51 mm
Hydraulic gradient =	62	Final water content =	9.7 %
		Final Dry Density =	2019 kg/m^3
Specific gravity of solids =	2.55 (assumed)	Final void ratio =	0.34
Initial sample condition			
Initial sample diameter =	74.35 mm		
Initial sample height =	25.97 mm	Permeant:	de-aired tap-water
Initial Water Content =	7.1 %		
Initial Dry Density =	2076 kg/m^3	**Final Hydraulic Conductivity:**	
Initial void ratio =	0.30	k = 2.0E-12 m/s @	35,720 minutes

Comments:

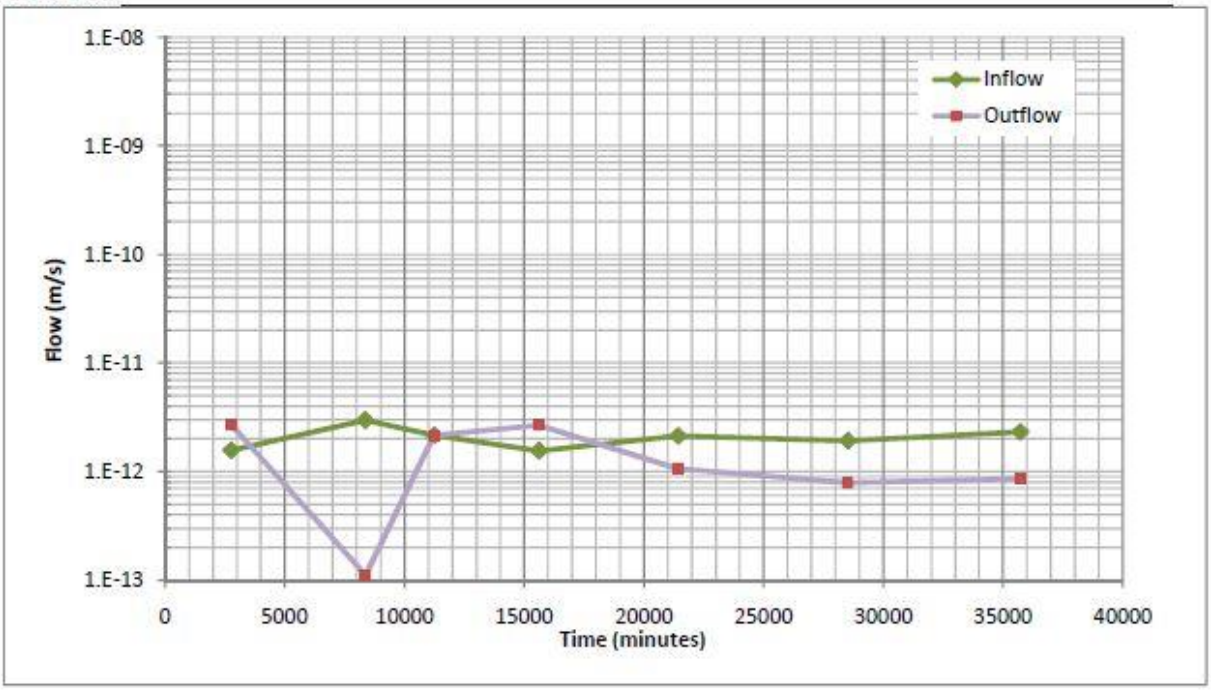

Appendix E6: Site 1, 2nd Speckled Shale- 277 m

TRIAXIAL HYDRAULIC CONDUCTIVITY TEST REPORT

Test reference: ASTM D 5084

MDH ENGINEERED SOLUTIONS

CLIENT:	-
PROJECT:	-
MDH Job No:	M1870
DATE:	17-Jan-11

SAMPLE: JNC-13 Core sample

Depth: 277.71m

Testing Summary:

Average back pressure =	200 kPa	**Post test condition**	
Effective confining pressure =	200 kPa	Final sample diameter =	73.28 mm
Head across sample =	15.8 kPa	Final sample height =	29.00 mm
Hydraulic gradient =	56	Final water content =	9.4 %
		Final Dry Density =	2161 kg/m^3
Specific gravity of solids =	2.55 (assumed)	Final void ratio =	0.23
Initial sample condition			
Initial sample diameter =	73.28 mm		
Initial sample height =	28.95 mm	Permeant:	salt solution @ 10g/L
Initial Water Content =	6.5 %		
Initial Dry Density =	2196 kg/m^3	**Final flow rate:**	
Initial void ratio =	0.21	k = 3.0E-12 m/s @	26,967 minutes

Comments:

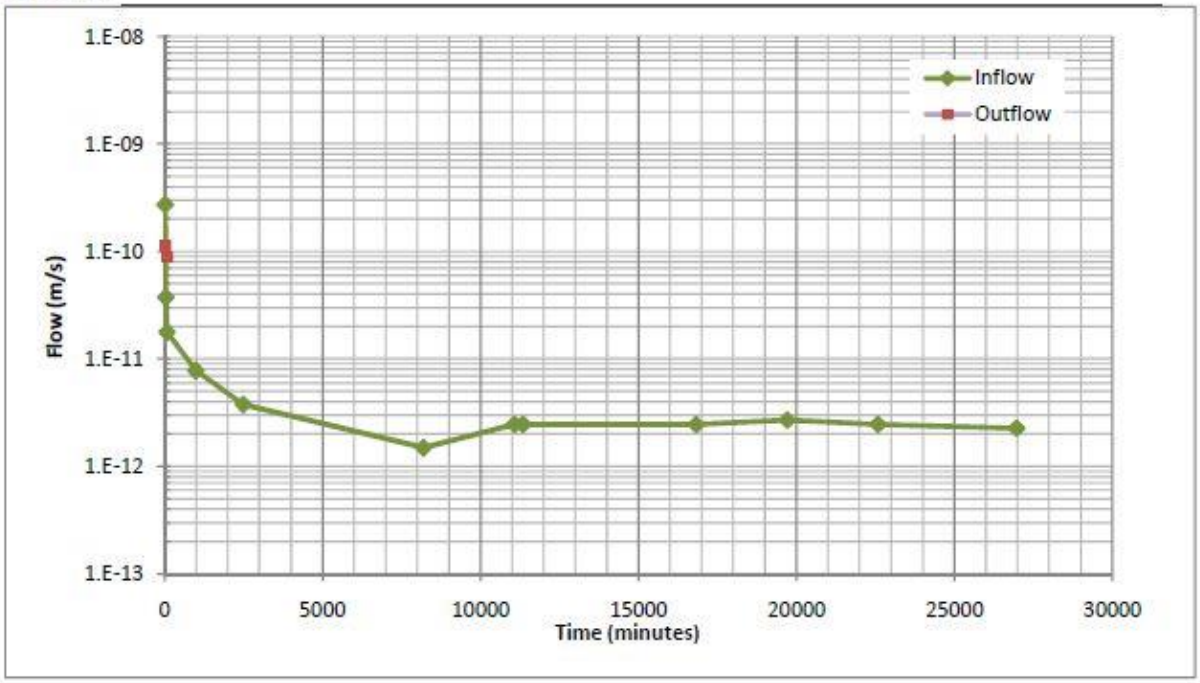

Appendix E7: Site 1, Belle Fourche- 311 m

TRIAXIAL HYDRAULIC CONDUCTIVITY TEST REPORT

Test reference: ASTM D 5084

MDH ENGINEERED SOLUTIONS

CLIENT:	-
PROJECT:	-
MDH Job No:	M1870
DATE:	17-Nov-10

SAMPLE: JNC-19 Core sample

Depth: 7.0m

Testing Summary:

Average back pressure =	200 kPa	**Post test condition**	
Effective confining pressure =	200 kPa	Final sample diameter =	74.34 mm
Head across sample =	15.8 kPa	Final sample height =	18.73 mm
Hydraulic gradient =	90	Final water content =	16.8 %
		Final Dry Density =	1848 kg/m^3
Specific gravity of solids =	2.55 (assumed)	Final void ratio =	0.45
Initial sample condition			
Initial sample diameter =	73.82 mm		
Initial sample height =	17.93 mm	Permeant:	de-aired tap-water
Initial Water Content =	11.2 %		
Initial Dry Density =	1947 kg/m^3	**Final Hydraulic Conductivity:**	
Initial void ratio =	0.36	k = 1.5E-12 m/s @	42,758 minutes

Comments:

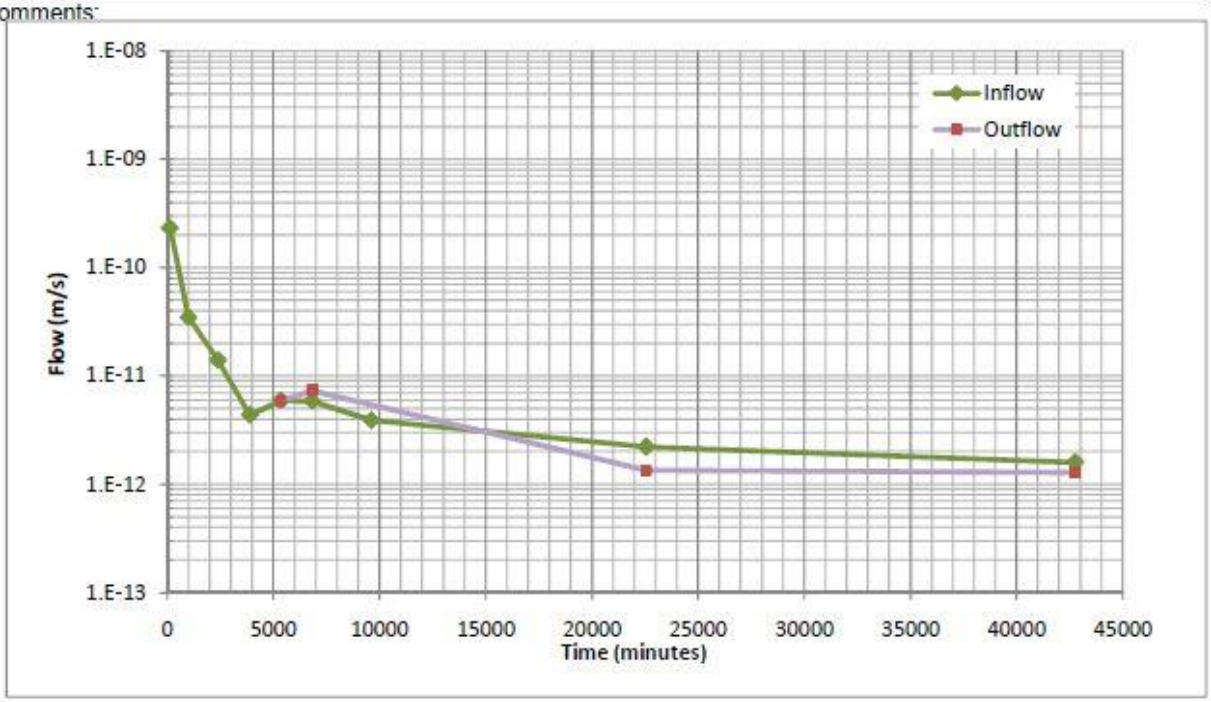

The testing services reported here have been performed in accordance with accepted local industry standards.

The results presented are for the sole use of the designated client only.

This report constitutes a testing service only. It does not represent any interpretation or opinion regarding specification compliance or material suitability.

Engineering interpretation will be provided by MDH Engineered Solutions Corp upon request.

Appendix E8: Site 1, Grout- Batch 1

TRIAXIAL HYDRAULIC CONDUCTIVITY TEST REPORT

Test reference: ASTM D 5084

MDH ENGINEERED SOLUTIONS

CLIENT:	University of Saskatchewan
PROJECT:	-
MDH Job No:	M1870
DATE:	23-Jun-10

SAMPLE: Batch #1 -

Testing Summary:			
Total back pressure =	215 kPa	Initial Water Content =	- %
Maximum effective stress =	24 kPa	Initial Dry Density =	- kg/m^3
Minimum effective stress =	17 kPa	Initial Deg of saturation =	- %
Hydraulic gradient =	36	Final Water Content =	- %
Initial sample diameter =	60.65 mm	Final Dry Density =	- kg/m^3
Initial sample height =	20.08 mm	Final deg of saturation =	- %
Permeant:	de-aired tap-water	**Final Hydraulic Conductivity:**	
		k = <2 E-10 cm/s @ 33,001 minutes	

Comments:

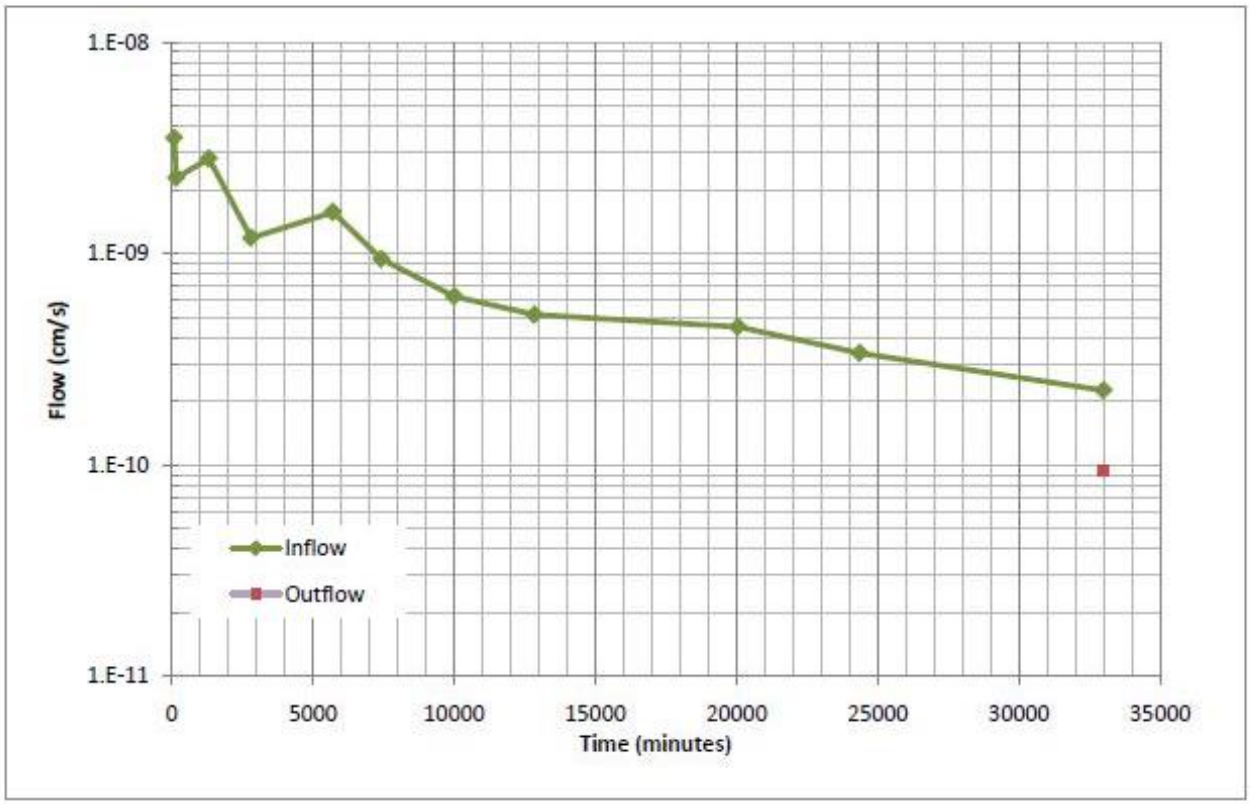

The testing services reported here have been performed in accordance with accepted local industry standards.

The results presented are for the sole use of the designated client only.

This report constitutes a testing service only. It does not represent any interpretation or opinion regarding specification compliance or material suitability.

Engineering interpretation will be provided by MDH Engineered Solutions Corp upon request.

Appendix E9: Site 1, Grout-Batch 24

TRIAXIAL HYDRAULIC CONDUCTIVITY TEST REPORT

Test reference: ASTM D 5084

MDH ENGINEERED SOLUTIONS

CLIENT:	University of Saskatchewan
PROJECT:	-
MDH Job No:	M1870
DATE:	23-Jun-10

SAMPLE: Batch #24 -

Testing Summary:			
Total back pressure =	215 kPa	Initial Water Content =	- %
Maximum effective stress =	24 kPa	Initial Dry Density =	- kg/m^3
Minimum effective stress =	17 kPa	Initial Deg of saturation =	- %
Hydraulic gradient =	34	Final Water Content =	- %
Initial sample diameter =	61.11 mm	Final Dry Density =	- kg/m^3
Initial sample height =	20.92 mm	Final deg of saturation =	- %
Permeant:	de-aired tap-water	**Final Hydraulic Conductivity:**	
		k = <6.0 E-10 cm/s @ 23,161 minutes	

Comments:

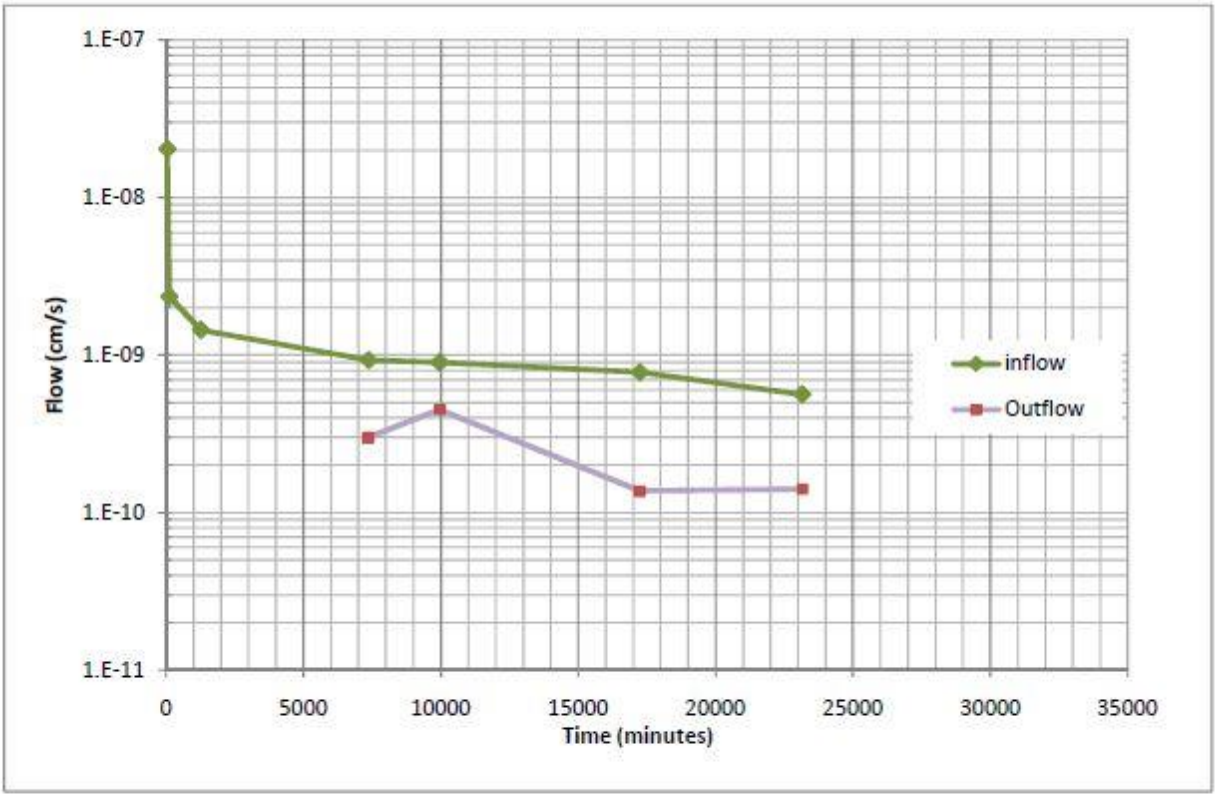

The testing services reported here have been performed in accordance with accepted local industry standards.

The results presented are for the sole use of the designated client only.

This report constitutes a testing service only. It does not represent any interpretation or opinion regarding specification compliance or material suitability.

Engineering interpretation will be provided by MDH Engineered Solutions Corp upon request.

Appendix E10: Site 1, Grout- Batch 48

TRIAXIAL HYDRAULIC CONDUCTIVITY TEST REPORT

Test reference: ASTM D 5084

MDH ENGINEERED SOLUTIONS

CLIENT:	University of Saskatchewan
PROJECT:	-
MDH Job No:	M1870
DATE:	04-Jun-10

SAMPLE: Batch #48 -

Testing Summary:			
Total back pressure =	215 kPa	Initial Water Content =	- %
Maximum effective stress =	24 kPa	Initial Dry Density =	- kg/m^3
Minimum effective stress =	17 kPa	Initial Deg of saturation =	- %
Hydraulic gradient =	29	Final Water Content =	- %
Initial sample diameter =	60.94 mm	Final Dry Density =	- kg/m^3
Initial sample height =	25.00 mm	Final deg of saturation =	- %
Permeant:	de-aired tap-water	**Final Hydraulic Conductivity:**	
		k = ~ 1.00E-08 cm/s @ 18,722 minutes	

Comments:

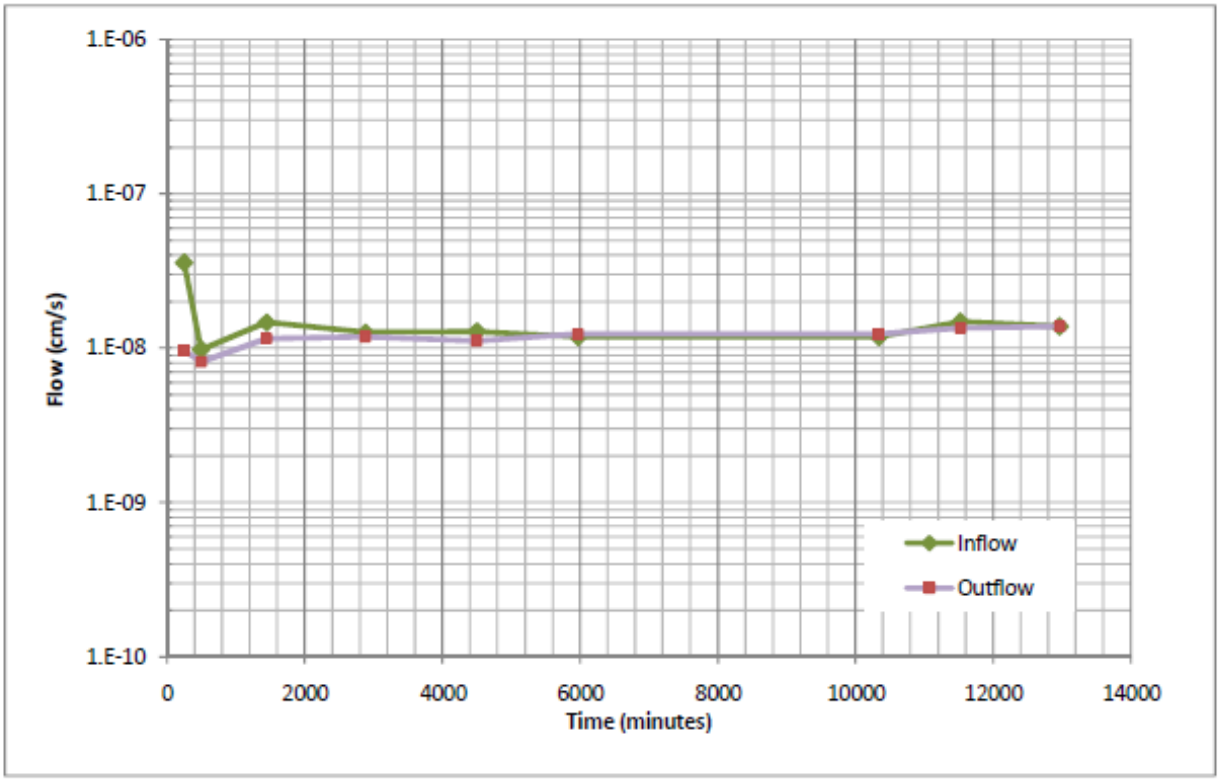

The testing services reported here have been performed in accordance with accepted local industry standards.

The results presented are for the sole use of the designated client only.

This report constitutes a testing service only. It does not represent any interpretation or opinion regarding specification compliance or material suitability.

Engineering interpretation will be provided by MDH Engineered Solutions Corp upon request.

Appendix E11: Site 2, Pierre Shale- 30 m

TRIAXIAL HYDRAULIC CONDUCTIVITY TEST REPORT

Test reference: ASTM D 5084

SNC·LAVALIN

CLIENT:	University of Saskatchewan
PROJECT:	-
PROJECT No:	617067
DATE:	3-Mar-14

SAMPLE: Kre-33 (30.03-30.12) Shelby specimen

Testing Summary:

Cell pressure =	528 kPa	Final Water Content =	16.7%
Average back pressure =	200 kPa	Final Dry Density =	1859 kg/m^3
Head across specimen =	67 cm	Final deg of saturation =	100%
Hydraulic gradient =	19.5		
Initial sample diameter =	68.02 mm	Inflow rate =	0.00035 cc/min
Initial sample height =	34.28 mm	Outflow rate =	0.00039 cc/min
Initial Water Content =	16.0%	Average flow rate =	0.00037 cc/min
Initial Dry Density =	1806 kg/m^3		
Initial Deg of saturation =	91%	**Hydraulic Conductivity (based on average flow rate):**	
Permeant:	de-aired tap-water	k = 8.65E-09 cm/s	

Comments:

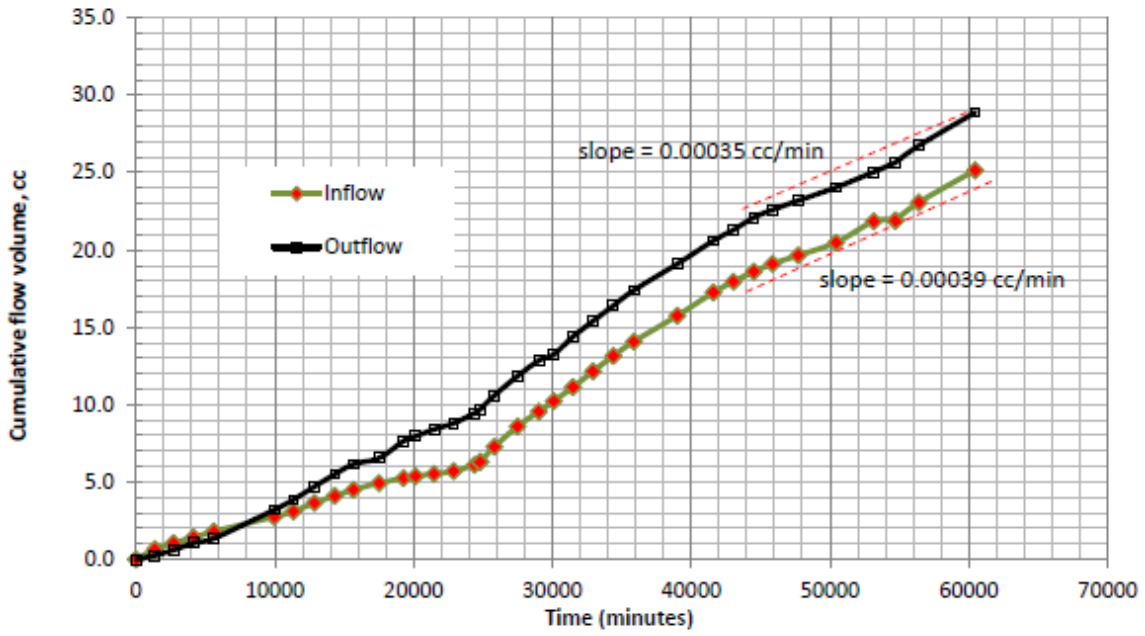

The testing services reported here have been performed in accordance with accepted local industry standards.

The results presented are for the sole use of the designated client only.

This report constitutes a testing service only. It does not represent any interpretation or opinion regarding specification compliance or material suitability.

Engineering interpretation will be provided by SNC-Lavalin upon request.

Appendix E12: Site 2, Pierre Shale- 82 m

TRIAXIAL HYDRAULIC CONDUCTIVITY TEST REPORT

Test reference: ASTM D 5084

SNC·LAVALIN

CLIENT:	University of Saskatchewan
PROJECT:	-
PROJECT No:	617067
DATE:	23-Jan-13

SAMPLE: KRE-43 (82.34-82.64) Shelby specimen

Testing Summary:

Cell pressure =	1363 kPa	Final Water Content =	21.1%
Average back pressure =	200 kPa	Final Dry Density =	1726 kg/m^3
Head across specimen =	67 cm	Final deg of saturation =	100%
Hydraulic gradient =	19.8		
Initial sample diameter =	68.67 mm	Inflow rate =	0.000034 cc/min
Initial sample height =	33.89 mm	Outflow rate =	0.000020 cc/min
Initial Water Content =	17.6%	Average flow rate =	0.000027 cc/min
Initial Dry Density =	1772 kg/m^3		
Initial Deg of saturation =	94%	**Hydraulic Conductivity (based on average flow rate):**	
Permeant:	de-aired tap-water	k = 6.1E-10 cm/s	

Comments:

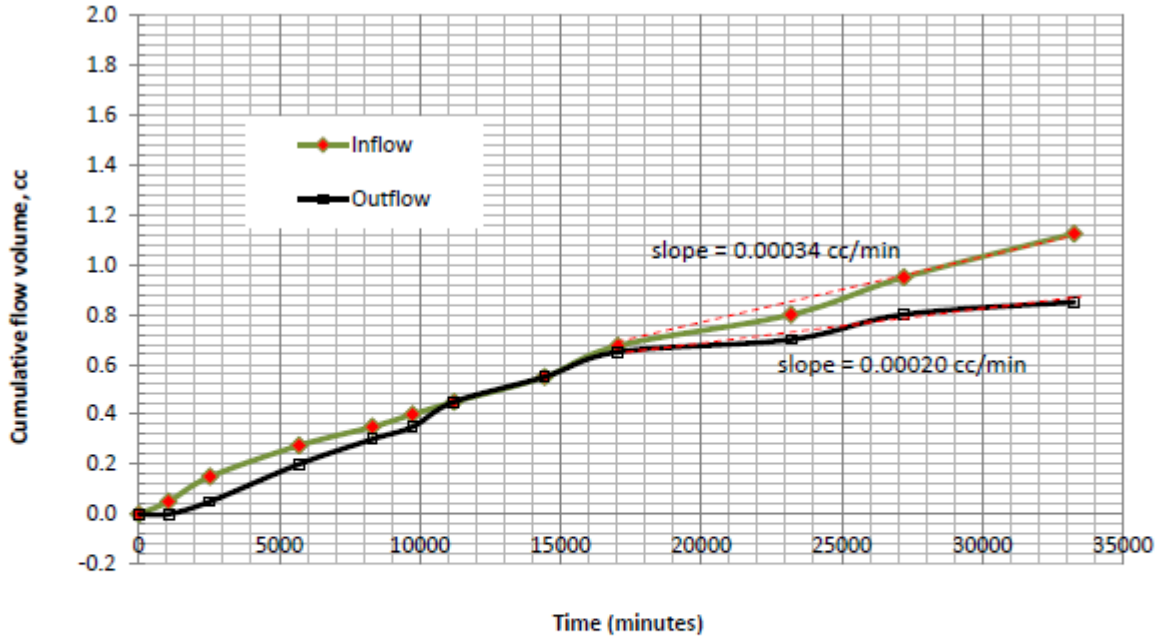

The testing services reported here have been performed in accordance with accepted local industry standards.

The results presented are for the sole use of the designated client only.

This report constitutes a testing service only. It does not represent any interpretation or opinion regarding specification compliance or material suitability.

Engineering interpretation will be provided by SNC-Lavalin upon request.

Appendix E13: Site 2, Pierre Shale- 126.77 m

TRIAXIAL HYDRAULIC CONDUCTIVITY TEST REPORT

Test reference: ASTM D 5084

SNC·LAVALIN

CLIENT:	University of Saskatchewan
PROJECT:	-
PROJECT No:	617067
DATE:	3-Mar-14

SAMPLE: Kre-150 (126.77-126.94) Shelby specimen

Testing Summary:

Cell pressure =	1903	kPa	Final Water Content =	29.8%	
Average back pressure =	200	kPa	Final Dry Density =	1524	kg/m^3
Head across specimen =	67	cm	Final deg of saturation =	100%	
Hydraulic gradient =	23.6				
Initial sample diameter =	68.13	mm	Inflow rate =	0.0000054	cc/min
Initial sample height =	28.41	mm	Outflow rate =	-	cc/min
Initial Water Content =	22.0%		Average flow rate =	-	cc/min
Initial Dry Density =	1677	kg/m^3			
Initial Deg of saturation =	100%		**Hydraulic Conductivity (based on inflow rate only):**		
Permeant:	de-aired tap-water		K << 1.05E-10	cm/s	

Comments: Confining pressure seal blew and test had to be curtailed. K was computed based on inflow alone, as no net outflow had yet occured. K of material was too low for this test set-up. Leaks, evaporation, humidity and temperature effects were significant in comparison to the minute flow volume. Actual K could not be obtained. It could only be concluded that K would be significantly lower than the 1.05 E-10 cm/s value computed based on limited inflow data.

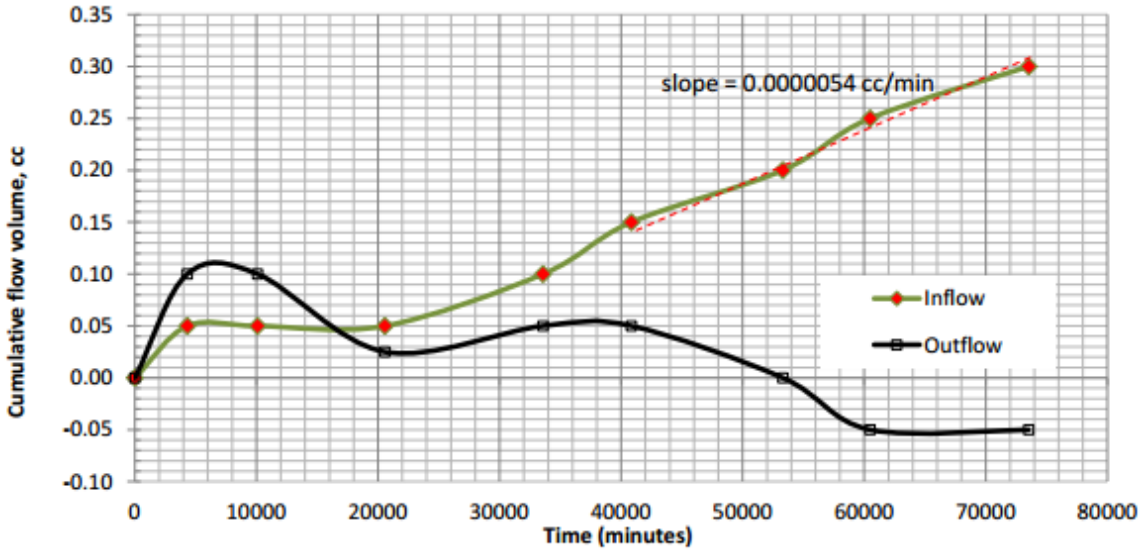

APPENDIX F: Geophysical log at Site 1 (0-215 m BG)

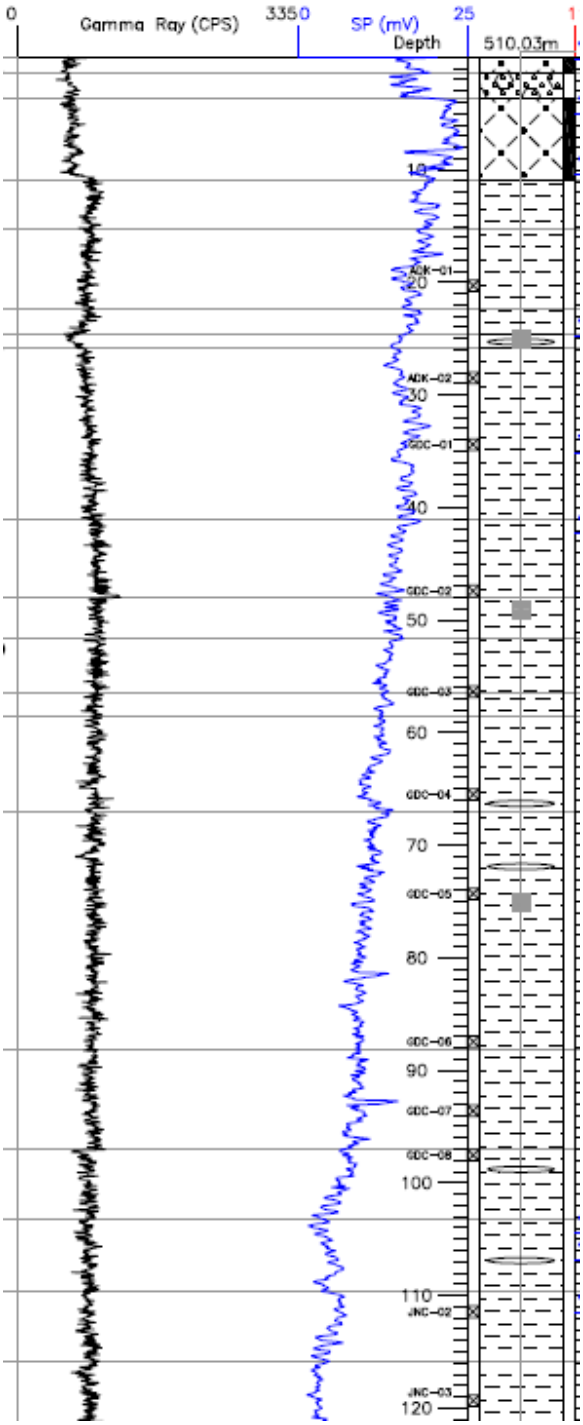

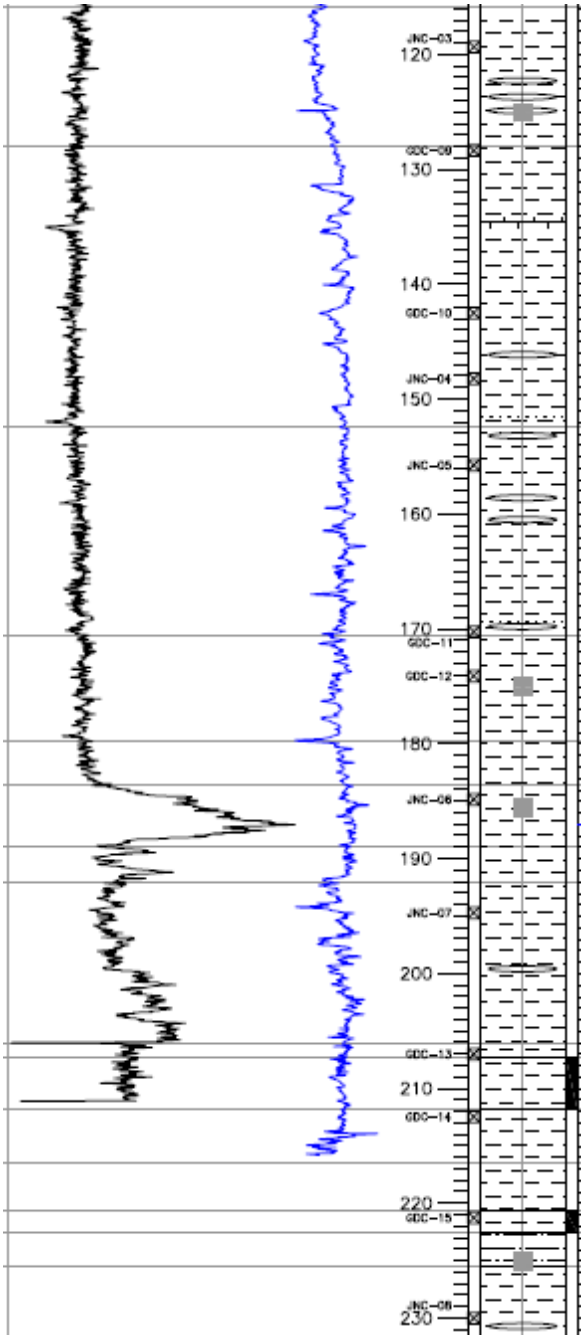

1 2 3 4